THE MANCHESTER METROPOLITAN
UNIVERSITY

MATHEMATICAL AND NUMERICAL STUDY OF TWO–PHASE FLOW MODELS

A THESIS SUBMITTED IN PARTIAL FULFILMENT OF
THE REQUIREMENTS FOR THE DEGREE OF
DOCTOR OF PHILOSOPHY

DEPARTMENT OF COMPUTING AND MATHEMATICS

BY

DIA HUSSEIN ABDULHAMEED ZEIDAN

MANCHESTER, UNITED KINGDOM
MARCH 2003

To my parents who nurtured me well and inculcated in me the spirit and appetite to learn more and more

To my sisters who have always given me their love, care and cheer

To my brothers who are not fully aware of the tools of mathematics

and beyond them to all my teachers and friends from whom I have learned so much and still do ..... year after year.

ABSTRACT

This research work has developed and investigated two different models that can be used in the study of two–phase flows. The first model, the simplified two–fluid model, was derived from the more fundamental two–fluid model for an isentropic two–phase flow. The model contains a mixture density conservation equation, a mixture momentum conservation equation and a relative velocity term between the two phases. The simplified two–fluid model is naturally written in a non–conservative form due to the presence of non–conservative products in the momentum equation. We show that the model is strictly hyperbolic provided that the relative velocity between the two–phases is much lower than the speed of sound of the two–phase mixture. We then present an exact Riemann solver for the model along with several approximate Riemann solvers. These solutions are then used locally to compute numerically the global solution of the general initial–value problem for the simplified two–fluid model. Total Variation Diminishing (TVD), shock–capturing, finite volume methods of Godunov–type of the upwind and centred type have been constructed. To illustrate the capabilities of the proposed numerical methods, results are presented for carefully selected challenging test problems. The results demonstrate that our numerical schemes are more accurate than other schemes currently used. A more complete model, the hyperbolic conservative model, for compressible two–phase flow governed by a hyperbolic system of conservative equations has also been developed. Extended thermodynamics principles are applied in the derivation of the three–dimensional governing equations and of their corresponding closure relations. The model involves six equations obtained from conservation principles applied to a one–dimensional mixture of gas and liquid completed by additional closure governing equations. The model is valid for pure fluids as well as for fluid mixtures. The system of partial differential equations with source terms is hyperbolic and has conservative form. Its numerical solution poses several difficulties. The model possesses a large number of acoustic waves and it is not easy to upwind all of these accurately and simply. We focus on relatively modern shock–capturing methods of a centred type such as the TVD SLIC scheme which solve these problems in a simple way and with good accuracy. Several numerical test problems were carried out to highlight the efficiency of our numerical scheme. The scheme provides reliable results, is able to compute strong shock waves and deals with complex equations of state.

ACKNOWLEDGEMENTS

This thesis is in partial fulfilment of the Degree of Doctor of Philosophy in Computational Applied Mathematics at the Manchester Metropolitan University. This work is the result of a research effort which I undertook between January 2000 and March 2003 under the guidance of Professor E. F. Toro (OBE), Dr A. Slaouti and Professor E. Romenski. I am very grateful to my research Supervisor Professor Toro who provided me with this research topic, shared with me his vast experience within this field and guided me through this work. I would also like to express my sincere thanks to my second Supervisor, Dr Slaouti, for his general help in the field of computational fluid dynamics and his constant supervision for more than three years. I deeply appreciate all of the hours he spent with me reviewing my work and discussing various numerical schemes. His enthusiasm, knowledge and readiness to answer my questions has been of great help during the entire duration of my PhD study. I am also greatly indebted to Professor Romenski (Formerly at Sobolev Institute of Mathematics, Russian Academy of Sciences, Novosibirsk, Russia) who came to work with Professor Toro for a short period and helped me learn and appreciate analytical methods and new techniques for the study of multiphase fluid flow problems.

The study of mathematics and the writing of a doctoral thesis is sometimes a solitary affair and social interaction and friendships are vital to emerge in a healthy and happy condition. I thank all my friends for making my time here in Manchester memorable. This research has also been a major family effort. My mum, Salwa deserves all the gratitude I can proffer for supporting me throughout this research with unlimited patience, love and encouragement. Many thanks too to my sisters Maysoon, Majedah, Muna and Dua'a for their steadfast encouragement during my PhD I am also indebted to my brothers for their understanding and support. Without all of the aforementioned contributions I would have been unable to complete this PhD work.

Dia H. A. Zeidan

Manchester, UK, March 2003

DECLARATION

No portion of the work referred to in this thesis has been submitted in support of an application for another degree or qualification of this or any other university or other institution of learning.

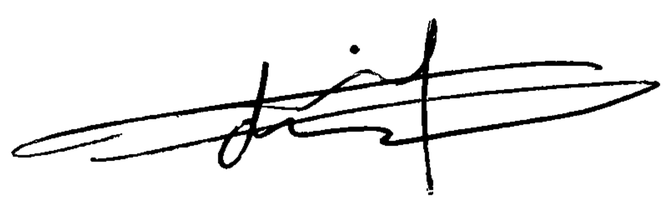

Dia H. A. Zeidan

March 2003

COPYRIGHT

Copyright in text of this thesis rests with the Author. Copies (by any process) either in full, or of extracts, may be made **only** in accordance with instructions given by the Author and lodged in the Manchester Metropolitan University Librarian. Details may be obtained from the Librarian. This page must form part of any such copies made. Further copies (by any process) of copies made in accordance with such instructions may not be made without the permission (in writing) of the Author.

The ownership of any intellectual property rights which may be described in this thesis is vested in the Manchester Metropolitan University, subject to any prior agreement to the contrary, and may not be made available for any third parties without the written permission of the University, which will prescribe the terms and conditions of any such agreement.

Further information on the conditions under which disclosures and exploitation may take place is available from the head of Department of Computing and Mathematics.

THE AUTHOR

The author graduated from Howarah Community College, Ministry of Higher Education, Amman, Jordan, in June 1990 with a First Degree in Mathematics. He then carried out a four year teaching period as a Mathematics teacher at governmental schools in the region until September 1994. This was followed by a two year programme of Applied Mathematics at Quaid–i–Azam University, Islamabad, Pakistan, and resulted in the award of MSc Degree in February 1998. He joined the Manchester Metropolitan University in January 2000, pursuing a PhD study in Computational Applied Mathematics under the supervision of Professor E. F. Toro (OBE), Dr A. Slaouti and Professor E. Romenski in the Department of Computing and Mathematics. In November 2002 he was appointed to a Research Officer position at Cranfield University, Royal Military College of Science at the Defence Academy of the United Kingdom. His PhD research was completed in March 2003.

TABLE OF CONTENTS

ABSTRACT iii

ACKNOWLEDGEMENTS iv

DECLARATION v

COPYRIGHT vi

THE AUTHOR vii

1 INTRODUCTION 1
- 1.1 Background 1
- 1.2 Objectives of the Thesis 8
- 1.3 Basic Mathematical Concepts for Hyperbolic Partial Differential Equations 10
  - 1.3.1 Basic Definitions 10
  - 1.3.2 The Riemann Problem 12
- 1.4 Two–Phase Flow Models 17
  - 1.4.1 The Simplified Two–Fluid Model 18
  - 1.4.2 The Hyperbolic Conservative Two–Fluid Model 22
- 1.5 Numerical Schemes for Conservation Laws 25
  - 1.5.1 The Godunov Upwind Method 30
  - 1.5.2 Stability and Boundary Conditions for Godunov's Method . . 32
  - 1.5.3 The Lax–Friedrichs Centred Method 32
  - 1.5.4 The FORCE Centred Method 33
- 1.6 Outline of the Thesis 34

2 MATHEMATICAL ANALYSIS OF A SIMPLIFIED TWO–FLUID MODEL 35
- 2.1 Governing Equations 35
- 2.2 Hyperbolicity Analysis of the Equations 39
- 2.3 Nature of Characteristic Fields 43
- 2.4 Conclusions 44

3 THE RIEMANN PROBLEM FOR THE SIMPLIFIED TWO–FLUID MODEL 46
- 3.1 The Riemann Problem and a Solution Strategy 46
- 3.2 An Exact Riemann Solver 49
  - 3.2.1 Function $\mathcal{F}_{\mathcal{L}}$ for a Left Shock 50

3.2.2 Function $\mathcal{F}_{\mathcal{L}}$ for a Left Rarefaction 53
3.2.3 Function $\mathcal{F}_{\mathcal{R}}$ for a Right Shock 56
3.2.4 Function $\mathcal{F}_{\mathcal{R}}$ for a Right Rarefaction 58
3.3 The Middle–Wave 59
3.3.1 The Middle–Shock Wave 60
3.3.2 The Middle–Rarefaction Wave 62
3.4 Numerical Solution for the Mixture Density $\rho^{\star}$ 63
3.4.1 Behaviour of the Mixture Density Function $\mathcal{F}(\rho)$ 63
3.4.2 Iterative Scheme for Finding the Mixture Density 65
3.5 The Complete Solution 66
3.5.1 Left Shock Wave 67
3.5.2 Left Rarefaction Wave 68
3.5.3 Right Shock Wave 70
3.5.4 Right Rarefaction Wave 71
3.6 Sampling the Solution 72
3.6.1 Sampling Point is to the Left of the Contact Wave 73
3.6.2 Sampling Point is to the Right of the Contact Wave 73
3.7 Conclusions 74

4 TEST PROBLEMS WITH EXACT SOLUTIONS 76
4.1 Test 1: Left Sonic Rarefaction and Right Shock Wave 78
4.2 Test 2: Left Rarefaction and Right Rarefaction 78
4.3 Test 3: Left Shock and Right Shock 78
4.4 Test 4: Left Shock and Right Rarefaction 79

5 APPROXIMATE RIEMANN SOLVERS 82
5.1 The Riemann Problem and Godunov Flux 82
5.2 Approximate–State Riemann Solvers 84
5.2.1 A Primitive–Variable Riemann Solver (PVRS) 84
5.2.2 A Two–Shock Riemann Solver (TSRS) 87
5.2.3 A Two–Rarefaction Riemann Solver (TRRS) 88
5.3 The HLL and HLLC Riemann Solvers 89
5.3.1 The HLL Riemann Solver 89
5.3.2 The HLLC Riemann Solver 91
5.4 Conclusions 93

6 HIGH–RESOLUTION AND TVD SCHEMES FOR THE SIMPLIFIED TWO–FLUID MODEL 94
6.1 Godunov–type Schemes 94
6.2 The Weighted Average Flux (WAF) Scheme 95
6.2.1 The Basic WAF Scheme 96
6.2.2 TVD Version of the WAF Scheme 98

6.2.3 Rarefactions in State Riemann Solvers 100
6.3 The MUSCL–Hancock Method 101
6.3.1 The Basic MUSCL–Hancock Method 102
6.3.2 TVD Version of the MUSCL–Hancock Method 103
6.4 Centred TVD Schemes 105
6.4.1 The SLIC Scheme 105
6.5 Numerical Results 106
6.6 Conclusions 122

7 MATHEMATICAL ANALYSIS OF THE HYPERBOLIC CONSERVATIVE TWO–FLUID MODEL 125
7.1 General Equations for Two–phase Flow 125
7.2 One–Dimensional Two–Phase Flow Model–Hyperbolic Conservative Model 133
7.3 Hyperbolicity Analysis of the Equations 138
7.4 Nature of Characteristic Fields 145
7.5 Conclusions 146

8 THE RIEMANN PROBLEM FOR THE HYPERBOLIC CONSERVATIVE TWO–FLUID MODEL 148
8.1 The Riemann Problem and a Solution Strategy 148
8.2 Study of the Sound Wave Propagation 152
8.3 Discontinuities in Two–Phase Flow Models 157
8.4 Study of Shock Waves of Small Amplitude 160
8.5 Conclusions 165

9 NUMERICAL STUDY OF WAVE PROPAGATION IN COMPRESSIBLE TWO–PHASE FLOW 167
9.1 The Numerical Method 167
9.2 Treatment of Source Terms 171
9.3 Test Problems and Numerical Results 173
9.3.1 Test 1: Air–Water Mixture Collision 175
9.3.2 Test 2: Grid Convergence Study 176
9.3.3 Test 3: Pressure Wave Propagation 177
9.3.4 Test 4: Relaxation of Volume Concentration 179
9.3.5 Test 5: Effect of Volume Concentration Relaxation and Interfacial Friction 180
9.3.6 Test 6: Mixture Two–Phase Shock–Tube Problem 181
9.3.7 Test 7: Four–Rarefactions Test Problem 182
9.4 Conclusions 183

10 OVERALL CONCLUSIONS AND SUGGESTIONS FOR FURTHER WORK 186

REFERENCES 190

A EXACT RIEMANN PROBLEM SOLVER FOR TWO–PHASE FLOW MODELS 205

B THE LAX–FRIEDRICHS SCHEME FOR TWO–PHASE FLOW MODELS 218

C MUSCL–HANCOCK SCHEME FOR TWO–PHASE FLOW MODELS 225

LIST OF FIGURES

1.1 Structure of the solution of the Riemann problem for a system of conservation laws. 15
1.2 Hyperbolic nature of the hyperbolic conservative two–fluid model. . . 25

3.1 Structure of the solution of the Riemann problem for the simplified two–fluid model. There are three wave families associated with the eigenvalues λ_1, λ_2 and λ_3. 48
3.2 Possible wave patterns in the solution of the Riemann problem for the one–dimensional simplified two–fluid model. (a) left rarefaction, contact and right shock (b) left shock, contact and right rarefaction (c) left rarefaction, contact and right rarefaction (d) left shock, contact and right shock. 49
3.3 Strategy for solving the Riemann problem by the mixture density function. The mixture velocity $u^\star$ is connected to data on the left and right via $\mathcal{F}_\mathcal{L}$ and $\mathcal{F}_\mathcal{R}$. 50
3.4 Left wave is a shock wave of speed $S_\mathcal{L}$: (a) stationary frame, shock speed is $S_\mathcal{L}$. (b) frame of reference moving with speed $S_\mathcal{L}$, shock speed is zero. 51
3.5 Left wave is a rarefaction wave that connects the data state $\mathbb{W}_\mathcal{L}$ with unknown state $\mathbb{W}^\star_\mathcal{L}$ in the star region to the left of the contact discontinuity. 54
3.6 Mixture density behaviour in the solution of the Riemann problem for the simplified two–fluid model. 64
3.7 Sampling the solution through the complete wave structure at time $t = t^\star$. 67
3.8 Two possible wave configurations at a point to the left of the contact wave: (a) left wave is a shock (b) left wave is a rarefaction wave. . . . 68
3.9 Two possible wave configurations to the right of the contact: (a) right wave is a shock wave (b) right wave is a rarefaction wave. 70

4.1 Exact solution for mixture density, mixture velocity, relative velocity and the pressure for test 1 at $t = 1.0$. 77
4.2 Exact solution for the mixture density, mixture velocity, relative velocity and the pressure for test 2 at $t = 0.04$. 79
4.3 Exact solution for mixture density, mixture velocity, relative velocity and the pressure for test 3 at $t = 0.1$. 80
4.4 Exact solution for the mixture density, mixture velocity, relative velocity and the pressure for test 4 at $t = 0.1$. 81

5.1 Structure of the exact solution of the Riemann problem for the simplified two–fluid model. There are three wave families associated with the eigenvalues λ_1, λ_2 and λ_3. Data and solution are given in terms of primitive variables. 83
5.2 Two–wave structure of the Riemann problem solution for the simplified two–fluid model assumed in the HLL approach. 90
5.3 HLLC approximate Riemann solver the simplified two–fluid model. Solution in the star region consists of two constant states separated from each other by a middle wave of speed $S^\star$. 91

6.1 The solution structure of the Riemann problem for the simplified two–fluid model with data $\mathbb{U}_i^n$ and $\mathbb{U}_{i+1}^n$. 96
6.2 The WAF intercell flux evaluation across the wave structure of the solution of the Riemann problem for the simplified two–fluid model. . 97
6.3 Treatment of right sonic rarefaction when evaluating the WAF flux based on exact or approximate Riemann solvers. 101
6.4 WAF scheme with HLLC Riemann solver and SUPERBEE TVD function applied to Test 1. Numerical (symbol) and exact (line) solutions are compared at $t = 1.0$. 108
6.5 MUSCL–Hancock scheme with exact Riemann solver and SUPERBEE TVD function applied to Test 1. Numerical (symbol) and exact (line) solutions are compared at $t = 1.0$. 109
6.6 Slope LImiter Centred (SLIC) scheme with SUPERBEE TVD function applied to Test 1. Numerical (symbol) and exact (line) solutions are compared at $t = 1.0$. 110
6.7 Lax–Friedrichs scheme applied to Test 1. Numerical (symbol) and exact (line) solutions are compared at $t = 1.0$. 111
6.8 WAF scheme with HLLC Riemann solver and SUPERBEE TVD function applied to Test 2. Numerical (symbol) and exact (line) solutions are compared at $t = 0.04$. 112
6.9 MUSCL–Hancock scheme with exact Riemann solver and SUPERBEE TVD function applied to Test 2. Numerical (symbol) and exact (line) solutions are compared at $t = 0.04$. 113
6.10 Slope LImiter Centred (SLIC) scheme with SUPERBEE TVD function applied to Test 2. Numerical (symbol) and exact (line) solutions are compared at $t = 0.04$. 114
6.11 Lax–Friedrichs scheme applied to Test 2. Numerical (symbol) and exact (line) solutions are compared at $t = 0.04$. 115
6.12 WAF scheme with HLLC Riemann solver and SUPERBEE TVD function applied to Test 3. Numerical (symbol) and exact (line) solutions are compared at $t = 0.1$. 116

6.13 MUSCL–Hancock scheme with exact Riemann solver and SUPERBEE TVD function applied to Test 3. Numerical (symbol) and exact (line) solutions are compared at $t = 0.1$. 117
6.14 Slope LImiter Centred (SLIC) scheme with SUPERBEE TVD function applied to Test 3. Numerical (symbol) and exact (line) solutions are compared at $t = 0.1$. 118
6.15 Lax–Friedrichs scheme applied to Test 3. Numerical (symbol) and exact (line) solutions are compared at $t = 0.1$. 119
6.16 WAF scheme with HLLC Riemann solver and SUPERBEE TVD function applied to Test 4. Numerical (symbol) and exact (line) solutions are compared at $t = 0.1$. 120
6.17 MUSCL–Hancock scheme with exact Riemann solver and SUPERBEE TVD function applied to Test 4. Numerical (symbol) and exact (line) solutions are compared at $t = 0.1$. 121
6.18 Slope LImiter Centred (SLIC) scheme with SUPERBEE TVD function applied to Test 4. Numerical (symbol) and exact (line) solutions are compared at $t = 0.1$. 122
6.19 Lax–Friedrichs scheme applied to Test 4. Numerical (symbol) and exact (line) solutions are compared at $t = 0.1$. 123

8.1 Structure of the solution of the Riemann problem on the x–t plane for the hyperbolic conservative two–fluid model. 149
8.2 Possible wave patterns in the solution of the Riemann problem for the hyperbolic conservative two–fluid model where one–left wave and one–right wave are shock waves. 150
8.3 Possible wave patterns in the solution of the Riemann problem for the hyperbolic conservative two–fluid model where one–left wave is a shock wave and one–right wave is a rarefaction wave. 151
8.4 Possible wave patterns in the solution of the Riemann problem for the hyperbolic conservative two–fluid model where one–left wave is a rarefaction wave and one–right wave is a shock wave. 152
8.5 Possible wave patterns in the solution of the Riemann problem for the hyperbolic conservative two–fluid model where one–left wave and one–right wave are rarefaction waves. 153
8.6 The acoustic velocity for a air–water mixture for the case of single pressure approximation as a function of void fraction α. The water and air are at rest under atmospheric conditions. 157
8.7 The shock in moving coordinates. 157

9.1 Structure of the exact solution of the symmetric Riemann problem in the x t plane for the hyperbolic conservative two–fluid model. There are six wave families associated with the eigenvalues (7.102)–(7.106). 174

9.2 Numerical solution of the Riemann problem. Pressure distribution in three–dimension at $t = 3$. 175
9.3 Pressure contours for the Riemann problem at $t = 3$. 177
9.4 Numerical solution (symbols) for pressure at time 3. SLIC and Lax–Friedrichs methods are compared with the reference solution at 1000 cells. 178
9.5 Numerical solution (SLIC scheme). Effect of the initial pressure on the structure of the solution at $t = 3$. 179
9.6 Riemann problem: grid convergence study for the pressure profile with SLIC scheme at $t = 3$. 180
9.7 A closer look at the strong 2–shocks propagating to the right obtained by SLIC scheme at $t = 3$. 181
9.8 Effect of the relaxation of volume concentration τ on the Pressure. . . 182
9.9 A closer look at the effect of source terms with relaxation time τ and interfacial friction on the structure of the solution of the Riemann problem (pressure). 183
9.10 Solution of the Riemann problem for the air–water mixture shock tube. SLIC and Lax–Friedrichs methods (symbols) compared with the reference solution (line) at 1000 cells. 184
9.11 Solution of the Riemann problem for the four rarefaction waves. SLIC and Lax–Friedrichs methods (symbols) compared with the reference solution (line) at 1000 cells. 185

LIST OF TABLES

4.1 Data for four test problems with exact solution. 76
4.2 Constants for the test problems with exact solution applied to test 1. 76
4.3 Constants for the test problems with exact solution applied to test 2. 78
4.4 Constants for the test problems with exact solution applied to test 3. 78

6.1 Initial states for the test problems with TVD Godunov–type methods. 107

8.1 Constants for the study of the sound wave propagation. 156

9.1 Parameters for the numerical study of wave propagation in compressible two–phase flow. 173

CHAPTER 1
INTRODUCTION

In this introductory chapter, the background and basic mathematical concepts will be described. These will be useful for the description and understanding of the mathematical models and numerical schemes considered. A more detailed discussion of the models is given in section 1.4. In section 1.5 a brief introduction to the numerical schemes is presented and an outline of the thesis is given in section 1.6.

1.1 Background

The field of Partial Differential Equations (PDE's) is a major link between mathematics and its applications. It began some three hundred years ago as a methodology for quantitative models of various physical phenomena. It has since developed into a major and central part of mathematics and it now has applications to other parts of mathematics, to modern science and to technology, including engineering, finance, medicine, and computer science. Partial differential equations and their solutions exhibit rich and complex structures. Unfortunately, closed analytical expressions for their solutions can be found only in very special circumstances and these are mostly of limited theoretical and practical interest. Thus, scientists and mathematicians have been naturally led to seeking techniques for the approximation of solutions. Indeed, the advent of computers has made the field more important than ever because it facilitates the computation of numerical solutions to equations which before could only be discussed qualitatively.

Focusing only on a particular field of PDE's such as fluid flow phenomena, one may develop a mathematical model as a starting point for a numerical method along with initial conditions, boundary conditions and closure relations. This requires a good understanding of the basic theory of PDE's and the processes they represent [2, 4, 17, 18, 27, 50, 53, 86, 94, 128, 148, 156, 157, 192, 204]. For instance, one

must be sure whether the boundary conditions are physically correct and that the problem to be solved is well–posed. When solving PDE's numerically one should be in a position of knowing what to expect from the numerical method. The physical and mathematical interpretation of the solution will be always an essential part of the computational work. Numerical solutions to PDE's observed early last century were unsuccessful due to the theoretical issues concerned with the stability of numerical methods and the practical reality of lacking fast computing machines and facilities. However, there had been significant success in closely related topics such as the governing PDE's for fluid flow. Such a success was not until the fundamental development on the theory of hyperbolic conservation laws was made in the existence and uniqueness of the solutions, well–posedness, stability and convergence of the numerical methods. Hyperbolic conservation laws (or quasi–linear hyperbolic systems in divergence form) govern a broad spectrum of physical phenomena such as compressible fluid dynamics and non–linear material science, etc. Such equations admit solutions that may exhibit various kinds of shocks and other non–linear waves (e.g. propagating phase boundaries and fluid interfaces) which play a dominant role in multiple areas of physics: astrophysics, cosmology, dynamics of (solid–solid) material interfaces, multi–phase (liquid–vapour) flows and combustion theory. In recent years, major progress has been made in both theoretical and the numerical aspects of the field [43, 57, 58, 75, 102], while the number of applications has increased.

Focusing in a typical engineering context, a substance exists in one of three physical phases or states (excluding the plasma state): a gas, a liquid, or a solid. Multiphase flow is the simultaneous flow of several phases. Two–phase flow is the simplest case of multiphase flow. The term two–component is sometimes used to describe flows in which the phases do not consist of the same chemical substance. For example, steam–water flows are two–phase flows with a single component, while air–water flows are two–component flows. Some two–component flows (liquid–liquid) consist of a single–phase but are often called two–phase flows in which the phases are identified as continuous or discontinuous components. Since the mathematics which describe two–phase or two component flows are identical, it does not matter which definitions are chosen. Two–phase flow research has application to a vast number of natural

and technological systems. A typical application to environmental problems involves predicting the effectiveness of natural flow phenomena for dispersing particulate pollutants to acceptable concentration levels. Many of these situations involve particulate releases from various local sources. The technological application of two–phase flow research involves a wide range of engineering systems, such as boiling water reactors, evaporators of refrigeration systems and evaporative and condensive heat exchangers in chemical and petroleum industries. There are also many important defence and military technology applications involving two–phase flow.

The ability to efficiently evaluate two–phase flow phenomena is needed to understand many processes of practical concern. For instance, nuclear reactor safety studies and pressure relief capabilities of many chemical reactors require this ability. In general, the ability to predict these phenomena depends on the availability of mathematical models and robust numerical methods. This is a very challenging task, as the numerical methods must combine robustness and accuracy and cover a wide domain of physical conditions, including the whole range of void fraction from single to mixture two–phase flow regime, and a wide range of pressure conditions. In two–phase flow problems, no procedure is universally accepted and several different approaches have been employed. On the other hand the degree of complexity of these equations makes the solution practically unachievable by numerical computations. Numerical methods [69, 70, 125] on which the current generation of two–phase flow codes used in the nuclear industry and in the thermal–hydraulic field are based are certainly robust but are known to suffer from excessive numerical dissipation. This in turn limits our ability to improve physical modeling and generally our understanding of compressible two–phase flow processes.

All current developments utilize a continuum approach which describes the field equations assuming the coexistence of the phases at every point in the flow field. The controversy lies in the derivation of these laws and in their final form. One approach to developing the two–phase flow equations makes use of the discrete nature of the separate phases through averaging techniques (over control volumes and time steps) [35, 84]. In this case the conservation equations are derived for averaged flow variables. Another approach to the derivation of the field equations utilizes contin-

uum mixture theory. In this case, conservation laws are determined for each phase which also account for the exchange of mass, momentum and energy between phases. In addition, conservation of mass, momentum and energy is required for the overall mixture [191] and this imposes constraints on the interaction between phases [197]. Comprehensive, formal mathematical theories of interpenetrating mixtures have been given in [13, 15, 44, 64, 65, 66, 67, 83, 90, 188, 189, 190, 200, 201]. Differences have been evidenced in the results among the workers in this area due in part to the originality and difficulty of the subject matter. Truesdell [191] has summarized existing mixture continuum theories and indicated that the results of [113, 114] and [40] are rigorously consistent with classical continuum mechanics theory. These generalized continuum mechanics studies are, for the most part, formal mathematical investigations that often result in equations with undetermined coefficients. In particular, the constitutive equations associated with these theories are quite complex and numerical values of most of the coefficients are not available. Application of the results of these theories is limited to special cases such as the mixture of linearly viscous, incompressible fluids as considered in [28]. Parts of the results of the above–mentioned studies have been employed in more practical areas of engineering fluid flow such as solid–fluid suspensions, combustion, dispersed single–component, two–phase flow, chemically reacting gas flows, the flow of blood in circulatory systems, fluidization and petroleum industry processes. Many of these areas have been discussed in [162] and [197].

A larger number of derivations of the balance equations are available for two–phase systems for engineering applications. The fact that each researcher is primarily interested in a particular flow regime has led to conflicts and differences in the resulting equations. A few derivations in the primary area of interest are listed here: fluidized beds [3, 117]; gas–particle mixtures [124]; liquid–phase dispersed, two–phase, single–component flows with interphase mass transfer [89]; gas–liquid flows [11, 30]; gas–solid [107, 162]. Previous work has shown that the resulting conservation equations are ill–posed, implying that the solutions to the initial–value problem can be unstable. In particular, characteristics associated with the partial differential equations have been shown to be imaginary and thus wave motion is non–physical.

It is clear from these various approaches that model closure centres on the issue of describing the final mathematical expressions when modeling two–phase flow. Two–phase flow models have in common that they must be supplied with closure relations. These are usually based on simple analytical models such as the relative motion between phases, correlations of experimental data, integral and differential analysis and a class of a powerful techniques based on universal phenomena that are independent of the flow regime, the analytical model or particular system. Typical of these methods are the various theories of wave motion and extremum techniques for obtaining the locus of the limiting behavior of a system. The resulting two–phase flow equations are a system of non–linear partial differential equations (PDE's) and they are expected to be hyperbolic in nature.

The difficulties associated with two–phase flow models can be significantly reduced by considering the following two approaches: The first approach makes use of homogeneous or diffusion models in which the relative velocity between phases is expressed by a constitutive equation in which one derives the simplified two–fluid model. The resulting model is a non–conservative two–fluid model and hyperbolicity of the model can be obtained under certain restrictions. The second approach formulates the two–phase problem in terms of extended thermodynamics which provides reliable results for modeling complicated media with rapidly varying and strongly inhomogeneous processes [116, 144, 146]. The resulting model is a hyperbolic conservative model which is a new model in understanding the mathematical character of the governing equations as well as studying the physical character of two–phase flow models. In fact it is important to note that the fundamental difference between the current two–fluid models and the hyperbolic conservative model is that the current models are based on ordinary thermodynamics which provides reliable results when the thermodynamic fields are smooth, in the sense that there are no steep gradients and rapid changes and thus the field equations are ill–posed. The hyperbolic conservative two–fluid model is based on extended thermodynamics as noted before and thus the field equations form a symmetric hyperbolic system. It guarantees well–posedness of initial–value problems.

Due to the complexity of two–phase flow models, we must look for numerical so-

lutions. There are as many different two–phase flow models as there are numerical methods for solving them. Each numerical method is usually dedicated to the specific problem considered and is therefore hard to generalize to other applications. More precisely, two–phase flows typically involve sharp gradient phenomena, for instance, sharp transitions between the different phases. One may use first–order finite difference methods for these models. But first–order methods suffer from a large amount of numerical diffusion. Thus, it is common to make explicit use of jump conditions, shock tracking techniques or grid refinement to minimize the numerical diffusion. On the other hand, classical second–order schemes typically produce oscillations around the discontinuities and have therefore not been used frequently.

Progress in numerical modeling of two–phase flow has been slower than for single–phase flow, for which the last two decades have seen the development and maturity of high–resolution numerical schemes such as shock–capturing methods and efficient unstructured mesh techniques. It was in the late eighties and beginning of the nineties that these advanced numerical methods were considered for the modeling of various types of two–phase flow, in sectors ranging from solid combustion [23, 131, 153, 155, 171] to nuclear thermal–hydraulics [10, 21, 150, 152, 164, 165, 183, 185] and to oil transport [46, 82, 140, 142]. In the past few years, a number of shock–capturing schemes have been constructed to solve systems of conservation laws. These methods are of first–order and are characterized by their degree of accuracy in the smooth regions of the solution, without presenting the spurious oscillations associated with the conventional second–order schemes in the presence of discontinuities. Advantages of shock–capturing are simplicity, generality and application to virtually any problem. The disadvantage is that the discontinuities are not completed as true discontinuities, as in the shock–fitting approach [111, 112]. Instead they are smeared or spread over a number of mesh points of computing cells where the amount of smearing depends on the particular shock–capturing methods being used. The name shock–capturing refers to numerical methods that have the ability to automatically deal with all flow features in the flow. A new class of shock–capturing methods are the high–resolution methods. These are oscillation–free near shock waves and retain high orders of accuracy in smooth parts of the flow. The shock–capturing may be classified into two

categories; upwind schemes and centred schemes. The fundamental work of Lax and Wendroff [97] was the first work considered in 1970s as the development period of high–resolution centred schemes. The idea behind this class of centred schemes is that shock–capturing can be accomplished by introducing artificial viscosity terms into the model considered. These terms introduce enough dissipation around the discontinuities to introduce oscillations. At the same time, these terms are negligible in smooth flow regions to maintain the accuracy of the solution. We refer to [81] for a comprehensive treatment of the family of Lax–Wendroff schemes.

An active area of research in the 1980s was the development of high–resolution upwind Godunov–type schemes. These modern shock–capturing schemes are more intelligent than artificial viscosity methods in the sense that they automatically introduce the correct amount of dissipation needed to reduce oscillations. Godunov methods are shock–capturing upwind methods and originate from the early works of Godunov in his PhD thesis which led to his paper of 1959 [59]. The work of Godunov generalised earlier work by Courant, Isaacson and Rees [26], who were the first to utilize this approach in their CIR (Courant, Isaacson and Rees) method, which is a first–order upwind scheme. The Godunov method regards the solution within each cell as a cell average instead of representing the solution in discrete form as pointwise values. This integral average is fundamentally linked with the conservative nature of the scheme which overcomes the disadvantage of traditional non–conservative methods. The interaction between two local constant states constitutes a Riemann problem and its solution can be calculated exactly or approximately for most hyperbolic systems. Then the solution to each local Riemann problem is used to calculate the inter–cell flux, which is used to update the solution to the next time level. A serious analysis of properties of conservation and monotonicity for convection problems by van Leer [193] made upwind schemes more and more popular, especially after the appearance of the concept of approximate Riemann solvers [123, 138].

In the 1990s, centred schemes received a considerable amount of renewed interest following the introduction of the Nessyahu–Tadmor Scheme [118] (see also [87, 88, 103]) which is a non–oscillatory van–Leer–type scheme constructed on the staggered Lax–Friedrichs scheme. It is a second order high–resolution centred method, a third order

extension of which using a non–oscillatory piecewise–quadratic reconstruction of point values from their given cell averages was utilized in [103]. The Lax–Friedrichs scheme is a first–order stable centred scheme which does not need, at least explicitly, Riemann solvers but suffers from excessive dissipation. A more recent first order centred approach is a First Order Centred (FORCE) scheme derived by Toro [176], which has less numerical viscosity than the Lax–Friedrich scheme.

In 2000, TVD versions of centred schemes were constructed by Toro and Billett [178] in order to obtain higher–order accurate numerical solutions. Toro and Billett abandoned the idea of imitating the Godunov first–order upwind method and put forward a new first–order centred method that is monotone. One of the extensions of the first–order centred scheme is the Slope LImiter Centred (SLIC) method. The SLIC scheme has been quite successful in providing accurate solutions to very complicated sets of equations, for which upwind methods are difficult or impossible to apply.

The development of the different shock–capturing schemes has been motivated from rather simple models such as the Euler equations where a detailed mathematical analysis is available. Hence, any shock–capturing scheme, such as any of the upwind Godunov–type schemes, requires mathematical properties. In addition, the analytical construction of an appropriate approximate Riemann solver is required. It is therefore not always obvious how these schemes should be extended to more complicated models like those found in two–phase problems. Here, a similar mathematical analysis is not always available and even the construction of an analytical solution can be a challenge.

1.2 Objectives of the Thesis

The main objectives are to investigate the mathematical analysis and modern shock–capturing schemes applied to non–linear partial differential equations with two–phase flow applications. The mathematical structure of two different two–phase flow models will be assessed. Schemes from both upwind and centred Godunov–type methods will be considered.

First, a simplified two–fluid model for an isentropic two–phase flow will be considered.

This model consists of a mixture density conservation equation, a mixture momentum conservation equation and an equation for the relative velocity between the two phases. We will develop an exact Riemann solver for the simplified two–fluid model along with several approximate Riemann solvers. The solutions will then be used locally to compute numerically the global solution of the general initial boundary value problem for the simplified two–fluid model.

The other model to be investigated is the hyperbolic conservative two–fluid model, describing one–dimensional compressible two–phase flow. Extended thermodynamics principles will be applied on the derivation of the three–dimensional governing equations and their corresponding closure relations. The field equations form a symmetric hyperbolic system of balance equations in conservative form. We will focus on a relatively modern shock–capturing method of centred type called the Slope LImiter Centred (SLIC) scheme. We emphasize that the SLIC scheme has never before been used to solve these models. The SLIC scheme is suitable for very complicated problems for which the Riemann problem solution is unavailable or is simply too complicated as in the hyperbolic conservative two–fluid model case.

Important subgoals for the investigations presented are

- To establish the hyperbolicity of the two–phase flow models.
- To give an overview of modern shock–capturing schemes that are flexible enough to be used for complex two–phase flow models.
- To compare the exact solution and numerical schemes of Godunov–type for two–phase flow models.
- To gain insight into the behaviour of two–fluid models through numerical tests.
- To assess whether modern shock–capturing schemes can become an alternative to existing solution techniques for the two–fluid models considered.

1.3 Basic Mathematical Concepts for Hyperbolic Partial Differential Equations

In this section we introduce the idea of the conservation laws through the mathematical formulation of a variety of systems. These systems are then used throughout the thesis to illustrate the applicability of the techniques that will be introduced. As we shall see in the later chapters, mathematical study of these systems is of interest since these are usually encountered in practice. The solution concepts for hyperbolic conservation laws are outlined and the general definition of the Riemann problem and of its expected solutions are discussed. The Riemann problem and its solution are the key elements in the development and application of modern shock–capturing methods. An excellent presentation of the mathematical theory of conservation laws can be found in [29, 78, 159].

1.3.1 Basic Definitions

A system of conservation laws in one space dimension is a set of partial differential equations of the form

$$\partial_t \mathbb{U} + \partial_x \mathbb{F}(\mathbb{U}) = \mathbb{S}(\mathbb{U}), \quad -\infty < x < \infty, \quad t \geq 0, \tag{1.1}$$

together with initial conditions

$$\mathbb{U}(x,0) = \mathbb{U}^{(0)}(x). \tag{1.2}$$

The symbol ∂_x stands for $\frac{\partial}{\partial x}$ and $\mathbb{U}$ and $\mathbb{F}$ are vector–valued functions

$$\mathbb{U} = \Big[u_1(x,t), \ldots, u_n(x,t)\Big]^T \equiv \mathbb{U}(x,t), \tag{1.3}$$

$$\mathbb{F}(\mathbb{U}) = \Big[f_1(\mathbb{U}), \ldots, f_n(\mathbb{U})\Big]^T, \tag{1.4}$$

$\mathbb{S} = \mathbb{S}(\mathbb{U})$ is the vector containing possible source terms

$$\mathbb{S}(\mathbb{U}) = \Big[\mathbb{S}_1(\mathbb{U}), \ldots, \mathbb{S}_{\mathfrak{n}}(\mathbb{U})\Big]^T, \tag{1.5}$$

and $\mathbb{U}^{(0)}(x)$ is vector for the initial conditions.

The conservation law (1.1) may also be written in quasi–linear form

$$\partial_t \mathbb{U} + \mathbb{A}(\mathbb{U})\partial_x \mathbb{U} = \mathbb{S}(\mathbb{U}), \tag{1.6}$$

where the coefficient matrix $\mathbb{A}(\mathbb{U})$ is the Jacobian matrix

$$\mathbb{A}(\mathbb{U}) = \frac{\partial \mathbb{F}}{\partial \mathbb{U}} = \left[\frac{\partial f_k(u_1, \ldots, u_{\mathfrak{n}})}{\partial u_l}\right]_{k,l}, \quad k, l = 1, \ldots, \mathfrak{n}. \tag{1.7}$$

The eigenvalues $\lambda_{\mathfrak{j}}$, $\mathfrak{j} = 1, \ldots, \mathfrak{n}$ of the Jacobian matrix $\mathbb{A}(\mathbb{U})$ are the solutions of the characteristic polynomial

$$\det\Big[\mathbb{A}(\mathbb{U}) - \lambda_{\mathfrak{j}}(\mathbb{U})I\Big] = 0, \tag{1.8}$$

and physically they represent the speeds of propagation of information.

Now for every $\mathbb{U} \in \mathbb{R}^{\mathfrak{n}}$ and $\mathbb{F} : \mathbb{R}^{\mathfrak{n}} \mapsto \mathbb{R}$ there exists a smooth basis $(\mathcal{K}^1(\mathbb{U}), \ldots, \mathcal{K}^{\mathfrak{j}}(\mathbb{U}))$ of $\mathbb{R}^{\mathfrak{n}}$ made with eigenvectors of $\mathbb{A}(\mathbb{U})$: $\exists\ \lambda_{\mathfrak{j}}(\mathbb{U}) \in \mathbb{R}$ such that $\mathbb{A}(\mathbb{U})\mathcal{K}^{\mathfrak{j}}(\mathbb{U})) = \lambda_{\mathfrak{j}}\mathcal{K}^{\mathfrak{j}}(\mathbb{U}))$. It is then possible to construct $(l^1(\mathbb{U}), \ldots, l^{\mathfrak{j}}(\mathbb{U}))$ such that $\mathbb{A}^T(\mathbb{U})l^{\mathfrak{j}}(\mathbb{U}) = \lambda_{\mathfrak{j}} l^{\mathfrak{j}}(\mathbb{U}))$ and $l^{\mathfrak{j}} \cdot \mathcal{K}^{\mathfrak{J}}(\mathbb{U}) = \delta_{\mathfrak{j},\mathfrak{J}}$. Thus system (1.6) is classified as hyperbolic if $\mathbb{A}(\mathbb{U})$ has real eigenvalues and a corresponding set of linearly independent eigenvectors. In addition, the system is said to be strictly hyperbolic if the eigenvalues are all distinct. It is sometimes convenient to formulate a system (1.1) in quasi–linear form as a function of primitive variables $\mathbb{W}$. This can make the mathematical analysis easier since the structure of the matrices can be less complicated. The primitive variables are often those observed and measured experimentally such as pressure, velocity, temperature, density, void fraction and the relative velocity. Therefore, these are also often referred to as physical variables. If we define the variable transformation between

conserved and primitive variables by $\mathbb{B}(\mathbb{W}) = \frac{\partial \mathbb{U}}{\partial \mathbb{W}}$, then system (1.1) can be written as

$$\mathbb{B}(\mathbb{W})\partial_t \mathbb{W} + \mathbb{A}(\mathbb{W})\mathbb{B}(\mathbb{W})\partial_x \mathbb{W} = \mathbb{S}(\mathbb{W}), \tag{1.9}$$

or

$$\partial_t \mathbb{W} + \mathbb{C}(\mathbb{W})\partial_x \mathbb{W} = \bar{\mathbb{S}}(\mathbb{W}), \tag{1.10}$$

where $\mathbb{C}(\mathbb{W}) = \mathbb{B}^{-1}(\mathbb{W})\mathbb{A}(\mathbb{W})\mathbb{B}(\mathbb{W})$ and $\bar{\mathbb{S}}(\mathbb{W}) = \mathbb{B}^{-1}(\mathbb{W})\mathbb{S}(\mathbb{W})$. In addition, the eigenvalues are invariant with respect to the choice of variables and thus $\lambda_j(\mathbb{U}) = \bar{\lambda}_j(\mathbb{W})$. The eigenvalues determine the characteristics in the (x, t) plane and given by

$$\frac{dx}{dt} = \bar{\lambda}_j(\mathbb{W}), \;\; x(0) = x_0, \;\; j = 1, \ldots, n. \tag{1.11}$$

In general, these will be curved for non–linear systems and straight lines for linear systems.

1.3.2 The Riemann Problem

In conservation law theory and computation, the Riemann problem is the building block for solving initial and boundary value problems. The Riemann problem was originally formulated, and solved, in the context of isentropic gas dynamics in a path-breaking paper of Riemann [151]. Early research on the Riemann problem for the equations of isentropic or adiabatic gas dynamics [27] was stimulated by the need to analyze wave interactions and shock tube experiments. The distillation of this work led to the solution of the Riemann problem with weak waves for general genuinely non–linear strictly hyperbolic systems of conservation laws [96]. Detailed expositions and references can be found in [16, 29, 73, 159, 161].

Non–linear conservation laws (1.1) can produce discontinuous solutions even for smooth initial data. When $\mathbb{U}(x, t)$ or $\mathbb{U}^{(0)}(x)$ are continuously differentiable, the differential form (1.1) can be derived from the integral form of conservation laws. For a control

volume V chosen on the x–t plane as $V = [x_1, x_2] \times [t_1, t_2]$, the integral form for conservation laws in one space dimension is

$$\partial_t \int_{x_1}^{x_2} \mathbb{U}(x,t)dx = \mathbb{F}(\mathbb{U}(x_1,t)) - \mathbb{F}(\mathbb{U}(x_2,t)), \tag{1.12}$$

where $\mathbb{U}(x,t)$ and $\mathbb{U}^{(0)}(x)$ are smooth.
If $\mathbb{U}(x,t)$ or $\mathbb{U}(x,0)$ is non–differentiable, we have to consider the integral form of conservation laws to obtain a weak solution in the classical sense. The integral form is more fundamentally physical than the differential form. It thus makes perfect sense to deal with and to define a generalised solution of (1.1) by introducing the weak solution concept. The weak solution is often not unique, and so an additional criterion has to be imposed to identify which weak solution is the physically correct vanishing dissipative solution (e.g. the viscosity solution). One would like to avoid working with the dissipative equation directly, but it turns out that there are other conditions one can impose in weak solutions that are easier to check and also pick out the correct solution. These are usually called entropy conditions to determine the physically relevant solution. The solution is also called the entropy weak solution.
The homogeneous conservation laws together with piecewise constant initial data having a single discontinuity is known as the Riemann problem and takes the following form

$$\partial_t \mathbb{U} + \partial_x \mathbb{F}(\mathbb{U}) = 0, \tag{1.13}$$

with the Riemann data

$$\mathbb{U}(x,0) = \begin{cases} \mathbb{U}_{\mathcal{L}} & \text{for} \quad x < 0, \\ \mathbb{U}_{\mathcal{R}} & \text{for} \quad x > 0, \end{cases} \tag{1.14}$$

and gives rise to the self–similar solution $\mathbb{U}(x,t) = \mathbb{U}(\frac{x}{t})$.
For a scalar non- linear case where $\lambda_1(\mathbb{U}) = \mathbb{F}'(\mathbb{U})$, and $\mathbb{F}(\mathbb{U})$ is strictly convex, the weak solution to this problem will be either a shock wave or a continuous rarefac-

tion wave. Generally, bounded, piecewise smooth weak solutions to a system of conservation laws satisfy the Rankine–Hugoniot condition at discontinuities. The Rankine–Hugoniot condition is

$$S[\mathbb{U}] = [\mathbb{F}], \tag{1.15}$$

where $[\cdot]$ represents the jump in a quantity across a shock of speed S, giving a relation between the speed S of the discontinuity and the constant states $\mathbb{U}_{\mathcal{L}}$ and $\mathbb{U}_{\mathcal{R}}$ on each side of the discontinuity. An additional condition, entropy condition, is required to pick out the physical correct weak solution. One such condition is the Lax entropy condition, which states that if $\mathbb{F}(\mathbb{U})$ is convex, a shock wave would satisfy the entropy condition

$$\lambda_1(\mathbb{U}_{\mathcal{L}}) > S > \lambda_1(\mathbb{U}_{\mathcal{R}}). \tag{1.16}$$

More general weak solutions for (1.13) are the non–linear wave solutions briefly described below:

- **Shock Wave.** If $\lambda_1(\mathbb{U}_{\mathcal{L}}) > \lambda_1(\mathbb{U}_{\mathcal{R}})$, the entropy satisfying weak solution is a shock wave given by

$$\mathbb{U}(x,t) = \begin{cases} \mathbb{U}_{\mathcal{L}} & \text{for} \quad \frac{x}{t} < S, \\ \mathbb{U}_{\mathcal{R}} & \text{for} \quad \frac{x}{t} \geq S, \end{cases} \tag{1.17}$$

  where S is the shock speed given by the Rankine–Hugoniot condition (1.15).

- **Rarefaction Wave.** If $\lambda_1(\mathbb{U}_{\mathcal{L}}) < \lambda_1(\mathbb{U}_{\mathcal{R}})$, then the correct entropy solution is a rarefaction wave given by

$$\mathbb{U}(x,t) = \begin{cases} \mathbb{U}_{\mathcal{L}} & \text{for} \quad \lambda_1(\mathbb{U}_{\mathcal{L}}) > \frac{x}{t}, \\ \mathbb{U}(\frac{x}{t}) & \text{for} \quad \lambda_1(\mathbb{U}_{\mathcal{L}}) \leq \frac{x}{t} \leq \lambda_1(\mathbb{U}_{\mathcal{R}}), \\ \mathbb{U}_{\mathcal{R}} & \text{for} \quad \lambda_1(\mathbb{U}_{\mathcal{R}}) \leq \frac{x}{t}, \end{cases} \tag{1.18}$$

  where $\mathbb{U}(\frac{x}{t})$ is the solution of $\mathbb{F}'(\mathbb{U}(\frac{x}{t})) = \frac{x}{t}$.

These elementary wave solutions also will be the key elements to describe the structure of the solution of the Riemann problem for non–linear systems.
For the non–linear $n \times n$ system of conservation laws with eigenvalues $\lambda_j(\mathbb{U}), j = 1, \ldots, n$, the jth characteristic field is said to be genuinely non–linear if

$$\nabla\lambda_j(\mathbb{U}) \cdot \mathcal{K}^j(\mathbb{U}) \neq 0, \ \forall \mathbb{U} \in \mathbb{R}^n.$$

Otherwise if

$$\nabla\lambda_j(\mathbb{U}) \cdot \mathcal{K}^j(\mathbb{U}) = 0, \ \forall \mathbb{U} \in \mathbb{R}^n,$$

then the field is said to be linearly degenerate.
The solution of the Riemann problem (1.13) is composed of $n + 1$ constant states separated by n waves corresponding to the different characteristic fields. The structure of the solution in the x–t plane is depicted in figure 1.1. If the jth characteristic field

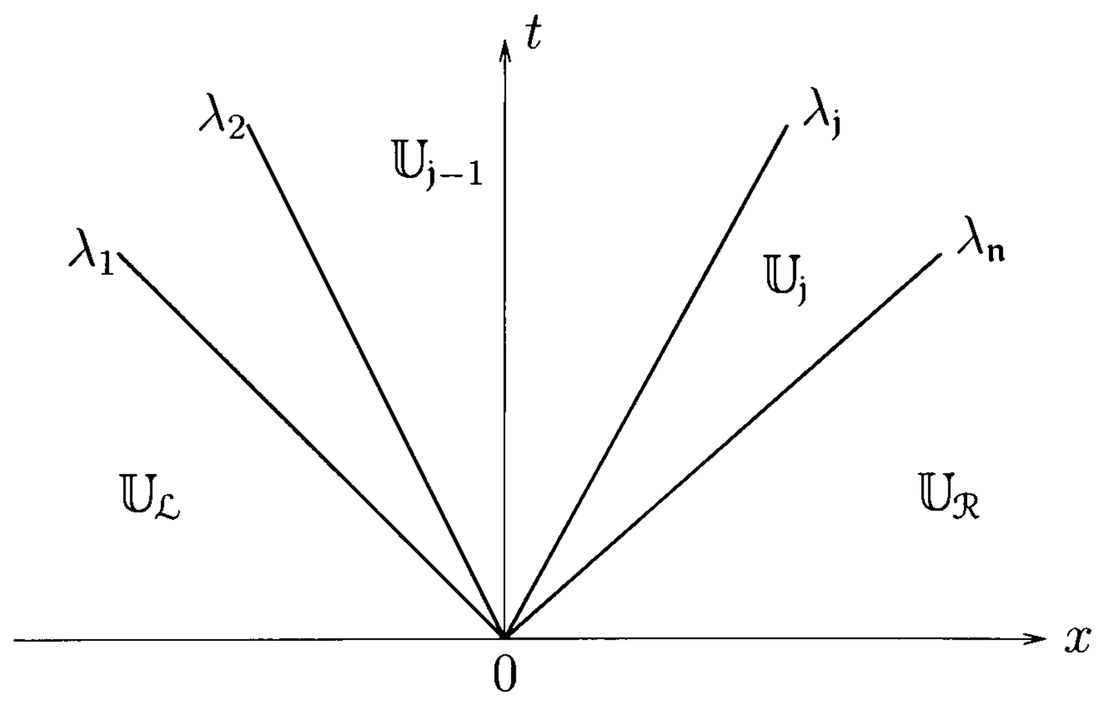

Figure 1.1: Structure of the solution of the Riemann problem for a system of conservation laws.

is genuinely non–linear, then the corresponding elementary wave solution connecting $\mathbb{U}_{j-1}$ and $\mathbb{U}_j$ will be either a shock or a rarefaction wave. If the jth characteristic field is linearly degenerate, then the possible weak solution is a contact discontinuity. In this case, the corresponding eigenvalue $\lambda_j(\mathbb{U})$ is constant across the wave and the j–characteristics are parallel to the discontinuity on each side. Moreover, to identify the correct physical solution, the Lax entropy condition (1.16) is generalised to systems.

If the jth field is a genuinely non–linear field then, a jth field is a j–shock or a contact discontinuity which are admissible only if

$$\lambda_j(\mathbb{U}_{j-1}) \geq S_j \geq \lambda_j(\mathbb{U}_j). \tag{1.19}$$

The general solution of the Riemann problem is now obtained by combining the possible types of waves and the corresponding constant states.
Finally, since the analytical solution of the Riemann problem for non–linear hyperbolic system of equations has limited application, we will present the solution of the Riemann problem for a linear system of equations. As the eigenvalues and the corresponding eigenvectors are in this case constant, the different characteristic fields are linearly degenerate. The solution is composed of n waves of speed λ_j and each wave carries a discontinuity. We expand the data $\mathbb{U}_{\mathcal{L}}$ (constant left state) and $\mathbb{U}_{\mathcal{R}}$ (constant right state) as linear combinations of the set $\mathcal{K}^{(1)}, \ldots, \mathcal{K}^{(j)}$, that is

$$\mathbb{U}_{\mathcal{L}} = \sum_{j=1}^{n} \aleph_j \mathcal{K}^j, \quad \mathbb{U}_{\mathcal{R}} = \sum_{j=1}^{n} \wp_j \mathcal{K}^j, \tag{1.20}$$

with constant coefficients $\aleph_j, \wp_j$, for $j = 1, \ldots, n$. Taking the difference between the left and right states $\mathbb{U}_{\mathcal{L}}$ and $\mathbb{U}_{\mathcal{R}}$

$$(\Delta \mathbb{U})_j = \sum_{j=1}^{n} \ell_j \mathcal{K}^j, \tag{1.21}$$

where

$$\ell_j = \aleph_j - \wp_j, \tag{1.22}$$

is the strength of wave j, we can write the final solution of the linear Riemann problem as

$$\mathbb{U}(x,t) = \mathbb{U}_{\mathcal{L}} + \sum_{\bar{\ell}>0} \aleph_j \mathcal{K}^j = \mathbb{U}_{\mathcal{R}} - \sum_{\bar{\ell}\leq 0} \wp_j \mathcal{K}^j,$$

where the integer $\bar{\ell} = x - \lambda_j t$.

1.4 Two–Phase Flow Models

The purpose of this section is to present the origin of the two–phase flow models and point out different models for two–phase flow. Two–phase flow modeling has undergone intensive development (see e.g. [5, 31, 48, 61, 62, 120, 122, 134, 168, 196, 198]). However, there are still no clear theoretical bases for deriving the final mathematical expressions when modeling two–phase flow models. According to the mathematical expressions, various gas–liquid two–phase flow models which have been proposed in the literature can roughly be classified into the following four different types [198]

- **Structural continuum fluid models**, formulated directly according to the conservation principles and expressed in terms of integro–differential balance equations by treating a two–phase mixture as a set of subregions of the individual phases.

- **Averaged continuum fluid models**, derived from structural continuum fluid models and expressed in terms of partial differential balance equations by treating a two–phase mixture as one or two averaged continua. The widely used homogeneous equilibrium models, the simplified two–fluid model, the drift flux model and the two–fluid models are typical examples.

- **Lumped–parameter fluid models**, derived from structural continuum fluid models or often averaged continuum fluid models. A lumped–parameter model is characterized by the use of globally averaged fluid properties for each phase or for the two–phase mixture in a control volume and is finally expressed in terms of ordinary differential equations.

- **Correlation models**, formulated in terms of algebraic or transcendental functions. They are often constructed according to experimental data or some ideal models under very special conditions.

The widely used two–fluid models are typical examples of the second approach. Early two–fluid models did not result in a system of hyperbolic equations (the eigenvalues can be complex–valued) [168, 171]. Some researchers introduce formulations for coupling the two separated momentum equations, including space and time derivatives of physical quantities such as virtual mass and interfacial pressure (see [1, 7, 12, 36, 37, 38, 42, 56, 93, 132, 133, 134, 166, 167, 169, 182]). Thus, the formulation for the basic two–fluid equations and the appropriate closure relations have been discussed in the past and, up to now, there does not seem to exist a commonly agreed approach. Two different two–phase flow models are considered in this thesis. In the first model we consider a simplified two–fluid model which is derived from the more basic three equation two–fluid model. The second model is the hyperbolic conservative two–fluid model for which a one–dimensional model describing a gas–liquid two–phase flow will be presented.

1.4.1 The Simplified Two–Fluid Model

For modeling two–phase flows, several sets of equations ranging in complexity from the homogeneous equilibrium model to two–fluid models involving unequal pressure for each phase have been used [84, 168]. The usual way to establish physical models for two–phase flows is to start with a single continuous description for each phase given by the Navier–Stokes equations. The presence of topologically complicated interfaces suggests the need for a multi–field model of the flow. Various averaging techniques have been used to obtain practical and computable two–fluid models involving mass, momentum and energy balance equations for each of the phases [84]. The averaging procedure leads to an ill–posed initial–value problem and differential quantities such as added mass and interfacial pressure are then included to make the models hyperbolic [168]. The resulting model is a non–conservative hyperbolic one, consisting in mass, momentum and energy balance equations for each phase. In addition to these mathematical difficulties, there are some complications due to uncertainties in specifying interfacial interaction terms between phases.

We now present one version of the two–fluid model equations. The appropriate,

one–dimensional governing equations which account for the conservation of mass, momentum and energy (see e.g. [168]) are, respectively,

$$\partial_t(\alpha_{\mathfrak{i}}\rho_{\mathfrak{i}}) + \partial_x(\alpha_{\mathfrak{i}}\rho_{\mathfrak{i}}u_{\mathfrak{i}}) = \Theta_{\mathfrak{i}}, \tag{1.23}$$

$$\partial_t(\alpha_{\mathfrak{i}}\rho_{\mathfrak{i}}u_{\mathfrak{i}}) + \partial_x(\alpha_{\mathfrak{i}}\rho_{\mathfrak{i}}u_{\mathfrak{i}}^2) + \alpha_{\mathfrak{i}}\partial_x\mathcal{P} = \Upsilon_{\mathfrak{i}}, \tag{1.24}$$

$$\partial_t(\alpha_{\mathfrak{i}}\rho_{\mathfrak{i}}(\mathfrak{e}_{\mathfrak{i}} + \frac{u_{\mathfrak{i}}^2}{2})) + \mathcal{P}\,\partial_t\alpha_{\mathfrak{i}} + \partial_x(\alpha_{\mathfrak{i}}\rho_{\mathfrak{i}}u_{\mathfrak{i}}\,(\mathfrak{h}_{\mathfrak{i}} + \frac{u_{\mathfrak{i}}^2}{2})) = \Omega_{\mathfrak{i}}. \tag{1.25}$$

Let us describe the physical meaning of each variable, the subscript $\mathfrak{i} = 1, 2$ refers to phase 1 and phase 2 respectively. t is the time, x is the flow direction (space coordinate), $\mathcal{P}$ is the thermodynamic pressure, $\alpha_{\mathfrak{i}}$ is the volume fraction of the phase $\mathfrak{i}$, $\rho_{\mathfrak{i}}$ is the density of phase $\mathfrak{i}$, $u_{\mathfrak{i}}$ denotes the velocity of phase $\mathfrak{i}$. Denoting by $\mathfrak{e}_{\mathfrak{i}}$ the specific internal energy of phase $\mathfrak{i}$, we have set $\mathcal{E}_{\mathfrak{i}} = \mathfrak{e}_{\mathfrak{i}} + \frac{1}{2}|u|^2$ as the total specific energy of phase $\mathfrak{i}$, $H_{\mathfrak{i}} = \mathcal{E}_{\mathfrak{i}} + \frac{\mathcal{P}}{\rho_{\mathfrak{i}}}$ as the total enthalpy of phase $\mathfrak{i}$ and $\mathfrak{h}_{\mathfrak{i}} \equiv \mathfrak{e}_{\mathfrak{i}} + \frac{\mathcal{P}}{\rho_{\mathfrak{i}}}$ as the specific enthalapy of phase $\mathfrak{i}$. Furthermore, the right–hand side of the equations (1.23)–(1.25) involve physical and chemical effects expressed in terms of the variables as well as some derivative terms. We have the relation

$$\alpha_1 + \alpha_2 = 1, \tag{1.26}$$

and we make the "single pressure" hypothesis

$$\mathcal{P}_1 \equiv \mathcal{P}_2, \tag{1.27}$$

which is often blamed for the controversial type of the equation. In fact the assumption that the two fluids share the same pressure, makes the two–fluid model ill–posed (in terms of the initial–value problem).

The most common numerical methods to solve these equations are methods based on staggered grids and donor–cell differencing [101, 187]. These methods, now almost universal in two–fluid codes developed for the nuclear industry like CATHARE [6], RELAP [135] and TRAC [186], introduce a large amount of numerical diffusion. However, the numerical diffusion is in some way necessary to stabilize the behaviour of

the mathematical model (see [129] for a more detailed discussion). Simulators like PeTra [95], PLAC [14], OLGA [9], TUFFP [109, 110] are also based on the two–fluid modeling approach. Moreover, it is shown in [136] that high frequency oscillations appear with a large number of cells. For numerical methods on non–staggered grids the Lax–Wendroff scheme was applied to two–fluid models in [134]. In [137], a split matrix method has been presented for the numerical solution of two–phase flow equations. This method solves the flow equations in their characteristic form and hence is not rigorously conservative. More accurate methods based on approximate Riemann solvers require modifications within the equations in order to obtain a hyperbolic system.

In recent years, several shock–capturing schemes have been used to solve the two–fluid model (see [25, 92, 106, 169, 170, 181, 182, 183, 184, 185]). Since these methods require that the model considered is hyperbolic, this has increased the need for establishing the hyperbolicity of the two–fluid model. Another interesting feature is the non–conservative form of the model equations which puts extra requirements on the shock–capturing schemes. The two–fluid model is known to be challenging from a modeling point of view. Several closure laws have to be supplied and especially the source terms relating to interphase of mass, momentum and energy are difficult to model. The two–fluid model has been widely used within the nuclear industry for describing steam–water flow and the first two–phase flow simulators were developed for these purposes.

The difficulties associated with the two–fluid model are greatly reduced by using homogeneous or diffusion models in which the velocity between the two–phase mixture is given by the mixture momentum equation and the relative velocity between phases is expressed by a constitutive equation. If we limit ourselves to considering isentropic flow no energy balance is needed and, assuming that there is no viscosity effect and no mass transfer between phases, then the simplified two–fluid model consisting of the mass and momentum conservation equations takes the following form

$$\partial_t(\alpha_i\rho_i) + \partial_x(\alpha_i\rho_i u_i) = 0, \tag{1.28}$$

$$\partial_t(\alpha_i\rho_i u_i) + \partial_x(\alpha_i\rho_i u_i^2) + \alpha_i\partial_x\mathcal{P} = 0. \tag{1.29}$$

This system is naturally written in a non–conservative form due to the presence of non–conservative products $\alpha_i \partial_x \mathcal{P}$ in the momentum equation. In this case distribution theory is not suitable to define weak solutions. Several approaches have been proposed to define weak solutions to non–conservative systems [22, 98]. Moreover, we need to add some information to a non–conservative system in order to obtain a complete definition of weak solutions [153]. To close the above system, several physical closure laws must be given which involve mass vapour concentration, equation of state for the two–phase flow, mixture relations and properties of the model. In addition, an equation is supplied which relates the velocities of the two phases at any point, the relative velocity balance equation or the slip relation. The slip relation has been described and discussed in [9, 19, 51, 210]. In general cases many researchers do not consider the slip relation in algebraic form but make use of it from empirical data given in tabular form. One will then obtain the drift flux model [49, 55, 85, 141] which is widely used in computer codes like RF–Kick [41], SIDEKICK [119, 199], TACITE [74, 126, 127] within the petroleum industry. In this thesis we will consider it as a hydrodynamic closure relating the two phase velocities by a kinetic constitutive equation such as

$$u_r = u_2 - u_1. \tag{1.30}$$

Thus the simplified two–fluid model for an isentropic two–phase flow can be written as a 3×3 system of conservation laws as

$$\partial_t \mathbb{U} + \partial_x \mathbb{F}(\mathbb{U}) = 0, \tag{1.31}$$

where $\mathbb{U}$ is the vector of conservative variables

$$\mathbb{U} = \begin{pmatrix} \rho \\ \rho u \\ u_r \end{pmatrix}, \tag{1.32}$$

and the flux function is given by

$$\mathbb{F}(\mathbb{U}) = \begin{pmatrix} \rho u \\ \rho u^2 + \rho\, c\, (1-c)\, u_r^2 + \mathcal{P} \\ u u_r + \frac{1-2c}{2}\, u_r^2 + \psi(\mathcal{P}) \end{pmatrix}. \tag{1.33}$$

The simplified two–fluid model (1.31) is analysed extensively in the next chapter. The model is shown to be hyperbolic (using perturbation methods) in a physically reasonable region of parameters and three distinct and real eigenvalues are obtained under the assumption that the relative velocity between the two phases is much lower than the speed of sound, a_m, of the two–phase mixture, that is

$$\eta = \frac{u_r}{a_m} \ll 1, \tag{1.34}$$

which is the case in many physically interesting mixtures such as steam and water. The simplified two–fluid model will be useful to study the Riemann problem for the system and develop an exact Riemann solver for the model. In addition, the model allows the application of Godunov–type methods of upwind and centred type for solving the model numerically.

1.4.2 The Hyperbolic Conservative Two–Fluid Model

The next model we consider in this thesis is the hyperbolic conservative two–fluid model. Models of this type are of great theoretical and practical interest in numerous applications. The difficulties associated with two–fluid models can be significantly reduced by formulating two–phase problems in terms of extended thermodynamics. Extended thermodynamics extends the number of fields beyond the ones of ordinary thermodynamics which are the densities of mass, momentum and energy and typical extensions are the fluxes of momentum and energy. Essential ingredients of the extended theory are [116]

- basic equations are of balance type

hence the possibility of weak solutions and shocks

- constitutive equations that are local in space and time
  hence quasi–linear first–order field equations

- entropy inequality with a concave entropy density
  hence symmetric hyperbolic field equations.

In all thermodynamic theories the velocity belongs to the basic fields which play a prominent role among thermodynamic variables because the constitutive quantities depend on it in a specific manner. For general background on extended thermodynamics we refer to [24, 39, 47, 113, 115, 130, 163] and particularly to [116].
The second model proposed in this thesis is developed by using the principles of extended thermodynamics. The resulting model is a conservative first order quasi–linear symmetric hyperbolic system of field equations and allows discontinuous solutions [52, 121, 143, 146, 158]. Symmetric hyperbolicity is a desirable feature mathematically because it ensures well–posedness of Cauchy problems, that is existence, uniqueness and continuous dependence of the solutions on the data [116]. The present model is a new model, at least in understanding the mathematical character of the governing equations as well as in studying the physical character of two–phase flow models. For a gas–liquid mixture two–phase flow the closed system of balance equations consists of conservation laws of mass, momentum and energy for the mixture, a balance law for the volume concentration of gas phase, a balance law for mass concentration of the gas phase and a balance law for the relative velocity between the two phases. The one–dimensional hyperbolic conservative model then takes the following form

$$\partial_t \mathbb{U} + \partial_x \mathbb{F}(\mathbb{U}) = \mathbb{S}(\mathbb{U}), \quad -\infty < x < \infty, \quad t > 0, \tag{1.35}$$

where the components of $\mathbb{U}$ are the conserved quantities

$$\mathbb{U} = \begin{pmatrix} \rho \\ \rho\alpha \\ \rho u \\ \rho c \\ u_r \\ \rho(\mathcal{E} + \frac{u^2}{2}) \end{pmatrix}, \tag{1.36}$$

and the flux vector $\mathbb{F}(\mathbb{U})$ is

$$\mathbb{F}(\mathbb{U}) = \begin{pmatrix} \rho u \\ \rho u\alpha \\ \rho u^2 + \mathcal{P} + \rho u_r \mathcal{E}_{u_r} \\ \rho u c + \rho \mathcal{E}_{u_r} \\ u u_r + \mathcal{E}_c \\ \rho u(\mathcal{E} + \frac{u^2}{2}) + \mathcal{P}u + \rho u u_r \mathcal{E}_{u_r} + \rho \mathcal{E}_c \mathcal{E}_{u_r} \end{pmatrix}, \tag{1.37}$$

with the source terms

$$\mathbb{S}(\mathbb{U}) = \Big[0, \phi, 0, 0, \pi, 0\Big]^T. \tag{1.38}$$

The model is presented in detail in chapter 7, with an extensive analysis. It is shown to be hyperbolic with four non–linear sonic waves and two contact waves. Further the characteristic fields corresponding to the acoustic waves were shown to be genuinely non–linear while the last two are linearly degenerate. A characteristic picture of the hyperbolic nature of the model is shown in figure 1.2. In general, the hyperbolic conservative two–fluid model has a very complex structure. It is therefore very difficult to develop any analytical calculations or solve the Riemann problem exactly. This implies using modern numerical schemes such as shock–capturing methods of centred type such as the TVD SLIC scheme which solve these problems in a simple way and with good accuracy. The SLIC scheme we use is flexible enough to handle

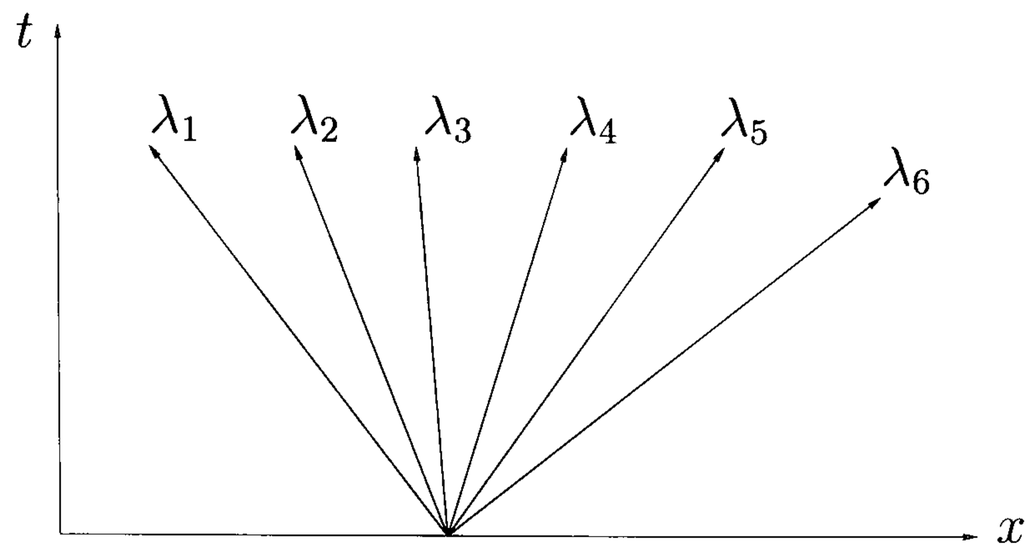

Figure 1.2: Hyperbolic nature of the hyperbolic conservative two–fluid model.

the model without relying on mathematical results obtained analytically. Generally, centred methods are methods that do not require the explicit solution of the Riemann problem, as they are not biased by the wave propagation direction. This feature is especially used for typical problems arising in two–phase flow modeling, where we often have to complete the equation model by extra equations. Thus the SLIC scheme will give more insight into the model and will resolve both rarefaction waves and shock waves.

1.5 Numerical Schemes for Conservation Laws

In this section we give a brief introduction on numerical schemes for partial differential equations of hyperbolic type, such as the two–phase flow equations. We limit ourselves to schemes which are robust and flexible enough to handle systems of conservation laws arising in two–phase flow models. These methods omit the analytical construction of an approximate Riemann solver and all calculations can be performed numerically if necessary. We will start with a brief discussion of some theoretical aspects related to numerical schemes for conservation laws and then continue with a description of the numerical schemes.

In this context we are mainly concerned with solving non–linear hyperbolic systems of conservation laws and we will consider the initial–value problem for the general

hyperbolic $\mathfrak{n} \times \mathfrak{n}$ system of conservation laws

$$\left.\begin{array}{ll} \text{PDE's}: & \partial_t \mathbb{U} + \partial_x \mathbb{F}(\mathbb{U}) = 0, \\ \text{IC's} & : \mathbb{U}(x,0) = \mathbb{U}^{(0)}(x), \\ \text{BC's} & : \mathbb{U}(0,t) = \mathbb{U}_l(t),\ \mathbb{U}(L,t) = \mathbb{U}_r(t), \end{array}\right\} \tag{1.39}$$

where the unknowns $\mathbb{U}$ depend on space x and a time–like variable t. $\mathbb{U}$ are the dependent variables, x and t are the independent variables expressed via the notation

$$\mathbb{U} = \mathbb{U}(x,t) = \Big[u_1(x,t), \ldots, u_{\mathfrak{n}}(x,t)\Big]^T, \tag{1.40}$$

and $\mathbb{F} = \mathbb{F}(\mathbb{U})$ is the vector of fluxes and each of its components is a function of $\mathbb{U}$

$$\mathbb{F}(\mathbb{U}) = \Big[f_1(\mathbb{U}), \ldots, f_{\mathfrak{n}}(\mathbb{U})\Big]^T. \tag{1.41}$$

$\mathbb{U}^{(0)}(x)$ is the initial data at time $t = 0$; $[0, L]$ is the spatial domain and boundary conditions are assumed to be represented by boundary functions $\mathbb{U}_l(t)$ and $\mathbb{U}_r(t)$.
To admit discontinuous solutions we adopt the use of the integral forms of conservation laws (1.39) such as

$$\int_{x_1}^{x_2} \mathbb{U}(x,t_2)dx = \int_{x_1}^{x_2} \mathbb{U}(x,t_1)dx + \int_{t_1}^{t_2} \mathbb{F}(\mathbb{U}(x_1,t))dt - \int_{t_1}^{t_2} \mathbb{F}(\mathbb{U}(x_2,t))dt, \tag{1.42}$$

for any control volume $[x_1, x_2] \times [t_1, t_2]$ in the domain of interest.
We discretise the spatial domain $[0, L]$ into M computing cells or finite volumes $I_i = [x_{i-\frac{1}{2}}, x_{i+\frac{1}{2}}]$ of size $\Delta x = x_{i+\frac{1}{2}} - x_{i-\frac{1}{2}}$ with $i = 1, \ldots, M$. The solution $\mathbb{U}(x,t)$ of (1.39) at the discrete location (x_i, t^n) is denoted by

$$\mathbb{U}_i^n \equiv \mathbb{U}(x_i, t^n). \tag{1.43}$$

The first methods introduced for solving conservation laws were the first–order Lax–Friedrichs and the second–order Lax–Wendroff schemes [96, 97]. The first order schemes typically produce results that are very smeared in regions near disconti-

nuities. The second–order schemes generate oscillations in these regions. Well developed theoretical concepts for numerical methods considered linear problems. If we can show that the numerical method is consistent with the mathematical model and stable, then the Lax Equivalence theorem ensures that the numerical method converges to the exact solution of (1.39). We also know that the domain of dependence of the numerical scheme should include the domain of the mathematical model. This condition is known as the CFL condition which is in general a necessary condition for stability (see [76, 77, 80, 160]).

When we attempt to solve non–linear conservation laws numerically we run into additional difficulties not encountered in the linear equation. More precisely, the non–linearity makes everything harder to analyze. In spite of this, a great deal of progress has been made in recent years [177, 179]. There can exist more than one weak solution for (1.39) and the method might converge to a function that is not a weak solution of the original equation, i.e. one that does not satisfy the entropy condition. It is possible to construct non–conservative schemes that converge to a solution which is not a weak solution of the original equation but they fail at shock waves. They give the wrong shock speed and thus the wrong shock position. Recent work by Hou and Le Floch [79] has shown that non–conservative schemes do not converge to the correct solution if a shock wave is present in the solution. They have also shown that if a method is not written in a conservative form, then in the presence of a shock wave, the scheme will, if convergent, converge to the solution of a new conservation law with a source term which only vanishes if the shock wave is not present. It is well known that conservative methods must be used when computing solutions to hyperbolic conservation laws containing shock waves as part of the solution. The Lax–Wendroff theorem states that if a conservative method is convergent, then it will converge to a weak solution of the conservation law. The proof of this result is presented in [99]. The Lax–Wendroff theorem is not a convergence theorem; it simply states that if the method, written in conservative form, is convergent then it converges to a weak solution of (1.39).

A numerical scheme in a conservative form should in some way initiate the integral form of the conservation laws. Thus a conservative scheme will typically take the

form

$$\mathbb{U}_i^{n+1} = \mathbb{U}_i^n - \frac{\Delta t}{\Delta x}\left[\mathbb{F}_{i+\frac{1}{2}} - \mathbb{F}_{i-\frac{1}{2}}\right], \tag{1.44}$$

where $\mathbb{F}_{i+\frac{1}{2}}$ is the inter–cell flux or numerical flux corresponding to the inter–cell boundary at $x = x_{i+\frac{1}{2}}$ between cells i and $i+1$ and takes the form

$$\mathbb{F}_{i+\frac{1}{2}} = \mathbb{F}_{i+\frac{1}{2}}\left(\mathbb{U}_{i-\jmath_{\mathcal{L}}}^n, \ldots, \mathbb{U}_{i+\jmath_{\mathcal{R}}}^n\right), \tag{1.45}$$

with the non–negative integers $\jmath_{\mathcal{L}}$ and $\jmath_{\mathcal{R}}$ depending on the particular choice of numerical flux.

In this thesis we are concerned with conservative numerical schemes based on the conservative formula (1.44), which is completely determined once the numerical fluxes $\mathbb{F}_{i\pm\frac{1}{2}}$ have been specified. If a conservation method converges, it will converge to a weak solution. Thus to ensure that this is the correct physical solution, the scheme must be entropy satisfying. In fact, the real issue concerning numerical methods is convergence. For non–linear systems convergence proofs rely on non–linear stability and the theory of functional analysis concepts such as compactness must be used. Sets of functions whose total variation is bounded lend to compact sets. Total Variation Stable methods are then defined as those whose mesh–dependent approximations lie in compact function sets [177]. It can be then shown that Total Variation Stable methods are convergent (see [72, 99, 100] for details). A subclass of Total Variation Stable methods are those whose total variation does not increase in time and are referred to as Total Variation Diminishing (TVD) methods. For a given grid function $\mathbb{U}^n = \{\mathbb{U}_i^n\}$, the total variation of $\mathbb{U}^n$ is defined as

$$TV(\mathbb{U}^n) = \sum_{i=-\infty}^{\infty} \left|\mathbb{U}_{i+1}^n - \mathbb{U}_i^n\right|, \tag{1.46}$$

for $TV(\mathbb{U}_i^n)$ to be finite, one must assume $\mathbb{U}_i^n = 0$ or $\mathbb{U}_i^n =$ constant as $i \to \pm\infty$.

If $TV(\mathbb{U}^{n+1})$ and $TV(\mathbb{U}^n)$ represent (1.46) evaluated at time level $n+1$ and n, re-

spectively, and if

$$TV(\mathbb{U}^{n+1}) \leq TV(\mathbb{U}^n), \ \forall n, \tag{1.47}$$

then the scheme is said to be a Total Variation Diminishing (TVD) .

TVD methods are one of the most significant achievements in the development of numerical solutions for partial differential equations (PDE's). The TVD concept has also been very useful for designing high–order non–oscillatory schemes for scalar problems. These have been extended to non–linear problems and have shown their significant achievements for these systems. High–order schemes are known for generating oscillations around discontinuities. Thus the basic idea is to construct higher order schemes where these oscillations are controlled or eliminated in high gradient regions by introducing some viscosity. Artificial viscosity methods [149] do this explicitly by introducing viscosity terms into the model. The form of these terms will typically depend on the problem considered. In TVD methods, the artificial viscosity is inherent to the scheme itself [177].

The TVD approach has managed to surround Godunov's theorem [59] by resorting to non–linear schemes, even when applied to linear problems. The inherent artificial viscosity of the schemes is controlled in a very precise manner so that spurious oscillations are eliminated and high–order accuracy in smooth parts of the solution is retained. Historically, TVD methods have almost exclusively been associated with high–order upwind methods. Recently it has been extended to centred schemes as distinct from upwind schemes [177]. This development has effectively provided Artificial Viscosity Methods with a more rational basis and has tended to unify the developments on numerical methods for conservation laws [177].

Because there are so many books and papers about the numerical schemes for conservation laws, further details can be found in the books by Hirsch [81], Kröner [91], LeVeque [99, 100], Toro [177], [179], the review paper by Roe [139], and the lecture notes by Yee [203].

The appeal of Godunov's method has been the success of the higher order extensions to it, such as Monotone Upstream–centred Schemes for Conservation Laws (MUSCL)

by van Leer [193], the Piecewise Parabolic Method (PPM) by Colella and Woodward [20], the MUSCL–Hancock method [195], the Generalised Riemann Problem (GRP) method by Ben–Artzi and Falcovitz [8, 45], and the Weighted Average Flux (WAF) method by Toro [172].

A brief description of the Godunov upwind method is given. Then the Lax–Friedrichs and FORCE centred schemes are described.

1.5.1 The Godunov Upwind Method

Godunov [59] suggested an approach for treating discontinuities on fluid flows by introducing explicit non–linearity into the difference method. This technique is fundamentally based upon the assumption that the solution is smooth. At a discontinuity this assumption is inappropriate, thus the need to force a well–behaved solution by introducing an unphysically large viscosity or an unphysical constraint of monotonicity. In 1959 Godunov found a new approach to this problem [59]. Instead of building up a full solution to the hydrodynamic equations by piecing together smooth, small–amplitude solutions, he built up a piecing together of discontinuous solutions. These discontinuous solutions closely approximate the smooth ones where those are appropriate, but they have the great additional advantage of approximating to the true solution reasonably well even when that solution is not smooth. We refer to [177] for details on the Godunov method. As most of the description applies to any system of hyperbolic conservation laws it also applies to the two–phase flow equations.

The Godunov method is a conservative method of the form

$$\mathbb{U}_i^{n+1} = \mathbb{U}_i^n - \frac{\Delta t}{\Delta x}\left[\mathbb{F}_{i+\frac{1}{2}} - \mathbb{F}_{i-\frac{1}{2}}\right], \tag{1.48}$$

where the fluxes $\mathbb{F}_{i+\frac{1}{2}}$ are computed by using the solution of the Riemann problem. As there are many choices for the flux $\mathbb{F}_{i+\frac{1}{2}}$ that will give a conservative numerical method, we are concerned here with the Godunov flux. The basic assumption of the method is that at the time $t = t^n$ the initial data $\mathbb{U}^n$ is a set of integral averages $\mathbb{U}_i^n$ over control volumes $I_i = [x_{i-\frac{1}{2}}, x_{i+\frac{1}{2}}]$ and results in a piecewise constant distribution of the data. Consider a short portion of the domain $x_{i-\frac{1}{2}} \leq x \leq x_{i+\frac{3}{2}}$, then locally one

has the set of conservation laws with initial data that consists of a pair of constant states separated by a discontinuity. Thus one can define a local Riemann problem as

$$\left.\begin{array}{l} \text{PDE's}: \ \partial_t \mathbb{U} + \partial_x \mathbb{F}(\mathbb{U}) = 0, \\ \text{IC's} \quad : \ \mathbb{U}(x,t^n) = \begin{cases} \mathbb{U}_i^n & \text{if} \quad x < x_{i+\frac{1}{2}}, \\ \mathbb{U}_{i+1}^n & \text{if} \quad x > x_{i+\frac{1}{2}}, \end{cases} \end{array}\right\} \tag{1.49}$$

with data states $\mathbb{U}_i^n$ (left) and $\mathbb{U}_{i+1}^n$ (right) and its solution denoted by $\mathbb{U}_{i+\frac{1}{2}}(x,t)$. Another local Riemann problem found in the portion $x_{i-\frac{3}{2}} \leq x \leq x_{i+\frac{1}{2}}$ is

$$\left.\begin{array}{l} \text{PDE's}: \ \partial_t \mathbb{U} + \partial_x \mathbb{F}(\mathbb{U}) = 0, \\ \text{IC's} \quad : \ \mathbb{U}(x,t^n) = \begin{cases} \mathbb{U}_{i-1}^n & \text{if} \quad x < x_{i-\frac{1}{2}}, \\ \mathbb{U}_i^n & \text{if} \quad x > x_{i-\frac{1}{2}}, \end{cases} \end{array}\right\} \tag{1.50}$$

where the solution in this case is denoted as $\mathbb{U}_{i-\frac{1}{2}}(x,t)$.
The Godunov flux $\mathbb{F}_{i+\frac{1}{2}}$ at the inter–cell boundary $x_{i+\frac{1}{2}}$ is defined as the physical function $\mathbb{F}(\mathbb{U})$ evaluated at the solution $\mathbb{U}_{i+\frac{1}{2}}(\frac{x}{t})$ in local coordinate $\frac{x}{t} = 0$ along the t–axis. Thus we express the Godunov flux as

$$\mathbb{F}_{i+\frac{1}{2}} = \mathbb{F}(\mathbb{U}_{i+\frac{1}{2}}(0)). \tag{1.51}$$

The method originates from the more basic definition

$$\mathbb{U}_i^{n+1} = \frac{1}{\Delta x} \int_0^{\frac{1}{2}\Delta x} \mathbb{U}_{i-\frac{1}{2}}(x,\Delta t)dx + \int_{-\frac{1}{2}\Delta x}^{0} \mathbb{U}_{i+\frac{1}{2}}(x,\Delta t)dx, \tag{1.52}$$

and allows the updating of the solution which is an integral average of $\mathbb{U}_i(\frac{x}{t})$ combining the solution of two local Riemann problem solutions $\mathbb{U}_{i-\frac{1}{2}}(\frac{x}{t})$ and $\mathbb{U}_{i+\frac{1}{2}}(\frac{x}{t})$ at time $t^{n+1} = t^n + \Delta t$ within the cell $I_i = [x_{i-\frac{1}{2}}, x_{i+\frac{1}{2}}]$. This is satisfied by imposing the following restriction

$$\Delta t = \frac{C\Delta x}{S_{\max}^n}, \tag{1.53}$$

where C is a Courant number or CFL coefficient satisfying

$$0 < C \leq 1. \tag{1.54}$$

In practical computations we take $C = 0.9$. $S^n_{\max}$ is the maximum wave speed at time level n.

1.5.2 Stability and Boundary Conditions for Godunov's Method

For non–linear systems, such as two–phase flow models, one implements the stability conditions (1.53) and (1.54) with a reliable estimate for $S^n_{\max}$ to be found. One may use the local solutions of the Riemann problem in one–dimensional problems to provide an estimate for $S^n_{\max}$. A practical choice is associated with non–linear waves present in the solution of the Riemann problem which can be shock or rarefaction waves as we shall see in later chapters.

Next, we discuss boundary conditions that are applied to the two–phase flow models considered here. For a domain $[0, L]$ discretised by M cells ($I_i = 1, \ldots, M$) we require two fictitious cells next to each boundary. For the left boundary at $x = 0$ the left fictitious cells are denoted by $i = -1$ and $i = 0$, and for the right boundary they are denoted by $i = M + 1$ and $i = M + 2$. We are only concerned with transmissive boundary conditions. The transmissive boundary conditions are given by

$$\left.\begin{aligned} \mathcal{V}^n_0 &= \mathcal{V}^n_1; & \mathcal{V}^n_{-1} &= \mathcal{V}^n_2, \\ \mathcal{V}^n_{M+1} &= \mathcal{V}^n_M; & \mathcal{V}^n_{M+2} &= \mathcal{V}^n_{M-1}, \end{aligned}\right\} \tag{1.55}$$

where $\mathcal{V}$ may be the vector of conserved variables or of some other variables such as the primitive variables. We refer to [177] for detailed and different types of boundary conditions for Godunov's method.

1.5.3 The Lax–Friedrichs Centred Method

Numerical schemes may be obtained from the conservative formula (1.48) using centred methods such as the Lax–Friedrichs method [96] which can be used to give the

inter–cell flux $\mathbb{F}_{i+\frac{1}{2}}$. The main feature of the scheme is that it does not require the differencing to be performed according to the upwind directions making the scheme more simple. The Lax–Friedrichs method takes the following numerical form

$$\mathbb{F}^{\text{LF}} = \frac{1}{2}\Big[\mathbb{F}_i^n + \mathbb{F}_{i+1}^n\Big] + \frac{1}{2}\frac{\Delta x}{\Delta t}\Big[\mathbb{U}_i^n - \mathbb{U}_{i+1}^n\Big]. \tag{1.56}$$

Mathematical analysis [177] shows that this scheme is too diffusive to be used in practical computations but it is extremely simple to implement. The scheme is monotone and has stability condition (1.53), (1.54), with $C = 0.9$ in practical computations.

1.5.4 The FORCE Centred Method

The FORCE (First–Order Centred) scheme is another first–order centred method proposed by Toro in [176]. The FORCE scheme can be written as [177]

$$\mathbb{F}_{i+\frac{1}{2}}^{\text{FORCE}} = \frac{1}{2}\Big[\mathbb{F}_{i+\frac{1}{2}}^{\text{LF}} + \mathbb{F}_{i+\frac{1}{2}}^{\text{RI}}\Big], \tag{1.57}$$

where $\mathbb{F}_{i+\frac{1}{2}}^{\text{LF}}$ is the Lax–Friedrichs flux and $\mathbb{F}_{i+\frac{1}{2}}^{\text{RI}}$ is the Richtmyer flux

$$\left.\begin{aligned} \mathbb{F}_{i+\frac{1}{2}}^{\text{RI}} &= \mathbb{F}(\mathbb{U}_{i+\frac{1}{2}}^{\text{RI}}), \\ \mathbb{U}_{i+\frac{1}{2}}^{\text{RI}} &= \frac{1}{2}(\mathbb{U}_i^n, \mathbb{U}_{i+1}^n) + \frac{1}{2}\frac{\Delta t}{\Delta x}\Big[\mathbb{F}_i^n - \mathbb{F}_{i+1}^n\Big]. \end{aligned}\right\} \tag{1.58}$$

The FORCE method has half the numerical viscosity of the Lax–Friedrichs method. The main disadvantage of this numerical viscosity can be reduced by using a high–resolution MUSCL interpolate [194], instead of the first order piecewise constant cell average values. This process is called the Slop LImiter Centred scheme (SLIC) suggested by Toro [178] and its effect can be significant in dealing with intricate problems as we shall see in later chapters.

1.6 Outline of the Thesis

This thesis is concerned with the mathematical analysis and modern shock–capturing schemes applied to non–linear partial differential equations with two–phase flow applications. Two–phase flow models in a non–conservative and conservative form are developed, studied mathematically and numerically. The thesis consists of two different models that can be used in the study of two–phase flows. The first model is the simplified two–fluid model and the second model is the hyperbolic conservative two–fluid model. In chapter 2 theoretical bases for the simplified two–fluid model are presented. The governing equations are developed. In particular, a great deal of attention has been given to the mathematical properties of the model.

Chapter 3 is devoted to the Riemann problem for the simplified two–fluid model. The Riemann problem is solved exactly for the model up to first order in η and under the assumption that the liquid phase is assumed to be incompressible with constant density.

Chapter 4 presents solutions for a selection of test problems using the exact solution of the Riemann problem developed in chapter 3. These solutions will be very useful in assessing the performance of numerical methods applied to the same problems.

In chapter 5 we present approximate Riemann solvers for the simplified two–fluid model using two different approaches.

Chapter 6 presents second–order TVD schemes of Godunov–type methods of upwind and centred type. Test problems are also presented to validate the schemes.

In chapter 7 the new hyperbolic conservative two–fluid model is introduced. The mathematical analysis is carried out for the one–dimensional two–phase flow case.

Chapter 8 investigates the Riemann problem for the hyperbolic conservative two–fluid model to study a possible wave patterns.

Chapter 9 deals with the numerical study of wave propagation in compressible two–phase flow. We construct a numerical method for the model and present a selection of test problems.

Conclusions and suggestions for further work are given in chapter 10. Appendices are included which contain listings of FORTRAN programs to solve the models.

CHAPTER 2
MATHEMATICAL ANALYSIS OF A SIMPLIFIED TWO–FLUID MODEL

In this chapter we present the simplified two–fluid model. We study the mathematical structure for the model to obtain and classify the wave fields associated with the model.

2.1 Governing Equations

In this section we derive a simplified isentropic one–dimensional model for two–phase flows. The isentropic 4–equation model consists of a mass equation and a momentum equation for each phase (see e.g. [168])

$$\partial_t(\alpha_2\rho_2) + \partial_x(\alpha_2\rho_2 u_2) = 0, \tag{2.1}$$

$$\partial_t(\alpha_1\rho_1) + \partial_x(\alpha_1\rho_1 u_1) = 0, \tag{2.2}$$

$$\partial_t(\alpha_2\rho_2 u_2) + \partial_x(\alpha_2\rho_2 u_2^2) + \alpha_2\partial_x\mathcal{P} = 0, \tag{2.3}$$

$$\partial_t(\alpha_1\rho_1 u_1) + \partial_x(\alpha_1\rho_1 u_1^2) + \alpha_1\partial_x\mathcal{P} = 0. \tag{2.4}$$

We refer to this as the simplified two–fluid model. Isentropic conditions are assumed within the model with no viscosity effects and no mass transfer between phases. The subscript 1 refers to the liquid phase and subscript 2 to the vapour phase; ρ_{i}, u_{i} and α_{i} are, respectively, the mass density, the velocity and the void fraction of phase i. $\mathcal{P}$ is the pressure assumed to be equal in the two phases. To close the system, we need to include the following additional equations:

- The volume fractions are related by

$$\alpha_1 + \alpha_2 = 1, \tag{2.5}$$

(i.e. there are no detachments between phases).

- Densities ρ_1, ρ_2 are linked to the fluid properties through a thermodynamic equation of state. We assume the form

$$\rho_i = \rho_i(\mathcal{P}). \tag{2.6}$$

- Hydrodynamic closure relating the two phase velocities is implemented by a kinetic constitutive equation such as

$$u_r = u_2 - u_1. \tag{2.7}$$

We can write the isentropic two–fluid 4–equation model in the following nonconservative form

$$\partial_t \mathbb{U} + \mathbb{A}(\mathbb{U})\partial_x \mathbb{U} = 0, \tag{2.8}$$

where $\mathbb{U}$ is the vector of conservative variables

$$\mathbb{U} = \Big[\alpha_2\rho_2,\ \alpha_1\rho_1,\ \alpha_2\rho_2 u_2,\ \alpha_1\rho_1 u_1\Big]^T. \tag{2.9}$$

The Jacobian matrix $\mathbb{A}(\mathbb{U})$ of the simplified two–fluid model cannot be written as the derivative of some flux function. However, as in the theory of conservative hyperbolic systems, we may expect that the solutions of the non–conservative system to show some discontinuities after a finite time even for smooth initial data. For a general matrix valued function $\mathbb{A}(\mathbb{U})$, the product $\mathbb{A}(\mathbb{U})\partial_x \mathbb{U}$ is not a distribution and we have to add some extra information to define it. Such non–conservative products have been considered in [22] and [98], within the functional framework of bounded variation functions.

The system of (2.8) cannot be written directly under a conservative form due to the presence of non–conservative products like $\alpha_1\partial_x\mathcal{P}$ and $\alpha_2\partial_x\mathcal{P}$ in the momentum equations (2.3) and (2.4). However, the basic two–fluid model, which is the sys-

tem (2.1)–(2.4) without the energy balance, has an equivalent conservative form for smooth solutions. We can write the phase momentum equations (2.3) and (2.4) using a sum and difference formulation

$$\partial_t(\alpha_2\rho_2u_2 + \alpha_1\rho_1u_1) + \partial_x(\alpha_2\rho_2u_2^2 + \alpha_1\rho_1u_1^2) + \partial_x\mathcal{P} = 0, \tag{2.10}$$

$$\partial_t(u_2 - u_1) + \partial_x(\frac{u_2^2}{2} - \frac{u_1^2}{2}) + \partial_x\psi(\mathcal{P}) = 0, \tag{2.11}$$

where

$$\psi'(\mathcal{P}) = \frac{1}{\rho_2} - \frac{1}{\rho_1} = \frac{1}{\rho_{21}}. \tag{2.12}$$

The sum momentum equation is obtained by the direct summation of the momentum equations, while the difference momentum equation is obtained by dividing the vapour phase momentum by $\alpha_2\partial_x\mathcal{P}$ and the liquid phase momentum by $\alpha_1\partial_x\mathcal{P}$ then subtracting the later from the former. Then, the system considered in our study takes the following form

$$\partial_t(\alpha_2\rho_2) + \partial_x(\alpha_2\rho_2u_2) = 0, \tag{2.13}$$

$$\partial_t(\alpha_1\rho_1) + \partial_x(\alpha_1\rho_1u_1) = 0, \tag{2.14}$$

$$\partial_t(\alpha_2\rho_2u_2 + \alpha_1\rho_1u_1) + \partial_x(\alpha_2\rho_2u_2^2 + \alpha_1\rho_1u_1^2) + \partial_x\mathcal{P} = 0, \tag{2.15}$$

$$\partial_t(u_2 - u_1) + \partial_x(\frac{u_2^2}{2} - \frac{u_1^2}{2}) + \partial_x\psi(\mathcal{P}) = 0, \tag{2.16}$$

where $\psi(\mathcal{P})$ can be obtained from (2.12).

For weak solutions, in order to prove the equivalence of the two systems (2.1)–(2.4) and (2.13)–(2.16), one must examine the classical and generalised Rankine–Hugoniot conditions for the conservative system (2.13)–(2.16) and the non–conservative system (2.1)–(2.4), respectively. Such a study has been realized in [154] for a model describing spray dynamics and is not within the scope of this problem.

Introducing the mixture density, ρ, and the mixture velocity u defined by

$$\rho = \alpha_2\rho_2 + \alpha_1\rho_1, \tag{2.17}$$

$$\rho u = \alpha_2\rho_2 u_2 + \alpha_1\rho_1 u_1, \tag{2.18}$$

then system (2.1)–(2.4) can be written in the following form

$$\partial_t(\alpha_2\rho_2 + \alpha_1\rho_1) + \partial_x(\alpha_2\rho_2 u_2 + \alpha_1\rho_1 u_1) = 0, \tag{2.19}$$

$$\partial_t(\alpha_2\rho_2 u_2 + \alpha_1\rho_1 u_1) + \partial_x(\alpha_2\rho_2 u_2^2 + \alpha_1\rho_1 u_1^2) + \partial_x\mathcal{P} = 0, \tag{2.20}$$

$$\partial_t(u_2 - u_1) + \partial_x(\frac{u_2^2}{2} - \frac{u_1^2}{2}) + \partial_x\psi(\mathcal{P}) = 0, \tag{2.21}$$

which may be viewed as a simplified version of (2.1) and (2.4), thus, this is a first step to study the system (2.1)–(2.4).

An additional relation is needed to close the system (2.19)–(2.21). We assume that the mass vapour concentration to be a function of pressure

$$c \equiv \frac{\alpha_2\rho_2}{\rho} \equiv c(\mathcal{P}). \tag{2.22}$$

Using the concentration function in the expression of the mixture density (2.17) gives

$$\frac{1}{\rho} = \frac{c}{\rho_2} - \frac{1-c}{\rho_1}, \tag{2.23}$$

then using (2.6) and (2.22) into (2.23) implies that

$$\rho = \rho(\mathcal{P}), \tag{2.24}$$

which is the generalised isentropic EOS in a mixture formulation.

Finally, for smooth solutions the simplified two–fluid model is equivalent to the following conservative system

$$\partial_t\mathbb{U} + \partial_x\mathbb{F}(\mathbb{U}) = 0,\ x \in \mathbb{R},\ t > 0, \tag{2.25}$$

with

$$\mathbb{U} = \begin{pmatrix} \rho \\ \rho u \\ u_r \end{pmatrix}, \tag{2.26}$$

and the flux function

$$\mathbb{F}(\mathbb{U}) = \begin{pmatrix} \rho u \\ \rho u^2 + \rho\, c\, (1-c)\, u_r^2 + \mathcal{P} \\ u u_r + \frac{1-2c}{2}\, u_r^2 + \psi(\mathcal{P}) \end{pmatrix}. \tag{2.27}$$

This conservative form of the isentropic mixture two–phase flow will be useful to study the Riemann problem for the system and to define jump conditions for the exact and approximate Riemann solvers. We call this system the simplified two–fluid model.

2.2 Hyperbolicity Analysis of the Equations

It is well known that the two–fluid model leads to a non–hyperbolic system, implying the resulting system of equations possesses some complex eigenvalues [168]. To determine the eigenvalues of system (2.25), we must find the three roots of a third degree polynomial given by the characteristic determinant. We assume that the relative velocity, u_r, between the two–phases is much lower than the speed of sound of the two–phase mixture, a_m, which is the case in many physically interesting mixtures such as steam and water. Consequently, we introduce the small parameter, η, given by the dimensionless relative velocity

$$\eta = \frac{u_r}{a_m} \ll 1, \tag{2.28}$$

from which we show that the simplified two–fluid model is strictly hyperbolic, with a_m defined as

$$a_m = \left(\frac{\partial \mathcal{P}}{\partial \rho}\right)^{\frac{1}{2}}. \tag{2.29}$$

We also assume that the following relations are satisfied

$$\frac{\partial \mathcal{P}}{\partial \rho} > 0, \quad 2\,\frac{\partial \mathcal{P}}{\partial \rho} + \rho\,\frac{\partial^2 \mathcal{P}}{\partial \rho^2} > 0, \tag{2.30}$$

to ensure that the pressure $\mathcal{P}$ is a convex function of the specific volume $\frac{1}{\rho}$. Further, for the generalised isentropic EOS (2.24), the system (2.25) is hyperbolic if and only if $\mathcal{P}^{'}(\rho) > 0$, that is, the pressure must be a monotone increasing function of the mixture density ρ.

The closed form expressions of the eigenvalues of the system (2.25) are rather lengthy and are not very suitable for analysis. Also, from a physical point of view, the vector of conservative variables $\mathbb{U}$ is not a convenient state vector to work with. Indeed, initial and boundary conditions are more often than not specified in terms of primitive variables, such as pressure, momentum or void fraction. In the case of the simplified two–fluid model, we will therefore consider as primitive variables the vector $\mathbb{W}$ defined as

$$\mathbb{W} = \left[\rho, u, u_r\right]^T. \tag{2.31}$$

Then the system (2.25) can be linearised to give

$$\mathbb{C}(\mathbb{W})\partial_t \mathbb{W} + \mathbb{A}(\mathbb{W})\partial_x \mathbb{W} = 0, \tag{2.32}$$

where the coefficient matrices are defined as

$$\mathbb{C}(\mathbb{W}) = \begin{pmatrix} a_m^{-2} & 0 & 0 \\ 0 & \rho & 0 \\ 0 & 0 & 1 \end{pmatrix}, \tag{2.33}$$

$$\mathbb{A}(\mathbb{W}) = \begin{pmatrix} \frac{u}{a_m^2} & \rho & 0 \\ 1 + c(1-c)\,\frac{u_r^2}{a_m^2} + (1-2c)\,c_{\mathcal{P}}\rho\,u_r^2 & \rho u & 2\rho c(1-c)\,u_r \\ \frac{1}{\rho_{21}} - c_{\mathcal{P}} u_r^2 & u_r & u + (1-2c)\,u_r \end{pmatrix}, \tag{2.34}$$

with $c_{\mathcal{P}} = \partial c/\partial \mathcal{P}$ and $1/\rho_{21}$ given by (2.12).

Let us introduce the set $\Omega \in \mathbb{R}^3$. Then for $\mathbb{U} \in \Omega$ we can choose a number $\eta^\star$ such that for any $\mathbb{U}$ lies in the set $\Omega^\star$ defined as $\Omega^\star = \left\{\mathbb{U} \in \Omega : \rho(\mathcal{P}) > 0, |\eta| \leq \eta^\star\right\}$ the eigenvalues λ_{j}, $1 \leq \mathrm{j} \leq 3$ are real and distinct for η small enough and $\rho(\mathcal{P})$ satisfies (2.30). Thus the eigenvalues of the matrix $\mathbb{A}(\mathbb{W})$ are the solutions of the characteristic polynomial

$$\det\Big[\mathbb{A}(\mathbb{W}) - \lambda I\Big] = 0,$$

which becomes

$$\mathfrak{p}_0(\mathcal{Y}) + \eta\mathfrak{p}_1(\mathcal{Y}) + \eta\mathfrak{p}_2(\mathcal{Y};\eta) = 0, \tag{2.35}$$

where

$$\begin{aligned} \mathfrak{p}_0(\mathcal{Y}) &= \mathcal{Y}^3 - \mathcal{Y}, \\ \mathfrak{p}_1(\mathcal{Y}) &= (1-2c)\mathcal{Y}^2 - \Big[1 - 2c - 2\,\frac{\rho}{\rho_{21}}\,c\,(1-c)\Big], \\ \mathfrak{p}_2(\mathcal{Y};\eta) &= -\Big\{\Big[3c\,(1-c) + c_{\mathcal{P}}\,a_m^2\,\rho\,(1-2c)\Big]\mathcal{Y} \\ &+ \Big[\big((1-2c)^2 + 2c\,(1-c)\big)\,c_{\mathcal{P}}\,a_m^2\,\rho + c\,(1-c)(1-2c)\Big]\eta\Big\}\eta, \end{aligned}$$

and

$$\mathcal{Y} = \frac{u - \lambda}{a_m}. \tag{2.36}$$

Following Goursat [63] we will use the following lemma:

LEMMA 1 Let $\mathfrak{p}(\mathcal{Y};\eta)$ be a polynomial with real coefficients in the variable $\mathcal{Y}$ depending on a parameter η. We set $\mathfrak{p}_0(\mathcal{Y}) = \mathfrak{p}(\mathcal{Y},0)$ and we assume that $\mathcal{Y}_0$ is a root of $\mathfrak{p}_0$. Moreover if we assume that $|\mathcal{Y} - \mathcal{Y}_0|$ is small enough, then the polynomial $\mathfrak{p}$ can be written as

$$\mathfrak{p}(\mathcal{Y};\eta) = \mathfrak{p}_0(\mathcal{Y}) + \eta\mathfrak{p}_1(\mathcal{Y}) + \eta\mathfrak{p}_2(\mathcal{Y};\eta),$$

with

$$\left|\mathfrak{p}_2(\mathcal{Y};\eta)\right| \leq \left(1 + |\mathcal{Y}|\right)^n \psi(\eta),\ n \in N,\ \exists \lim_{\eta\to 0}\psi(\eta) = 0.$$

We look for the roots of the polynomial $\mathfrak{p}(\mathcal{Y};\eta)$ in the neighbourhood of $\mathcal{Y}_0$. If $\mathcal{Y}_0$ is a simple root of $\mathfrak{p}_0$ there exists C^1 function in η

$$\mathcal{Y}(\eta) = \mathcal{Y}_0 + \mathcal{Y}_1\eta + \mathcal{O}(\eta^2), \tag{2.37}$$

where

$$\mathcal{Y}_1 = -\frac{\mathfrak{p}_1(\mathcal{Y}_0)}{\mathfrak{p}_0'(\mathcal{Y}_0)}, \tag{2.38}$$

defined in a neighbourhood $(-\eta_0, \eta_0)$ of 0 such as $\mathfrak{p}\big(\mathcal{Y}(\eta);\eta\big) = 0$ for all $\eta \in (-\eta_0, \eta_0)$. If $\mathcal{Y}_0$ is a real, $\mathcal{Y}(\eta)$ is real.

In equation (2.35) the polynomials $\mathfrak{p}_0$, $\mathfrak{p}_1$ and $\mathfrak{p}_2$ satisfy the assumptions of Lemma (1) and (2.36). Thus with aid of Lemma (1) we find that the eigenvalues of the simplified

two–fluid model have the following behaviour up to first order in η

$$\lambda_{\mathrm{j}} = \begin{cases} u - a_m + \frac{\rho}{\rho_{21}}\, c(1-c)\, u_r + a_m \mathcal{O}(\eta^2) & \mathrm{j} = 1, \\ u + \left[1 - 2c - 2\frac{\rho}{\rho_{21}}\, c(1-c)\right] u_r + a_m \mathcal{O}(\eta^2) & \mathrm{j} = 2, \\ u + a_m + \frac{\rho}{\rho_{21}}\, c(1-c)\, u_r + a_m \mathcal{O}(\eta^2) & \mathrm{j} = 3. \end{cases} \tag{2.39}$$

Thus, we have proved that the simplified two–fluid is hyperbolic up to first order in η. In fact system (2.25) is strictly hyperbolic because the eigenvalues are real and distinct as long as the speed of sound a_m remain positive. Further we compute the corresponding eigenvectors up to first order in η as

$$\mathcal{K}^{1,3} = \begin{pmatrix} \rho a_m \\ \pm 1 + \frac{\rho}{\rho_{21}}\, c(1-c) \frac{u_r}{a_m} \\ \pm \frac{\rho}{\rho_{21}} + \frac{\rho}{\rho_{21}} \left(1 - 2c - c(1-c)\frac{\rho}{\rho_{21}} + \frac{\rho_{21}}{\rho}\right) \frac{u_r}{a_m} \end{pmatrix}, \tag{2.40}$$

$$\mathcal{K}^{2} = \begin{pmatrix} -2\rho c(1-c) u_r \\ 0 \\ 1 \end{pmatrix}. \tag{2.41}$$

Finally, we find that the first and third characteristic fields are genuinely non–linear and the second characteristic field is neither genuinely non–linear nor linearly degenerate as we shall see in the next section.

2.3 Nature of Characteristic Fields

In view of the hyperbolicity analysis demonstrated in the previous section, we study the nature of the characteristic fields of the simplified two–fluid model. Using the

following expressions

$$\frac{\partial a_m}{\partial \mathcal{P}} = -\frac{a_m^3}{2}\frac{\partial^2 \rho}{\partial \mathcal{P}^2} = -\frac{a_m^3}{2}(-a_m^{-6})\frac{\partial^2 \rho}{\partial \mathcal{P}^2} = \frac{a_m^3}{2}\frac{\partial^2 \rho}{\partial \mathcal{P}^2}, \tag{2.42}$$

we find that

$$\lim_{\eta \to 0} \nabla \lambda_1(\mathbb{U}) \cdot \mathcal{K}^1(\mathbb{U}) = -\frac{a_m^{-2}}{2}\Big[2\,\frac{\partial \mathcal{P}}{\partial \rho} + \rho\frac{\partial^2 \mathcal{P}}{\partial \rho^2} + 2a_m^2\,(\frac{\rho}{\rho_{21}})^2\,c(1-c)\Big], \tag{2.43}$$

$$\lim_{\eta \to 0} \nabla \lambda_3(\mathbb{U}) \cdot \mathcal{K}^3(\mathbb{U}) = \frac{a_m^{-2}}{2}\Big[2\,\frac{\partial \mathcal{P}}{\partial \rho} + \rho\frac{\partial^2 \mathcal{P}}{\partial \rho^2} + 2a_m^2\,(\frac{\rho}{\rho_{21}})^2\,c(1-c)\Big]. \tag{2.44}$$

Using (2.29) and (2.30) we find the first and the third characteristic fields are genuinely non–linear.

For the second characteristic field we obtain

$$\lim_{\eta \to 0} \nabla \lambda_2(\mathbb{U}) \cdot \mathcal{K}^2(\mathbb{U}) = 1 - 2c - 2c(1-c)\,\frac{\rho}{\rho_{21}}. \tag{2.45}$$

The expression in (2.45) is positive for $c = 0$ and negative for $c = 1$, thus this field is neither genuinely non–linear nor linearly degenerate. Equation (2.12) together with the mixture density from system (2.17) and (2.22), (2.45) can be written as

$$\lim_{\eta \to 0} \nabla \lambda_2(\mathbb{U}) \cdot \mathcal{K}^2(\mathbb{U}) = 1 - 2\alpha, \tag{2.46}$$

where $\alpha = \alpha_2$ is the void fraction for the vapour phase.

2.4 Conclusions

This study shows how the simplified two–fluid model for an isentropic two–phase flow was derived. The model was written in a non–conservative form due to the presence of non–conservative products in the momentum equations. It showed that the phase momentum equations can be written in a sum and a difference formulation in which the velocity between the two–phase mixture is given by the mixture momen-

tum equation and in which the relative velocity between phases can be expressed by a constitutive equation. Thus the simplified two–fluid model consists of a mixture density conservation equation, a mixture momentum conservation equation and an equation for the relative velocity between the two phases written in a conservative form.

From that the Jacobian matrix of the model was derived and it is shown that the model is hyperbolic in a physically reasonable region of parameters; three distinct and real eigenvalues are obtained under the assumption that the relative velocity between the two phases is much lower than the speed of sound of the two–phase mixture. Also the corresponding eigenvectors for the system were determined and it is shown that the first and third characteristic fields are genuinely non–linear while the second characteristic field is neither genuinely non–linear nor linearly degenerate. Having established this mathematical study, sufficient framework has been provided towards the development of an exact Riemann solver as we shall see in the next chapter.

CHAPTER 3

THE RIEMANN PROBLEM FOR THE SIMPLIFIED TWO–FLUID MODEL

The simplified two–fluid model for an isentropic two–phase flow problem was developed in the previous chapter. The simplified two–fluid model is useful for understanding the physical and mathematical concepts associated with two–phase flow equations. In this chapter we introduce and solve exactly the Riemann problem for the simplified two–fluid model up to first order in η.

3.1 The Riemann Problem and a Solution Strategy

In this section we describe the structure of the Riemann problem for the simplified two–fluid model as a set of elementary waves such as shocks, contact and rarefaction waves. The Riemann problem for the one–dimensional simplified two–fluid model up to first order in η with data $\mathbb{U}_{\mathcal{L}}$ and $\mathbb{U}_{\mathcal{R}}$ is the initial value problem (IVP) for the conservation law

$$\partial_t \mathbb{U} + \partial_x \mathbb{F}(\mathbb{U}) = 0, \quad x \in \mathbb{R}, \ t > 0, \tag{3.1}$$

with the initial conditions (IC)

$$\mathbb{U}(x,0) = \mathbb{U}^{(0)}(x) = \begin{cases} \mathbb{U}_{\mathcal{L}} & \text{if} \quad x < 0, \\ \mathbb{U}_{\mathcal{R}} & \text{if} \quad x > 0, \end{cases} \tag{3.2}$$

where the subscripts $\mathcal{L}$ and $\mathcal{R}$ denote the left and right states respectively and $\mathbb{U}$ and $\mathbb{F}(\mathbb{U})$ are vectors of conserved variables and fluxes respectively given by

$$\mathbb{U} = \begin{pmatrix} \rho \\ \rho u \\ u_r \end{pmatrix}, \quad \mathbb{F}(\mathbb{U}) = \begin{pmatrix} \rho u \\ \rho u^2 + \rho\, c\,(1-c)\, u_r^2 + \mathcal{P} \\ u u_r + \frac{1-2c}{2}\, u_r^2 + \psi(\mathcal{P}) \end{pmatrix}. \tag{3.3}$$

The initial conditions (3.2) consists of two constant states $\mathbb{U}_{\mathcal{L}}$ and $\mathbb{U}_{\mathcal{R}}$ with

$$\mathbb{U}_{\mathcal{L}} = \begin{pmatrix} \rho_{\mathcal{L}} \\ \rho_{\mathcal{L}} u_{\mathcal{L}} \\ u_{r\mathcal{L}} \end{pmatrix}, \quad \mathbb{U}_{\mathcal{R}} = \begin{pmatrix} \rho_{\mathcal{R}} \\ \rho_{\mathcal{R}} u_{\mathcal{R}} \\ u_{r\mathcal{R}} \end{pmatrix}, \tag{3.4}$$

and represent conditions at time $t = 0$, to the left of $x = 0$ and to the right of $x = 0$, respectively.

In solving the Riemann problem for the simplified two–fluid model up to first order in η we shall use the vector of primitive variables $\mathbb{W}$ rather than the vector $\mathbb{U}$ of conserved variables where $\mathbb{W}$ is chosen as

$$\mathbb{W} = \left[\rho, u, u_r\right]^T, \tag{3.5}$$

where ρ is the mixture density, u is the mixture velocity and u_r is the relative velocity between phases. The structure of the general solution of the Riemann problem (3.1)–(3.3) can be represented in the half x–t plane as in figure 3.1. There are three waves present which are associated with the eigenvalues $\lambda_1 = u - a_m + \frac{\rho}{\rho_{21}}\, c(1-c)\, u_r + a_m \mathcal{O}(\eta^2)$, $\lambda_2 = u + \left[1 - 2c - 2\frac{\rho}{\rho_{21}}\, c(1-c)\right] u_r + a_m \mathcal{O}(\eta^2)$ and $\lambda_3 = u + a_m + \frac{\rho}{\rho_{21}}\, c(1-c)\, u_r + a_m \mathcal{O}(\eta^2)$. The left wave is either a shock or rarefaction, the right wave is either a shock or rarefaction and the middle wave is a contact discontinuity. The waves separate four constant states, namely $\mathbb{W}_{\mathcal{L}}$ to the left of the left wave, $\mathbb{W}^{\star}_{\mathcal{L}}$, $\mathbb{W}^{\star}_{\mathcal{R}}$ and $\mathbb{W}_{\mathcal{R}}$ to the right of the right wave. The states $\mathbb{W}^{\star}_{\mathcal{L}}$ and $\mathbb{W}^{\star}_{\mathcal{R}}$ cover the unknown region between the left and right waves. This unknown region, called the

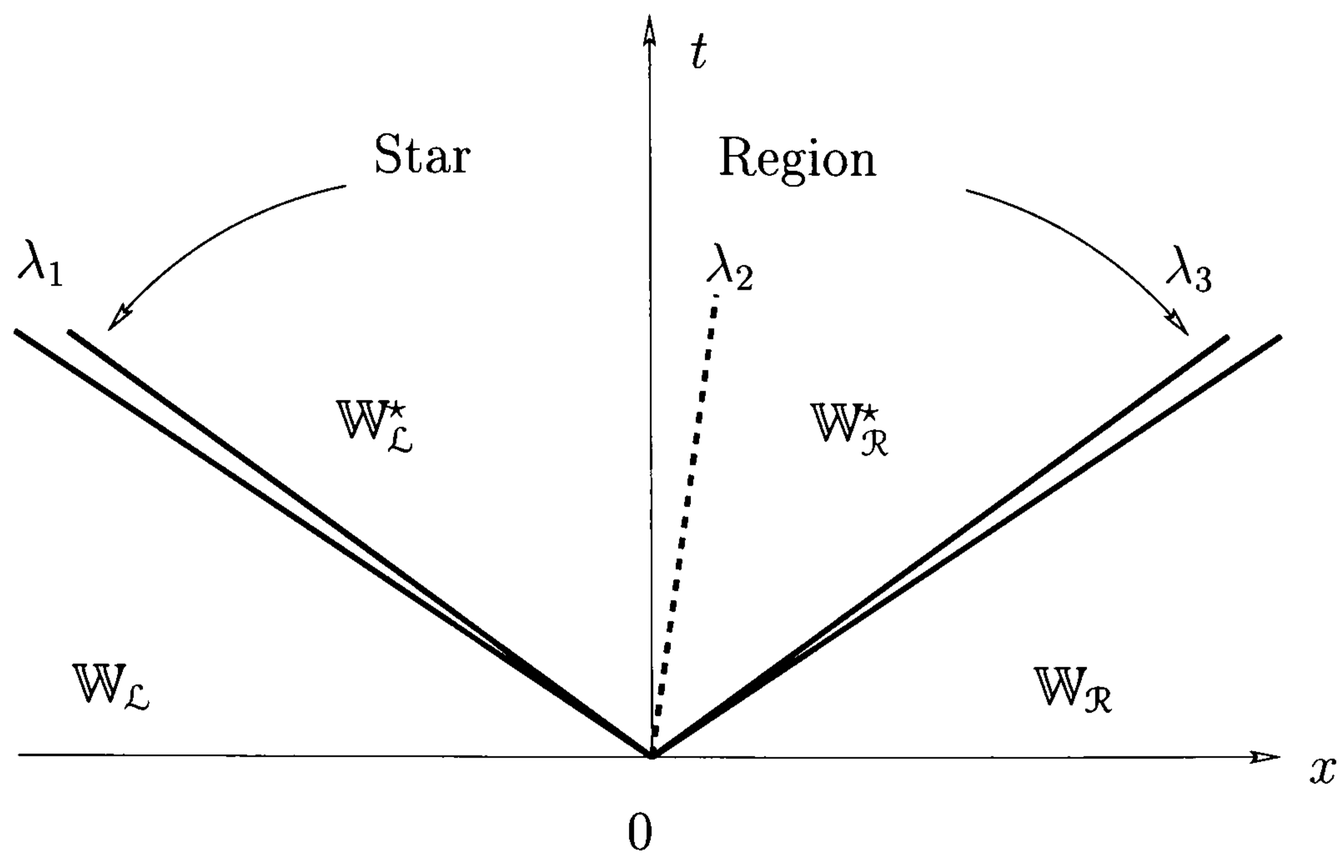

Figure 3.1: Structure of the solution of the Riemann problem for the simplified two–fluid model. There are three wave families associated with the eigenvalues λ_1, λ_2 and λ_3.

star region, is divided by the middle wave into two subregions $\mathbb{W}^\star_{\mathcal{L}}$ (star left) and $\mathbb{W}^\star_{\mathcal{R}}$ (star right). The solution is equal to constant state $\mathbb{W}_{\mathcal{L}}$ in the region of the left wave and equal to $\mathbb{W}_{\mathcal{R}}$ in the region of the right wave, and varies continuously with x at $t > 0$ through the rarefaction waves while it jumps discontinuously through the shock waves. Thus, there are four possible wave patterns according to the type of non–linear waves in the solution of the Riemann problem as shown in figure 3.2. There are also two possible variations of these waves when the left or right non–linear wave is a sonic rarefaction wave. The interest of these two cases is important when utilizing the solution of the Riemann problem in Godunov–type methods. However, for the purpose of constructing a solution scheme for the problem it is sufficient to consider the four wave patterns of figure 3.2. The analysis based on the eigenstructure of the simplified two–fluid model (see chapter 2) reveals that mixture density ρ, mixture velocity u and the relative velocity u_r change across the left and right waves, and the mixture density $\rho^\star$ and mixture velocity $u^\star$ remain constant across the middle wave while the relative velocity changes discontinuously to the two constant values $u_r = u^\star_{r\mathcal{L}}$ and $u_r = u^\star_{r\mathcal{R}}$. As we shall see later the solution strategy makes use of the constant mixture density and mixture velocity in the star region to derive a single,

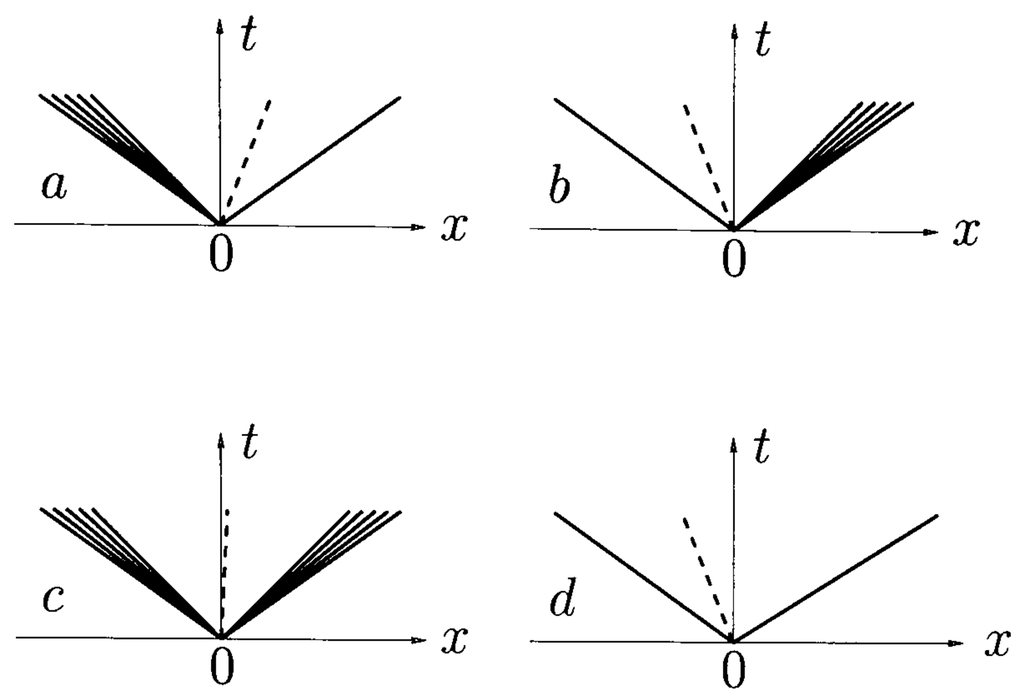

Figure 3.2: Possible wave patterns in the solution of the Riemann problem for the one–dimensional simplified two–fluid model. (a) left rarefaction, contact and right shock (b) left shock, contact and right rarefaction (c) left rarefaction, contact and right rarefaction (d) left shock, contact and right shock.

algebraic non–linear equation for the mixture density $\rho^\star$.

3.2 An Exact Riemann Solver

In the previous section we saw that the solution of the Riemann problem in the x–t plane consists of four wave patterns. We looked specifically at the star region. In dealing with the star region, we shall necessarily be concerned with the solution procedure to determine the solution in the star region up to first order in η. The basic step is to derive a single algebraic, non–linear equation for the mixture density $\rho^\star$, the value of ρ in the star region, namely

$$\mathcal{F}(\rho, \mathbb{W}_\mathcal{L}, \mathbb{W}_\mathcal{R}) \equiv \mathcal{F}_\mathcal{L}(\rho, \mathbb{W}_\mathcal{L}) + \mathcal{F}_\mathcal{R}(\rho, \mathbb{W}_\mathcal{R}) + \Delta u = 0, \quad \Delta u \equiv u_\mathcal{R} - u_\mathcal{L}, \tag{3.6}$$

where $u_\mathcal{L}$ and $u_\mathcal{R}$ are the mixture velocity in a left and right data, respectively. $\mathcal{F}_\mathcal{L}(\rho, \mathbb{W}_\mathcal{L})$ and $\mathcal{F}_\mathcal{R}(\rho, \mathbb{W}_\mathcal{R})$ are functions connecting the left and right data to the star region as illustrated in figure 3.3. Referring to figure 3.3, we see that the function $\mathcal{F}_\mathcal{L} = \mathcal{F}_\mathcal{L}(\rho, \mathbb{W}_\mathcal{L})$ governs relations across the left non–linear wave which is dependent on the type of wave (shock or rarefaction) and serves to connect the unknown mixture velocity $u^\star$ to the known states $\mathbb{W}_\mathcal{L}$ on the left side of the wave. Similarly, the function

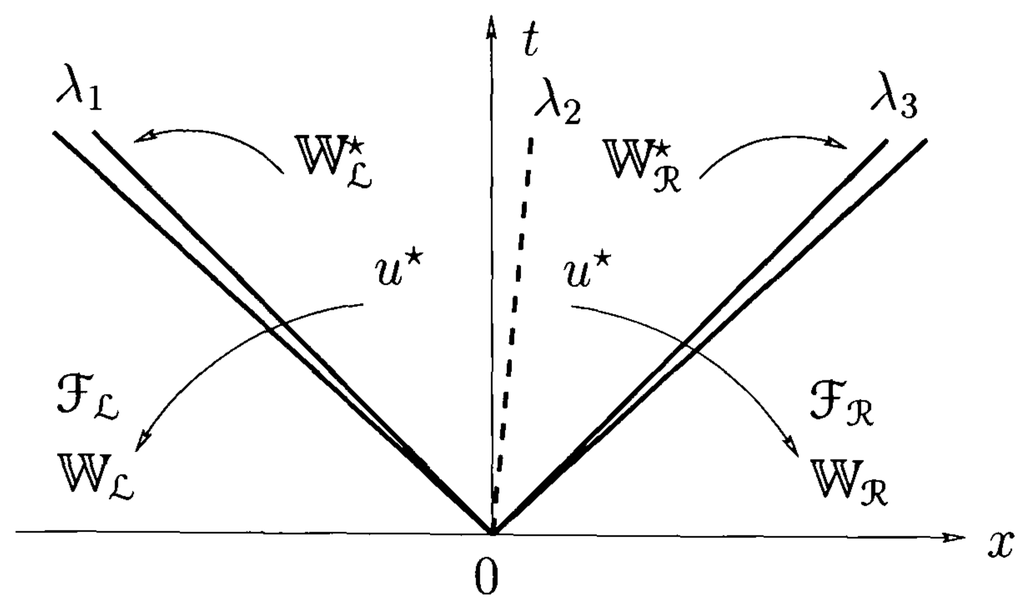

Figure 3.3: Strategy for solving the Riemann problem by the mixture density function. The mixture velocity $u^\star$ is connected to data on the left and right via $\mathcal{F}_{\mathcal{L}}$ and $\mathcal{F}_{\mathcal{R}}$.

$\mathcal{F}_{\mathcal{R}} = \mathcal{F}_{\mathcal{R}}(\rho, \mathbb{W}_{\mathcal{R}})$ governs the relation across the right wave and connects the unknown $u^\star$ to the right state, while the solution of the mixture velocity $u^\star$ in the star region is

$$u^\star = \frac{1}{2}(u_{\mathcal{L}} + u_{\mathcal{R}}) + \frac{1}{2}\big[\mathcal{F}_{\mathcal{R}}(\rho^\star) - \mathcal{F}_{\mathcal{L}}(\rho^\star)\big]. \tag{3.7}$$

Next we consider each non–linear wave separately to derive these functions.

3.2.1 Function $\mathcal{F}_{\mathcal{L}}$ for a Left Shock

Here we assume that the left wave is a shock wave travelling with velocity $S_{\mathcal{L}}$ as shown in figure 3.4 (a) where pre–shock values are $\rho_{\mathcal{L}}$, $u_{\mathcal{L}}$, $u_{r\mathcal{L}}$ and post–shock values are $\rho^\star$, $u^\star$, $u^\star_{r\mathcal{L}}$. It is more convenient to transform coordinates to a stationary form as shown in figure 3.4 (b) where the shock speed is zero in the new frame and the relative velocities are

$$\hat{u}_{\mathcal{L}} = u_{\mathcal{L}} - S_{\mathcal{L}}, \;\; \hat{u}^\star = u^\star - S_{\mathcal{L}}. \tag{3.8}$$

In chapter 2 we have proved that our system is strictly hyperbolic. Thus if $\mathbb{U}$ is a piecewise weak solution of (3.1), then $\mathbb{U}$ satisfies the Rankine–Hugoniot jump condition

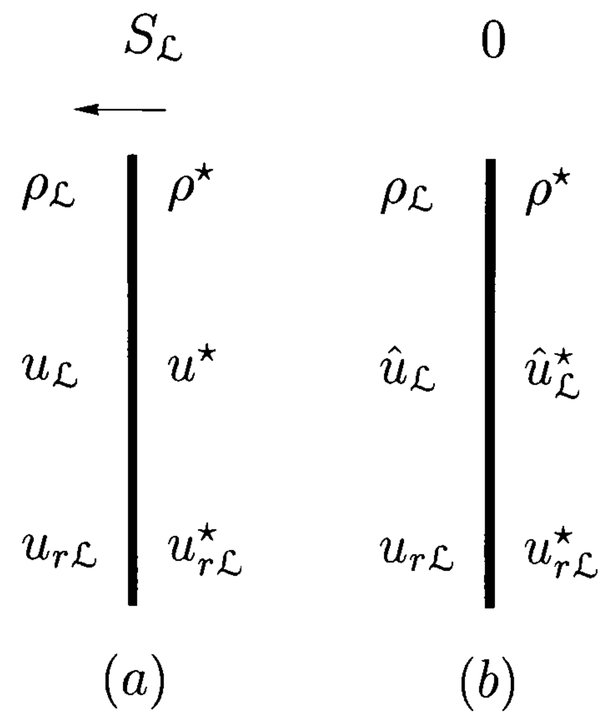

Figure 3.4: Left wave is a shock wave of speed $S_{\mathcal{L}}$: (a) stationary frame, shock speed is $S_{\mathcal{L}}$. (b) frame of reference moving with speed $S_{\mathcal{L}}$, shock speed is zero.

$$S\Big[\,\mathbb{U}\,\Big] = \Big[\,\mathbb{F}(\mathbb{U})\Big], \tag{3.9}$$

where S is the shock speed and $[\cdot]$ represent the jump across the discontinuity. The jump condition across a left shock wave can be written as

$$S_{\mathcal{L}}(\rho_{\mathcal{L}} - \rho^\star) = (\rho_{\mathcal{L}} u_{\mathcal{L}} - \rho^\star u^\star), \tag{3.10}$$

$$S_{\mathcal{L}}(\rho_{\mathcal{L}} u_{\mathcal{L}} - \rho^\star u^\star) = \rho_{\mathcal{L}} u_{\mathcal{L}}^2 - \rho^\star u^{2\star} + \mathcal{P}_{\mathcal{L}} - \mathcal{P}^\star + \Big[\,\rho\, c(1-c) u_r^2\Big], \tag{3.11}$$

$$S_{\mathcal{L}}(u_{r\mathcal{L}} - u^\star_{r\mathcal{L}}) = u u_{r\mathcal{L}} - u^\star u^\star_{r\mathcal{L}} + \psi(\mathcal{P}_{\mathcal{L}}) - \psi(\mathcal{P}^\star) + \left[\frac{1-2c}{2} u_r^2\right]. \tag{3.12}$$

Application of the Rankine–Hugoniot conditions in the new frame in which the shock speed is zero gives

$$\rho_{\mathcal{L}} \hat{u}_{\mathcal{L}} = \rho^\star \hat{u}^\star, \tag{3.13}$$

$$\rho_{\mathcal{L}} \hat{u}_{\mathcal{L}}^2 + \mathcal{P}_{\mathcal{L}} = \rho^\star \hat{u}^{2\star} + \mathcal{P}^\star, \tag{3.14}$$

$$\hat{u}_{\mathcal{L}} u_{r\mathcal{L}} + \psi(\mathcal{P}_{\mathcal{L}}) = \hat{u}^\star u^\star_{r\mathcal{L}} + \psi(\mathcal{P}^\star). \tag{3.15}$$

We now introduce the mixture mass flux $Q_{\mathcal{L}}$, which in view of (3.13) may be written as

$$Q_{\mathcal{L}} \equiv \rho_{\mathcal{L}} \hat{u}_{\mathcal{L}} = \rho^\star \hat{u}^\star. \tag{3.16}$$

From equation (3.14) we write

$$(\rho_{\mathcal{L}}\hat{u}_{\mathcal{L}})\hat{u}_{\mathcal{L}} + \mathcal{P}_{\mathcal{L}} = (\rho^{\star}\hat{u}^{\star})\hat{u}^{\star} + \mathcal{P}^{\star}. \tag{3.17}$$

Use of equation (3.16) and solving for $Q_{\mathcal{L}}$ gives

$$Q_{\mathcal{L}} = -\frac{\mathcal{P}^{\star} - \mathcal{P}_{\mathcal{L}}}{\hat{u}^{\star} - \hat{u}_{\mathcal{L}}}. \tag{3.18}$$

In view of equation (3.8), equation (3.18) becomes

$$Q_{\mathcal{L}} = -\frac{\mathcal{P}^{\star} - \mathcal{P}_{\mathcal{L}}}{u^{\star} - u_{\mathcal{L}}}, \tag{3.19}$$

from which we obtain

$$u^{\star} = u_{\mathcal{L}} - \frac{\mathcal{P}^{\star} - \mathcal{P}_{\mathcal{L}}}{Q_{\mathcal{L}}}. \tag{3.20}$$

The value of $\hat{u}^{\star}$ and $\hat{u}_{\mathcal{L}}$ from equations (3.16)–(3.18) gives

$$Q_{\mathcal{L}}^2 = \left(\rho^{\star}\rho_{\mathcal{L}}\ \frac{\mathcal{P}^{\star} - \mathcal{P}_{\mathcal{L}}}{\rho^{\star} - \rho_{\mathcal{L}}}\right). \tag{3.21}$$

Substituting equation (3.21) into equation (3.20) reduces equation (3.20) to

$$u^{\star} = u_{\mathcal{L}} - \mathcal{F}_{\mathcal{L}}(\rho^{\star}, \mathbb{W}_{\mathcal{L}}), \tag{3.22}$$

with

$$\mathcal{F}_{\mathcal{L}}(\rho^{\star}, \mathbb{W}_{\mathcal{L}}) = (\rho^{\star} - \rho_{\mathcal{L}})\left[\frac{\mathcal{B}_{\mathcal{L}}}{\mathcal{A}_{\mathcal{L}}(\rho^{\star} - \rho_{\mathcal{L}})}\right]^{\frac{1}{2}}, \tag{3.23}$$

and

$$\mathcal{A}_{\mathcal{L}} = \frac{\rho^{\star}}{\rho_{\mathcal{L}}},\ \mathcal{B}_{\mathcal{L}} = \frac{\mathcal{P}^{\star} - \mathcal{P}_{\mathcal{L}}}{\rho_{\mathcal{L}}^2}. \tag{3.24}$$

This is the required expression for $\mathcal{F}_{\mathcal{L}}$ for the case in which the left wave is a shock wave.

Next we find the jump relative velocity across a left shock wave. We can write (3.13) and (3.15) as

$$S_{\mathcal{L}}(\rho^{\star} - \rho_{\mathcal{L}}) = (\rho^{\star}u^{\star} - \rho_{\mathcal{L}}u_{\mathcal{L}}), \tag{3.25}$$

$$S_{\mathcal{L}}(u^{\star}_{r\mathcal{L}} - u_{r\mathcal{L}}) = u^{\star}u^{\star}_{r\mathcal{L}} - u_{\mathcal{L}}u_{r\mathcal{L}} + \psi(\mathcal{P}^{\star}) - \psi(\mathcal{P}_{\mathcal{L}}). \tag{3.26}$$

From equation (3.25)–(3.26) we find

$$(\rho_{\mathcal{L}}u^{\star}_{r\mathcal{L}} - \rho^{\star}u_{r\mathcal{L}})(u^{\star} - u_{\mathcal{L}}) = (\rho^{\star} - \rho_{\mathcal{L}})(\psi(\mathcal{P}^{\star}) - \psi(\mathcal{P}_{\mathcal{L}})). \tag{3.27}$$

Substituting the value of $(u^{\star} - u_{\mathcal{L}})$ from equation (3.20) we obtain

$$u^{\star}_{r\mathcal{L}} = \mathcal{A}_{\mathcal{L}}u_{r\mathcal{L}} - (\psi(\mathcal{P}^{\star}) - \psi(\mathcal{P}_{\mathcal{L}}))\left[\frac{\mathcal{A}_{\mathcal{L}}}{\rho^2_{\mathcal{L}}}\,\frac{\rho^{\star} - \rho_{\mathcal{L}}}{\mathcal{B}_{\mathcal{L}}}\right]^{\frac{1}{2}}, \tag{3.28}$$

where $\psi(\mathcal{P})$ can be derived from equation (2.12) and $\mathcal{A}_{\mathcal{L}}$, $\mathcal{B}_{\mathcal{L}}$ are given by equation (3.24).

3.2.2 Function $\mathcal{F}_{\mathcal{L}}$ for a Left Rarefaction

Here we derive an expression for the function $\mathcal{F}_{\mathcal{L}}$ for the case in which the left wave is a rarefaction wave as shown in figure 3.5. First, let us demonstrate the use of generalised Riemann invariants for the case of the eigenvector $\mathcal{K}^1(\mathbb{U})$. This will help us to connect the unknown state $\mathbb{W}^{\star}_{\mathcal{L}}$ to the left data state $\mathbb{W}_{\mathcal{L}}$. Using the eigenstructure (2.39), we obtain

$$\frac{d\mathcal{P}}{\rho a_m} = \frac{du}{-1} = -\rho_{21}\,\frac{du_r}{\rho}. \tag{3.29}$$

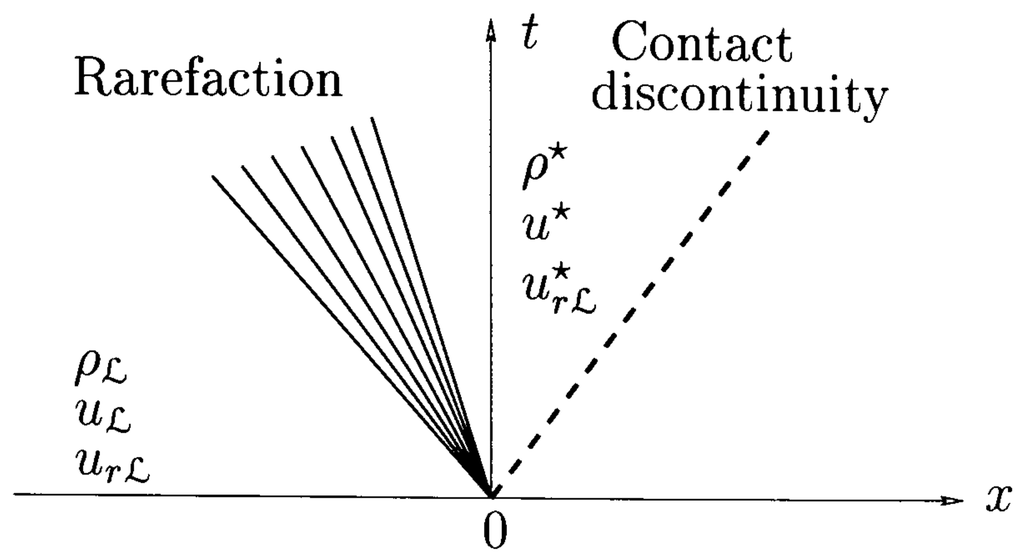

Figure 3.5: Left wave is a rarefaction wave that connects the data state $\mathbb{W}_{\mathcal{L}}$ with unknown state $\mathbb{W}^\star_{\mathcal{L}}$ in the star region to the left of the contact discontinuity.

Manipulating of these quantities gives us

$$\mathbb{I}_{\mathcal{L}}(\rho, \rho u) = u + \int^{\mathcal{P}} \frac{1}{\rho a_m}\, d\mathcal{P} = \textbf{constant}, \tag{3.30}$$

$$\mathbb{I}_{\mathcal{L}}(\rho, u_r) = u_r + \int^{\mathcal{P}} \frac{1}{\rho_{21} a_m}\, d\mathcal{P} = \textbf{constant}, \tag{3.31}$$

$$\mathbb{I}_{\mathcal{L}}(\rho u, u_r) = u_r - \frac{\rho u}{\rho_{21}} = \textbf{constant}. \tag{3.32}$$

Now we evaluate the integrals in equation (3.30) and equation (3.31). Since the entropy is constant across $\mathcal{K}^1$, we may use the isentropic laws for the mixture and for the vapour phase, respectively

$$\mathcal{P} = \mathfrak{K}\rho^\gamma, \tag{3.33}$$

$$\mathcal{P} = k_2 \rho_2^\gamma, \tag{3.34}$$

with the constants $\mathfrak{K}$, k_2 evaluated at the appropriate data state.
As the mixture speed of sound is a function of ρ we can evaluate the integral term exactly as

$$\int^{\mathcal{P}} \frac{1}{\rho a_m} d\mathcal{P} = \frac{2}{\gamma - 1}\, a_m. \tag{3.35}$$

Therefore equation (3.30) becomes

$$\mathbb{I}_{\mathcal{L}}(\rho, \rho u) = u + \frac{2}{\gamma - 1}\, a_m = \textbf{constant}. \tag{3.36}$$

The integral in equation (3.31) is

$$\int^{\mathcal{P}} \frac{1}{\rho_{21} a_m}\, d\mathcal{P} = \frac{2}{\gamma + 1}\left(\mathfrak{C}\frac{\gamma + 1}{\gamma - 1} - \frac{\rho}{\rho_1}\right)\, a_m = \textbf{constant}, \tag{3.37}$$

where

$$\mathfrak{C} = \left(\frac{k_2}{\mathfrak{K}}\right)^{\frac{1}{\gamma}}. \tag{3.38}$$

Thus equation (3.31) becomes

$$\mathbb{I}_{\mathcal{L}}(\rho, u_r) = u_r + \frac{2}{\gamma + 1}\left(\mathfrak{C}\frac{\gamma + 1}{\gamma - 1} - \frac{\rho}{\rho_1}\right)\, a_m = \textbf{constant}. \tag{3.39}$$

Next we derive an expression for $\mathcal{F}_{\mathcal{L}}$ for the case in which the left wave is a rarefaction wave. Evaluating the constant on the left data state equation (3.36) we write

$$u_{\mathcal{L}} + \frac{2}{\gamma - 1}\, a_{m\mathcal{L}} = u^{\star} + \frac{2}{\gamma - 1}\, a_m^{\star}, \tag{3.40}$$

where $a_{m\mathcal{L}}$ and $a_m^{\star}$ denote the mixture speeds of sound on the left and star states bounding the left rarefaction wave.

From equation (3.33) we can write

$$a_m^{\star} = a_{m\mathcal{L}}\left(\frac{\rho^{\star}}{\rho_{\mathcal{L}}}\right)^{\frac{\gamma - 1}{2}}, \tag{3.41}$$

and equation (3.40) leads to

$$u^{\star} = u_{\mathcal{L}} - \mathcal{F}_{\mathcal{L}}(\rho^{\star}, \mathbb{W}_{\mathcal{L}}), \tag{3.42}$$

where

$$\mathcal{F}_{\mathcal{L}}(\rho^\star, \mathbb{W}_{\mathcal{L}}) = \frac{2}{\gamma - 1}\, a_{m\mathcal{L}} \left[\left(\frac{\rho^\star}{\rho_{\mathcal{L}}} \right)^{\frac{\gamma-1}{2}} - 1 \right]. \tag{3.43}$$

Thus, we have obtained the function $\mathcal{F}_{\mathcal{L}}$ for the case in which the left wave is a rarefaction wave.

Next we evaluate the constant in (3.39)

$$u_{r\mathcal{L}} + \frac{2}{\gamma+1}\left[\mathcal{C}\, \frac{\gamma+1}{\gamma-1} - \frac{\rho_{\mathcal{L}}}{\rho_1} \right] a_{m\mathcal{L}} = u^\star_{r\mathcal{L}} + \frac{2}{\gamma+1}\left[\mathcal{C}\, \frac{\gamma+1}{\gamma-1} - \frac{\rho^\star}{\rho_1} \right] a^\star_m. \tag{3.44}$$

Solving these two equations simultaneously for $u^\star_{r\mathcal{L}}$ and $a^\star_m$ leads to the relative velocity solution in the star region

$$u^\star_{r\mathcal{L}} = u_{r\mathcal{L}} - \frac{2}{\gamma+1}\left\{ \mathcal{C}\, \frac{\gamma+1}{\gamma-1}\left[\left(\frac{\rho^\star}{\rho_{\mathcal{L}}} \right)^{\frac{\gamma-1}{2}} - 1 \right] + \frac{\rho^\star}{\rho_1}\left[\frac{\rho_{\mathcal{L}}}{\rho^\star} - \left(\frac{\rho_{\mathcal{L}}}{\rho^\star} \right)^{\frac{\gamma-1}{2}} \right] \right\} a_{m\mathcal{L}}. \tag{3.45}$$

3.2.3 Function $\mathcal{F}_{\mathcal{R}}$ for a Right Shock

Now we assume the right wave is a shock wave travelling with speed $S_{\mathcal{R}}$, pre–shock values $\rho_{\mathcal{R}}$, $u_{\mathcal{R}}$, $u_{r\mathcal{R}}$ and post–shock values $\rho^\star$, $u^\star$, $u^\star_{r\mathcal{R}}$. As for the left shock case the analysis here is carried out in a similar manner. Thus we transform the equations to a frame of reference moving with the shock speed $S_{\mathcal{R}}$. In the transformed frame moving with the shock, the shock speed is zero and the relative velocities are

$$\hat{u}_{\mathcal{R}} = u_{\mathcal{R}} - S_{\mathcal{R}}, \;\; \hat{u}^\star = u^\star - S_{\mathcal{R}}. \tag{3.46}$$

The jump condition across a right shock wave can be written as

$$S_{\mathcal{R}}(\rho^\star - \rho_{\mathcal{R}}) = (\rho^\star u^\star - \rho_{\mathcal{R}} u_{\mathcal{R}}), \tag{3.47}$$

$$S_{\mathcal{R}}(\rho^\star u^\star - \rho_{\mathcal{R}} u_{\mathcal{R}}) = \rho^\star u^{2\star} - \rho_{\mathcal{R}} u^2_{\mathcal{R}} + \mathcal{P}^\star - \mathcal{P}_{\mathcal{R}} + \left[\rho\, c(1-c) u_r^2 \right], \tag{3.48}$$

$$S_{\mathcal{R}}(u^\star_{r\mathcal{R}} - u_{r\mathcal{R}}) = u^\star u^\star_{r\mathcal{R}} - u u_{r\mathcal{R}} + \psi(\mathcal{P}^\star) - \psi(\mathcal{P}_{\mathcal{R}}) + \left[\frac{1-2c}{2} u_r^2 \right]. \tag{3.49}$$

Then the Rankine–Hugoniot conditions in the transformed frame of reference give

$$\rho^\star \hat{u}^\star = \rho_\mathcal{R} \hat{u}_\mathcal{R}, \tag{3.50}$$

$$\rho^\star \hat{u}^{2\star} + \mathcal{P}^\star = \rho_\mathcal{R} \hat{u}_\mathcal{R}^2 + \mathcal{P}_\mathcal{R}, \tag{3.51}$$

$$\hat{u}^\star u_{r\mathcal{R}}^\star + \psi(\mathcal{P}^\star) = \hat{u}_\mathcal{R} u_{r\mathcal{R}} + \psi(\mathcal{P}_\mathcal{R}). \tag{3.52}$$

Defining the mixture mass flux $Q_\mathcal{R}$ as

$$Q_\mathcal{R} \equiv -\rho_\mathcal{R} \hat{u}_\mathcal{R} = -\rho^\star \hat{u}^\star, \tag{3.53}$$

then, with some algebraic manipulation similar to those for a left shock we derive the following expression for the mixture mass flux

$$Q_\mathcal{R} = \left(\rho^\star \rho_\mathcal{R} \, \frac{\mathcal{P}^\star - \mathcal{P}_\mathcal{R}}{\rho^\star - \rho_\mathcal{R}} \right)^{\frac{1}{2}}. \tag{3.54}$$

Therefore, the mixture velocity in the star region takes the following form

$$u^\star = u_\mathcal{R} + \mathcal{F}_\mathcal{R}(\rho^\star, \mathbb{W}_\mathcal{R}), \tag{3.55}$$

with

$$\mathcal{F}_\mathcal{R}(\rho^\star, \mathbb{W}_\mathcal{R}) = (\rho^\star - \rho_\mathcal{R}) \left[\frac{\mathcal{B}_\mathcal{R}}{\mathcal{A}_\mathcal{R}(\rho^\star - \rho_\mathcal{R})} \right]^{\frac{1}{2}}, \tag{3.56}$$

and

$$\mathcal{A}_\mathcal{R} = \frac{\rho^\star}{\rho_\mathcal{R}}, \; \mathcal{B}_\mathcal{R} = \frac{\mathcal{P}^\star - \mathcal{P}_\mathcal{R}}{\rho_\mathcal{R}^2}, \tag{3.57}$$

which is the required expression for $\mathcal{F}_\mathcal{R}$ for the case in which the right wave is a shock wave.

Finally, we derive the jump relative velocity across a right shock wave. From (3.46),

(3.50) and (3.52) we find that

$$(\rho_{\mathcal{R}} u^{\star}_{r\mathcal{R}} - \rho^{\star} u_{r\mathcal{R}})(u^{\star} - u_{\mathcal{R}}) = (\rho^{\star} - \rho_{\mathcal{R}})(\psi(\mathcal{P}^{\star}) - \psi(\mathcal{P}_{\mathcal{R}})), \tag{3.58}$$

and using (3.55) in (3.58) gives

$$u^{\star}_{r\mathcal{R}} = \mathcal{A}_{\mathcal{R}} u_{r\mathcal{R}} + (\psi(\mathcal{P}^{\star}) - \psi(\mathcal{P}_{\mathcal{R}})) \left[\frac{\mathcal{A}_{\mathcal{R}}}{\rho^2_{\mathcal{R}}} \frac{\rho^{\star} - \rho_{\mathcal{R}}}{\mathcal{B}_{\mathcal{R}}} \right]^{\frac{1}{2}}. \tag{3.59}$$

3.2.4 Function $\mathcal{F}_{\mathcal{R}}$ for a Right Rarefaction

For the case of a right rarefaction wave we find an expression for the function $\mathcal{F}_{\mathcal{R}}$ to connect the unknown state $\mathbb{W}^{\star}_{\mathcal{R}}$ to the state $\mathbb{W}_{\mathcal{R}}$ using the isentropic relations and generalised Riemann invariants. The derivation is similar to the case of a left rarefaction. The generalised Riemann invariant for the right rarefaction wave are found to be

$$\mathbb{I}_{\mathcal{R}}(\rho, \rho u) = u - \frac{2}{\gamma - 1} a_m = \textbf{constant}, \tag{3.60}$$

$$\mathbb{I}_{\mathcal{R}}(\rho, u_r) = u_r - \frac{2}{\gamma + 1} \left(\mathcal{C} \frac{\gamma + 1}{\gamma - 1} - \frac{\rho}{\rho_1} \right) a_m = \textbf{constant}. \tag{3.61}$$

Evaluating the constant on the right data state we write (3.60) as

$$u_{\mathcal{R}} - \frac{2}{\gamma - 1} a_{m\mathcal{R}} = u^{\star} - \frac{2}{\gamma - 1} a^{\star}_m, \tag{3.62}$$

where $a^{\star}_m$ and $a_{m\mathcal{R}}$ denote the mixture speed of sound on the star states and right data bounding the right rarefaction wave.

Using the isentropic law (3.33) to obtain

$$a^{\star}_m = a_{m\mathcal{R}} \left(\frac{\rho^{\star}}{\rho_{\mathcal{R}}} \right)^{\frac{\gamma - 1}{2}}, \tag{3.63}$$

substitution of $a_m^\star$ from (3.63) into (3.62) leads to

$$u^\star = u_{\mathcal{R}} + \mathcal{F}_{\mathcal{R}}(\rho^\star, \mathbb{W}_{\mathcal{R}}), \tag{3.64}$$

with

$$\mathcal{F}_{\mathcal{R}} = \frac{2}{\gamma - 1}\, a_{m\mathcal{R}} \left[(\frac{\rho^\star}{\rho_{\mathcal{R}}})^{\frac{\gamma-1}{2}} - 1 \right]. \tag{3.65}$$

This is the required function $\mathcal{F}_{\mathcal{R}}$ for the case in which the right wave is a rarefaction wave.

To find the relative velocity in the star region, we evaluate the constant in (3.61) at the right data state as

$$u_{r\mathcal{R}}^\star - \frac{2}{\gamma+1}\left(\mathcal{C}\frac{\gamma+1}{\gamma-1} - \frac{\rho^\star}{\rho_1} \right) a_m^\star = u_{r\mathcal{R}} - \frac{2}{\gamma+1}\left(\mathcal{C}\frac{\gamma+1}{\gamma-1} - \frac{\rho_{\mathcal{R}}}{\rho_1} \right) a_{m\mathcal{R}}, \tag{3.66}$$

thus solving for $u_{r\mathcal{R}}^\star$ gives

$$u_{r\mathcal{R}}^\star = u_{r\mathcal{R}} + \frac{2}{\gamma+1}\left\{ \mathcal{C}\,\frac{\gamma+1}{\gamma-1}\left[\left(\frac{\rho^\star}{\rho_{\mathcal{R}}}\right)^{\frac{\gamma-1}{2}} - 1 \right] + \frac{\rho^\star}{\rho_1}\left[\frac{\rho_{\mathcal{R}}}{\rho^\star} - \left(\frac{\rho^\star}{\rho_{\mathcal{R}}}\right)^{\frac{\gamma-1}{2}} \right] \right\} a_{m\mathcal{R}}. \tag{3.67}$$

3.3 The Middle–Wave

We now study the middle–wave "slip line" connecting a state $\mathbb{W}_{\mathcal{L}}^\star = (\rho^\star, u^\star, u_{r\mathcal{L}}^\star)$ on the left hand of the discontinuity to the state $\mathbb{W}_{\mathcal{R}}^\star = (\rho^\star, u^\star, u_{r\mathcal{R}}^\star)$ on the right hand side. As seen in chapter 2 the second characteristic field is neither GNL nor LD since $\nabla\lambda_2(\mathbb{U}) \cdot \mathcal{K}^2(\mathbb{U})$ may change sign. As we shall see the middle–wave present in the solution is a contact wave up to first order in η. In order to identify the type of the middle–wave we make the following proposition.

Proposition 1 Along the middle–wave curve, the pressure and the mixture velocity are constant up to first order in η

$$\mathcal{O}^2(\mathbb{W}^\star) = \left\{ \mathbb{W} \in \Omega^\star; \mathcal{P} = \mathcal{P}^\star, u = u^\star \right\}.$$

Proof 1 For a proof of the proposition we distinguish between two cases for the middle–wave. The first case is a middle–rarefaction wave and the second is a middle–shock wave. We start with the middle–shock wave.

3.3.1 The Middle–Shock Wave

We look for the third solution of the Rankine–Hugoniot jump conditions

$$S\,[\rho] = [\rho u]\,, \tag{3.68}$$

$$S\,[\rho u] = \left[\rho u^2\right] + \left[\rho c(1-c)u_r^2\right] + [\mathcal{P}]\,, \tag{3.69}$$

$$S\,[u_r] = [u u_r] + \left[\frac{1-2c}{2}\,u_r^2\right] + \Big[\,\psi(\mathcal{P})\Big]\,. \tag{3.70}$$

At zero order in η equation (3.70) gives

$$\Big[\,\psi(\mathcal{P})\Big] = 0, \text{ or } \mathcal{P} = \mathcal{P}^\star. \tag{3.71}$$

Equation (3.69) gives

$$S = [u]\,. \tag{3.72}$$

Equation (3.68) and equation (3.69) leads to

$$u = u^\star \;\text{ and }\; S \equiv S^\star = u^\star. \tag{3.73}$$

Now we can write the solution in the following form

$$u = u^\star + u^1\eta + \mathcal{O}(\eta^2), \tag{3.74}$$

$$\mathcal{P} = \mathcal{P}^\star + \mathcal{P}^1\eta + \mathcal{P}^2\eta^2 + \mathcal{O}(\eta^3), \tag{3.75}$$

$$S = S^\star + S^1\eta + \mathcal{O}(\eta^2). \tag{3.76}$$

Up to first order in η equation (3.74) can be written as

$$\rho u - \rho^\star u^\star = \rho^1 u^\star \eta + \rho^\star u^1 \eta, \tag{3.77}$$

and using (3.73) we find that

$$\rho - \rho^\star = \rho^1 \eta. \tag{3.78}$$

Equations (3.77) and (3.78) into (3.68) give

$$S\rho^1 = \rho^1 u^\star + \rho^\star u^1, \tag{3.79}$$

which leads to

$$u^1 = 0, \text{ and } S = u^\star. \tag{3.80}$$

Equations (3.68)–(3.69) acquire the form

$$S^2(\rho - \rho^\star) = \rho u^2 - \rho^\star {u^\star}^2 + \mathcal{P} - \mathcal{P}^\star. \tag{3.81}$$

Equations (3.75) and (3.78) together with (3.81) lead to

$$S^2 \rho^1 = \rho^1 {u^\star}^2 + \rho {u^1}^2 + \mathcal{P}^1. \tag{3.82}$$

Using of equations (3.79) and (3.80) we find that

$$\mathcal{P}^1 = 0. \tag{3.83}$$

Thus the pressure and the mixture velocity remain constant up to first order in η.

3.3.2 The Middle–Rarefaction Wave

The generalised Riemann invariant across the λ_2–wave is

$$\frac{d\mathcal{P}}{-2\rho c(1-c)u_r} = \frac{du}{0} = \frac{du_r}{1}. \tag{3.84}$$

Manipulation of these quantities gives us

$$\mathbb{I}(\rho, u) = u = \textbf{constant}, \tag{3.85}$$

$$\mathbb{I}(\rho, u_r) = u_r^2 + \int^{\mathcal{P}} \frac{1}{\rho c(1-c)}\, d\mathcal{P} = \textbf{constant}. \tag{3.86}$$

Using the Riemann invariant, equation (3.86) reveals a second order dependency in η as follows

$$\frac{u_r^2}{a_m^2} = \int^{\rho} \frac{a_m^2}{\rho c(1-c)} \frac{d\rho}{a_m^2} = \mathcal{O}(\eta^2), \tag{3.87}$$

and

$$u_{\mathcal{R}}^\star - u_{\mathcal{L}}^\star = \mathcal{O}(\eta^2). \tag{3.88}$$

Thus

$$\mathcal{P}_{\mathcal{L}}^\star = \mathcal{P}_{\mathcal{R}}^\star, \tag{3.89}$$

and

$$u_{\mathcal{L}}^\star = u_{\mathcal{R}}^\star, \tag{3.90}$$

up to first order in η.

In view of the above proposition, we have now established the existence of the contact wave in the solution of Riemann problem for the simplified two–fluid model up to first

order in η. This contact wave is a discontinuous wave across which both pressure (or mixture density) and mixture velocity are constant up to first order in η, while there is a wave jump in the relative velocity u_r.

3.4 Numerical Solution for the Mixture Density $\rho^\star$

The single, non–linear algebraic equation (3.6) can be solved numerically in the star region to find the unknown mixture density $\rho^\star$ by finding the roots of (3.6) using an iterative technique. Thus the exact solver for the simplified two–fluid model must be understood as an iterative solution to the accuracy provided by the computation.

3.4.1 Behaviour of the Mixture Density Function $\mathcal{F}(\rho)$

The behaviour of $\mathcal{F}(\rho)$ is useful to determine whether the solution for $\rho^\star$ exists, unique and what the best numerical approach is to find its roots. For convenience we summarize the expressions for $\mathcal{F}_\mathcal{L}$ and $\mathcal{F}_\mathcal{R}$, namely

$$\mathcal{F}_\mathfrak{s}(\rho, \mathbb{W}_\mathfrak{s}) = \begin{cases} (\rho - \rho_\mathfrak{s})\left[\frac{\mathcal{B}_\mathfrak{s}}{\mathcal{A}_\mathfrak{s}(\rho-\rho_\mathfrak{s})}\right]^{\frac{1}{2}} & \text{if} \quad \rho > \rho_\mathfrak{s} \quad \text{(Shock)}, \\ \\ \frac{2}{\gamma-1}\left[\left(\frac{\rho}{\rho_\mathfrak{s}}\right)^{\frac{\gamma-1}{2}} - 1\right] a_{m\mathfrak{s}} & \text{if} \quad \rho \leq \rho_\mathfrak{s} \quad \text{(Rarefaction)}, \end{cases} \tag{3.91}$$

where

$$\mathcal{A}_\mathfrak{s} = \frac{\rho}{\rho_\mathfrak{s}}, \ \mathcal{B}_\mathfrak{s} = \frac{\mathcal{P} - \mathcal{P}_\mathfrak{s}}{\rho_\mathfrak{s}^2}, \tag{3.92}$$

and $\mathfrak{s}$ stands for $\mathcal{L}, \mathcal{R}$.

The first derivative of $\mathcal{F}_\mathfrak{s}$ is

$$\mathcal{F}_\mathfrak{s}^{'} = \begin{cases} \frac{1}{2\rho}\left[\frac{\rho_\mathfrak{s}}{\rho-\rho_\mathfrak{s}} + \frac{\gamma\rho^\gamma}{\rho^\gamma-\rho_\mathfrak{s}^\gamma}\right] \mathcal{F}_\mathfrak{s} & \text{if} \quad \rho > \rho_\mathfrak{s} \quad \text{(Shock)}, \\ \\ \frac{a_{m\mathfrak{s}}}{\rho}\left[\left(\frac{\rho}{\rho_\mathfrak{s}}\right)^{\frac{\gamma-1}{2}}\right] & \text{if} \quad \rho \leq \rho_\mathfrak{s} \quad \text{(Rarefaction)}, \end{cases} \tag{3.93}$$

and expressions for the second derivatives are easily found but not given here. However, we note that the mixture density function $\mathcal{F}(\rho)$ is concave down, that is $\mathcal{F}'' < 0$ and $\mathcal{F}'' = \mathcal{F}''_{\mathcal{L}} + \mathcal{F}''_{\mathcal{R}}$. Since $\mathcal{F}' = \mathcal{F}'_{\mathcal{L}} + \mathcal{F}'_{\mathcal{R}}$ and $\mathcal{F}' > 0$, the function $\mathcal{F}(\rho)$ is a monotone increasing function of ρ and concave down as shown in figure 3.6. Thus for appro-

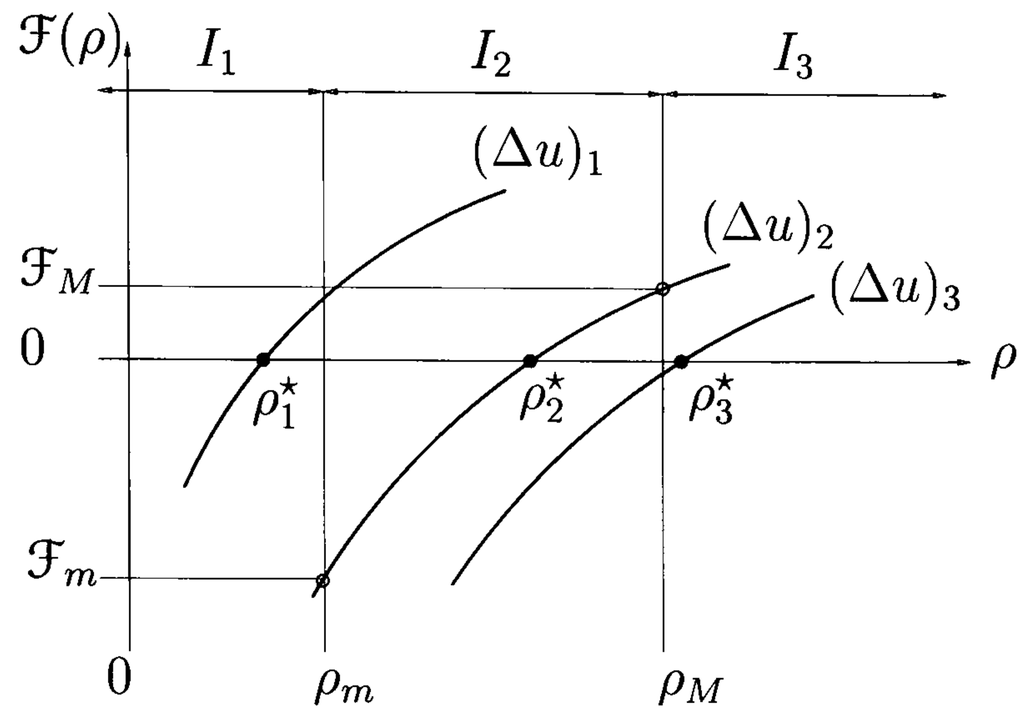

Figure 3.6: Mixture density behaviour in the solution of the Riemann problem for the simplified two–fluid model.

priate combinations of data the equation of $\mathcal{F}(\rho)$ has a unique solution. The mixture density data $\rho_{\mathcal{L}}$, $\rho_{\mathcal{R}}$ and the velocity difference $\Delta u = u_{\mathcal{R}} - u_{\mathcal{L}}$ are the most important parameters of $\mathcal{F}(\rho)$ to determine the roots. Referring to figure 3.6, there are three intervals of physical interest ($\rho^\star > 0$). Within each interval along the $\rho -$ axis the complete wave pattern in the Riemann solution is also determined. These intervals can be identified as

$$\left.\begin{array}{lll} \rho^\star \text{ lies in } I_1 = (0, \rho_{\min}) & \text{if } \mathcal{F}_{\min} > 0 \text{ and } \mathcal{F}_{\max} > 0, \\ \rho^\star \text{ lies in } I_2 = [\rho_{\min}, \rho_{\max}] & \text{if } \mathcal{F}_{\min} \leq 0 \text{ and } \mathcal{F}_{\max} \geq 0, \\ \rho^\star \text{ lies in } I_3 = (\rho_{\max}, \infty) & \text{if } \mathcal{F}_{\min} < 0 \text{ and } \mathcal{F}_{\max} < 0, \end{array}\right\} \tag{3.94}$$

where

$$\begin{aligned} \rho_{\min} &= \min(\rho_{\mathcal{L}}, \rho_{\mathcal{R}}), \quad \mathcal{F}_{\min} = \mathcal{F}(\rho_{\min}), \\ \rho_{\max} &= \max(\rho_{\mathcal{L}}, \rho_{\mathcal{R}}), \quad \mathcal{F}_{\max} = \mathcal{F}(\rho_{\max}). \end{aligned}$$

For a choice such as $(\Delta u)_3$ in figure 3.6 the solution $\rho^\star = \rho_3^\star$ lies in I_3 and $\rho^\star > \rho_{\mathcal{L}}$, $\rho^\star > \rho_{\mathcal{R}}$, thus the solution in this case consists of two–shock waves. For Δu as $(\Delta u)_2$ in figure 3.6 $\rho^\star = \rho_2^\star$ lies in I_2 and hence one wave is a rarefaction and the other one is a shock. If $\Delta u = (\Delta u)_1$ in figure 3.6 the solution $\rho^\star = \rho_1^\star$ lies in I_1 and thus $\rho^\star < \rho_{\mathcal{L}}$, $\rho^\star < \rho_{\mathcal{R}}$, hence the two waves are rarefaction waves.

3.4.2 Iterative Scheme for Finding the Mixture Density

In the previous section we have given the behaviour of $\mathcal{F}(\rho)$ and the availability of its analytical derivative $\mathcal{F}^{'}(\rho)$. Thus we use a Newton–Raphson [105] iteration procedure to find the root of $\mathcal{F}(\rho) = 0$.

Assuming that a guess value ρ_0 for the true solution of $\rho^\star$ is available, since $\mathcal{F}(\rho)$ is a smooth function, we can find an approximate value of $\mathcal{F}(\rho)$ at a neighbouring point $\rho_0 + \delta$ via the Taylor expression [177]

$$\mathcal{F}(\rho_0 + \delta) = \mathcal{F}(\rho_0) + \delta\mathcal{F}^{'}(\rho_0) + \mathcal{O}(\delta^2). \tag{3.95}$$

If the $\rho_0 + \delta$ is a solution of $\mathcal{F}(\rho_0) = 0$ then

$$\mathcal{F}(\rho_0) + \delta\mathcal{F}^{'}(\rho_0) = 0, \tag{3.96}$$

and so the corrected value $\rho_1 = \rho_0 + \delta$ is

$$\rho_1 = \rho_0 - \frac{\mathcal{F}(\rho_0)}{\mathcal{F}^{'}(\rho_0)}. \tag{3.97}$$

The above procedure generalises to

$$\rho_{(\jmath)} = \rho_{(\jmath-1)} - \frac{\mathcal{F}(\rho_{(\jmath-1)})}{\mathcal{F}^{'}(\rho_{(\jmath-1)})}, \tag{3.98}$$

where $\rho_{(\jmath)}$ is the $\jmath$–th iterate.

Now to start the iteration we require a guess value $\rho_{(0)}$ for the mixture density. One

could take the arithmetic mean of data, namely,

$$\rho_0 = \frac{1}{2}(\rho_{\mathcal{L}} + \rho_{\mathcal{R}}), \tag{3.99}$$

which is simple but not very accurate and can increase the number of iterations required for convergence. The initial guess (see chapter 5 for details)

$$\rho^\star = \frac{1}{2}\left\{\rho_{\mathcal{L}}\left[1 + \frac{\mathcal{Z}}{a_{m\mathcal{L}}}(u_{\mathcal{L}} - u^\star)\right]^{\frac{1}{\mathcal{Z}}} + \rho_{\mathcal{R}}\left[1 + \frac{\mathcal{Z}}{a_{m\mathcal{R}}}(u^\star - u_{\mathcal{R}})\right]^{\frac{1}{\mathcal{Z}}}\right\}, \tag{3.100}$$

is found to be very accurate and results from the exact solver (3.6) for the mixture density under the assumption that the two non–linear waves are rarefaction waves. Another two guess values, resulting from the approximation to the solution $\rho^\star$ for the mixture density, are presented in chapter 5.

The iteration (3.98) is stopped whenever the change in the mixture density ρ is smaller than a prescribed tolerance value $\mathcal{TOL}$, that is when

$$\mathcal{CHA} = \frac{\left|\rho^\star_{(\jmath)} - \rho^\star_{(\jmath-1)}\right|}{0.5\left[\rho^\star_{(\jmath)} + \rho^\star_{(\jmath-1)}\right]} < \mathcal{TOL}, \tag{3.101}$$

where the value of $\mathcal{TOL} = 10^{-8}$ was found to be satisfactory.

Having formulated and solved numerically the equation for $\rho^\star$, the solution for $u^\star$ follows directly in terms of $\mathcal{F}(\rho^\star, \mathbb{W}_{\mathcal{L}})$ and $\mathcal{F}(\rho^\star, \mathbb{W}_{\mathcal{R}})$ (see equation (3.7)). The rest of the solution through the complete wave structure then follows by using standard wave relations as we shall see in the next section.

3.5 The Complete Solution

Up to now we have concentrated mainly on the algorithm for computing the mixture density $\rho^\star$, the mixture velocity $u^\star$ and the relative velocities $u^\star_{r\mathcal{L}}$ and $u^\star_{r\mathcal{R}}$ in the star region. These are computed by identifying the types of non–linear waves shown in figure 3.7. Figure 3.7 shows that there are two regions to consider, one to the left of the contact wave $\frac{x}{t} = u^\star$ (dashed line) and one to the right. As we shall see later the

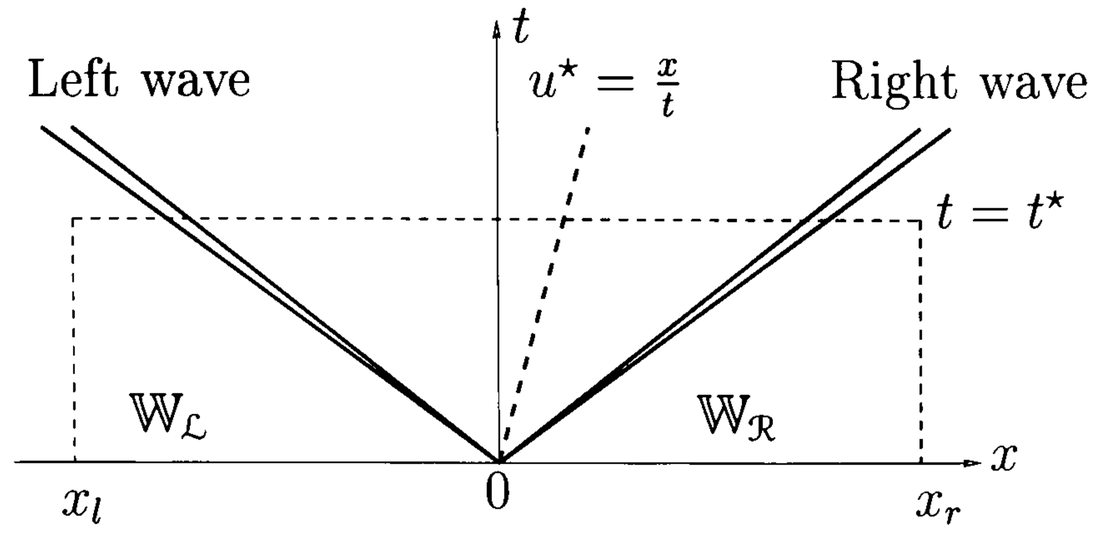

Figure 3.7: Sampling the solution through the complete wave structure at time $t = t^\star$.

type of non–linear left and right waves are determined by comparing $\rho^\star$ with $\rho_\mathcal{L}$ and $\rho_\mathcal{R}$ using the following conditions:

$$\left.\begin{array}{l} \rho^\star > \rho_\mathcal{L} : \text{left wave is a shock wave,} \\ \rho^\star \leq \rho_\mathcal{L} : \text{left wave is a rarefaction wave,} \end{array}\right\} \tag{3.102}$$

and

$$\left.\begin{array}{l} \rho^\star > \rho_\mathcal{R} : \text{right wave is a shock wave,} \\ \rho^\star \leq \rho_\mathcal{R} : \text{right wave is a rarefaction wave.} \end{array}\right\} \tag{3.103}$$

For shock waves we only need to find the mixture density behind the wave and the shock speed. For rarefaction waves we need ρ behind the wave, equations for the head and tail of the wave and the full solution inside the rarefaction fan. Thus there are two cases to consider. The first case has the sampling point (x, t) to the left of the contact discontinuity as illustrated in figure 3.7, with two different possibilities to study. The second case has the sampling point (x, t) to the right of the contact discontinuity. These two cases are investigated separately next.

3.5.1 Left Shock Wave

The left wave is a shock wave if $\rho^\star > \rho_\mathcal{L}$, see (3.103), and from (3.8) it has speed

$$S_\mathcal{L} = u_\mathcal{L} - \hat{u}_\mathcal{L} = u_\mathcal{L} + \frac{Q_\mathcal{L}}{\rho_\mathcal{L}}. \tag{3.104}$$

Using (3.21) we write the shock speed $S_{\mathcal{L}}$ as

$$S_{\mathcal{L}} = u_{\mathcal{L}} - \left[\frac{\rho^\star}{\rho_{\mathcal{L}}}\frac{\mathcal{P}^\star - \mathcal{P}_{\mathcal{L}}}{\rho^\star - \rho_{\mathcal{L}}}\right]^{\frac{1}{2}}. \tag{3.105}$$

This case is shown in figure 3.8 (a). Thus we have completely determined the solution

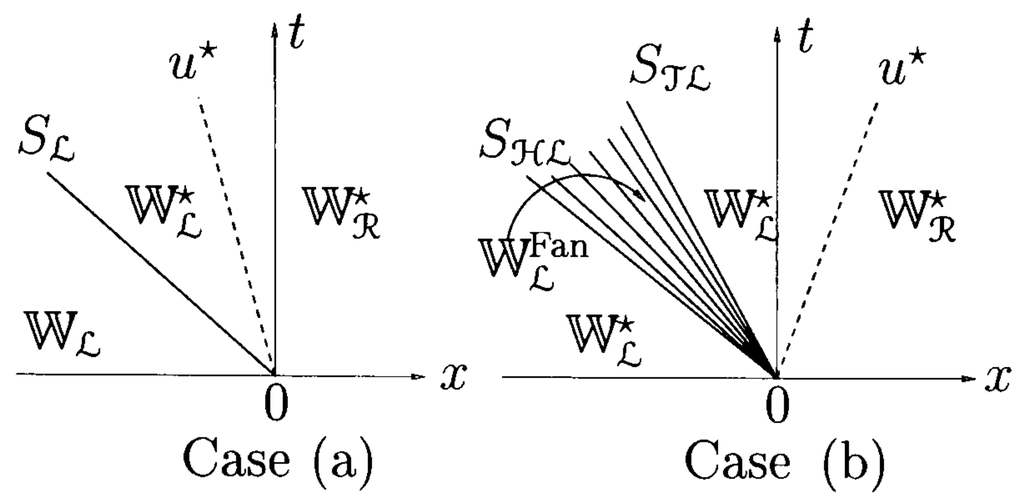

Figure 3.8: Two possible wave configurations at a point to the left of the contact wave: (a) left wave is a shock (b) left wave is a rarefaction wave.

for the entire region to the left of the contact discontinuity in the case of a shock wave.

3.5.2 Left Rarefaction Wave

If $\rho^\star \leq \rho_{\mathcal{L}}$ then the left wave is a rarefaction wave as shown in figure 3.8 (b). The mixture density $\rho^\star$, mixture velocity $u^\star$ and the relative velocity $u^\star_{r\mathcal{L}}$ in the star region are known. Figure 3.8 (b) shows that the rarefaction wave is enclosed by the head and the tail which are the characteristics of speeds given respectively by

$$S_{\mathcal{HL}} = u_{\mathcal{L}} - a_{m\mathcal{L}} + \frac{\rho_{\mathcal{L}}}{\rho_{21\mathcal{L}}}\, c_{\mathcal{L}}\,(1 - c_{\mathcal{L}})\, u_{r\mathcal{L}}, \tag{3.106}$$

$$S_{\mathcal{TL}} = u^\star - a^\star_m + \frac{\rho^\star}{\rho^\star_{21}}\, c^\star\,(1 - c^\star)\, u^\star_{r\mathcal{L}}. \tag{3.107}$$

To find the solution for $\mathbb{W}^{\text{Fan}}_{\mathcal{L}}$ inside the left rarefaction fan we consider a point $\hat{y} = (\hat{x}, \hat{t})$ inside the wave and a characteristic ray joining the origin $(0, 0)$ inside and $\hat{y}$. The slope of the characteristic is

$$\frac{dx}{dt} = u - a_m + \frac{\rho}{\rho_{21}} c(1 - c) u_r = \frac{\hat{x}}{\hat{t}}, \tag{3.108}$$

where u, a_m, ρ, ρ_{21} and u_r are unknown values at $\hat{y}$. Now we use the Riemann invariant given by (3.36) to connect the point $\hat{y}$ to the left data. Thus equations (3.36) and (3.108) give

$$\frac{a_m}{a_{m\mathcal{L}}} = \frac{2}{\gamma+1} + \frac{1}{a_{m\mathcal{L}}}\,(u_{\mathcal{L}} - S)\,\frac{\gamma-1}{\gamma+1} + \frac{\gamma-1}{\gamma+1}\,\frac{\rho}{\rho_{21}}\,\frac{c}{a_{m\mathcal{L}}}\,(1-c)\,u_r. \tag{3.109}$$

By the definition (3.41) of mixture speed of sound and isentropic relation, with $\rho^\star$ replaced by ρ, at point $\tilde{y}$ we obtain

$$\rho = \rho_{\mathcal{L}}\left[\frac{2}{\gamma+1} + \frac{1}{a_{m\mathcal{L}}}\,(u_{\mathcal{L}} - S)\,\frac{\gamma-1}{\gamma+1} + \frac{\gamma-1}{\gamma+1}\,\frac{\rho}{\rho_{21}}\,\frac{c}{a_{m\mathcal{L}}}\,(1-c)\,u_r\right]^{\frac{2}{\gamma-1}}. \tag{3.110}$$

For the mixture velocity we have

$$u = \frac{2}{\gamma+1}\left[S + \frac{\gamma-1}{2}\,u_{\mathcal{L}} + a_{m\mathcal{L}} - \frac{\rho}{\rho_{21}}\,c\,(1-c)\,u_r\right]. \tag{3.111}$$

Finally, using the invariant (3.39) we find the relative velocity between the two phases as

$$\begin{aligned} u_r &= u_{r\mathcal{L}} - \frac{2}{\gamma+1}\left\{\mathcal{C}\,\frac{\gamma+1}{\gamma-1}\left[\left(\frac{\rho}{\rho_{\mathcal{L}}}\right)^{\frac{\gamma-1}{2}} - 1\right]\right. \\ &+ \left.\frac{\rho}{\rho_1}\left[\frac{\rho_{\mathcal{L}}}{\rho} - \left(\frac{\rho}{\rho_{\mathcal{L}}}\right)^{\frac{\gamma-1}{2}}\right]\right\} a_{m\mathcal{L}}. \end{aligned} \tag{3.112}$$

Substituting the value of u_r from (3.112) into (3.110) gives the solution for the mixture density ρ inside left rarefaction fan as

$$\begin{aligned}
\rho &= \rho_{\mathcal{L}}\Bigg\{\Bigg[\frac{2}{\gamma+1}+\frac{1}{a_{m\mathcal{L}}}\,(u_{\mathcal{L}}-S)\,\frac{\gamma-1}{\gamma+1}\Bigg] \\
&+ \frac{2}{\gamma+1}\,c(1-c)\big[\mathcal{C}-\frac{\rho}{\rho_1}\big]\frac{u_{r\mathcal{L}}}{a_{m\mathcal{L}}} \\
&+ \frac{2}{\gamma+1}\,c(1-c)\mathcal{C}\Bigg\{\Bigg[\mathcal{C}+\frac{\rho}{\rho_1}\big[\frac{\rho}{\rho_{\mathcal{L}}}^{\frac{\gamma-1}{2}}-1\big]-\frac{\rho}{\rho_{\mathcal{L}}}^{\frac{\gamma-1}{2}}\Bigg] \\
&+ \frac{\gamma-1}{\gamma+1}\Bigg[\frac{\rho}{\rho_{\mathcal{L}}}^{\frac{\gamma-1}{2}}\big[\frac{\rho}{\rho_{\mathcal{L}}}-\frac{\rho^2}{\rho_{\mathcal{L}}^2}\big]+\frac{\rho_{\mathcal{L}}}{\rho_1}\big[\frac{\rho}{\rho_1}-1\big]\Bigg]\Bigg\}\Bigg\}^{\frac{2}{\gamma-1}}, \qquad (3.113)
\end{aligned}$$

where $\mathcal{C}$ can be found from (3.38).

Equation (3.113) is a non–linear algebraic equation for ρ. Thus, we solve this equation using the Newton–Raphson method. Once ρ is found to a given accuracy, the mixture velocity u and relative velocity u_r follow immediately from equations (3.111)–(3.112).

3.5.3 Right Shock Wave

A right shock wave, see figure 3.9 (a), is identified by the condition $\rho^\star > \rho_{\mathcal{R}}$ with

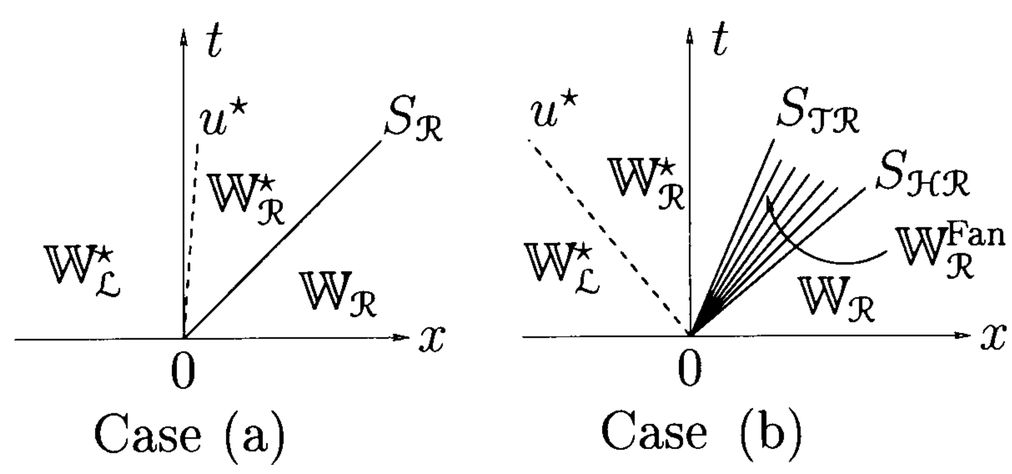

Figure 3.9: Two possible wave configurations to the right of the contact: (a) right wave is a shock wave (b) right wave is a rarefaction wave.

shock speed

$$S_{\mathcal{R}} = u_{\mathcal{R}} + \hat{u}_{\mathcal{R}} = u_{\mathcal{R}} + \frac{Q_{\mathcal{R}}}{\rho_{\mathcal{R}}}. \qquad (3.114)$$

From (3.54), the shock speed $S_{\mathcal{R}}$ can be written explicitly as

$$S_{\mathcal{R}} = u_{\mathcal{R}} + \left[\frac{\rho^\star}{\rho_{\mathcal{R}}}\frac{\mathcal{P}^\star - \mathcal{P}_{\mathcal{R}}}{\rho^\star - \rho_{\mathcal{R}}}\right]^{\frac{1}{2}}. \tag{3.115}$$

3.5.4 Right Rarefaction Wave

If $\rho^\star \leq \rho_{\mathcal{R}}$ then the right wave is a rarefaction wave as shown in figure 3.9 (b). Referring to figure 3.9 (b) we can see that the rarefaction wave is enclosed by the tail and the head which are the characteristics of speeds given respectively by

$$S_{\mathcal{TR}} = u^\star + a_m^\star + \frac{\rho^\star}{\rho_{21}^\star}\, c^\star\,(1 - c^\star)\, u_{r\mathcal{R}}^\star, \tag{3.116}$$

$$S_{\mathcal{HR}} = u_{\mathcal{R}} + a_{m\mathcal{R}} + \frac{\rho_{\mathcal{R}}}{\rho_{21\mathcal{R}}}\, c_{\mathcal{R}}\,(1 - c_{\mathcal{R}})\, u_{r\mathcal{R}}. \tag{3.117}$$

To find the solution for $\mathbb{W}_{\mathcal{R}}^{\text{Fan}}$ inside the right rarefaction fan we follow a similar analysis as the one for the left rarefaction fan . Thus for a point $\hat{y} = (\hat{x}, \hat{t})$ inside the wave and a characteristic ray joining the origin $(0, 0)$ inside and $\hat{y}$, the slope of the characteristic is

$$\frac{dx}{dt} = u + a_m + \frac{\rho}{\rho_{21}} c(1 - c)u_r = \frac{\hat{x}}{\hat{t}}, \tag{3.118}$$

where u, a_m, ρ, ρ_{21} and u_r are known values at $\hat{y}$. Using the Riemann invariant given by (3.64) and (3.65) the mixture density inside the right fan takes the the following form

$$\rho = \rho_{\mathcal{R}}\left[\frac{2}{\gamma+1} + \frac{1}{a_{m\mathcal{R}}}\,(S - u_{\mathcal{R}})\,\frac{\gamma-1}{\gamma+1} + \frac{\gamma-1}{\gamma+1}\,\frac{\rho}{\rho_{21}}\,\frac{c}{a_{m\mathcal{R}}}\,(1-c)\,u_r\right]^{\frac{2}{\gamma-1}}. \tag{3.119}$$

The mixture velocity is

$$u = \frac{2}{\gamma+1}\left[S + \frac{\gamma-1}{2}\,u_{\mathcal{R}} - a_{m\mathcal{R}} - \frac{\rho}{\rho_{21}}\,c\,(1-c)\,u_r\right], \tag{3.120}$$

and the relative velocity between the two phases is

$$
\begin{aligned}
u_r &= u_{r\mathcal{R}} + \frac{2}{\gamma+1}\left\{ \mathcal{C}\,\frac{\gamma+1}{\gamma-1}\left[\left(\frac{\rho}{\rho_{\mathcal{R}}}\right)^{\frac{\gamma-1}{2}} - 1\right]\right. \\
&+ \left.\frac{\rho}{\rho_1}\left[\frac{\rho_{\mathcal{R}}}{\rho} - \left(\frac{\rho}{\rho_{\mathcal{R}}}\right)^{\frac{\gamma-1}{2}}\right]\right\} a_{m\mathcal{R}}. \qquad (3.121)
\end{aligned}
$$

The solution inside the right rarefaction fan is obtained using the Newton–Raphson method for ρ from which we find u and u_r as described for the left rarefaction fan.

3.6 Sampling the Solution

So far we have developed a solver to find the exact solution $\mathbb{W}(x,t)$ of the complete wave structure of the Riemann problem at any point (x,t), where $t > 0$ and x lies in the domain $[x_l, x_r]$ with $x_l < 0 < x_r$ as shown in figure 3.7. Here we provide a sampling procedure which should be of practical use for programming the exact Riemann solver and utilizing the solution in numerical schemes. For a given time $t > 0$, the solution $\mathbb{W}(x,t)$ is a function of the space x alone and gives a profile at time t. As the solution $\mathbb{W}(x,t)$ is a similarity solution we perform the sampling in terms of the speed

$$S = \frac{x}{t}, \qquad (3.122)$$

and using the vector of primitive variables

$$\mathbb{W} = \left[\rho, u, u_r\right]^T, \qquad (3.123)$$

the solution appears as depicted in figure 3.7 with the character of the left and right waves determined from the ratios $\frac{\rho^\star}{\rho_{\mathcal{L}}}$ and $\frac{\rho^\star}{\rho_{\mathcal{R}}}$ respectively. In sampling the complete solution the sampling strategy divides the wave patterns into two subregions (see figure 3.7), to the left of contact wave $u^\star = \frac{dx}{dt}$ and to the right of $u^\star = \frac{dx}{dt}$. Thus there are two cases to consider in sampling the complete solution. The first case is when

the sampling point is to the left of the contact wave and the second case is when it is to the right of the contact wave.

3.6.1 Sampling Point is to the Left of the Contact Wave

The solution on the left side of the contact wave $S = \frac{x}{t} \leq u^\star$ is determined by the character of the left wave as shown in figure 3.8. There are two possible cases, if $\rho^\star > \rho_{\mathcal{L}}$ the left wave is a shock wave and the complete solution on the left side of the contact wave is

$$\mathbb{W}(x,t) = \begin{cases} \mathbb{W}^\star_{\mathcal{L}} & \text{if} \quad S_{\mathcal{L}} \leq \frac{x}{t} \leq u^\star, \\ \mathbb{W}_{\mathcal{L}} & \text{if} \quad S_{\mathcal{L}} \geq \frac{x}{t}, \end{cases} \tag{3.124}$$

where $S_{\mathcal{L}}$ is the speed of the left shock wave given by (3.105), $u^\star_{r\mathcal{L}}$ given by (3.28) and $\mathbb{W}_{\mathcal{L}}$ is the left data state.

Now if $\rho^\star \leq \rho_{\mathcal{L}}$ then the left wave is a rarefaction wave and the solution on the left of the contact wave is

$$\mathbb{W}(x,t) = \begin{cases} \mathbb{W}_{\mathcal{L}} & \text{if} \quad \frac{x}{t} \leq S_{\mathcal{HL}}, \\ \mathbb{W}^{\text{Fan}}_{\mathcal{L}} & \text{if} \quad S_{\mathcal{HL}} \leq \frac{x}{t} \leq S_{\mathcal{TL}}, \\ \mathbb{W}^\star_{\mathcal{L}} & \text{if} \quad S_{\mathcal{TL}} \leq \frac{x}{t} \leq u^\star, \end{cases} \tag{3.125}$$

where the characteristic speeds $S_{\mathcal{HL}}$ and $S_{\mathcal{TL}}$ are the speeds of the head and the tail of the rarefaction as described in section 3.5.2.

3.6.2 Sampling Point is to the Right of the Contact Wave

For right side sampling there are two possible wave configurations as shown in figure 3.9. In the case that the right wave is a shock wave, $\rho^\star > \rho_{\mathcal{R}}$, then the complete solution of the right hand side of the contact wave is given by

$$\mathbb{W}(x,t) = \begin{cases} \mathbb{W}^\star_{\mathcal{R}} & \text{if} \quad u^\star \leq \frac{x}{t} \leq S_{\mathcal{R}}, \\ \mathbb{W}_{\mathcal{R}} & \text{if} \quad S_{\mathcal{R}} \leq \frac{x}{t}, \end{cases} \tag{3.126}$$

where $S_{\mathcal{R}}$ is the shock speed given by (3.115).

If $\rho^\star \leq \rho_{\mathcal{R}}$ then the right wave is a rarefaction and the solution to the right of the contact wave is

$$\mathbb{W}(x,t) = \begin{cases} \mathbb{W}^\star_{\mathcal{R}} & \text{if} \quad u^\star \leq \frac{x}{t} \leq S_{\mathcal{TR}}, \\ \mathbb{W}^{\text{Fan}}_{\mathcal{R}} & \text{if} \quad S_{\mathcal{TR}} \leq \frac{x}{t} \leq S_{\mathcal{HR}}, \\ \mathbb{W}_{\mathcal{R}} & \text{if} \quad S_{\mathcal{HR}} \leq \frac{x}{t}. \end{cases} \tag{3.127}$$

The exact solution of the Riemann problem for simplified two–fluid model is now known everywhere in the half x–t plane up to first order in η.

3.7 Conclusions

In this chapter the Riemann problem was presented for the simplified two–fluid model as a set of elementary waves such as shocks, contact and rarefaction waves. The Riemann invariants were derived constructing a simple wave solution up to first order in η. A solution procedure is presented in order to determine the solution in the star region up to first order in η and the existence of the contact wave is also established in the solution of Riemann problem for the simplified two–fluid model up to first order in η. This contact wave is a discontinuous wave across which both pressure (or mixture density) and mixture velocity are constant up to first order in η, while there is a wave jump in the relative velocity u_r. Additionally, the mixture density $\rho^\star$, the value of ρ in the star region, between the acoustic waves is found by solving a single non–linear algebraic equation numerically using a Newton–Raphson iterative procedure. The mixture velocity $u^\star$ and the relative velocities $u^\star_{r\mathcal{L}}$ and $u^\star_{r\mathcal{R}}$ follow directly. For the complete solution of the Riemann problem the mixture density behind the wave and the shock speeds were obtained for the shock waves while for the rarefaction waves the mixture density behind the waves and the equations for the head and the tail of the waves with the full solution inside the rarefaction fans were derived. The solution is then completed by sampling the solution to the left and to the right of the contact wave as described. The solution of the Riemann problem for the simplified two–fluid model is validated by direct application to four test problems as we shall see in the

next chapter.

CHAPTER 4

TEST PROBLEMS WITH EXACT SOLUTIONS

In this chapter we present four Riemann problems to test the performance of the Riemann solver developed in chapter 3. These tests can also be of use to other researchers involved in testing numerical schemes or developing codes for two–phase flow models. Exact solutions are very important to assess numerical methods as we shall see in later chapters. The Riemann problems presented here are selected to show some typical wave patterns resulting from the solution of the Riemann problem for the simplified two–fluid model. Each of the tests has been carefully designed and

$\mathcal{TEST}$	$\rho_{\mathcal{L}}$	$u_{\mathcal{L}}$	$u_{r\mathcal{L}}$	$\rho_{\mathcal{R}}$	$u_{\mathcal{R}}$	$u_{r\mathcal{R}}$
1	799.9459	3.96918	0.0	470.5632	2.94636	0.0
2	492.93	2.0	0.0	492.93	4.3394	0.0
3	483.0	3.34144	4.0	483.0	3.0	-3.0
4	483.0	2.94636	4.0	484.93902	3.5	5.0

Table 4.1: Data for four test problems with exact solution.

offers a particular degree of difficulty to numerical methods. The two–phase flow is assumed to be isentropic while the liquid phase is assumed to be incompressible with a constant mass density ρ_1 and the vapour phase is assumed to be an ideal isentropic gas. The first test problem is characterized by a left sonic rarefaction and

Constants for for test 1	
$\gamma = 1.4$	$k_2 = 1.15$
$c = 0.65$	$\rho_1 = 958.0 \quad kg/m^3$

Table 4.2: Constants for the test problems with exact solution applied to test 1.

a right shock wave. Test 2 has a solution consisting of two strong rarefactions and a contact discontinuity. The third test deals with a right and a left shocks separated

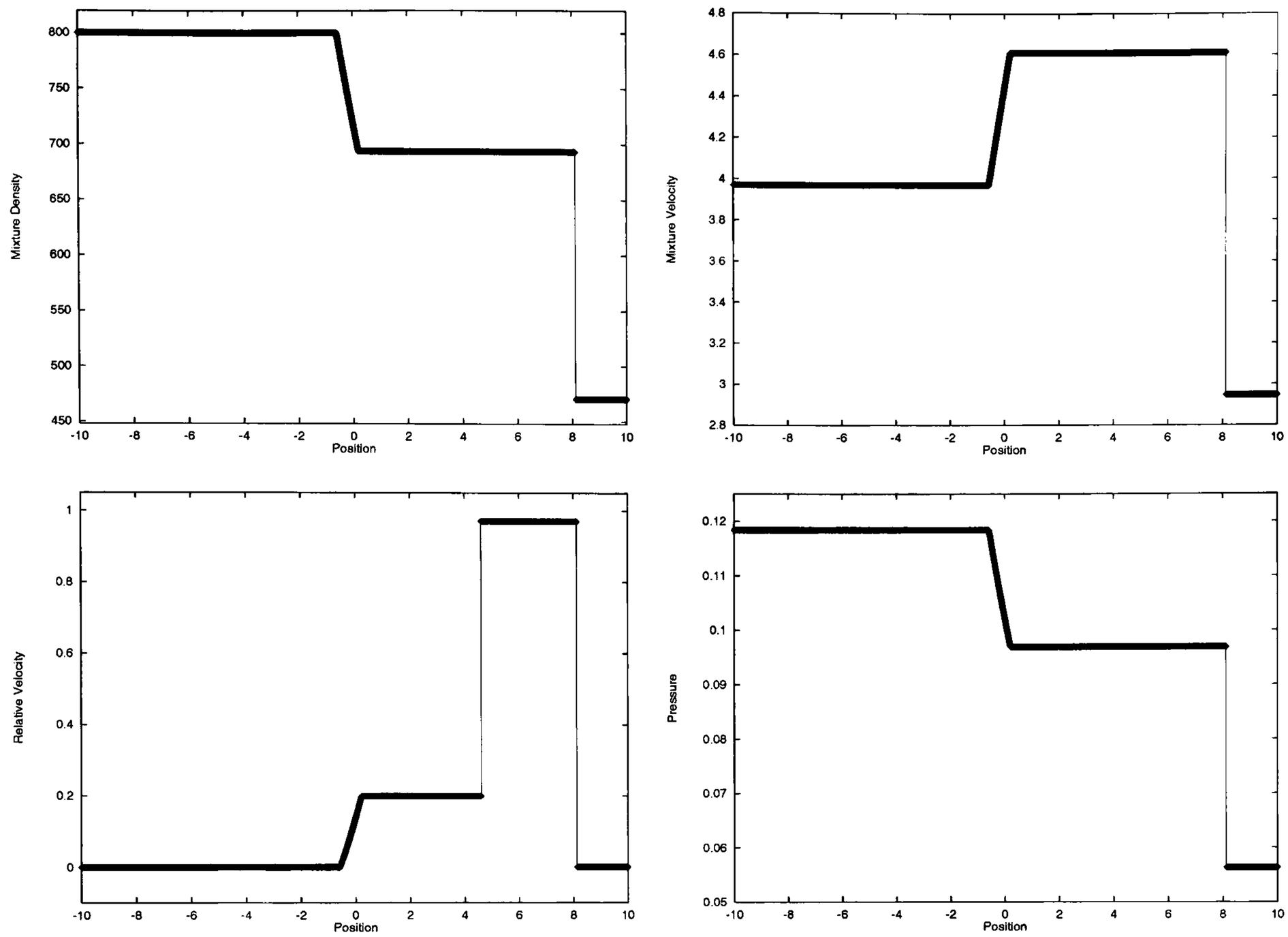

Figure 4.1: Exact solution for mixture density, mixture velocity, relative velocity and the pressure for test 1 at $t = 1.0$.

by a contact discontinuity. Test 4 consists of a single left shock wave associated with the left eigenvalue and a right rarefaction wave associated with the right eigenvalue separated by a contact discontinuity

As noted previously, these tests will also be used to assess numerical methods applied to the simplified two–fluid model. Table 4.1 shows the initial data for all tests in terms of primitive variables. The exact solutions to these tests are obtained by running a FORTRAN 90 program in the spatial domain $-10 \leq x \leq 10$ with a tolerance $\mathcal{TOL}$ of 10^{-8} and the use of 10000 cells.

Constants for for test 2	
$\gamma = 1.4$	$k_2 = 70000.0$
$c = 0.05$	$\rho_1 = 958.0 \quad kg/m^3$

Table 4.3: Constants for the test problems with exact solution applied to test 2.

Constants for for test 3	
$\gamma = 1.4$	$k_2 = 70000.0$
$c = 0.01$	$\rho_1 = 958.0 \quad kg/m^3$

Table 4.4: Constants for the test problems with exact solution applied to test 3.

4.1 Test 1: Left Sonic Rarefaction and Right Shock Wave

In this test problem the initial data has been chosen to produce a sonic or critical left rarefaction wave and a strong right propagating shock wave. A feature of this test is that the left rarefaction is sonic (or critical), that is, the eigenvalue $\lambda_1 = u - a_m + \frac{\rho}{\rho_{21}} c(1-c)u_r + a_m \mathcal{O}(\eta^2)$ changes from a negative value to a positive value as the wave is crossed from left to right. Figure 4.1 shows solution profiles for the mixture density, mixture velocity, relative velocity and the pressure at the output time $t = 1.0$ with the parameters given in table 4.2.

4.2 Test 2: Left Rarefaction and Right Rarefaction

The initial data for this test problem was chosen so that the solution consists of two strong rarefaction waves travelling in opposite directions separated by a contact discontinuity. Figure 4.2 shows profiles for the mixture density, mixture velocity, relative velocity and the pressure solution at $t = 0.04$ with the parameters defined in table 4.3.

4.3 Test 3: Left Shock and Right Shock

This test problem deals with a strong left shock wave and a strong right shock wave. Its solution represents the collision of these two strong shocks separated by a contact

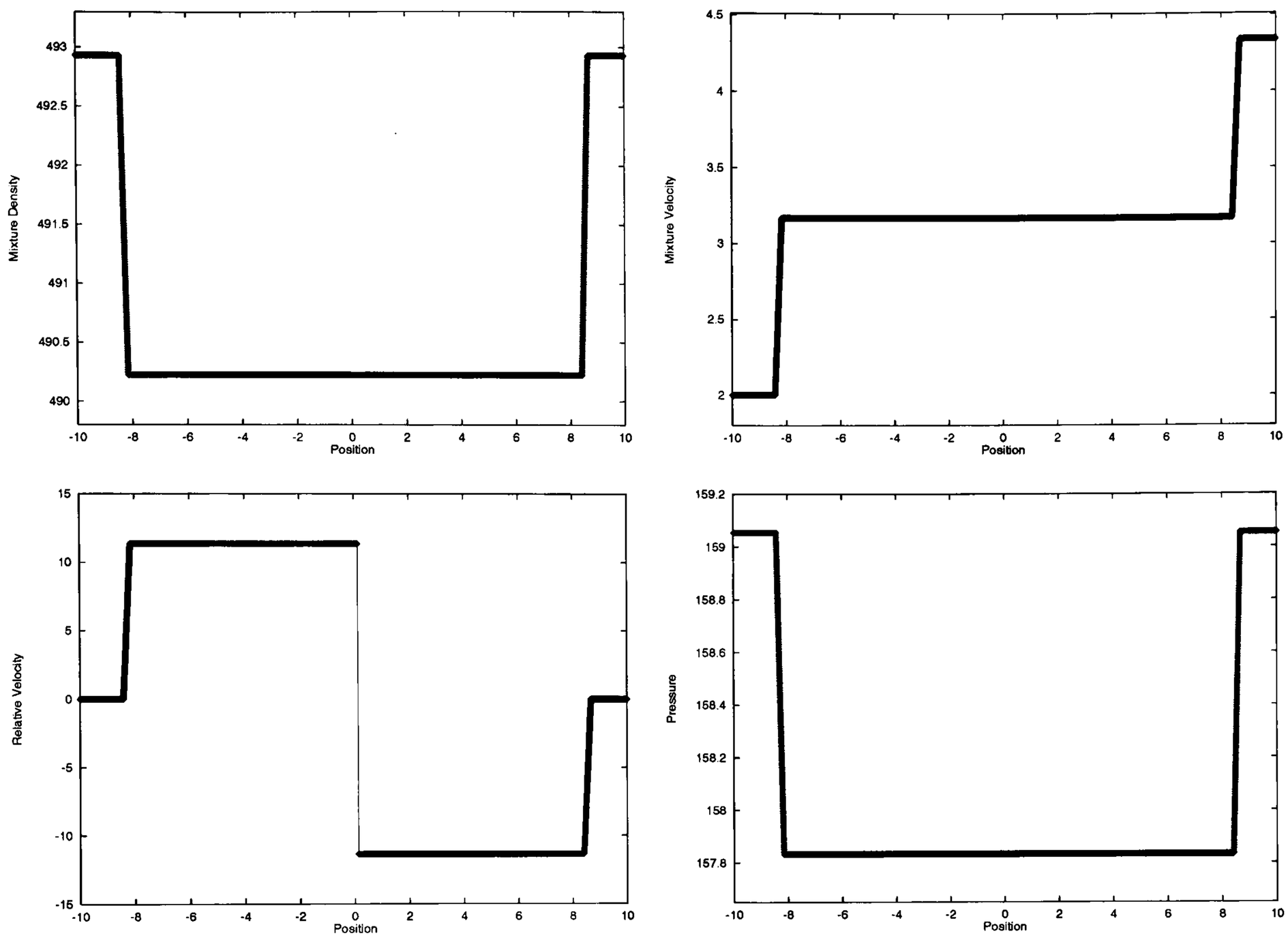

Figure 4.2: Exact solution for the mixture density, mixture velocity, relative velocity and the pressure for test 2 at $t = 0.04$.

discontinuity. The solution profiles for the mixture density, mixture velocity, relative velocity and the pressure are shown in figure 4.3 at the output time $t = 0.1$ using the parameters given in table 4.4.

4.4 Test 4: Left Shock and Right Rarefaction

Test 3 uses initial data such that the solution consisting of a single left shock wave associated with the left eigenvalue and a right rarefaction wave associated with the right eigenvalue are separated by a contact discontinuity as shown in figure 4.4. Figure 4.4 shows profiles for the mixture density, mixture velocity, relative velocity and the pressure for the solution at $t = 0.1$ with the parameters of test 3 (see table 4.4).

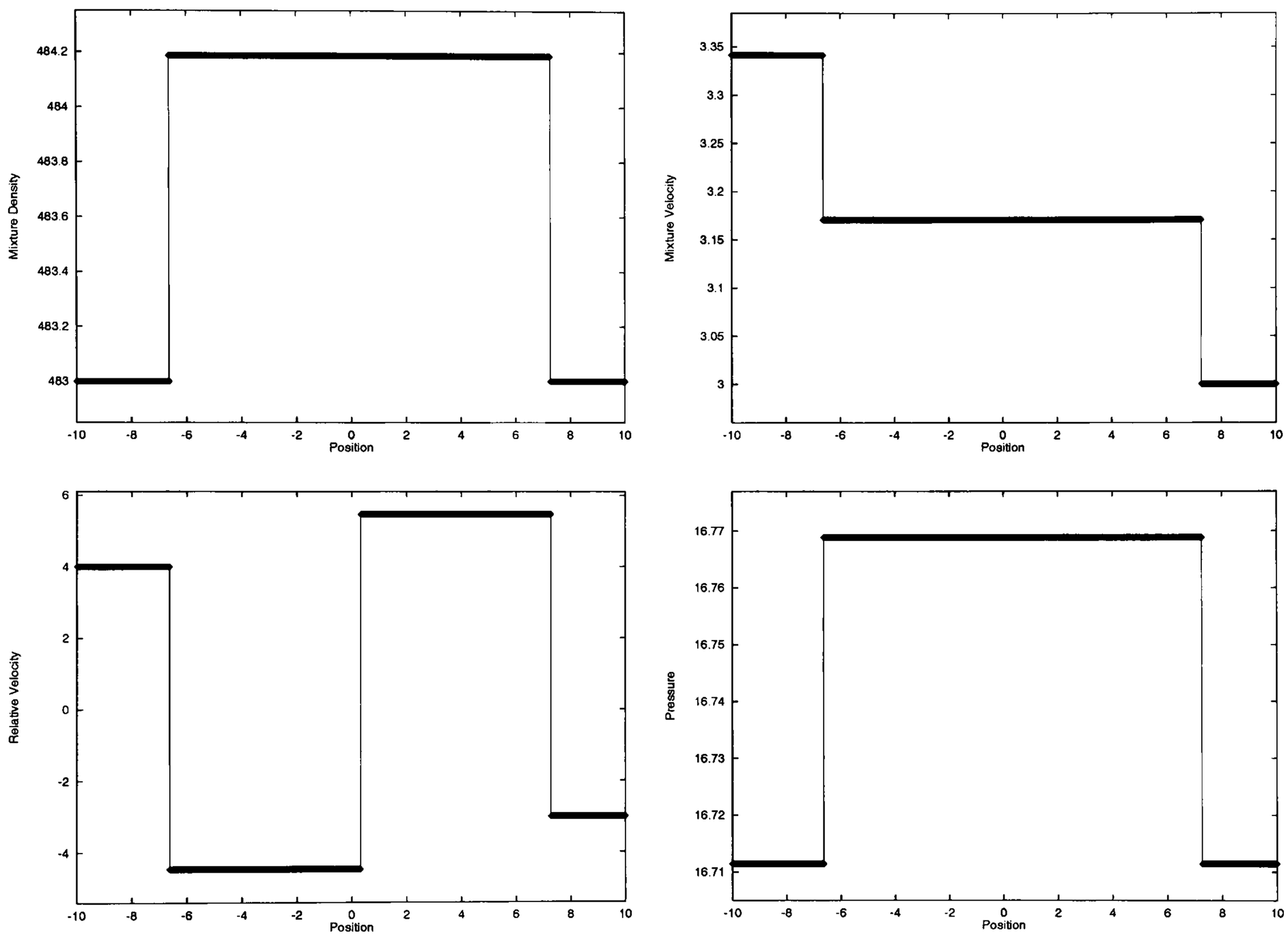

Figure 4.3: Exact solution for mixture density, mixture velocity, relative velocity and the pressure for test 3 at $t = 0.1$.

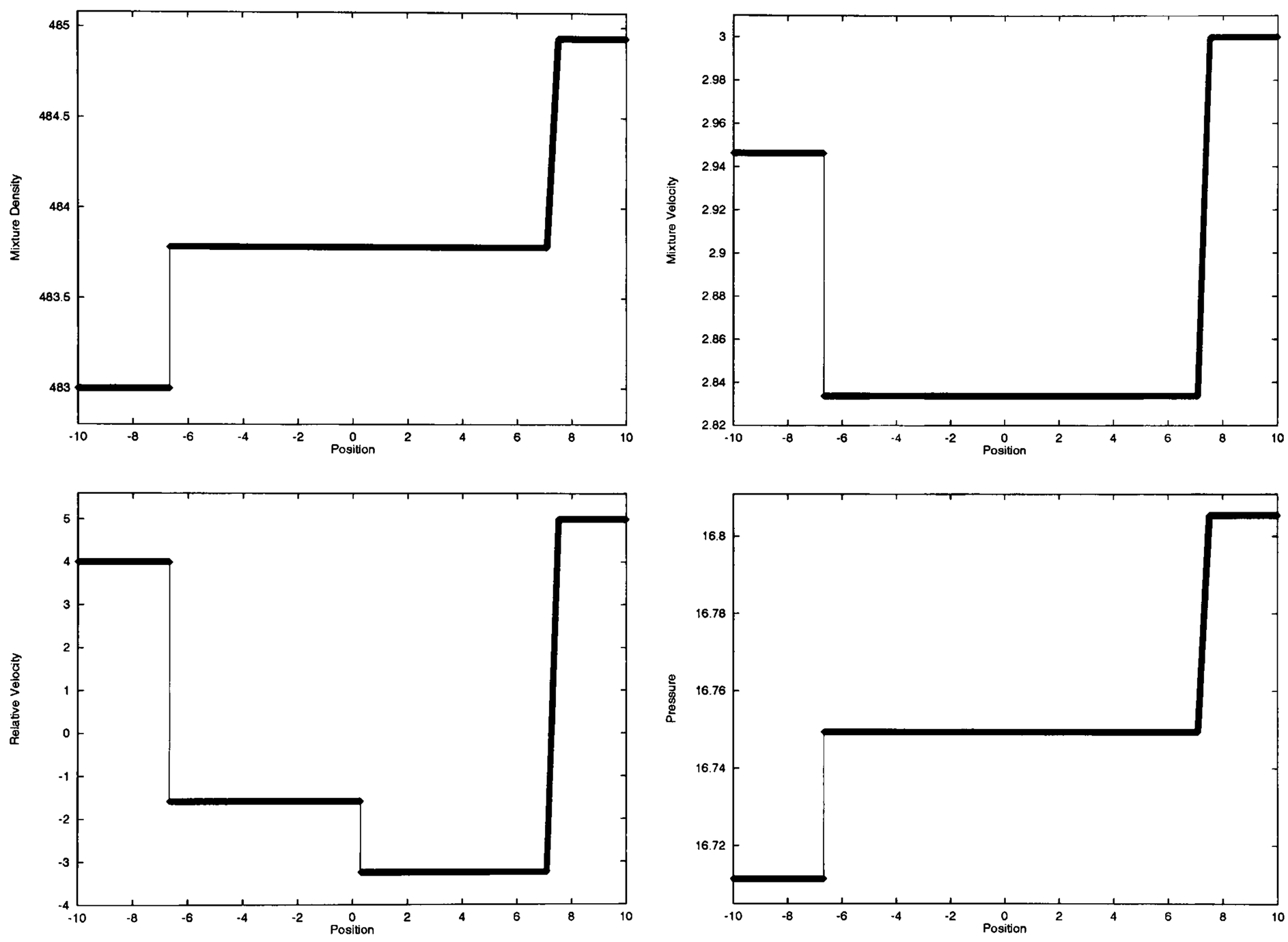

Figure 4.4: Exact solution for the mixture density, mixture velocity, relative velocity and the pressure for test 4 at $t = 0.1$.

CHAPTER 5
APPROXIMATE RIEMANN SOLVERS

In this chapter we describe two classes of approximate Riemann solvers applied to the simplified two–fluid model. In the first class of solvers we provide approximate solvers where one can compute an approximate solution to a state and then the numerical flux is obtained by evaluating the exact physical flux vector at this approximate state. In the second class of solvers an approximation for the intercell numerical flux is obtained directly. These solvers will provide effective computational tools at a competitive cost for the simplified two–fluid model.

5.1 The Riemann Problem and Godunov Flux

In this section we are concerned with solving numerically the general initial–boundary value problem (IBVP) for the simplified two–fluid model

$$\left.\begin{array}{ll} \text{PDE's}: & \partial_t \mathbb{U} + \partial_x \mathbb{F}(\mathbb{U}) = 0, \\ \text{IC's} & : \mathbb{U}(x,0) = \mathbb{U}^{(0)}, \\ \text{BC's} & : \mathbb{U}(0,t) = \mathbb{U}_l(t),\ \mathbb{U}(L,t) = \mathbb{U}_r(t), \end{array}\right\} \tag{5.1}$$

in a domain $x_l \leq x \leq x_r$, utilising a Godunov–type method based on the explicit conservative formula

$$\mathbb{U}_i^{n+1} = \mathbb{U}_i^n - \frac{\Delta t}{\Delta x}\left[\mathbb{F}_{i+\frac{1}{2}} - \mathbb{F}_{i-\frac{1}{2}}\right], \tag{5.2}$$

where the Godunov intercell numerical flux is defined as

$$\mathbb{F}_{i+\frac{1}{2}} = \mathbb{F}(\mathbb{U}_{i+\frac{1}{2}}(0)), \tag{5.3}$$

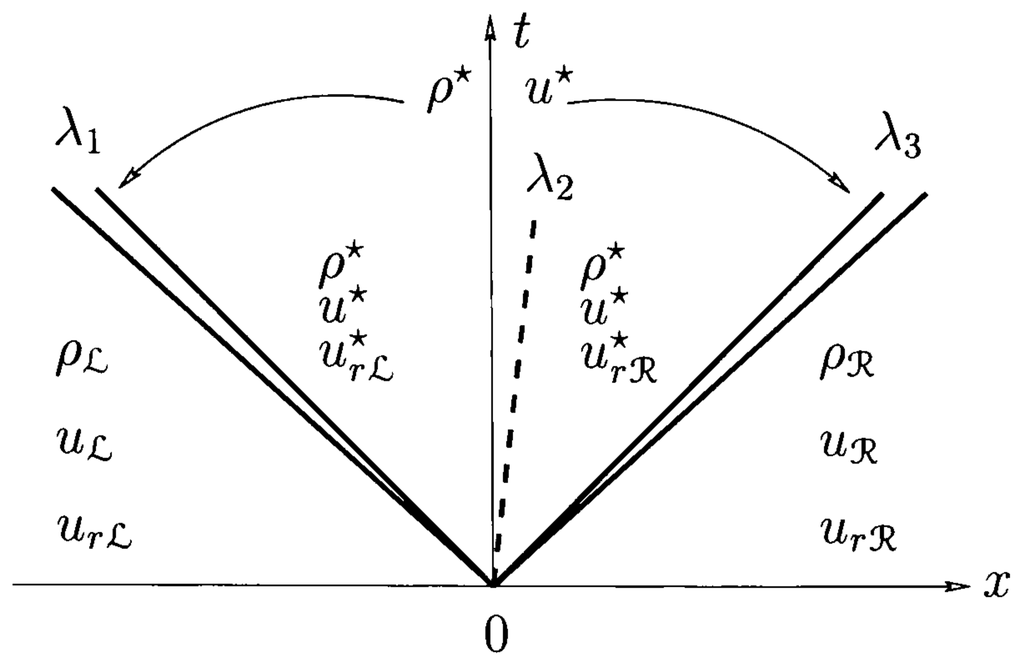

Figure 5.1: Structure of the exact solution of the Riemann problem for the simplified two–fluid model. There are three wave families associated with the eigenvalues λ_1, λ_2 and λ_3. Data and solution are given in terms of primitive variables.

with $\mathbb{U}_{i+\frac{1}{2}}(0)$ is the exact similarity solution $\mathbb{U}_{i+\frac{1}{2}}(\frac{x}{t})$ of the Riemann problem

$$\left.\begin{array}{c} \partial_t \mathbb{U} + \partial_x \mathbb{F}(\mathbb{U}) = 0, \\ \mathbb{U}(x,0) = \begin{cases} \mathbb{U}_{\mathcal{L}} & \text{if} \quad x < 0, \\ \mathbb{U}_{\mathcal{R}} & \text{if} \quad x > 0, \end{cases} \end{array}\right\} \tag{5.4}$$

evaluated at $\frac{x}{t} = 0$ as shown in figure 5.1. The vector of conserved variables and fluxes are

$$\mathbb{U} = \begin{pmatrix} \rho \\ \rho u \\ u_r \end{pmatrix}, \quad \mathbb{F}(\mathbb{U}) = \begin{pmatrix} \rho u \\ \rho u^2 + \rho\, c\, (1-c)\, u_r^2 + \mathcal{P} \\ u u_r + \frac{1-2c}{2}\, u_r^2 + \psi(\mathcal{P}) \end{pmatrix}. \tag{5.5}$$

The piecewise constant initial data $\mathbb{U}$ in terms of primitive variables can be written as

$$\mathbb{W}_{\mathcal{L}} = \begin{pmatrix} \rho_{\mathcal{L}} \\ u_{\mathcal{L}} \\ u_{r\mathcal{L}} \end{pmatrix}, \quad \mathbb{W}_{\mathcal{R}} = \begin{pmatrix} \rho_{\mathcal{R}} \\ u_{\mathcal{R}} \\ u_{r\mathcal{R}} \end{pmatrix}. \tag{5.6}$$

As shown in figure 5.1, the general structure of the exact solution of the Riemann problem for the simplified two–fluid model for which the value of the solution along $\frac{x}{t} = 0$ for the Godunov flux corresponding to the t–axis (see chapter 3 for details on the exact solution of the Riemann problem). One can compute numerical solutions by Godunov–type methods using the exact Riemann solver of chapter 3 or approximate Riemann solvers. In the rest of this chapter we develop approximate Riemann solvers that do not require an iteration process. We start with approximate–state Riemann solvers.

5.2 Approximate–State Riemann Solvers

In the approximate–state Riemann solvers approach, first we compute the approximate solution $\mathbb{W}_{i+\frac{1}{2}}(\frac{x}{t})$ to the Riemann problem. Then the approximate numerical flux is obtained by evaluating the physical flux

$$\mathbb{F}_{i+\frac{1}{2}} = \mathbb{F}(\mathbb{W}_{i+\frac{1}{2}}(0)), \tag{5.7}$$

where $\mathbb{W}_{i+\frac{1}{2}}(0)$ is the approximate value along the t–axis.

There are two steps in the process of finding the approximate solution $\mathbb{W}_{i+\frac{1}{2}}(\frac{x}{t})$. The first step is to compute the approximate solution in the star region, $\rho^\star$, $u^\star$, $u^\star_{r\mathcal{L}}$ and $u^\star_{r\mathcal{R}}$ (see figure 5.1). The second step is to sample the solution to obtain the correct values along the t–axis and evaluate the Godunov flux as in (5.7). Note that in the presence of a left (or right) sonic rarefaction the approximate Godunov scheme will take the solution inside the rarefaction along the t–axis in which case the exact solution is given in closed form as presented in chapter 3.

In the rest of this section we study three approaches of finding approximate solution for $\rho^\star$, $u^\star$, $u^\star_{r\mathcal{L}}$ and $u^\star_{r\mathcal{R}}$ in the star region.

5.2.1 A Primitive–Variable Riemann Solver (PVRS)

This solver is obtained as an extension of the Toro [173] primitive–variable Riemann solver for Euler equations which is based on a local linearization of the equations

in primitive variables form. The solution is direct and involves few and very simple arithmetic operations. The corresponding governing equations in primitive variables formulation (see chapter 3) are

$$\mathbb{C}(\mathbb{W})\partial_t \mathbb{W} + \mathbb{A}(\mathbb{W})\partial_x \mathbb{W} = 0, \tag{5.8}$$

where

$$\mathbb{W} = \begin{pmatrix} \rho \\ u \\ u_r \end{pmatrix}, \quad \mathbb{C}(\mathbb{W}) = \begin{pmatrix} a_m^{-2} & 0 & 0 \\ 0 & \rho & 0 \\ 0 & 0 & 1 \end{pmatrix}, \tag{5.9}$$

and

$$\mathbb{A}(\mathbb{W}) = \begin{pmatrix} \frac{u}{a_m^2} & \rho & 0 \\ 1 + c(1-c)\,\frac{u_r^2}{a_m^2} + (1-2c)\,c_{\mathcal{P}}\rho\,u_r^2 & \rho u & 2\rho c(1-c)\,u_r \\ \frac{1}{\rho_{21}} - c_{\mathcal{P}} u_r^2 & u_r & u + (1-2c)\,u_r \end{pmatrix}. \tag{5.10}$$

The eigenvalues of $\mathbb{A}(\mathbb{W})$ are

$$\lambda_{\mathrm{j}} = \begin{cases} u - a_m + \frac{\rho}{\rho_{21}}\,c(1-c)\,u_r + a_m\mathcal{O}(\eta^2) & \mathrm{j} = 1, \\ u + \left[1 - 2c - 2\frac{\rho}{\rho_{21}}\,c(1-c)\right]u_r + a_m\mathcal{O}(\eta^2) & \mathrm{j} = 2, \\ u + a_m + \frac{\rho}{\rho_{21}}\,c(1-c)\,u_r + a_m\mathcal{O}(\eta^2) & \mathrm{j} = 3, \end{cases} \tag{5.11}$$

and the matrices of corresponding eigenvectors are

$$\mathcal{K}^{1,3} = \begin{pmatrix} \rho a_m \\ \pm 1 + \frac{\rho}{\rho_{21}}\,c(1-c)\frac{u_r}{a_m} \\ \pm\frac{\rho}{\rho_{21}} + \frac{\rho}{\rho_{21}}\left(1 - 2c - c(1-c)\frac{\rho}{\rho_{21}} + \frac{\rho_{21}}{\rho}\right)\frac{u_r}{a_m} \end{pmatrix}, \tag{5.12}$$

$$\mathcal{K}^2 = \begin{pmatrix} -2\rho c(1-c)u_r \\ 0 \\ 1 \end{pmatrix}. \tag{5.13}$$

It is more convenient to express (5.8) as

$$\partial_t \mathbb{W} + \mathbb{B}(\mathbb{W})\partial_x \mathbb{W} = 0, \ \mathbb{B}(\mathbb{W}) = \mathbb{C}^{-1}(\mathbb{W})\mathbb{A}(\mathbb{W}). \tag{5.14}$$

We now perform a local linearization as follows; suppose that the data states $\mathbb{W}_{\mathcal{L}}$ and $\mathbb{W}_{\mathcal{R}}$ and the solution $\mathbb{W}(\frac{x}{t})$ are close to their mean value

$$\overline{\mathbb{W}} = \frac{1}{2}(\mathbb{W}_{\mathcal{L}} + \mathbb{W}_{\mathcal{R}}), \tag{5.15}$$

then we approximate the non–linear problem (5.8) by the linear constant coefficient system

$$\partial_t \mathbb{W} + \overline{\mathbb{B}}\ \partial_x \mathbb{W} = 0, \tag{5.16}$$

where

$$\overline{\mathbb{B}} = \mathbb{B}(\overline{\mathbb{W}}). \tag{5.17}$$

Next we solve this approximate system exactly by applying the Rankine–Hugoniot conditions across each wave of speed $\bar{\lambda}_j$. Thus we deal with (5.14) as the system in conservative form

$$\partial_t \mathbb{W} + \partial_x \mathbb{F}(\mathbb{W}) = 0, \ \mathbb{F}(\mathbb{W}) \equiv \overline{\mathbb{B}}\mathbb{W}. \tag{5.18}$$

Then across a wave of speed $\bar{\lambda}_j$ we have

$$\Delta\mathbb{F} \equiv \overline{\mathbb{B}}\ \Delta\mathbb{W} = \bar{\lambda}_j\ \Delta\mathbb{W}. \tag{5.19}$$

Applying (5.19) to the $\bar{\lambda}_j$ waves gives the solution in the star region up to first order in η as

$$\begin{aligned}
\rho^\star &= \frac{1}{2}(\rho_\mathcal{R} + \rho_\mathcal{L}) + \frac{1}{2}\frac{\bar{\rho}}{\bar{a}_m}\,(u_\mathcal{L} - u_\mathcal{R}) + \frac{1}{2}\frac{\bar{u}}{\bar{a}_m}\,(\rho_\mathcal{R} - \rho_\mathcal{L}) \\
&+ \frac{1}{2}\frac{\bar{\rho}}{\bar{\rho}_{21}}\,\overline{c(1-c)}\,(\rho_\mathcal{R} - \rho_\mathcal{L})\,\frac{\bar{u}_r}{\bar{a}_m}, \qquad (5.20)\\
u^\star &= \frac{\bar{u}}{\bar{a_m}^2} - \frac{\bar{u}}{\bar{a_m}^2}\frac{\rho^\star}{\bar{\rho}} - \frac{\bar{a_m}}{\bar{\rho}}\frac{\rho_\mathcal{R} - \rho_\mathcal{L}}{2} + \frac{\bar{u}}{\bar{\rho}}\rho^\star \\
&- \frac{\bar{\rho}}{\bar{\rho}_{21}}\overline{c(1-c)}\bar{u}_r + \frac{\bar{u}_r}{\bar{\rho}_{21}}\overline{c(1-c)}\bar{u}_r\rho^\star, \qquad (5.21)\\
u^\star_{r\mathcal{L}} &= u_{r\mathcal{L}} - \frac{1}{\bar{a}_m\,\bar{\rho}_{21}}\,(\rho^\star - \rho_\mathcal{L}), \qquad (5.22)\\
u^\star_{r\mathcal{R}} &= u_{r\mathcal{R}} + \frac{1}{\bar{a}_m\,\bar{\rho}_{21}}\,(\rho^\star - \rho_\mathcal{R}), \qquad (5.23)
\end{aligned}$$

where we have chosen the arithmetic mean $\mathcal{M}$ as

$$\overline{\mathcal{M}} = \frac{1}{2}(\mathcal{M}_\mathcal{L} + \mathcal{M}_\mathcal{R}) \text{ for } \overline{\mathcal{M}} = \rho,\ u,\ u_r,\ \mathcal{P},\ a_m,\ c,\ \rho_{21}. \qquad (5.24)$$

Finally, in order to evaluate the Godunov flux (5.7) we need to sample the solution to find the value $\mathbb{W}_{i+\frac{1}{2}}(0)$ along the t–axis. This sampling procedure is identical to the sampling procedure of the exact Riemann problem solution of chapter 3.

5.2.2 A Two–Shock Riemann Solver (TSRS)

The two–shock Riemann solver was proposed by Toro [175]. This results from assuming that the acoustic waves in the Riemann problem are both shock waves and evaluating further the mixture density function $\mathcal{F}(\rho)$ in the exact solver of chapter 3. Thus the two–shock Riemann solver is an approximation based on the exact solver and the solution values in the star region for the mixture density found to be

$$\rho^\star = \frac{\mathcal{G}_\mathcal{R}(\rho_0)\rho_\mathcal{R} + \mathcal{G}_\mathcal{L}(\rho_0)\rho_\mathcal{L} - (u_\mathcal{R} - u_\mathcal{L})}{\mathcal{G}_\mathcal{R}(\rho_0) + \mathcal{G}_\mathcal{L}(\rho_0)}, \qquad (5.25)$$

while the solution for the mixture velocity $u^\star$ is

$$u^\star = \frac{1}{2}(u_{\mathcal{L}} + u_{\mathcal{R}}) + \frac{1}{2}\Big[(\rho^\star - \rho_{\mathcal{R}})\mathcal{G}_{\mathcal{R}}(\rho_0) - (\rho^\star - \rho_{\mathcal{L}})\mathcal{G}_{\mathcal{L}}(\rho_0)\Big], \tag{5.26}$$

where the function $\mathcal{G}(\rho_0), k = \mathcal{L}, \mathcal{R}$, is

$$\mathcal{G}_{\mathfrak{s}}(\rho_0) = \left[\ \frac{\mathcal{B}_{\mathfrak{s}}}{\mathcal{A}_{\mathfrak{s}}(\rho^\star - \rho_{\mathfrak{s}})}\ \right]^{\frac{1}{2}}, \tag{5.27}$$

with $\mathcal{A}_{\mathfrak{s}}$, $\mathcal{B}_{\mathfrak{s}}$ are given by (3.92) and the choice for the density estimate ρ_0 as

$$\rho_0 = \max(0, \rho_{\mathtt{PVRS}}),$$

and $\rho_{\mathtt{PVRS}}$ is the solution for the mixture density given by **PVRS** solver (5.20). Next we give another approximate Riemann solver.

5.2.3 A Two–Rarefaction Riemann Solver (TRRS)

The two–rarefaction Riemann Solver is another approximate solver based on the exact solver of chapter 3. If we assume both non–linear waves are rarefactions then the closed form solution $\rho^\star$ for $\mathcal{F}(\rho) = 0$ is obtained as

$$\rho^\star \ = \ \frac{1}{2}\Big\{\rho_{\mathcal{L}}\big[1 + \frac{\mathcal{Z}}{a_{m\mathcal{L}}}\,(u_{\mathcal{L}} - u^\star)\big]^{\frac{1}{\mathcal{Z}}} + \rho_{\mathcal{R}}\big[1 + \frac{\mathcal{Z}}{a_{m\mathcal{R}}}\,(u^\star - u_{\mathcal{R}})^{\frac{1}{\mathcal{Z}}}\big]\Big\}, \tag{5.28}$$

and the solution for $u^\star$ is

$$u^\star = \frac{\rho_{\mathcal{L}\mathcal{R}}\,\frac{u_{\mathcal{L}}}{a_{m\mathcal{L}}} + \frac{u_{\mathcal{R}}}{a_{m\mathcal{R}}} + (\rho_{\mathcal{L}\mathcal{R}} - 1)/\mathcal{Z}}{\frac{\rho_{\mathcal{L}\mathcal{R}}}{a_{m\mathcal{L}}} + \frac{1}{a_{m\mathcal{R}}}}, \tag{5.29}$$

where

$$\rho_{\mathcal{L}\mathcal{R}} = \left(\frac{\rho_{\mathcal{L}}}{\rho_{\mathcal{R}}}\right)^{\mathcal{Z}},\ \mathcal{Z} = \frac{\gamma - 1}{2}.$$

The TRRS is exact for the case of two rarefaction waves in the Riemann problem which is clear by the condition

$$\mathcal{F}(\rho_{\min}) \geq 0, \quad \text{with} \quad \rho_{\min} = \min(\rho_{\mathcal{L}}, \rho_{\mathcal{R}}). \tag{5.30}$$

See section 3.4 of chapter 3 for details on the behaviour of the mixture density function. Next we study approximate Riemann solver in which an approximation to the numerical flux is obtained directly.

5.3 The HLL and HLLC Riemann Solvers

In the previous section we presented a class of solvers for solving the Riemann problem by computing an approximate solution to a state and then the numerical flux is obtained by evaluating the exact physical flux vector at this approximate state. In this section we develop an approximation to the flux $\mathbb{F}_{i+\frac{1}{2}}$ by constructing the HLL Riemann solver of Harten, Lax and van Leer [71] and the HLLC modification of Toro et al [174] applied to the simplified two–fluid model.

5.3.1 The HLL Riemann Solver

A very simple type of approximation to the solution of the Riemann problem was proposed by Harten et al. [71] and denoted by HLL. Their approach assumes that the four possible wave patterns in the exact solution of the Riemann problem are represented by a single wave pattern; the only waves present are the left and right non–linear waves and estimates $S_{\mathcal{L}}$ and $S_{\mathcal{R}}$ for the lower and upper bounds of the speeds of the non–linear waves are available. In this context, there is no contact discontinuity and the whole range of star region is given by a constant vector $\mathbb{U}^{\star}_{i+\frac{1}{2}}$, that is, $\mathbb{U}^{\text{HLL}}$. A star region is shown in figure 5.2 in which $S_{\mathcal{L}} \leq 0$ and $S_{\mathcal{R}} \geq 0$. We are interested in determining the constant vector $\mathbb{U}^{\star}_{i+\frac{1}{2}}$ and the corresponding flux vector $\mathbb{F}^{\star}_{i+\frac{1}{2}}$ ($\mathbb{F}^{\text{HLL}}$) for the simplified two–fluid model using these assumptions. Refer again to figure 5.2. Apply the integral form of the conservation laws in appropriate

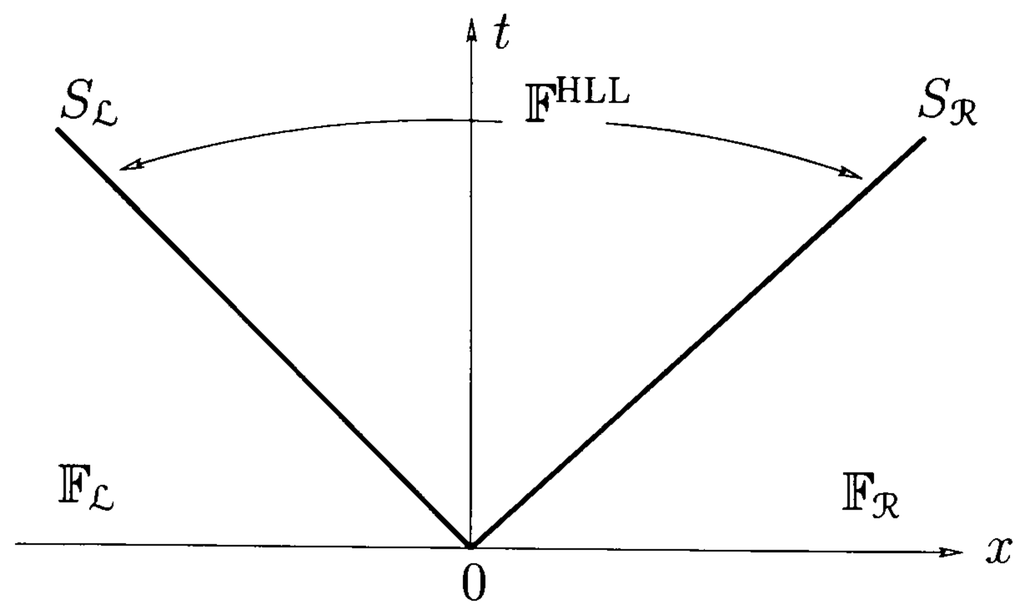

Figure 5.2: Two–wave structure of the Riemann problem solution for the simplified two–fluid model assumed in the HLL approach.

control volumes to obtain

$$\mathbb{U}^{\star}_{i+\frac{1}{2}} = \frac{S_{\mathcal{R}}\mathbb{U}_{\mathcal{R}} - S_{\mathcal{L}}\mathbb{U}_{\mathcal{L}} - (\mathbb{F}_{\mathcal{R}} - \mathbb{F}_{\mathcal{L}})}{S_{\mathcal{R}} - S_{\mathcal{L}}}, \tag{5.31}$$

where the subscripts $\mathcal{L}$ and $\mathcal{R}$ replace i and $i+1$ and $\mathbb{F}_{\mathcal{L}} \equiv \mathbb{F}(\mathbb{U}_{\mathcal{L}})$, $\mathbb{F}_{\mathcal{R}} \equiv \mathbb{F}(\mathbb{U}_{\mathcal{R}})$, and the corresponding flux vector $\mathbb{F}^{\star}_{i+\frac{1}{2}}$ as

$$\mathbb{F}^{\star}_{i+\frac{1}{2}} = \frac{S_{\mathcal{R}}\mathbb{F}_{\mathcal{L}} - S_{\mathcal{L}}\mathbb{F}_{\mathcal{R}} + S_{\mathcal{L}}S_{\mathcal{R}}(\mathbb{U}_{\mathcal{R}} - \mathbb{U}_{\mathcal{L}})}{S_{\mathcal{R}} - S_{\mathcal{L}}}, \tag{5.32}$$

which is the basis for a Godunov–type method based on the conservative formula with intercell numerical flux

$$\mathbb{F}^{\star}_{i+\frac{1}{2}} = \begin{cases} \mathbb{F}_i \equiv \mathbb{F}_{\mathcal{L}} & \text{if} \quad S_{\mathcal{L}} \geq 0, \\ \mathbb{F}^{\star}_{i+\frac{1}{2}} \equiv \mathbb{F}^{\mathrm{HLL}} & \text{if} \quad S_{\mathcal{L}} \leq 0 \leq S_{\mathcal{R}}, \\ \mathbb{F}_{i+1} \equiv \mathbb{F}_{\mathcal{R}} & \text{if} \quad S_{\mathcal{R}} \leq 0. \end{cases} \tag{5.33}$$

As to the wave speed estimates $S_{\mathcal{L}}$ and $S_{\mathcal{R}}$, there are a number of procedures available [177]. A possible choice of wave speed estimates that leads to accurate and robust

schemes can be

$$S_{\mathcal{L}} = u - a_{m\mathcal{L}} + \frac{\rho_{\mathcal{L}}}{\rho_{21}} c_{\mathcal{L}}(1 - c_{\mathcal{L}}) u_{r\mathcal{L}}, \tag{5.34}$$

$$S_{\mathcal{R}} = u + a_{m\mathcal{R}} + \frac{\rho_{\mathcal{R}}}{\rho_{21}} c_{\mathcal{R}}(1 - c_{\mathcal{R}}) u_{r\mathcal{R}}. \tag{5.35}$$

The HLL scheme is corrected by restoring the missing wave which is the contact discontinuity associated with the eigenvalue λ_2 (see figure 5.1).

5.3.2 The HLLC Riemann Solver

The HLLC Riemann solver was first presented in terms of the time–dependent, two–dimensional Euler equations [174] and is a modification to the basic HLL scheme to take into account the influence of intermediate waves. In [177], a more detailed description of this approach is given. Figure 5.3 shows the assumed wave structure in the HLLC Riemann solver. To solve the non–linear Riemann problem (5.1) for

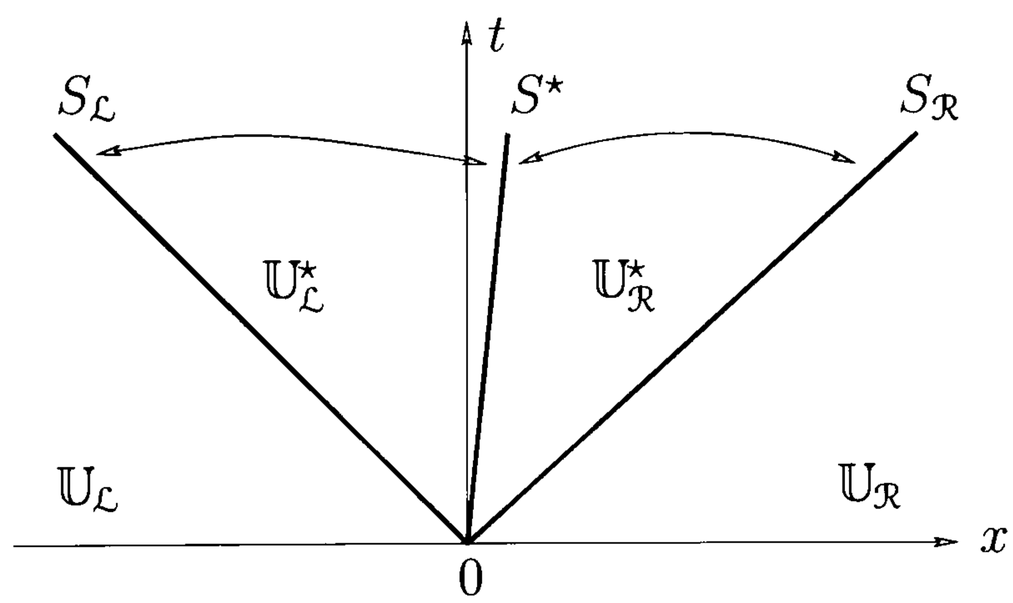

Figure 5.3: HLLC approximate Riemann solver the simplified two–fluid model. Solution in the star region consists of two constant states separated from each other by a middle wave of speed $S^\star$.

hyperbolic systems of conservation laws, we construct a HLLC Riemann solver to solve the simplified two–fluid model. Our HLLC Riemann solver is accurate and robust in comparison with other approximate Riemann solvers such as Roe's solver [138] which would require an explicit entropy fix. In addition, the HLLC Riemann solver forms the basis of very efficient and robust approximate Godunov–type methods. Referring

to figure 5.3 there are two distinct fluxes for the star region in comparison with the wave structure of HLL solver of figure 5.2. Also we need an estimate for the speed of the middle wave in addition to the wave estimates $S_{\mathcal{L}}$ and $S_{\mathcal{R}}$ in the HLL solver. Thus the HLLC Riemann solver assumes an estimate of the left and right wave speed $S_{\mathcal{L}}$ and $S_{\mathcal{R}}$ at cell boundary and an estimate $S^\star$ for the speed of the middle wave which is $S^\star = u^\star$ (see section 3.3 of chapter 3 for details on the middle wave). Assuming all wave speed estimates are available we can derive the HLLC numerical flux as

$$\mathbb{F}^{\text{HLLC}}_{i+\frac{1}{2}} = \begin{cases} \mathbb{F}_{\mathcal{L}} & \text{if} \quad 0 \leq S_{\mathcal{L}}, \\ \mathbb{F}^\star_{\mathcal{L}} & \text{if} \quad S_{\mathcal{L}} \leq 0 \leq S^\star, \\ \mathbb{F}^\star_{\mathcal{R}} & \text{if} \quad S^\star \leq 0 \leq S_{\mathcal{R}}, \\ \mathbb{F}_{\mathcal{R}} & \text{if} \quad 0 \geq S_{\mathcal{R}}, \end{cases} \tag{5.36}$$

where

$$\mathbb{F}^\star_{\mathcal{L}} = \mathbb{F}_{\mathcal{L}} + S_{\mathcal{L}}(\mathbb{U}^\star_{\mathcal{L}} - \mathbb{U}_{\mathcal{L}}), \tag{5.37}$$

$$\mathbb{F}^\star_{\mathcal{R}} = \mathbb{F}_{\mathcal{R}} + S_{\mathcal{R}}(\mathbb{U}^\star_{\mathcal{R}} - \mathbb{U}_{\mathcal{R}}). \tag{5.38}$$

The states $\mathbb{U}^\star_{\mathcal{L}}$ and $\mathbb{U}^\star_{\mathcal{R}}$ are given by

$$\mathbb{U}^\star_k = \rho_k \left(\frac{S_k - u_k}{S_k - S^\star} \right) \begin{pmatrix} 1 \\ S^\star \\ \mathcal{H} \end{pmatrix}, \tag{5.39}$$

which is obtained by manipulating relations (5.37) and (5.38) with $k = \mathcal{L}, \mathcal{R}$ and replacing $u^\star = S^\star$, and $\mathcal{H}$ by

$$\begin{aligned} \mathcal{H} &= \frac{S_k - u_k}{S_k - S^\star} \frac{u_{rk}}{\rho_k} \\ &+ \frac{1}{\rho_k(S_k - S^\star)} \left[\frac{1 - 2c^\star}{2} u^{2\star}_{rk} - \frac{1 - 2c_k}{2} u^2_{rk} + \psi(\mathcal{P}^\star) - \psi(\mathcal{P}_k) \right]. \end{aligned} \tag{5.40}$$

5.4 Conclusions

It is shown in this chapter that there are essentially two ways of extracting approximate information from the solution of the Riemann problem to be used in Godunov–type methods to solve the simplified two–fluid model numerically. The first approach is to find an approximation to a state and then to evaluate the physical flux function at this state. This approximation can be found using three different approaches: the primitive variable Riemann solver which is based on a local linearization of the equations in primitive variables form and two–shock and two–rarefaction Riemann solvers in which they are based on the exact Riemann solver of the simplified two–fluid model. The two–rarefaction Riemann solver is generally robust, accurate and more exact than the primitive variable Riemann solver or the two–shock Riemann solver.

The other approach presented in this chapter was to find an approximation to the numerical flux directly by constructing the HLL and HLLC Riemann solvers. The HLLC Riemann solver put back the missing middle wave in the HLL Riemann solver into the structure of the approximate Riemann solver. Accurate and robust estimates are also provided for the wave speeds for the numerical flux computations in both HLL and HLLC Riemann solvers for the simplified two–fluid model. These wave speed estimates are based on the solution of the Riemann problem together with the exact Riemann solver. The HLLC approximate Riemann solver developed in this chapter is accurate and robust in comparison with other approximate Riemann solvers. In addition, the HLLC Riemann solver forms the basis of very efficient and robust approximate Godunov–type methods. All the approximate Riemann solvers developed in this chapter lead to an approximate scheme of Godunov–type methods of second–order accuracy in space and time as we shall see in the next chapter.

CHAPTER 6

HIGH–RESOLUTION AND TVD SCHEMES FOR THE SIMPLIFIED TWO–FLUID MODEL

In this chapter we present second–order Total Variation Diminishing (TVD) upwind and centred schemes for solving numerically the simplified two–fluid model. The upwind schemes are extensions of the Godunov first–order upwind of chapter 1 which can be used with the exact Riemann solver of chapter 3 or with any of the Riemann solvers presented in chapter 5. The centred schemes are extensions of the First–Order Centred (FORCE) method presented in chapter 1.

6.1 Godunov–type Schemes

Godunov–type schemes are a large subset of high–order methods based on solutions of the local Riemann problems. They are high–order extensions of the first–order accurate method of Godunov [59]. These methods are conservative, have the ability to automatically capture clean, sharp and correctly positioned discontinuities such as shock and contact waves, and Total Variation Diminishing (TVD). This means that they are at least second–order accurate almost everywhere. The methods are applied to the initial–boundary value problem

$$\left.\begin{array}{ll} \text{PDE's}: & \partial_t \mathbb{U} + \partial_x \mathbb{F}(\mathbb{U}) = 0, \\ \text{IC's} & : \mathbb{U}(x,0) = \mathbb{U}^{(0)}, \\ \text{BC's} & : \mathbb{U}(0,t) = \mathbb{U}_l(t),\ \mathbb{U}(L,t) = \mathbb{U}_r(t), \end{array}\right\} \tag{6.1}$$

where the spatial domain $[0, L]$ is discretised into M computing cells $I_i = [x_{i-\frac{1}{2}}, x_{i+\frac{1}{2}}]$ with a constant mesh size $\Delta x = x_{i+\frac{1}{2}} - x_{i-\frac{1}{2}}$.

The simplified two–fluid model uses typical conservation laws in (6.1) where the vector

$\mathbb{U}$ of conserved variables and $\mathbb{F} = \mathbb{F}(\mathbb{U})$, the vector of fluxes, are

$$\mathbb{U} = \begin{pmatrix} \rho \\ \rho u \\ u_r \end{pmatrix}, \quad \mathbb{F}(\mathbb{U}) = \begin{pmatrix} \rho u \\ \rho u^2 + \rho\, c\,(1-c)\, u_r^2 + \mathcal{P} \\ u u_r + \frac{1-2c}{2}\, u_r^2 + \psi(\mathcal{P}) \end{pmatrix}. \tag{6.2}$$

The background for the simplified two–fluid model was given in chapter 2.
All the schemes applied to the model are based on the explicit conservative formula to solve (6.1) namely

$$\mathbb{U}_i^{n+1} = \mathbb{U}_i^n - \frac{\Delta t}{\Delta x}\left[\mathbb{F}_{i+\frac{1}{2}} - \mathbb{F}_{i-\frac{1}{2}}\right], \tag{6.3}$$

where $\mathbb{F}_{i+\frac{1}{2}}$ is the numerical flux at the cell interface position $x = x_{i+\frac{1}{2}}$ between cells i and $i+1$. The choice of the numerical flux $\mathbb{F}_{i+\frac{1}{2}}$ in (6.3) determines the scheme. The choice of the time step Δt in (6.3) satisfies the condition

$$\Delta t = C\frac{\Delta x}{S_{\max}^{(n)}}, \tag{6.4}$$

where C is the CFL (Courant–Friedrichs–Lewy) number with $0 < C \leq 1$ and $S_{\max}^{(n)}$ is the maximum wave speed present at time level n chosen as

$$S_{\max}^{(n)} = \max_i \left\{ \left|u_i^n\right| + a_{mi}^n + \frac{\rho_i^n}{\rho_{21i}^n} c_i^n (1 - c_i^n) u_{ri}^n \right\}. \tag{6.5}$$

In the rest of this chapter we will study two Godunov–type methods. We follow the procedures given by Toro [177]. The first method deals with two upwind–based second–order TVD schemes. The second method uses a centred second–order TVD scheme.

6.2 The Weighted Average Flux (WAF) Scheme

In this section we present a Weighted Average Flux (WAF) scheme for the numerical solution of the simplified two–fluid model. The WAF scheme was proposed in [172]

for the Euler equations. Further details can be found in [177]. The WAF scheme is a generalisation of the Lax–Wendroff and Godunov first–order upwind method.

6.2.1 The Basic WAF Scheme

In the section we present the basic WAF scheme without TVD modification. As in the following section we introduce the TVD version to deal with shock waves. The WAF scheme for the simplified two–fluid model defines a numerical flux via the integral average

$$\mathbb{F}^{\text{WAF}}_{i+\frac{1}{2}} = \frac{1}{t_2 - t_1}\frac{1}{x_2 - x_1}\int_{t_1}^{t_2}\int_{x_1}^{x_2} \mathbb{F}\big(\mathbb{U}^\star(x,t)\big)\, dxdt, \tag{6.6}$$

in the x–t plane where the choices for the integration volume $[x_1, x_2]\times[t_1, t_2]$ are assumed to be

$$x_1 = -\frac{\Delta x}{2},\ x_2 = \frac{\Delta x}{2}, \quad t_1 = 0,\ t_2 = \Delta t. \tag{6.7}$$

The vector $\mathbb{U}^\star(x,t)$ in the integral is the solution $\mathbb{U}_{i+\frac{1}{2}}(\frac{x}{t})$ of the Riemann problem with piecewise constant data $\mathbb{U}_i^n$, $\mathbb{U}_{i+1}^n$ at the interface position $i+\frac{1}{2}$. The structure of the solution of the Riemann problem for the simplified two–fluid model is presented in figure 6.1. As shown in figure 6.1 three waves of speed S_1, S_2 and S_3 separate four

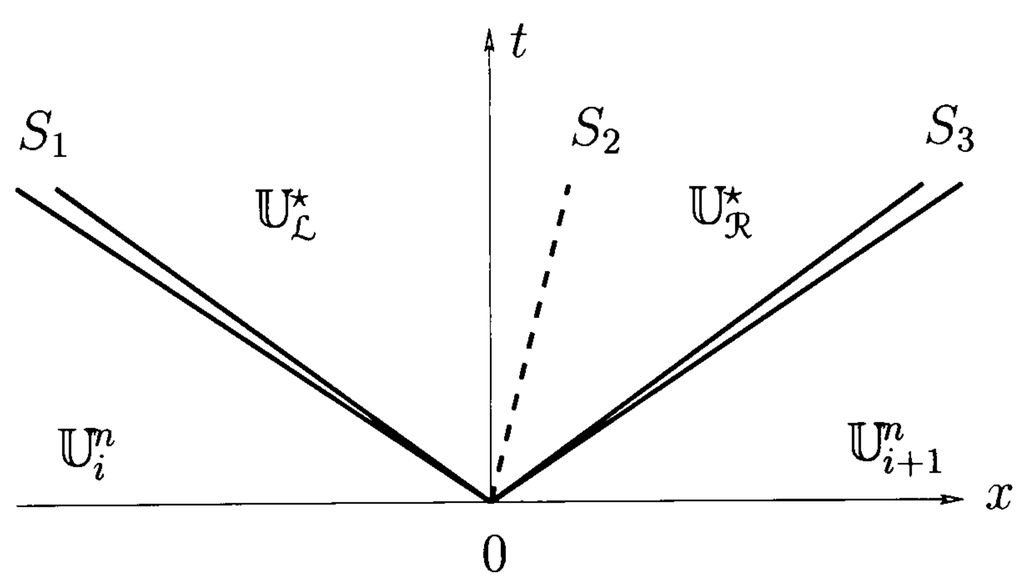

Figure 6.1: The solution structure of the Riemann problem for the simplified two–fluid model with data $\mathbb{U}_i^n$ and $\mathbb{U}_{i+1}^n$.

constant states $\mathbb{U}_i^n$, $\mathbb{U}_{\mathcal{L}}^\star$, $\mathbb{U}_{\mathcal{R}}^\star$ and $\mathbb{U}_{i+1}^n$. The left and right waves may be rarefaction or shock waves.

Now we approximate the time integration (6.6) by the midpoint rule to obtain

$$\mathbb{F}_{i+\frac{1}{2}}^{\text{WAF}} = \frac{1}{\Delta x} \int_{-\frac{1}{2}\Delta x}^{\frac{1}{2}\Delta x} \mathbb{F}(\mathbb{U}_{i+\frac{1}{2}}(x, \frac{1}{2}\Delta t))\, dx. \tag{6.8}$$

Setting $\mathbb{U}^{(1)} = \mathbb{U}_i^n$, $\mathbb{U}^{(2)} = \mathbb{U}_{\mathcal{L}}^\star$, $\mathbb{U}^{(3)} = \mathbb{U}_{\mathcal{R}}^\star$ and $\mathbb{U}^{(4)} = \mathbb{U}_{i+1}^n$ and considering a wave structure such that all waves are represented by a single ray through the origin as shown in figure 6.2, then the integral (6.8) becomes a weighted average flux and is

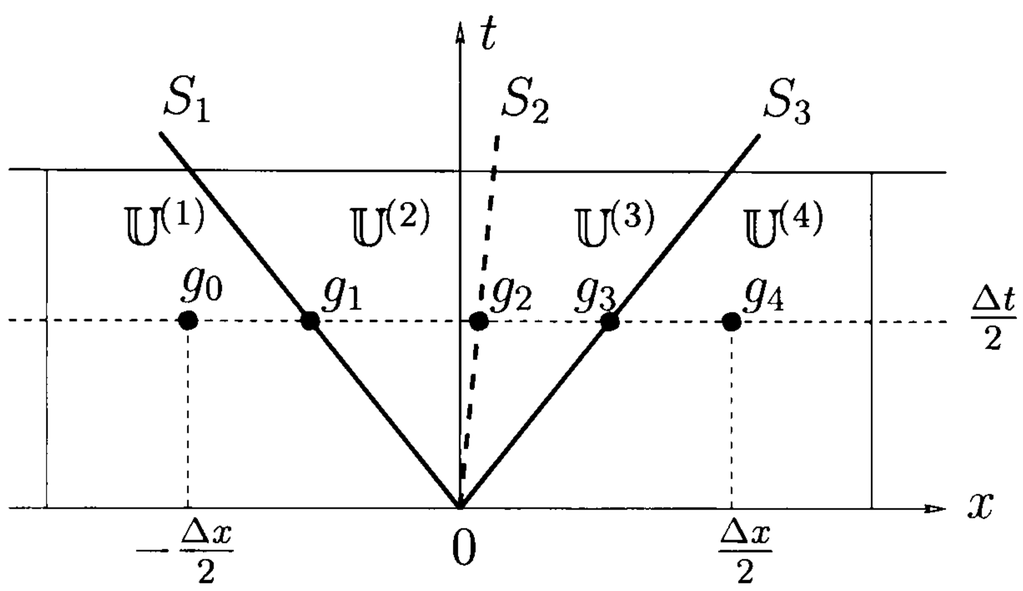

Figure 6.2: The WAF intercell flux evaluation across the wave structure of the solution of the Riemann problem for the simplified two–fluid model.

given by the summation

$$\mathbb{F}_{i+\frac{1}{2}}^{\text{WAF}} = \sum_{k=1}^{N+1} \varphi_k \mathbb{F}_{i+\frac{1}{2}}^{(k)}, \tag{6.9}$$

where $\mathbb{F}_{i+\frac{1}{2}}^{(k)} = \mathbb{F}(\mathbb{U}^{(k)})$, N is the number of waves in the solution of the Riemann problem ($N = 3$ for the simplified two–fluid model). The coefficients φ_k, $k = 1, \ldots, 4$ are normalised lengths of the segments $g_{k-1} - g_k$ given by

$$\varphi_k = \frac{|g_{k-1} - g_k|}{\Delta x}. \tag{6.10}$$

The weights φ_k can be written in terms of the wave speed S_k as

$$\varphi_k = \frac{1}{2}(C_k - C_{k-1}),\ C_0 = -1,\ C_{N+1} = 1, \tag{6.11}$$

with the Courant number for wave k given by

$$C_k = \frac{\Delta t S_k}{\Delta x}. \tag{6.12}$$

Substitution of φ_k in (6.11) into (6.9) leads to an alternative expression for the WAF flux, namely

$$\mathbb{F}^{\text{WAF}}_{i+\frac{1}{2}} = \frac{1}{2}\Big[\mathbb{F}_i + \mathbb{F}_{i+1}\Big] - \frac{1}{2}\sum_{k=1}^{N} C_k \Delta\mathbb{F}^{(k)}_{i+\frac{1}{2}}, \tag{6.13}$$

with

$$\Delta\mathbb{F}^{(k)}_{i+\frac{1}{2}} = \mathbb{F}^{(k+1)}_{i+\frac{1}{2}} - \mathbb{F}^{(k)}_{i+\frac{1}{2}}, \tag{6.14}$$

representing the flux jump across the wave k.

Finally, instead of obtaining an intercell averaged flux one could obtain an averaged state $\mathbb{U}^{\text{WAF}}_{i+\frac{1}{2}}$ as

$$\mathbb{U}^{\text{WAF}}_{i+\frac{1}{2}} = \frac{1}{2}\Big[\mathbb{F}_i + \mathbb{F}_{i+1}\Big] - \frac{1}{2}\sum_{k=1}^{N} C_k \Delta\mathbb{F}^{(k)}_{i+\frac{1}{2}}, \tag{6.15}$$

with the numerical flux defined as

$$\mathbb{F}^{\text{WAF}}_{i+\frac{1}{2}} = \mathbb{F}\big(\mathbb{U}^{\text{WAF}}_{i+\frac{1}{2}}\big). \tag{6.16}$$

6.2.2 TVD Version of the WAF Scheme

The WAF scheme presented in the previous section is second–order accurate in space and time. It is well known that higher order schemes produce spurious oscillations in the vicinity of large gradients according to Godunov's theorem [59]. Thus we

require a non–linear oscillation–free version of the WAF flux to avoid such unphysical or spurious oscillations. This is achieved by applying a Total Variation Diminishing (TVD) constraint on the scheme. We refer to [177] for details on the weighted average state version.

The TVD modification of the WAF flux (6.13) is

$$\mathbb{F}^{\text{TVD}}_{i+\frac{1}{2}} = \frac{1}{2}\Big[\mathbb{F}_i + \mathbb{F}_{i+1}\Big] - \frac{1}{2}\sum_{k=1}^{N} \text{sign}(C_k)\phi_k \Delta\mathbb{F}^{(k)}_{i+\frac{1}{2}}, \tag{6.17}$$

where ϕ_k is a WAF limiter function which is designed to ensure the scheme is TVD. There exists a variety of limiters that can be used to calculate the slopes in the WAF scheme. We refer to [177] for a detailed description of the available limiters. In this thesis we will only use the SUPERBEE limiter which is known to be overcompressive, that is, which tends to sharpen profiles into discontinuities. The SUPERBEE limiter is given by

$$\phi(r,|C|) = \begin{cases} 1 & \text{if} \quad r \leq 0, \\ 1-2(1-|C|)r & \text{if} \quad 0 \leq r \leq \frac{1}{2}, \\ |C| & \text{if} \quad \frac{1}{2} \leq r \leq 1, \\ 1-(1-|C|)r & \text{if} \quad 1 \leq r \leq 2, \\ 2|C|-1 & \text{if} \quad r \geq 2. \end{cases} \tag{6.18}$$

The WAF limiter functions are related to conventional flux limiters $\Psi(r)$ by

$$\phi(r) = 1-(1-|C|)\Psi(r), \tag{6.19}$$

where the flow parameter $r = r^{(k)}$, referring to wave k in the solution $\mathbb{U}_{i+\frac{1}{2}}(x,t)$ of the Riemann problem, is the ratio

$$r^{(k)} = \begin{cases} \dfrac{\Delta q^{(k)}_{i-\frac{1}{2}}}{\Delta q^{(k)}_{i+\frac{1}{2}}} & \text{if} \quad C_{(k)} > 0, \\ \\ \dfrac{\Delta q^{(k)}_{i+\frac{3}{2}}}{\Delta q^{(k)}_{i+\frac{1}{2}}} & \text{if} \quad C_{(k)} < 0, \end{cases} \tag{6.20}$$

which is the ratio of upwind change $\Delta q^{(k)}_{i-\frac{1}{2}}$ if $C_k > 0$ or $\Delta q^{(k)}_{i+\frac{3}{2}}$ if $C_k < 0$, to the local change $\Delta q^{(k)}_{i+\frac{1}{2}}$ of a suitable variable q. One selects a simple quantity q which is known to change across each wave family in the solution of the Riemann problem. For the simplified two–fluid model the choice $q \equiv u_r$ gives very satisfactory results. The notations $\Delta q^{(k)}_{i-\frac{1}{2}}$ denotes the jump in q across wave k in the solution $\mathbb{U}_{i-\frac{1}{2}}(x,t)$ of the Riemann problem with data $(\mathbb{U}^n_{i-1}, \mathbb{U}^n_i)$, $\Delta q^{(k)}_{i+\frac{3}{2}}$ denotes the jump in q across wave k in the solution $\mathbb{U}_{i+\frac{3}{2}}(x,t)$ of the Riemann problem with data $(\mathbb{U}^n_{i+1}, \mathbb{U}^n_{i+2})$, while $\Delta q^{(k)}_{i+\frac{1}{2}}$ is the corresponding jump across wave k in the local Riemann problem solution $\mathbb{U}_{i+\frac{1}{2}}(x,t)$ with data $(\mathbb{U}^n_i, \mathbb{U}^n_{i+1})$.

6.2.3 Rarefactions in State Riemann Solvers

For the WAF intercell flux it was assumed that the waves in the solution of the Riemann problem were single rays. For contacts and shocks this assumption is correct and the summation (6.13) or (6.17) is exact, but it is not for rarefaction waves. Thus special care is necessary in the WAF scheme.

In a fan–like configuration, the approximate expression (6.13) or (6.17) works well when the rarefaction is non–sonic or non–critical and the speeds of the head and the tail of the wave are the wave speed for that wave family. Consequently, one may lump the rarefaction wave together with the closest of the star states $\mathbb{U}^\star_5$ into a single state in the direction of the t–axis. Thus the flux for the state in that summation (6.15) is

$$\mathbb{F}^{(k)}_{i+\frac{1}{2}} = \mathbb{F}(\mathbb{U}^\star_5). \tag{6.21}$$

A special treatment is needed in the case of a sonic or critical rarefaction. Figure 6.3 shows the case in which the right rarefaction is a sonic rarefaction fan. The required

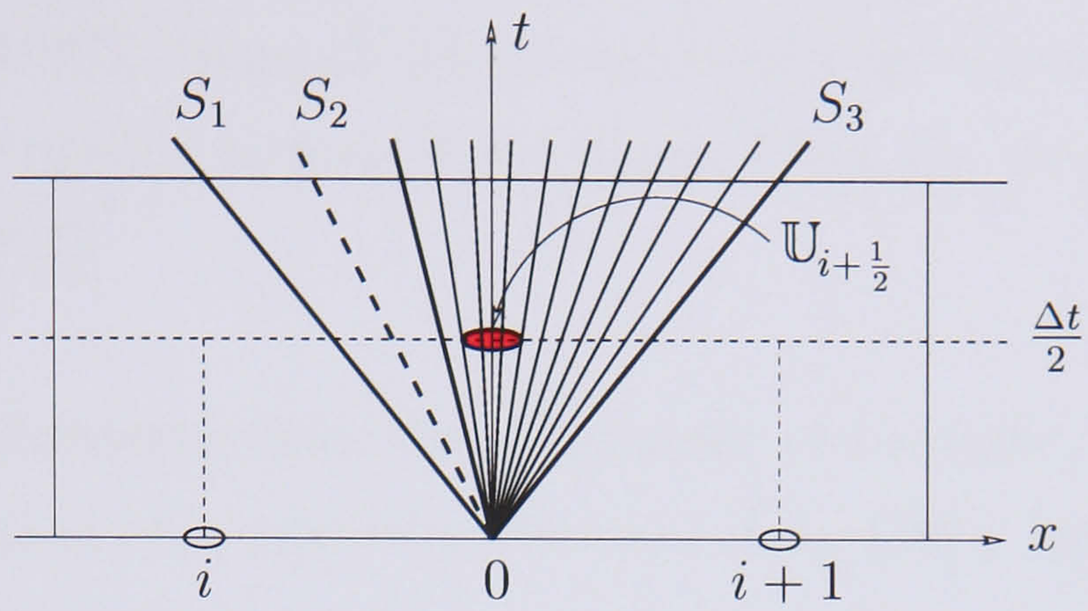

Figure 6.3: Treatment of right sonic rarefaction when evaluating the WAF flux based on exact or approximate Riemann solvers.

state $\mathbb{U}_{\mathfrak{s}}^{\star}$ for the solution of the Riemann problem lies inside the rarefaction region along the t–axis where the rarefaction zone is incorporated with the closest star state. The state used for evaluating the flux in the star region is $\mathbb{U}_{i+\frac{1}{2}}^{(0)}$ which is the solution of the Riemann problem along the t–axis which is the Godunov flux as it is always one term in the solution summation (6.15) for the WAF flux. This special treatment of sonic rarefaction waves is needed only when the exact Riemann solver and approximate Riemann solvers are used.

6.3 The MUSCL–Hancock Method

MUSCL–Hancock method is another second–order extension of the Godunov upwind method applied to the simplified two–fluid model. Details of the MUSCL–Hancock method as applied to any system of hyperbolic conservation laws are given in [177]. The scheme achieves a second–order accuracy in space and time by (i) data reconstruction, (ii) by evolving boundary extrapolated values in time and (iii) by solving a conventional piecewise constant data Riemann problem with initial data consisting of evolved boundary extrapolated values.

6.3.1 The Basic MUSCL–Hancock Method

Here we present the basic MUSCL–Hancock scheme applied to the simplified two–fluid model. The MUSCL–Hancock scheme achieves a second–order extension of the Godunov first–order upwind method if the intercell flux $\mathbb{F}_{i+\frac{1}{2}}$ is calculated in the following three steps [177]:

Step(I): Data Reconstruction, for a given set of constant, average data states $\{\mathbb{W}_i^n\}$, a reconstruction of a piecewise constant data $\{\mathbb{W}_i^n\}$ into a piecewise linear distribution of the data given as

$$\mathbb{W}_i(x) = \mathbb{W}_i^n + (x - x_i)\frac{\Delta_i}{\Delta x}, x \in I_i, \tag{6.22}$$

where $\mathbb{W} = (\rho, u, u_r)^T$, is a vector of primitive variables, $x_i = (i - \frac{1}{2})\Delta x$ is the centre of the computing cell $I_i = [x_{i-\frac{1}{2}}, x_{i+\frac{1}{2}}]$, Δ_i are the slopes of three components for the simplified two–fluid model defined as

$$\Delta_i = \frac{1}{2}(1 + \Im)\mathbb{W}_{i-\frac{1}{2}} + \frac{1}{2}(1 - \Im)\mathbb{W}_{i+\frac{1}{2}}, \tag{6.23}$$

with the parameter $\Im \in [-1, 1]$ (for the simplified two–fluid model $\Im = 0$) and the average between the intercell slopes

$$\mathbb{W}_{i-\frac{1}{2}} = \mathbb{W}_i^n - \mathbb{W}_{i-1}^n, \quad \mathbb{W}_{i+\frac{1}{2}} = \mathbb{W}_{i+1}^n - \mathbb{W}_i^n. \tag{6.24}$$

Now the boundary extrapolated values are obtained by setting $x = 0$ and $x = \Delta x$ in (6.22) to obtain

$$\mathbb{W}_i^{\mathcal{L}} = \mathbb{W}_i^n - \frac{1}{2}\Delta_i, \quad \mathbb{W}_i^{\mathcal{R}} = \mathbb{W}_i^n + \frac{1}{2}\Delta_i. \tag{6.25}$$

These are the values of the vector function (6.22) at the left and right boundaries of I_i.

Step(II): Evolution, the extrapolated values $\mathbb{W}_i^{\mathcal{L}}$, $\mathbb{W}_i^{\mathcal{R}}$ are then evolved in each

cell I_i by a time $t = \frac{1}{2}\Delta t$ in terms of the corresponding variables and according to

$$\overline{\mathbb{U}}_i^{\mathcal{L}} = \mathbb{U}_i^{\mathcal{L}} + \frac{1}{2}\frac{\Delta t}{\Delta x}\Big[\mathbb{F}(\mathbb{W}_i^{\mathcal{L}}) - \mathbb{F}(\mathbb{W}_i^{\mathcal{R}})\Big], \tag{6.26}$$

$$\overline{\mathbb{U}}_i^{\mathcal{R}} = \mathbb{U}_i^{\mathcal{R}} + \frac{1}{2}\frac{\Delta t}{\Delta x}\Big[\mathbb{F}(\mathbb{W}_i^{\mathcal{L}}) - \mathbb{F}(\mathbb{W}_i^{\mathcal{R}})\Big], \tag{6.27}$$

where the values $\mathbb{U}_i^{\mathcal{L}}$ and $\mathbb{U}_i^{\mathcal{R}}$ are computed from the boundary extrapolated values $\mathbb{W}_i^{\mathcal{L}}$ and $\mathbb{W}_i^{\mathcal{R}}$.
The flux vector is evaluated at the two boundary extrapolated vectors to provide a flux difference.

Step(III): The Riemann Problem, we solve the conventional piecewise constant data Riemann problem with data $\overline{\mathbb{W}}_i^{\mathcal{R}}$, $\overline{\mathbb{W}}_{i+1}^{\mathcal{L}}$ at each interface $x_{i+\frac{1}{2}}$ to find the similarity solution $\mathbb{W}_{i+\frac{1}{2}}(\frac{x}{t})$. The intercell flux is

$$\mathbb{F}_{i+\frac{1}{2}} = \mathbb{F}(\mathbb{W}_{i+\frac{1}{2}}(0)), \tag{6.28}$$

where $\mathbb{W}_{i+\frac{1}{2}}(0)$ denote the solution along the t–axis.
The scheme resulting from applying the previous three steps is second–order accurate in space and time.

6.3.2 TVD Version of the MUSCL–Hancock Method

A TVD version of MUSCL–Hancock method is needed to avoid the expected spurious oscillations. This is achieved by limiting the slopes Δ_i in the data reconstruction step by limited slopes $\bar{\Delta}_i$ according to TVD constraints. Let $\mathfrak{u}$ be any of the variables of the vector $\mathbb{W}$ to be reconstructed, then at the interface $i+\frac{1}{2}$ we have left $\mathfrak{u}_{\mathcal{L}}$ and right $\mathfrak{u}_{\mathcal{R}}$ data for a Riemann problem where

$$\mathfrak{u}_{\mathcal{L}} \equiv \bar{\mathfrak{u}}_i^{\mathcal{R}} = \mathfrak{u}_i^{\,n} + \frac{1}{2}\bar{\Delta}_i, \tag{6.29}$$

$$\mathfrak{u}_{\mathcal{R}} \equiv \bar{\mathfrak{u}}_{i+1}^{\mathcal{L}} = \mathfrak{u}_{i+1}^{\,n} - \frac{1}{2}\bar{\Delta}_i, \tag{6.30}$$

with the limited slopes

$$\bar{\Delta}_i = \begin{cases} \max\Big[0, \min(\beta\Delta_{i-\frac{1}{2}}, \Delta_{i+\frac{1}{2}}), \min(\Delta_{i-\frac{1}{2}}, \beta\Delta_{i+\frac{1}{2}})\Big], & \Delta_{i+\frac{1}{2}} > 0, \\ \min\Big[0, \max(\beta\Delta_{i-\frac{1}{2}}, \Delta_{i+\frac{1}{2}}), \max(\Delta_{i-\frac{1}{2}}, \beta\Delta_{i+\frac{1}{2}})\Big], & \Delta_{i+\frac{1}{2}} < 0, \end{cases} \tag{6.31}$$

for particular values of the parameter β with

$$\Delta_{i-\frac{1}{2}} = \mathfrak{u}_i - \mathfrak{u}_{i-1}, \quad \Delta_{i+\frac{1}{2}} = \mathfrak{u}_{i+1} - \mathfrak{u}_i. \tag{6.32}$$

As mentioned before we will only use the SUPERBEE flux limiter in this thesis. Thus the value for $\beta = 2$ in (6.31) reproduces the SUPERBEE flux limiter. Note that $\bar{\Delta}_i$ is a vector and thus the limiting process is applied to each component of the system being solved.

Another approach is to find a slope limiter ξ such that

$$\bar{\Delta}_i = \xi\Delta_i, \tag{6.33}$$

where Δ_i is given by (6.23). The use of the slope limiter approach leads to a TVD region for $\xi(r)$ given such that

$$\xi(r) \begin{cases} = 0 & r \leq 0, \\ \leq \min\Big\{\xi_{\mathcal{L}}(r), \xi_{\mathcal{R}}(r)\Big\} & r > 0, \end{cases} \tag{6.34}$$

where

$$\left.\begin{aligned} \xi_{\mathcal{L}}(r) &= \frac{2\beta_{i-\frac{1}{2}}r}{1 - \Im + (1 + \Im)r}, \\ \xi_{\mathcal{R}}(r) &= \frac{2\beta_{i+\frac{1}{2}}}{1 - \Im + (1 + \Im)r}, \\ r &= \frac{\Delta_{i-\frac{1}{2}}}{\Delta_{i+\frac{1}{2}}}, \end{aligned}\right\} \tag{6.35}$$

and

$$\beta_{i-\frac{1}{2}} = \frac{2}{1 + C}, \quad \beta_{i+\frac{1}{2}} = \frac{2}{1 - C}. \tag{6.36}$$

For limiting values of $\beta_{i-\frac{1}{2}}$ and $\beta_{i+\frac{1}{2}}$ one may eliminate the dependence on C and set $\beta_{i-\frac{1}{2}} = 1 = \beta_{i+\frac{1}{2}}$ in (6.35) to obtain a slope limiter that is similar to the SUPERBEE flux limiter given by

$$\xi(r)_{sb} = \begin{cases} 0 & \text{if} \quad r \leq 0, \\ 2r & \text{if} \quad 0 \leq r \leq \frac{1}{2}, \\ 1 & \text{if} \quad \frac{1}{2} \leq r \leq 1, \\ \min\{r, \xi_{\mathcal{R}}(r), 2\} & \text{if} \quad r \geq 1. \end{cases} \tag{6.37}$$

6.4 Centred TVD Schemes

Centred schemes applied to the simplified two–fluid model are called Godunov–type methods. These schemes do not require explicit Riemann solvers as in the case of upwind schemes. Here we present a second–order TVD scheme that is an extension of the first–order centred FORCE scheme [176, 178]. The scheme is of the slope limiter type and results from replacing the Godunov flux by the FORCE flux in the MUSCL–Hancock scheme of section 6.3. A key issue in constructing TVD centred schemes is the fact that the dependence of the scheme on the limiter functions in direction of wave propagation is simply undesirable.

6.4.1 The SLIC Scheme

Let us first recall the FORCE flux for a system of hyperbolic conservation laws

$$\partial_t \mathbb{U} + \partial_x \mathbb{F}(\mathbb{U}) = 0, \; x \in \mathbb{R}, \; t > 0, \tag{6.38}$$

such as the simplified two–fluid model, for which $\mathbb{U}$ and $\mathbb{F}(\mathbb{U})$ are given by (6.2). The FORCE flux is given by

$$\mathbb{F}^{\text{FORCE}}_{i+\frac{1}{2}} = \mathbb{F}^{\text{FORCE}}_{i+\frac{1}{2}}(\mathbb{U}_{\mathcal{L}}, \mathbb{U}_{\mathcal{R}}) = \frac{1}{2}\Big[\mathbb{F}^{\text{LF}}_{i+\frac{1}{2}}(\mathbb{U}_{\mathcal{L}}, \mathbb{U}_{\mathcal{R}}) + \mathbb{F}^{\text{RI}}_{i+\frac{1}{2}}(\mathbb{U}_{\mathcal{L}}, \mathbb{U}_{\mathcal{R}})\Big], \tag{6.39}$$

which is an arithmetic mean between the Lax–Friedrichs flux $\mathbb{F}^{\text{LF}}_{i+\frac{1}{2}}$ and the Richtmyer flux $\mathbb{F}^{\text{RI}}_{i+\frac{1}{2}}$.

Now we construct a second–order extension of the FORCE Scheme by replacing the Godunov upwind flux in the MUSCL–Hancock scheme by the FORCE flux. A TVD version is derived in detail in [177] and results from limiting the slopes in the data reconstruction step. The slope limiter centred scheme SLIC has three steps. Step (I) and step (II) are exactly the same as in the MUSCL–Hancock scheme described in the previous section. The first step results in boundary extrapolated values $\mathbb{U}_i^{\mathcal{L}}$ and $\mathbb{U}_i^{\mathcal{R}}$ in each cell $I_i = [x_{i-\frac{1}{2}}, x_{i+\frac{1}{2}}]$. In the second step one evolves $\mathbb{U}_i^{\mathcal{L}}$, $\mathbb{U}_i^{\mathcal{R}}$ by a time $\frac{1}{2}\Delta t$ according to (6.26)–(6.27). In step(III) instead of solving the Riemann problem with data

$$\mathbb{W}_{\mathcal{L}} \equiv \overline{\mathbb{U}}_i^{\mathcal{R}},\ \mathbb{W}_{\mathcal{R}} \equiv \overline{\mathbb{U}}_{i+1}^{\mathcal{L}}, \tag{6.40}$$

to find the Godunov flux at (6.28) the intercell position $i+\frac{1}{2}$, we evaluate the FORCE flux

$$\mathbb{F}_{i+\frac{1}{2}}^{\text{FORCE}} = \mathbb{F}_{i+\frac{1}{2}}^{\text{FORCE}}(\overline{\mathbb{U}}_{\mathcal{L}}, \overline{\mathbb{U}}_{\mathcal{R}}), \tag{6.41}$$

as given by (6.39). The resulting model is second–order accurate in space and time and stable with CFL number C satisfying $|C| \leq 1$. For TVD version implementation for the simplified two–fluid model, the slopes Δ_i in the reconstruction step (6.22) are replaced by limited slopes $\bar{\Delta}_i$ with SUPERBEE limiters and $\beta_{i-\frac{1}{2}} = 1 = \beta_{i+\frac{1}{2}}$ in (6.35).

6.5 Numerical Results

In this section we present numerical results obtained with TVD upwind and centred schemes based on HLLC Riemann solver of chapter 5 applied to the simplified two–fluid model. The exact and numerical solution are found in the spatial domain $-10 \leq x \leq 10$. The numerical solution is computed with $M = 100$ cells, the Courant number coefficient is $C = 0.9$ and S_{max}^n is found using the simplified formula (6.5). The test problems were introduced in chapter 3 and applied to a two–fluid shock–tube problem consisting of a Riemann problem with transmissive boundary conditions in which there are three wave families as a part of the solution. The first test problem

is characterized by a left sonic rarefaction and a right shock wave. The second test deals with a solution consisting of a left rarefaction and a right rarefaction separated by a contact discontinuity while the third test deals with a left shock and a right shock. The fourth test consists of a single left shock wave associated with the left eigenvalue and a right rarefaction wave associated with the right eigenvalue separated by a contact discontinuity. The left and right states are defined in table 6.1.

$\mathcal{TEST}$	$\rho_{\mathcal{L}}$	$u_{\mathcal{L}}$	$u_{r\mathcal{L}}$	$\rho_{\mathcal{R}}$	$u_{\mathcal{R}}$	$u_{r\mathcal{R}}$
1	799.9459	3.96918	0.0	470.5632	2.94636	0.0
2	492.93	2.0	0.0	492.93	4.3394	0.0
3	483.0	3.34144	4.0	483.0	3.0	-3.0
4	483.0	2.94636	4.0	484.93902	3.5	5.0

Table 6.1: Initial states for the test problems with TVD Godunov–type methods.

We present four sets of results for each test problem. The first set of each test correspond to the WAF scheme of section 6.2 (see figures 6.4, 6.8, 6.12 and 6.16). The MUSCL–Hancock scheme results are shown in the second set of each test problem (see figures 6.5, 6.9, 6.13 and 6.17). The third set correspond to the SLIC scheme (see figures 6.6, 6.10, 6.14 and 6.18) while the fourth set belong to the Lax–Friedrichs scheme (see figure 6.7, 6.11, 6.15 and 6.19). Figures 6.4, 6.8, 6.12 and 6.16 show results obtained for the WAF TVD scheme used in conjunction with the HLLC Riemann solver of chapter 5 using the flux limiter SUPERBEE (6.18). The results gives a very sharp resolution of discontinuities but small spurious oscillations are just visible on the plots. Figures 6.5, 6.9, 6.13 and 6.17 show results from the MUSCL–Hancock method obtained from the limiter slopes (6.34) and corresponds to the flux limiter SUPERBEE. Figures 6.6, 6.10, 6.14 and 6.18 show results obtained from the SLIC scheme, a second–order TVD scheme, with SUPERBEE (6.37). These schemes are less accurate than those from upwind methods. Figures 6.7, 6.11, 6.15 and 6.19 shows results obtained from the Lax–Friedrichs scheme, a first–order centred scheme. As expected, the Lax–Friedrichs scheme (see figures 6.7, 6.11, 6.15 and 6.19) has much more numerical diffusion than the other numerical schemes, but the results obtained with the schemes are in good agreement.

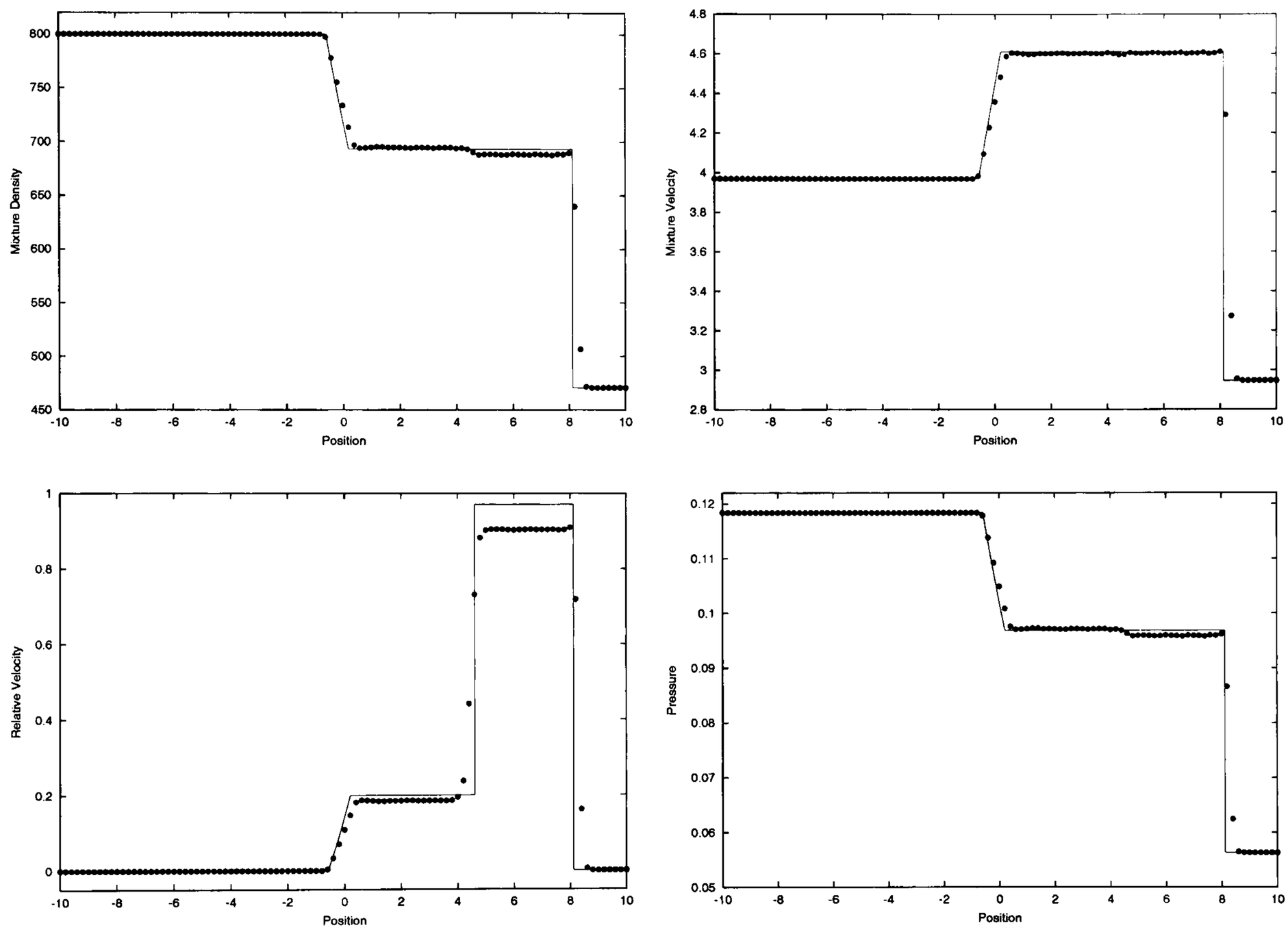

Figure 6.4: WAF scheme with HLLC Riemann solver and SUPERBEE TVD function applied to Test 1. Numerical (symbol) and exact (line) solutions are compared at $t = 1.0$.

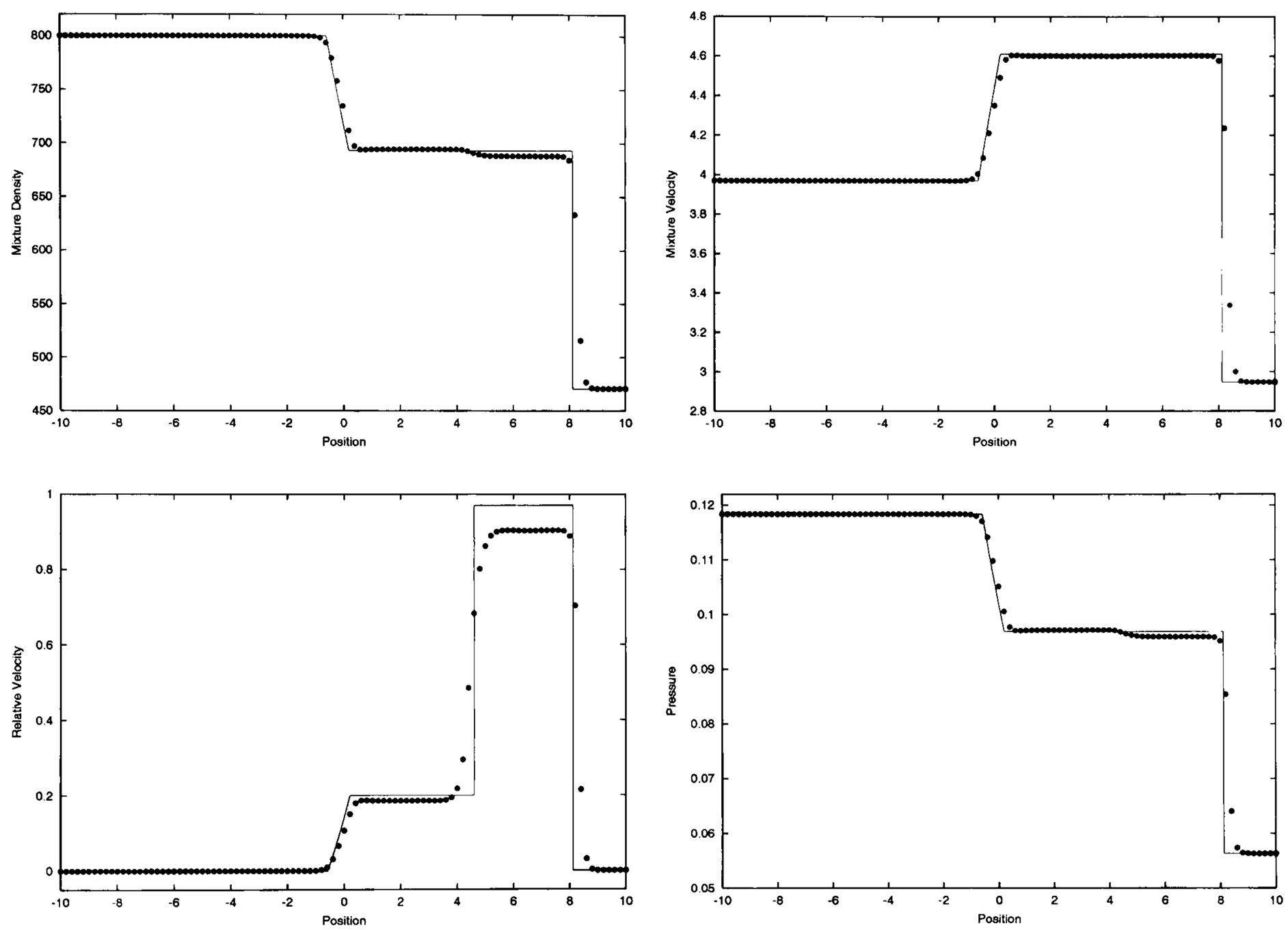

Figure 6.5: MUSCL–Hancock scheme with exact Riemann solver and SUPERBEE TVD function applied to Test 1. Numerical (symbol) and exact (line) solutions are compared at $t = 1.0$.

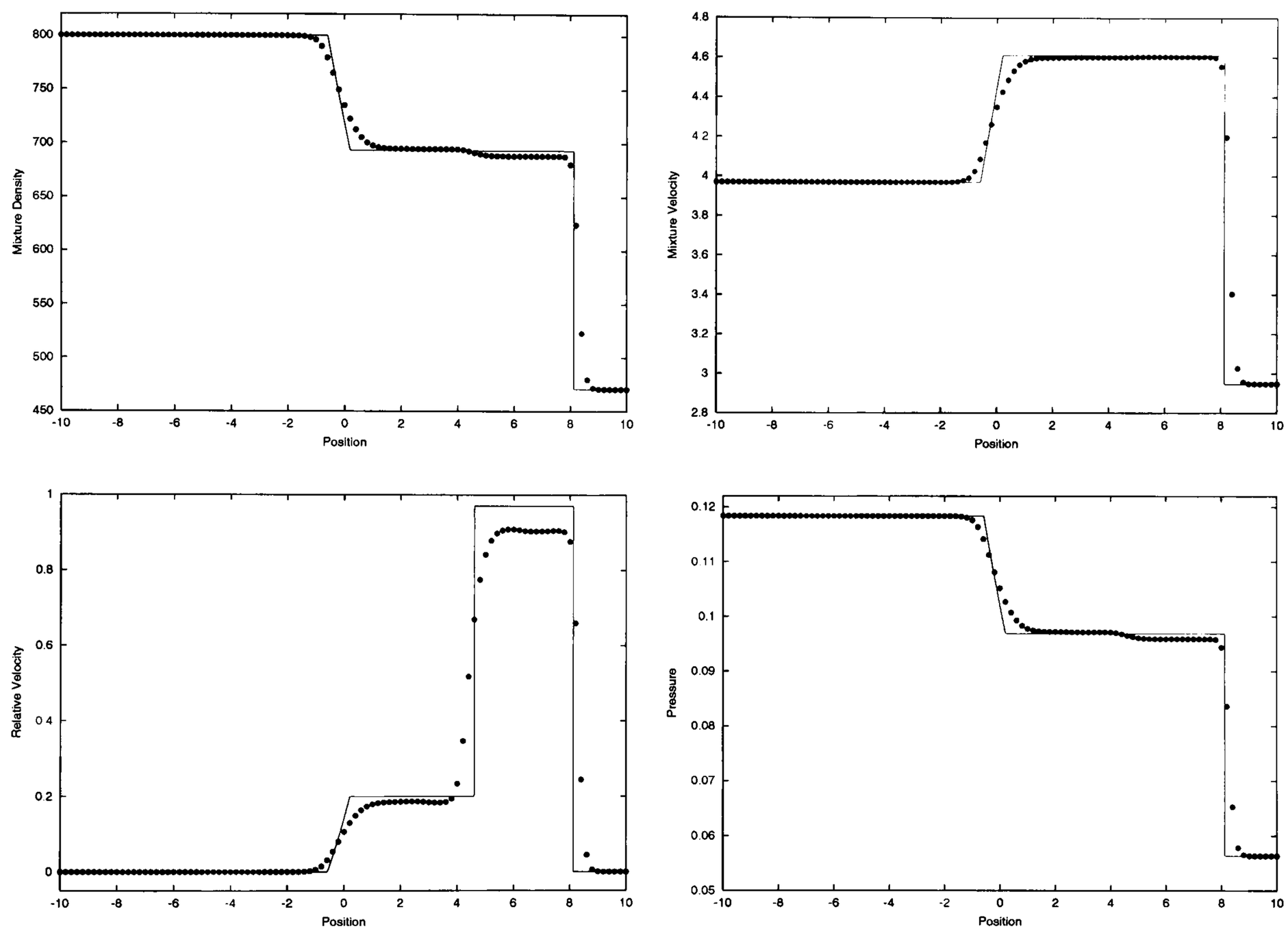

Figure 6.6: Slope LImiter Centred (SLIC) scheme with SUPERBEE TVD function applied to Test 1. Numerical (symbol) and exact (line) solutions are compared at $t = 1.0$.

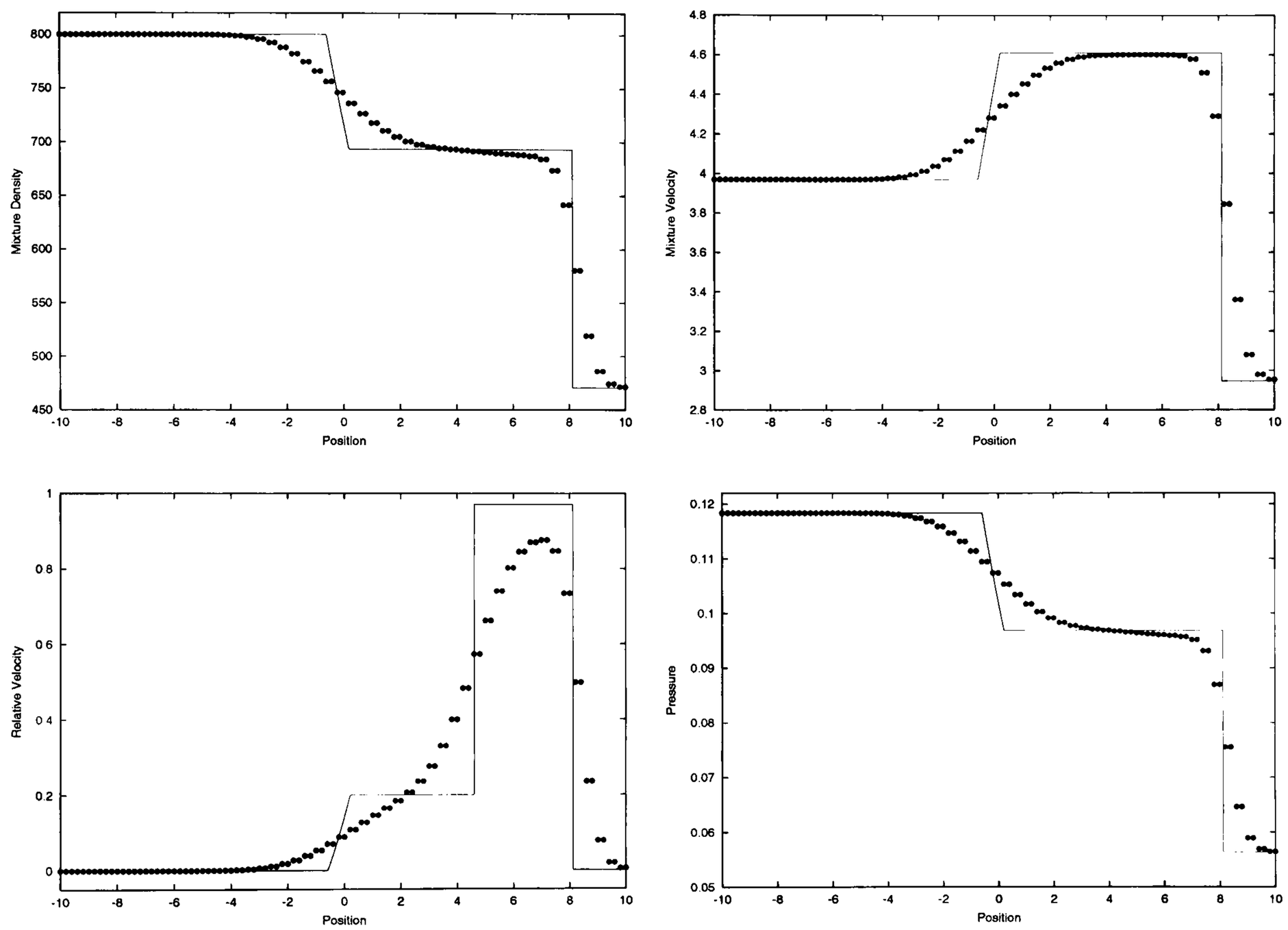

Figure 6.7: Lax–Friedrichs scheme applied to Test 1. Numerical (symbol) and exact (line) solutions are compared at $t = 1.0$.

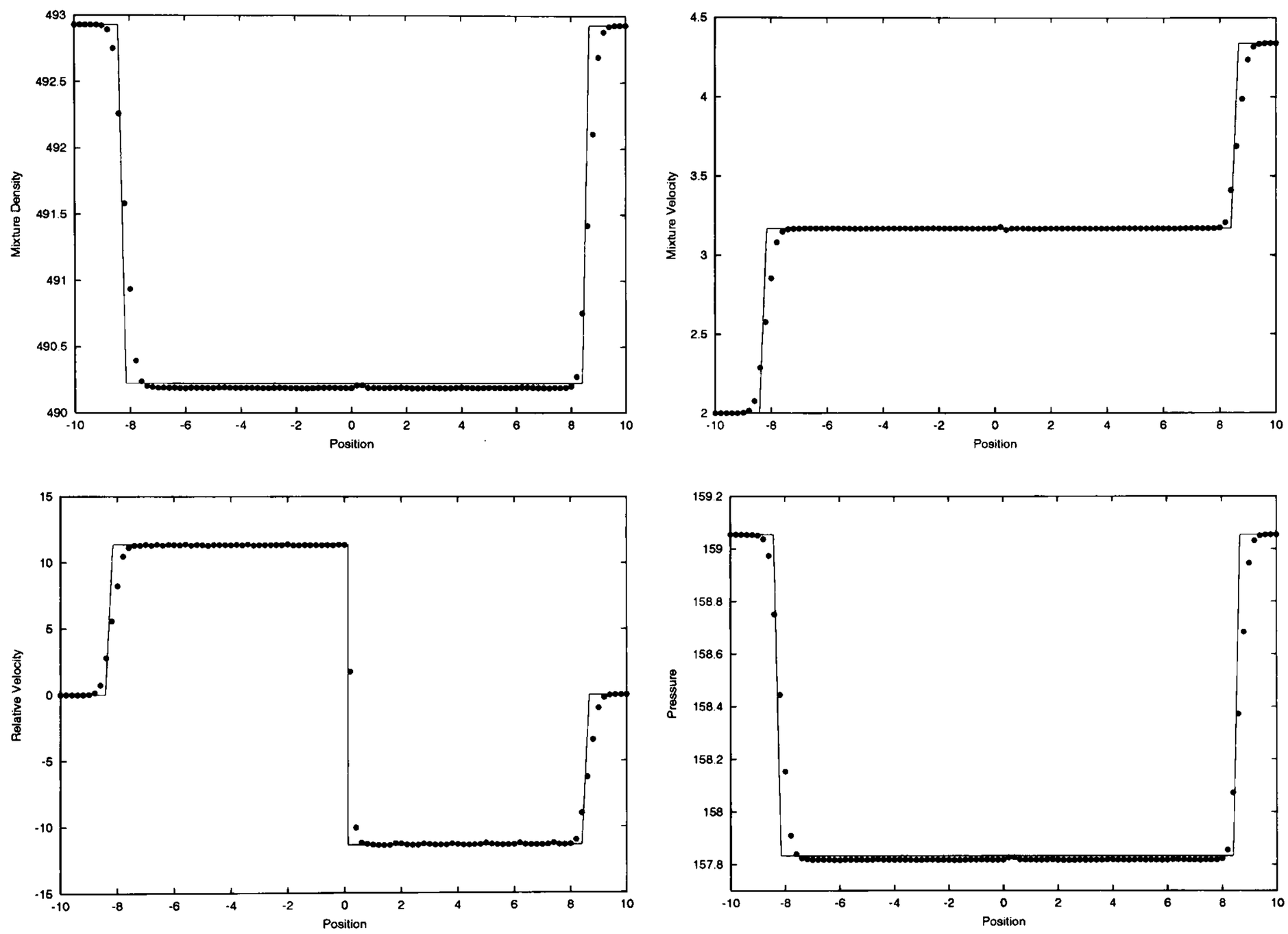

Figure 6.8: WAF scheme with HLLC Riemann solver and SUPERBEE TVD function applied to Test 2. Numerical (symbol) and exact (line) solutions are compared at $t = 0.04$.

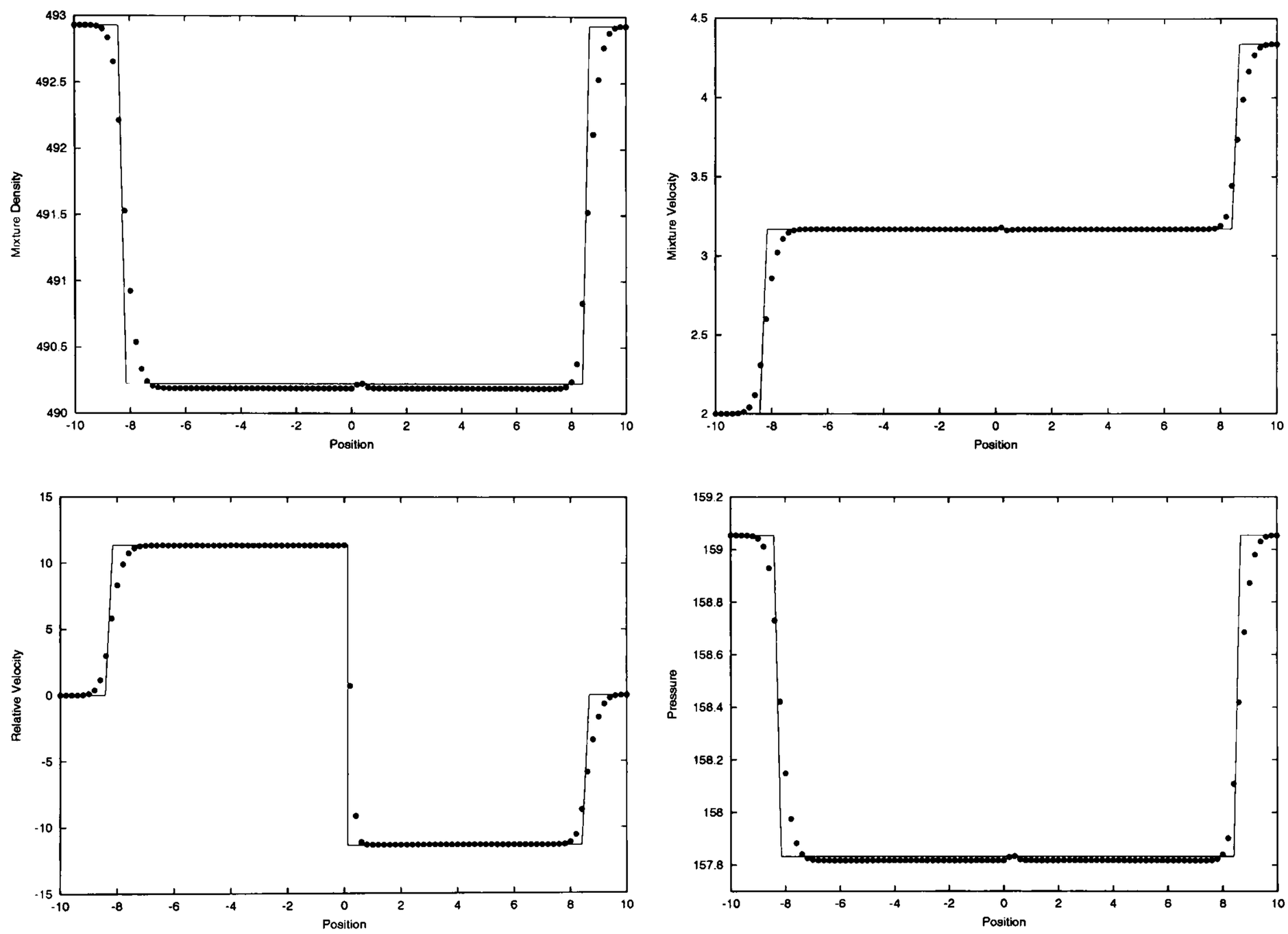

Figure 6.9: MUSCL–Hancock scheme with exact Riemann solver and SUPERBEE TVD function applied to Test 2. Numerical (symbol) and exact (line) solutions are compared at $t = 0.04$.

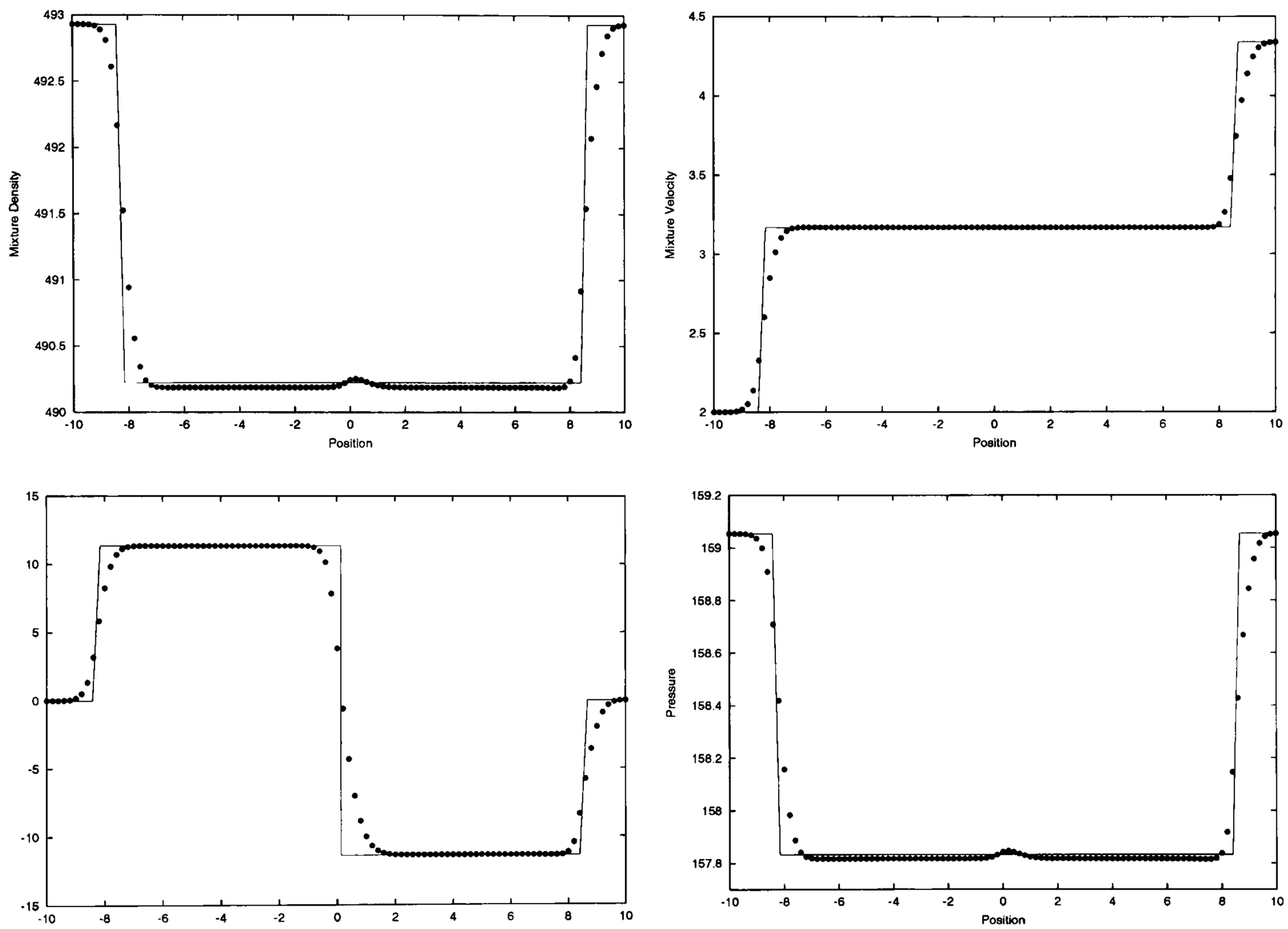

Figure 6.10: Slope LImiter Centred (SLIC) scheme with SUPERBEE TVD function applied to Test 2. Numerical (symbol) and exact (line) solutions are compared at $t = 0.04$.

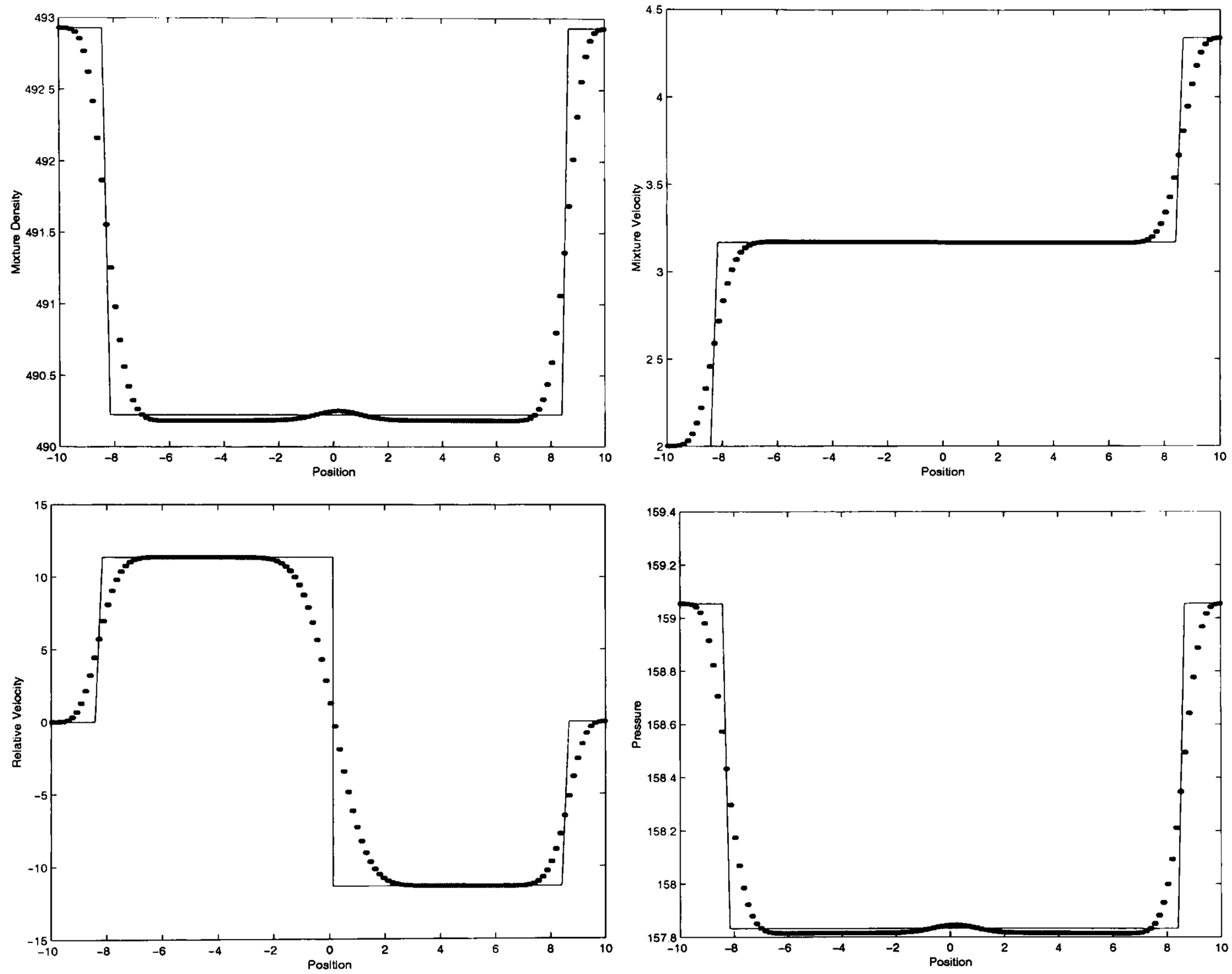

Figure 6.11: Lax–Friedrichs scheme applied to Test 2. Numerical (symbol) and exact (line) solutions are compared at $t = 0.04$.

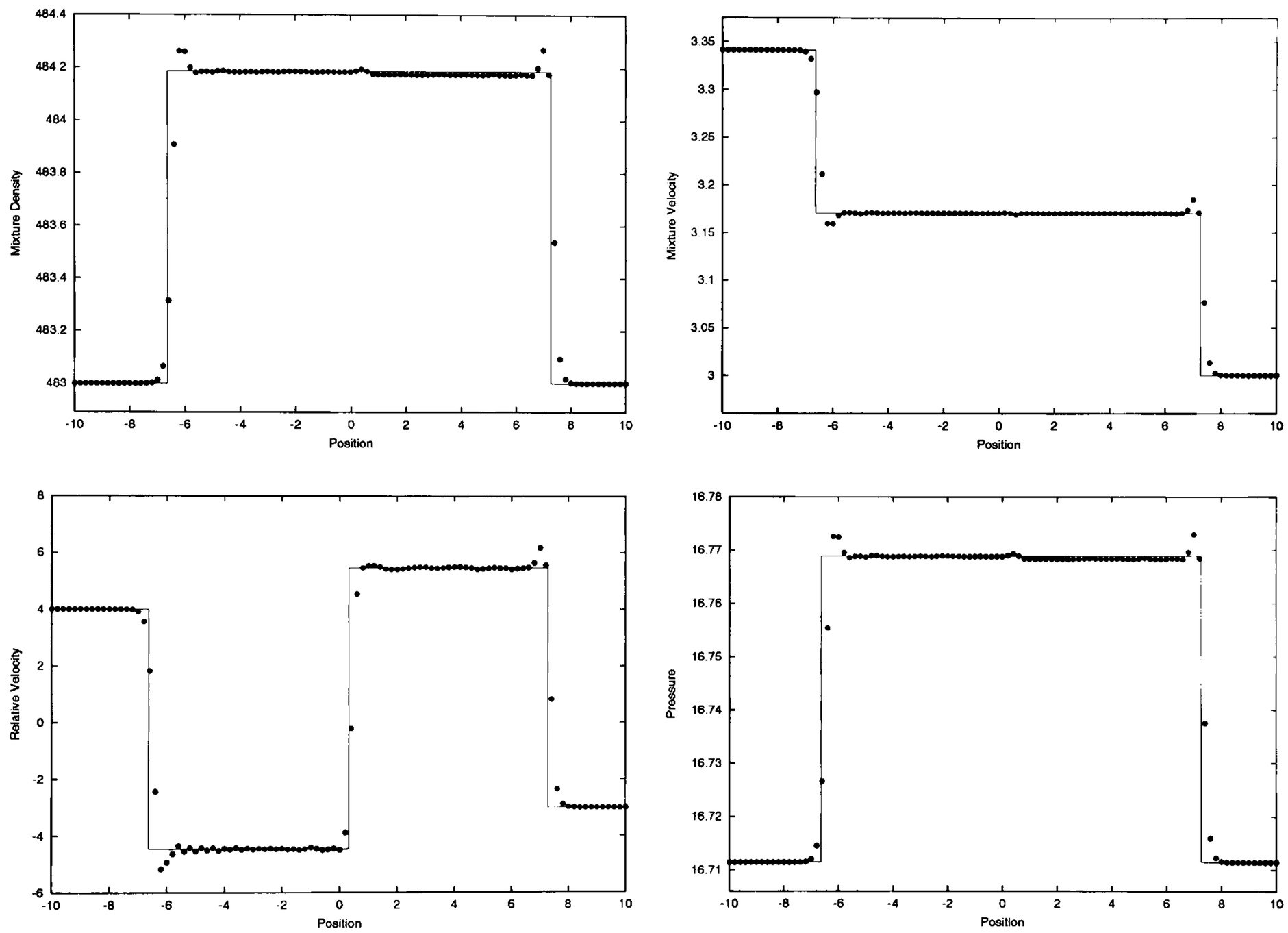

Figure 6.12: WAF scheme with HLLC Riemann solver and SUPERBEE TVD function applied to Test 3. Numerical (symbol) and exact (line) solutions are compared at $t = 0.1$.

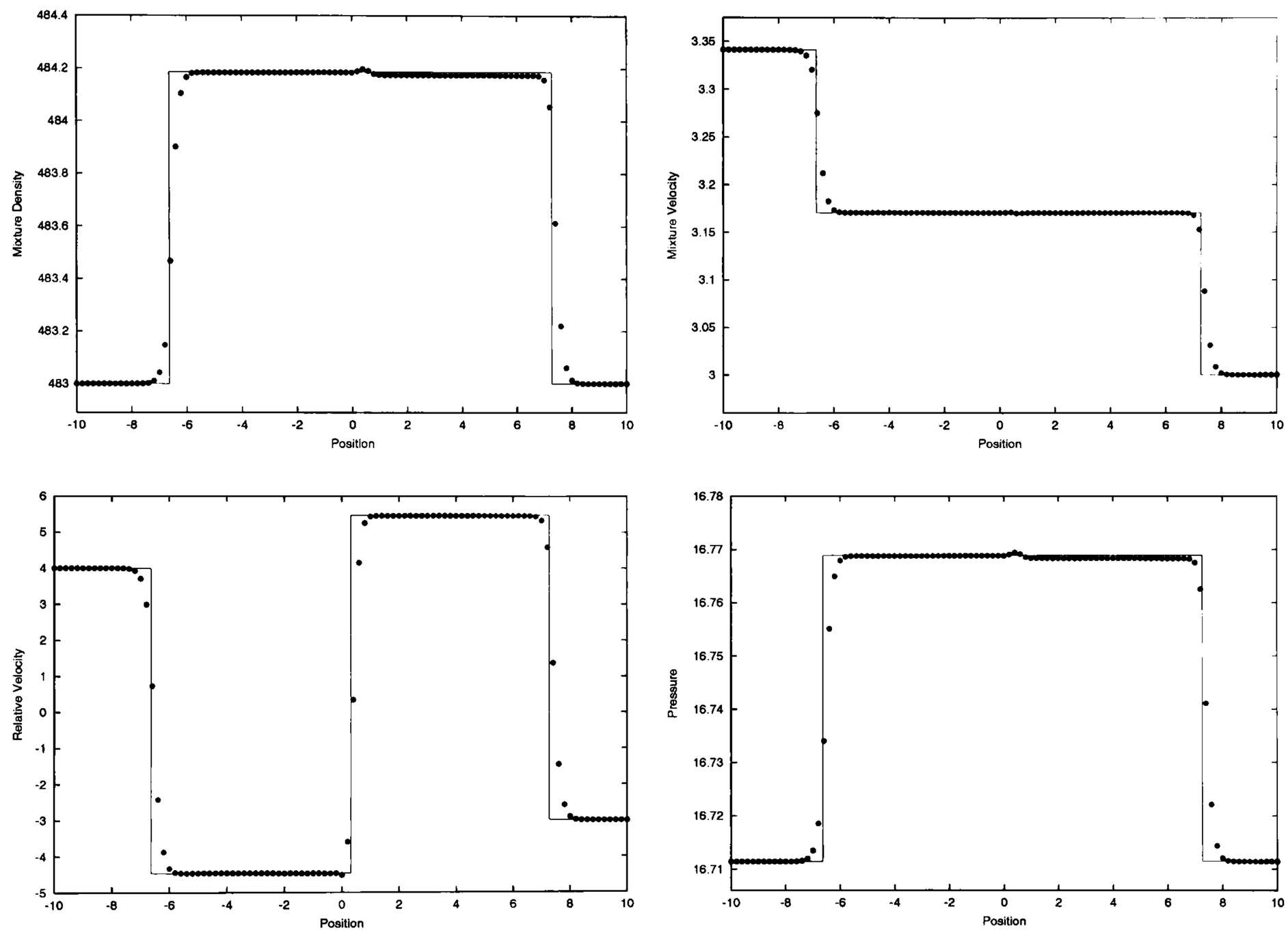

Figure 6.13: MUSCL–Hancock scheme with exact Riemann solver and SUPERBEE TVD function applied to Test 3. Numerical (symbol) and exact (line) solutions are compared at $t = 0.1$.

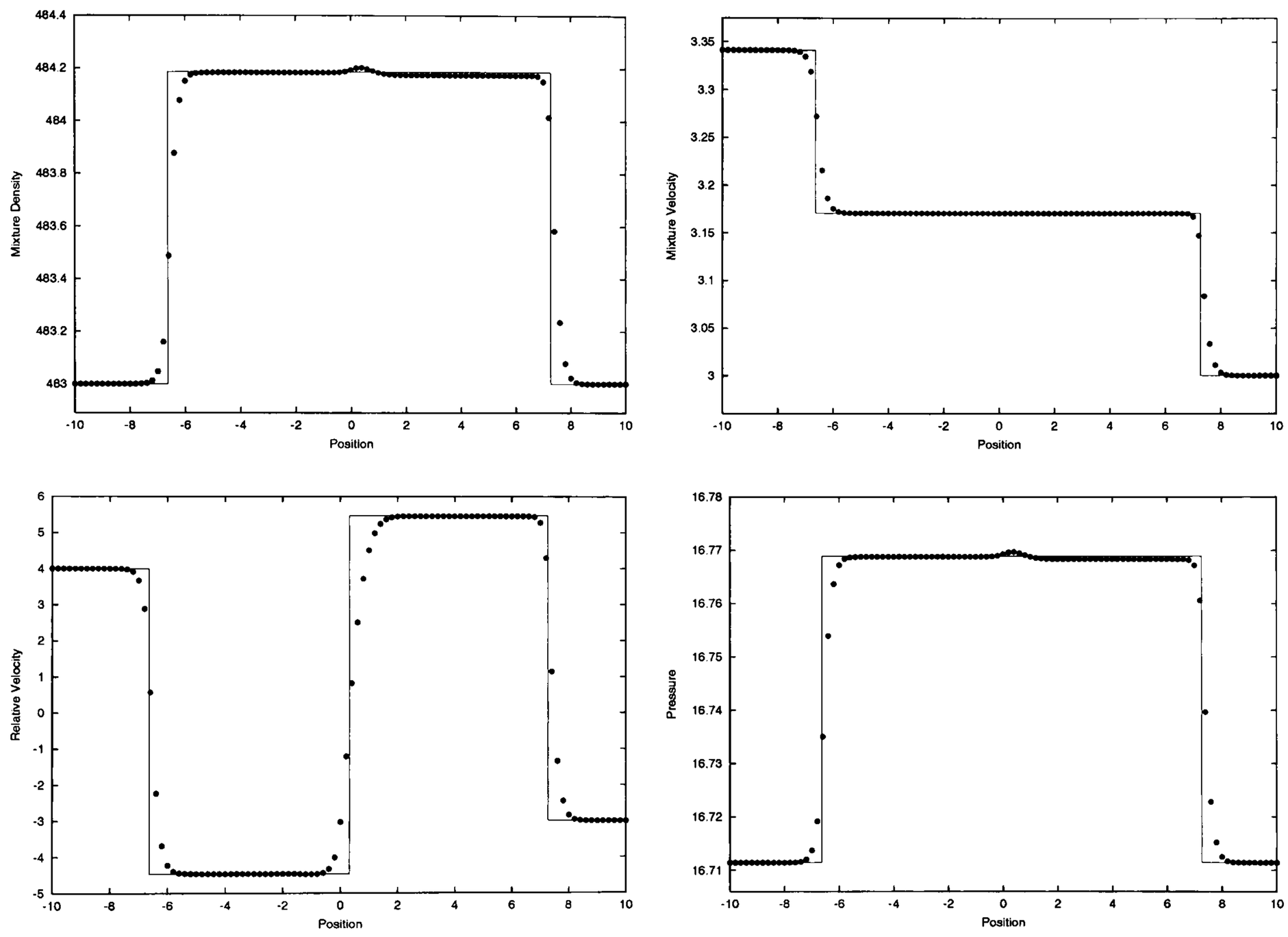

Figure 6.14: Slope LImiter Centred (SLIC) scheme with SUPERBEE TVD function applied to Test 3. Numerical (symbol) and exact (line) solutions are compared at $t = 0.1$.

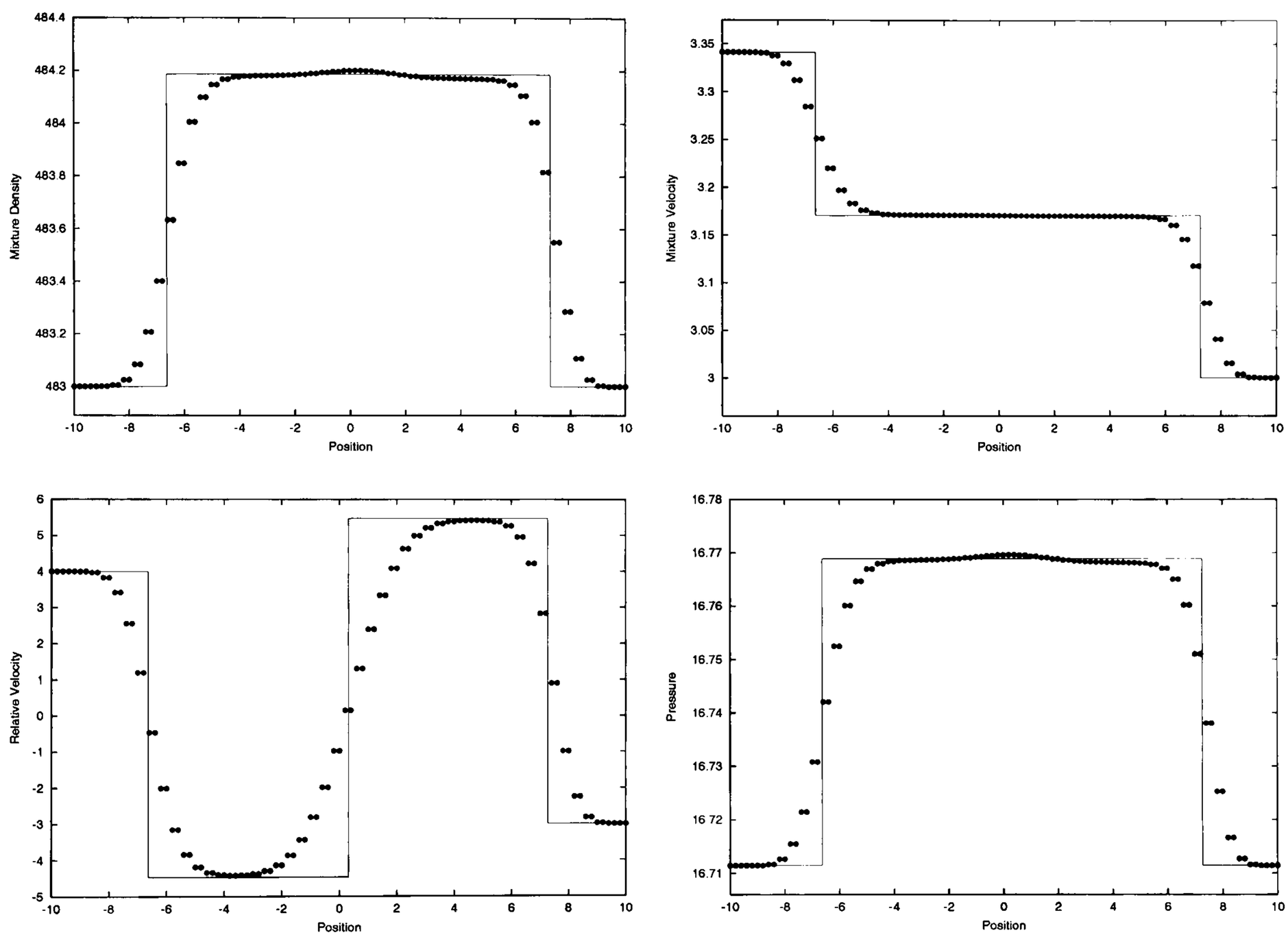

Figure 6.15: Lax–Friedrichs scheme applied to Test 3. Numerical (symbol) and exact (line) solutions are compared at $t = 0.1$.

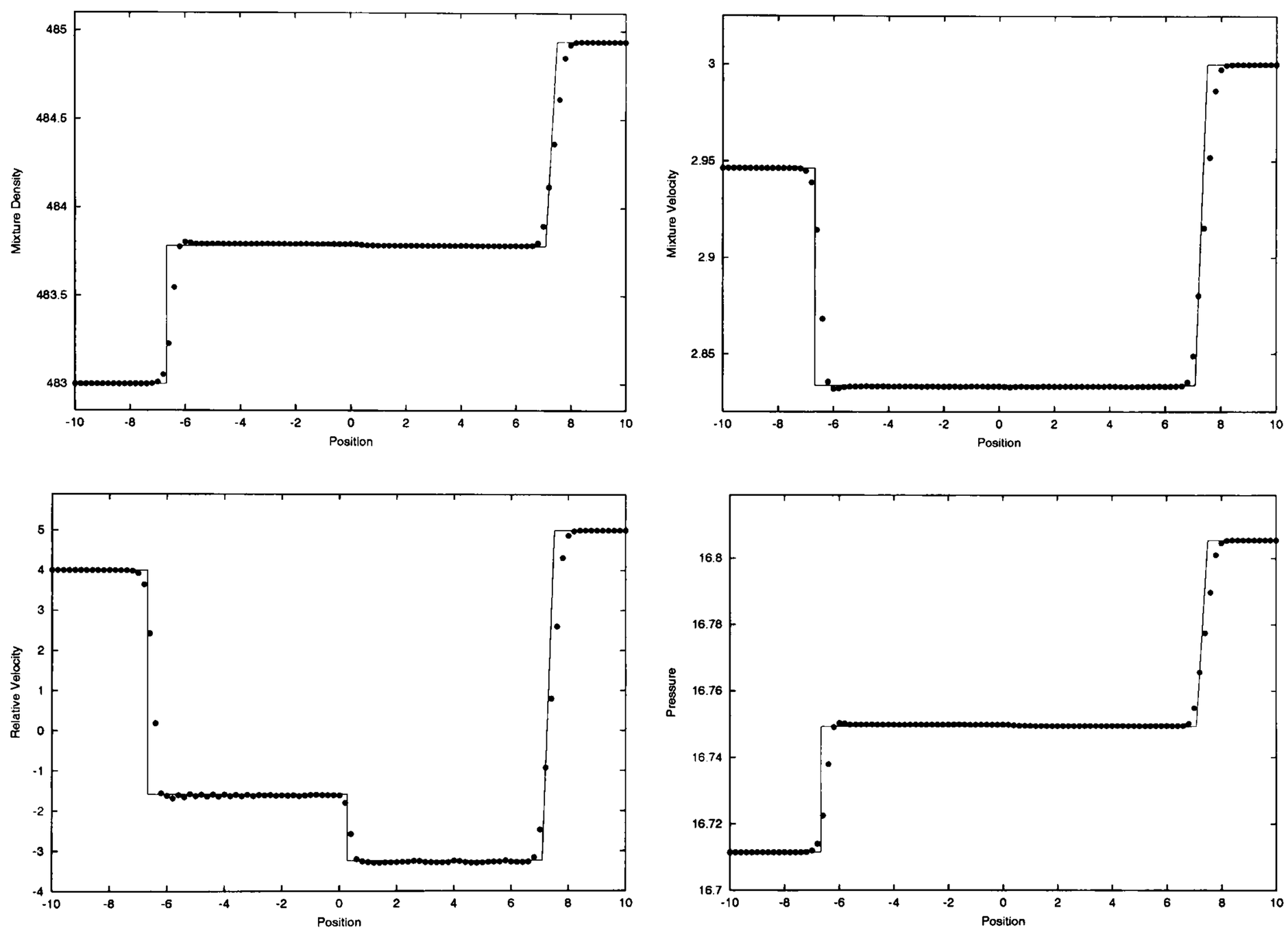

Figure 6.16: WAF scheme with HLLC Riemann solver and SUPERBEE TVD function applied to Test 4. Numerical (symbol) and exact (line) solutions are compared at $t = 0.1$.

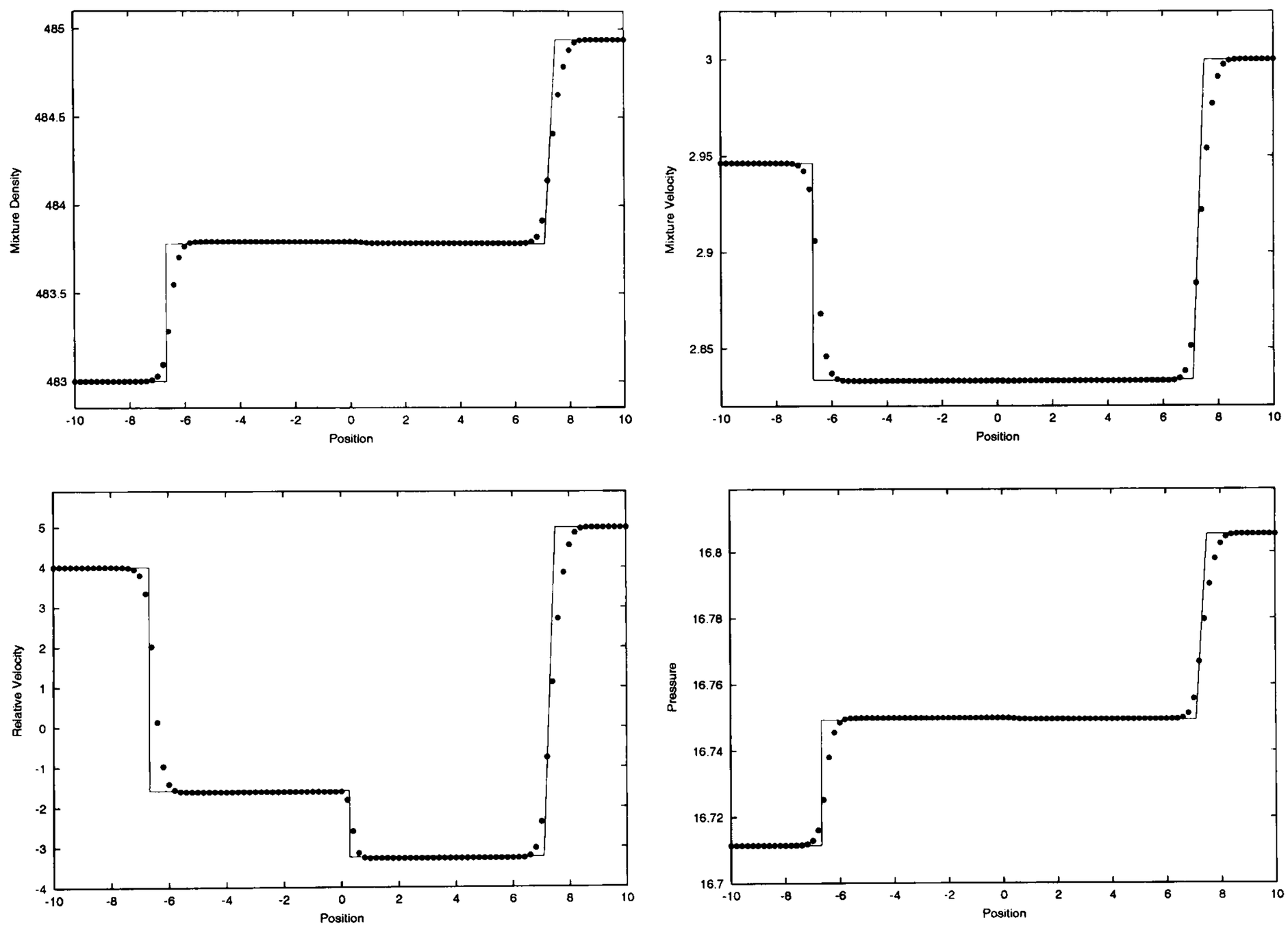

Figure 6.17: MUSCL–Hancock scheme with exact Riemann solver and SUPERBEE TVD function applied to Test 4. Numerical (symbol) and exact (line) solutions are compared at $t = 0.1$.

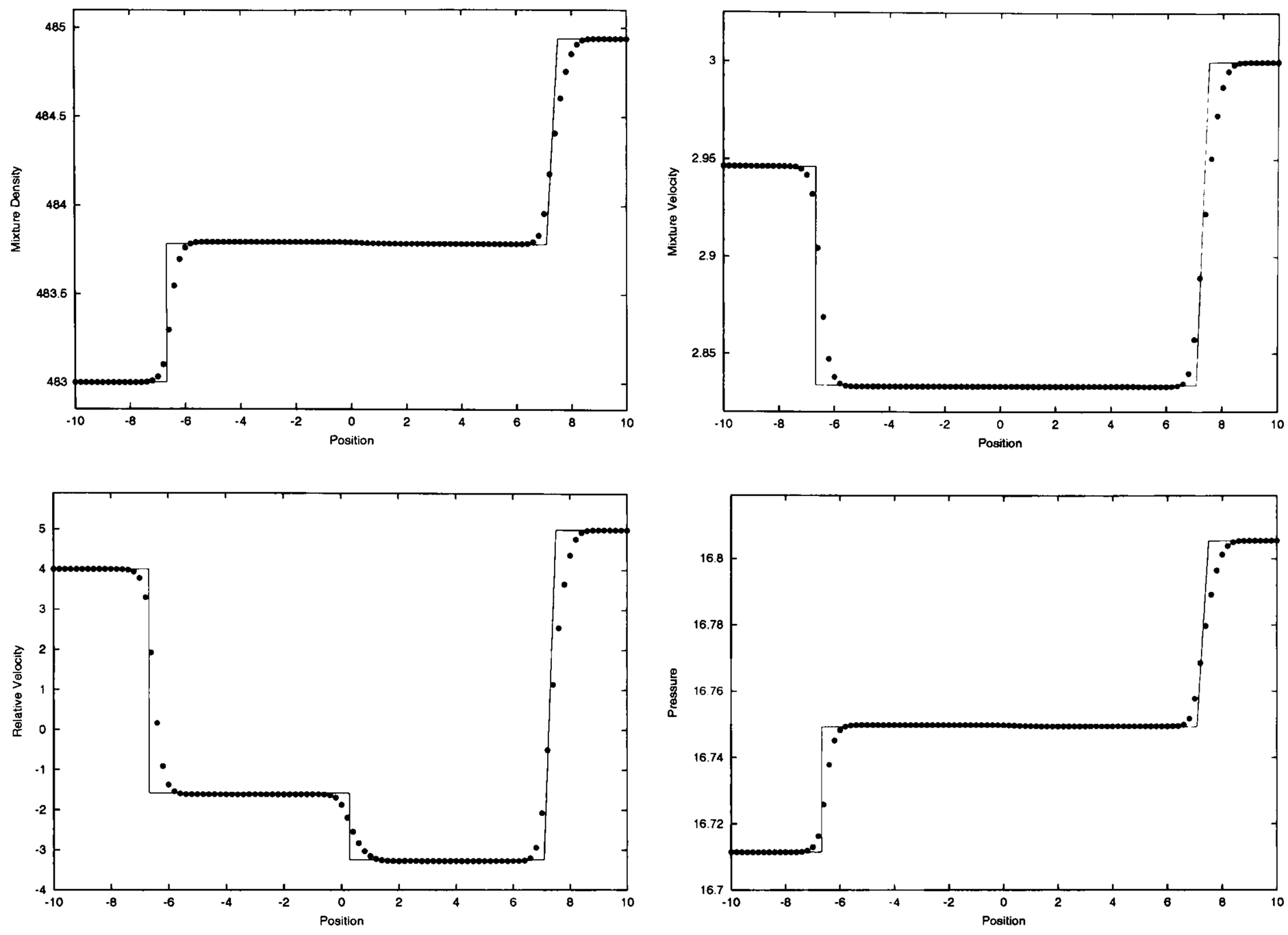

Figure 6.18: Slope LImiter Centred (SLIC) scheme with SUPERBEE TVD function applied to Test 4. Numerical (symbol) and exact (line) solutions are compared at $t = 0.1$.

6.6 Conclusions

This chapter shows the development of TVD upwind and centred schemes for the numerical solution of the simplified two–fluid model. The upwind schemes are an extension of the Godunov first–order upwind methods and are applied with exact and approximate Riemann solvers of the simplified two–fluid model. The TVD WAF scheme is second–order accurate in space and time. As the simplified two–fluid model is a non–linear system of conservation laws with three wave families, the TVD WAF scheme is applied to the system. The solution to the complete system is characterized by jumps in a single quantity u_r which is known to change across each of the three waves in the solution of the Riemann problem. The TVD MUSCL–Hancock scheme

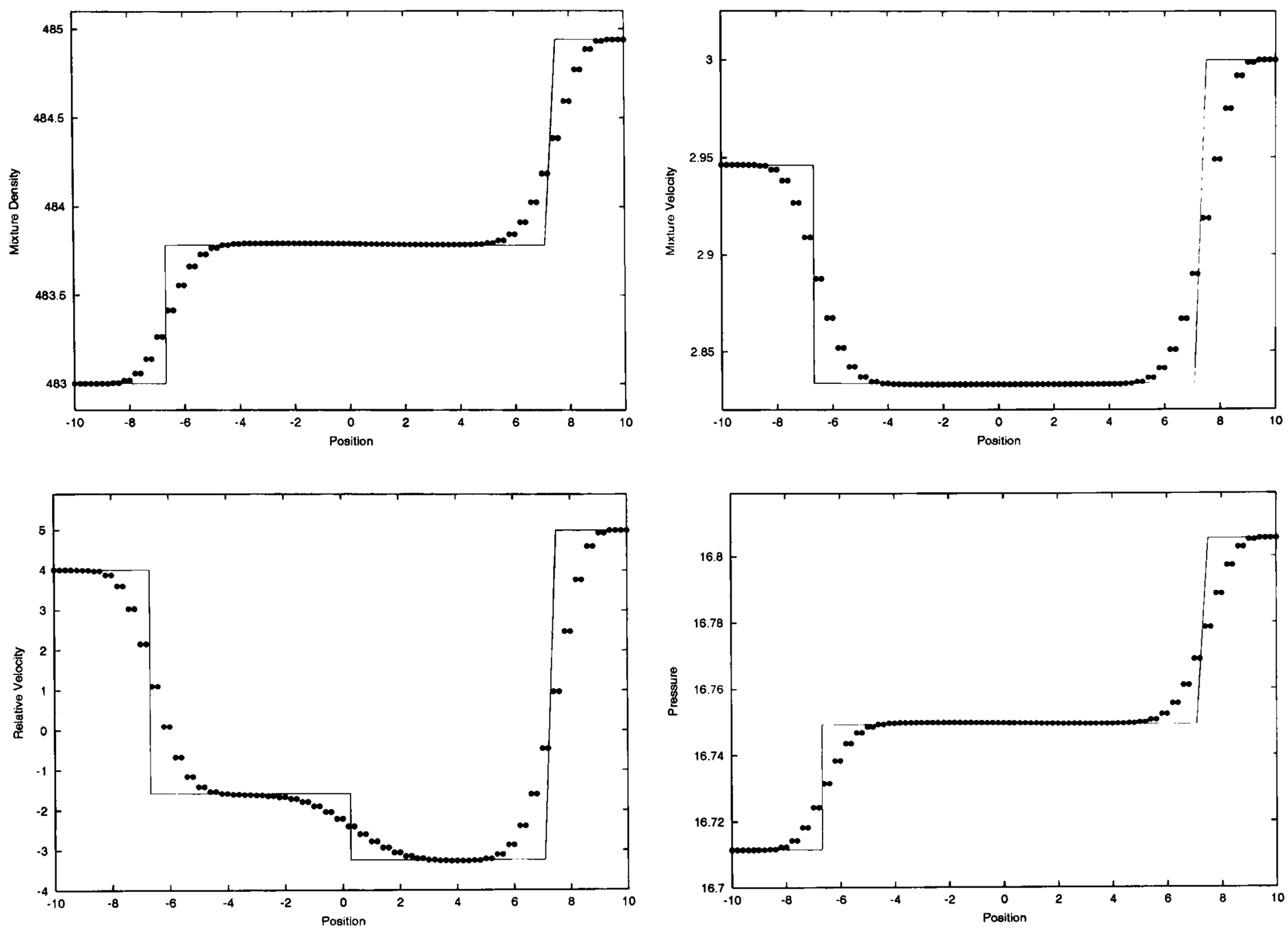

Figure 6.19: Lax–Friedrichs scheme applied to Test 4. Numerical (symbol) and exact (line) solutions are compared at $t = 0.1$.

is another second–order extension of the Godunov upwind methods developed in this chapter for the simplified two–fluid model. The centred scheme implemented in this chapter is another TVD scheme applied to the simplified two–fluid model. The SLIC scheme is a second–order scheme in space and time resulting from replacing the Godunov upwind flux in the MUSCL–Hancock scheme by the FORCE flux.

The efficiency of the subsequent methods have been demonstrated on difficult test problems and numerical results are also presented for both upwind and centred schemes as applied to the simplified two–fluid model. These results are compared with the exact solution of the simplified two–fluid model developed earlier in the thesis. The upwind results for the WAF and MUSCL–Hancock schemes have been obtained with the HLLC Riemann solver developed in the previous chapter. It is

clear that the WAF scheme gives better results than the MUSCL–Hancock scheme. The centred TVD SLIC scheme results are less accurate than those from the upwind methods. The methods developed in this chapter for the simplified two–fluid model are accurate, robust and they are expected to provide an efficient way to calculate more realistic two–phase flow problems as we shall see in the next chapters.

CHAPTER 7
MATHEMATICAL ANALYSIS OF THE HYPERBOLIC CONSERVATIVE TWO–FLUID MODEL

In previous chapters we discussed the simplified two–fluid model, derived and examined carefully the mathematical behaviour of the governing equations of the model, and constructed the numerical solution of the model. In this chapter we develop the fundamental governing equations of the hyperbolic conservative two–fluid model. The purpose is to present the origin of the one–dimensional hyperbolic conservative two–fluid model and to study the mathematical structure of the model.

7.1 General Equations for Two–phase Flow

In describing two–phase mixtures, we treat the two fluid media as constituents in which the stress tensor reduces to the pressure. The system of governing equations generalises the model developed by Romensky [145]. This theory is based on the principles of extended thermodynamics and formulates a class of thermodynamically compatible systems of conservation laws. Such a class is remarkable for its properties, namely that every system of the class is a symmetric hyperbolic one, generated by one thermodynamic potential alone and has an additional conservation law as a consequence. A complete description of the thermodynamically compatible conservation laws in continuum mechanics can be found in [60, 116, 144, 146]. The closed system of balance equations for two–phase media with different phase velocities comprises the following conservation laws of density, momentum and energy for the mixture and

additional closure governing equations:

$$\frac{\partial}{\partial t}(\rho) + \frac{\partial}{\partial x_k}(\rho u_k) = 0, \tag{7.1}$$

$$\frac{\partial}{\partial t}(\rho u_l) + \frac{\partial}{\partial x_k}(\rho u_l u_k + \mathcal{P}\delta_{kl} + \rho u_{r,l}\mathcal{E}_{u_{r,k}}) = 0, \tag{7.2}$$

$$\frac{\partial}{\partial t}\Big(\rho(\mathcal{E} + \frac{u_l u_l}{2})\Big) + \frac{\partial}{\partial x_k}\Big(\rho u_k(\mathcal{E} + \frac{u_l u_l}{2}) + \Pi_k\Big) = 0, \tag{7.3}$$

$$\frac{\partial}{\partial t}(\rho\alpha) + \frac{\partial}{\partial x_k}(\rho u_k \alpha) = \phi, \tag{7.4}$$

$$\frac{\partial}{\partial t}(\rho c) + \frac{\partial}{\partial x_k}(\rho u_k c + \rho\mathcal{E}_{u_{r,k}}) = 0, \tag{7.5}$$

$$\frac{\partial}{\partial t}(u_{r,k}) + \frac{\partial}{\partial x_k}(u_l u_{r,l} + \mathcal{E}_c) = -(e_{klj}u_l\omega_j + \pi_k). \tag{7.6}$$

Here equations (7.1)–(7.3) correspond to the mass, momentum and energy conservation laws for the mixture (although they could also be applied to each one of the two phases). Equation (7.4) is the balance law for the volume concentration of the second phase, equation (7.5) is the conservation law for the mass concentration of the second phase (with no phase transition assumption) and the last equation (7.6) is the balance law for the relative velocity. Subscripts k, l and j denote one of the three–dimensional components of the physical variables. Other subscripts denotes differentiation with respect to these subscripts. In the system (7.1)–(7.6), t is the time; x_k are the Cartesian coordinates; $\alpha = \alpha_2$ is the volume concentration for the second phase which is related to the first phase volume concentration α_1 by the relation

$$\alpha_1 + \alpha_2 = (1 - \alpha) + \alpha = 1. \tag{7.7}$$

The mixture density ρ is given by

$$\rho = \alpha_1\rho_1 + \alpha_2\rho_2, \tag{7.8}$$

where ρ_1, ρ_2 are the mass densities of phases.
The mass concentrations for the phases are

$$c_2 = \frac{\alpha\rho_2}{\rho} = c, \tag{7.9}$$

$$c_1 = \frac{(1-\alpha)\rho_1}{\rho} = (1-c). \tag{7.10}$$

The mixture momentum is given by

$$\rho u_l = (\alpha_1\rho_1 u_{1,l} + \alpha_2\rho_2 u_{2,l}), \tag{7.11}$$

where $u_{1,l}$ and $u_{2,l}$ are the velocities of the phases.
The relative velocity $u_{r,l}$ is such that

$$u_{r,l} = u_{2,l} - u_{1,l}. \tag{7.12}$$

We also define the mixture internal energy [145] as

$$\mathcal{E}(\rho, \alpha, c, u_{r,l}, \mathcal{S}) = \mathfrak{e}(\rho, \alpha, c, \mathcal{S}) + c(1-c)\frac{u_{r,l}u_{r,l}}{2}, \tag{7.13}$$

where $\mathcal{S}$ is the entropy of the mixture and $\mathfrak{e}(\rho, \alpha, c, \mathcal{S})$ is the specific potential energy of the mixture.
The pressure of the mixture [145] is defined by

$$\mathcal{P} = \rho^2\mathcal{E}_\rho = \rho^2\mathfrak{e}_\rho, \tag{7.14}$$

and ω_j is the vorticity vector. The term Π_k in equation (7.3) is given by

$$\Pi_k = \mathcal{P}u_k + \rho u_k u_{r,l}\mathcal{E}_{r_{r,l}} + \rho\mathcal{E}_c\mathcal{E}_{u_{r,k}}. \tag{7.15}$$

The source term in the volume concentration equation (7.4) describes the relaxation of volume concentration to the equilibrium state with relaxation time τ which can be

a function of parameters of state, that is,

$$\phi = -\frac{\rho}{\tau}\mathcal{E}_\alpha. \tag{7.16}$$

The source term in the relative velocity equation (7.6) dominates the interfacial friction

$$\pi_k = \kappa\mathcal{E}_{u_{r,k}} = \kappa c(1-c)u_{r,k}, \tag{7.17}$$

where κ can depend on the parameters of state and ω_j is the relative–velocity vorticity vector.

The system (7.1)–(7.6) is compatible with two additional conservation laws [145]

$$\frac{\partial u_{r,k}}{\partial x_l} - \frac{\partial u_{r,l}}{\partial x_k} = e_{klj}\omega_j, \tag{7.18}$$

$$\frac{\partial \omega_k}{\partial t} + \frac{\partial(u_l\omega_k - u_k\omega_l + e_{klj}\pi_j)}{\partial x_l} = 0. \tag{7.19}$$

Equation (7.18) is the definition of the relative velocity vorticity vector, while equation (7.19) is the compatibility condition between vorticity and interfacial friction. Here, the vorticity ω_j, which is not a parameter of state, allows us to write the conservative form for the relative velocity equation. More precisely, from equation (7.18), equation (7.6) can be written as

$$\frac{\partial u_{r,k}}{\partial t} + u_l\frac{\partial u_{r,k}}{\partial x_l} + \frac{\partial \mathcal{E}_c}{\partial x_k} + u_{r,l}\frac{\partial u_l}{\partial x_k} = -\pi_k. \tag{7.20}$$

The equations (7.1)–(7.5) and (7.20) form a closed system for $\rho, u_l, \mathcal{S}, \alpha, c, u_{r,k}$ and after solving these equations, the vorticity ω_l can be found using (7.18).

An additional entropy balance law is valid for the solution to the system (7.1)–(7.6)

$$\frac{\partial \rho\mathcal{S}}{\partial t} + \frac{\partial \rho u_k\mathcal{S}}{\partial x_k} = \frac{1}{\mathcal{E}_\mathcal{S}}\left(\mathcal{E}_\alpha\phi + \rho\mathcal{E}_{u_{r,k}}\pi_k\right). \tag{7.21}$$

The right hand side in the above equation is the entropy production and it is a non negative quantity due to appropriate definitions of ϕ and π_k.

The important fact is the possibility to reduce the system (7.1)–(7.6) in process without dissipation to symmetric hyperbolic form with the use of stationary law for the vorticity (7.18). The proof can be done by introducing a special generating potential and the hyperbolicity is provided by the convexity of this potential. The symmetric hyperbolicity was proved for a simpler system in which a balance law for the volume concentration was not included in the complete system of balance laws [60, 145].

To close the system of governing equations it is necessary to define the equation of state (7.13), namely the specific potential energy $\mathfrak{e}$. Assuming that the equations of state for each constituent are given functions of their own parameters of state we develop the derivation of a common equation of state for the mixture. From the definition of the mixture parameters of state follows that the mass densities of each phase are

$$\rho_1 = \frac{(1-c)\rho}{(1-\alpha)}, \tag{7.22}$$

and

$$\rho_2 = \frac{c\rho}{\alpha}. \tag{7.23}$$

Let us suppose that $\mathfrak{e}_1(\rho_1, \mathcal{S}_1)$ and $\mathfrak{e}_2(\rho_2, \mathcal{S}_2)$ are the equations of state for the two phases and define the specific potential energy for the mixture as

$$\tilde{\mathfrak{e}}(\rho, \alpha, c, \mathcal{S}_1, \mathcal{S}_2) = c_1\mathfrak{e}_1(\rho_1, \mathcal{S}_1) + c_2\mathfrak{e}_2(\rho_2, \mathcal{S}_2) + \mathfrak{e}_0(c), \tag{7.24}$$

where $\mathfrak{e}_0(c)$ is the excess energy providing in particular the thermodynamic equilibrium condition $\mathfrak{e}_c = 0$ if $c = 0$ or $c = 1$ at normal conditions (by convention "normal conditions" can be regarded as the state under atmospheric pressure and temperature 293K and its parameters can be defined as $\rho_1 = \rho_1^0$, $\rho_2 = \rho_2^0$, $\mathcal{S} = 0$). Further we

choose

$$\mathfrak{e}_0(c) = \frac{1}{2}B_1c_1^2 + \frac{1}{2}B_2c_2^2 = \frac{1}{2}B_1(1-c)^2 + \frac{1}{2}B_2c^2, \tag{7.25}$$

with

$$B_1 = \frac{A_1}{\gamma_1 - 1}(\gamma_1 - 1) - \frac{A_2}{\gamma_2 - 1}(\gamma_2 - 1) - A_0, \tag{7.26}$$

where A_0, A_1 and A_2 are given constants, and $B_2 = -B_1$ in (7.25).

The definition (7.24) of the equation of state of the mixture allows us to derive the governing equations in terms of the individual parameters of state of the phases. Moreover, using the relations (7.8), (7.9) and (7.10) we derive a thermodynamic identity as

$$\begin{aligned} d\tilde{\mathfrak{e}}(\rho, \alpha, c, \mathcal{S}_1, \mathcal{S}_2) &= \tilde{\mathfrak{e}}_\rho d\rho + \tilde{\mathfrak{e}}_c dc + \tilde{\mathfrak{e}}_\alpha d\alpha + \tilde{\mathfrak{e}}_{\mathcal{S}_1} d\mathcal{S}_1 + \tilde{\mathfrak{e}}_{\mathcal{S}_2} d\mathcal{S}_2 \\ &= \frac{1}{\rho^2}(\alpha_1\mathcal{P}_1 + \alpha_2\mathcal{P}_2)d\rho + \frac{1}{\rho}(\mathcal{P}_1 - \mathcal{P}_2)d\alpha \\ &+ (\mathfrak{e}_2 - \mathfrak{e}_1 + \frac{\mathcal{P}_2}{\rho_2} - \frac{\mathcal{P}_1}{\rho_1} + \mathfrak{e}_{0_c})dc \\ &+ c_1\mathcal{T}_1 d\mathcal{S}_1 + c_2\mathcal{T}_2 d\mathcal{S}_2, \end{aligned} \tag{7.27}$$

where the pressures $\mathcal{P}_j$ $(j = 1, 2)$ and temperatures $\mathcal{T}_j$ $(j = 1, 2)$ of the two phases are

$$\mathcal{P}_j = \rho_j^2(\mathfrak{e}_j)_{\rho_j}, \tag{7.28}$$

$$\mathcal{T}_j = (\mathfrak{e}_j)_{\mathcal{S}_j}. \tag{7.29}$$

Now we pass to the new thermodynamic variables connected with the phase entropies and temperatures. We can define

$$\mathcal{S}_1 = \mathcal{S} - \Delta, \tag{7.30}$$

$$\mathcal{S}_2 = \mathcal{S} + \Delta, \tag{7.31}$$

where $\mathcal{S}$ is the mean entropy of the mixture and Δ is the parameter characterizing thermal nonequilibriumity.

Using the above definition, equality (7.27) can be rewritten in the form

$$\begin{aligned}
d\tilde{\mathfrak{e}}(\rho,\alpha,c,\mathcal{S}_1,\mathcal{S}_2) &= d\hat{\mathfrak{e}}(\rho,\alpha,c,\mathcal{S},\Delta) \\
&= \hat{\mathfrak{e}}_\rho d\rho \\
&+ \hat{\mathfrak{e}}_c dc + \hat{\mathfrak{e}}_\alpha d\alpha \\
&+ \hat{\mathfrak{e}}_\mathcal{S} d\mathcal{S} + \hat{\mathfrak{e}}_\Delta d\Delta \\
&= \frac{1}{\rho^2}(\alpha_1\mathcal{P}_1 + \alpha_2\mathcal{P}_2)d\rho \\
&+ \frac{1}{\rho}(\mathcal{P}_1 - \mathcal{P}_2)d\alpha \\
&+ (\mathfrak{e}_2 - \mathfrak{e}_1 + \frac{\mathcal{P}_2}{\rho_2} - \frac{\mathcal{P}_1}{\rho_1} + \mathfrak{e}_{0c})dc \\
&+ (c_1\mathcal{T}_1 + c_2\mathcal{T}_2)d\mathcal{S} \\
&+ (c_2\mathcal{T}_2 - c_1\mathcal{T}_1)d\Delta. \qquad (7.32)
\end{aligned}$$

The final step in the definition of the equation of state for our model is the assumption that the potential energy for the mixture does not depend on Δ, that is

$$\mathfrak{e}(\rho,\alpha,c,\mathcal{S}) = \hat{\mathfrak{e}}(\rho,\alpha,c,\mathcal{S},\Delta)|_{\Delta=0}. \qquad (7.33)$$

This assumption is correct for the processes in which the variation of entropy is not too large. A more complicated case could be considered in a more sophisticated two–temperature model of two–phase flow with thermal nonequilibriumity.

Thus we have the thermodynamic identity defining the equation of state for the system (7.1)–(7.6)

$$\begin{aligned}
d\mathfrak{e}(\rho,\alpha,c,\mathcal{S}) &= \mathfrak{e}_\rho d\rho + \mathfrak{e}_c dc + \mathfrak{e}_\alpha d\alpha + \mathfrak{e}_\mathcal{S} d\mathcal{S} \\
&= \frac{1}{\rho^2}(\alpha_1\mathcal{P}_1 + \alpha_2\mathcal{P}_2)d\rho + \frac{1}{\rho}(\mathcal{P}_1 - \mathcal{P}_2)d\alpha \\
&+ (\mathfrak{e}_2 - \mathfrak{e}_1 + \frac{\mathcal{P}_2}{\rho_2} - \frac{\mathcal{P}_1}{\rho_1} + \mathfrak{e}_{0c})dc \\
&+ (c_1\mathcal{T}_1 + c_2\mathcal{T}_2)d\mathcal{S}, \qquad (7.34)
\end{aligned}$$

from which we conclude that

$$\mathcal{P} = \rho^2 \mathfrak{e}_\rho = \alpha_1 \mathcal{P}_1 + \alpha_2 \mathcal{P}_2, \tag{7.35}$$

$$\mathfrak{e}_\alpha = \frac{1}{\rho}(\mathcal{P}_1 - \mathcal{P}_2), \tag{7.36}$$

$$\mathfrak{e}_c = (\mathfrak{e}_2 - \mathfrak{e}_1 + \frac{\mathcal{P}_2}{\rho_2} - \frac{\mathcal{P}_1}{\rho_1} + \mathfrak{e}_{0c}), \tag{7.37}$$

$$\mathcal{T} = \mathfrak{e}_{\mathcal{S}} = c_1 \mathfrak{e}_{1_{\mathcal{S}}} + c_2 \mathfrak{e}_{2_{\mathcal{S}}}. \tag{7.38}$$

Here $\mathfrak{e}_c$ is the difference of the enthalpies [116] for the two phases supplemented by the normalizing term $\mathfrak{e}_{0c}$ arising from excess energy and $\mathcal{T}$ is the temperature of the mixture.

Using the above relationships between the parameters of state for the mixture and individual phases the closed system of balance laws selected from the above equations can be written in terms of parameters $\rho_1, \rho_2, \alpha, u_{1,l}, u_{2,l}, \mathcal{S}$ as follows:

$$\frac{\partial}{\partial t}(\alpha_1\rho_1 + \alpha_2\rho_2) + \frac{\partial}{\partial x_k}(\alpha_1\rho_1 u_{1,k} + \alpha_2\rho_2 u_{2,k}) = 0, \tag{7.39}$$

$$\frac{\partial}{\partial t}(\alpha_1\rho_1 u_{1,l} + \alpha_2\rho_2 u_{2,l}) + \frac{\partial}{\partial x_k}(\alpha_1\rho_1 u_{1,l}u_{1,k} + \alpha_2\rho_2 u_{2,l}u_{2,k} + \mathcal{P}\delta_{lk}) = 0, \tag{7.40}$$

$$\frac{\partial}{\partial t}((\alpha_1\rho_1 + \alpha_2\rho_2)\alpha) + \frac{\partial}{\partial x_k}((\alpha_1\rho_1 u_{k,1} + \alpha_2\rho_2 u_{k,2})\alpha) = \phi, \tag{7.41}$$

$$\frac{\partial}{\partial t}(\alpha_2\rho_2) + \frac{\partial}{\partial x_k}(\alpha_2\rho_2 u_{2,k}) = 0, \tag{7.42}$$

$$\frac{\partial}{\partial t}(u_{2,k} - u_{1,k}) + \frac{\partial}{\partial x_k}(\frac{u_{2,l}u_{2,l}}{2} - \frac{u_{1,l}u_{1,l}}{2} + \mathfrak{e}_2 - \mathfrak{e}_1 + \frac{\mathcal{P}_2}{\rho_2} - \frac{\mathcal{P}_1}{\rho_1} + \mathfrak{e}_{0c}) = \Gamma, \tag{7.43}$$

$$\frac{\partial}{\partial t}((\alpha_1\rho_1 + \alpha_2\rho_2)\mathcal{S}) + \frac{\partial}{\partial x_k}((\alpha_1\rho_1 u_{1,k} + \alpha_2\rho_2 u_{2,k})\mathcal{S}) = \Lambda, \tag{7.44}$$

$$\frac{\partial u_{r,k}}{\partial x_j} - \frac{\partial u_{r,j}}{\partial x_k} = \Theta, \tag{7.45}$$

where the source terms are

$$\phi = -\frac{1}{\tau}(\mathcal{P}_1 - \mathcal{P}_2), \tag{7.46}$$

$$\Gamma = -(e_{klj}u_l\omega_j + \pi_k), \quad \pi_k = \kappa c(1-c)u_{r,k}. \tag{7.47}$$

$$\Lambda = \frac{1}{\mathcal{T}}\left(\frac{(\mathcal{P}_1 - \mathcal{P}_2)^2}{\rho\tau} + \rho\kappa c(1-c)u_{r,k}u_{r,k}\right) \geq 0, \tag{7.48}$$

$$\Theta = -e_{klj}\omega_j. \tag{7.49}$$

We can see that the two–phase flow conservation laws are supplemented here by the balance law for the relative velocity. This law postulates that the relative velocity arises if there exists a gradient of the difference of enthalpies and (or) kinetic energies of phases.

It is significant to note that if the relaxation process leading to the equilibrium of volume concentration is sufficiently fast ($\tau \to 0$), then the above system gives the single–pressure approximation within the framework of the formulated model, because in this case the approximation

$$\mathcal{E}_\alpha = \frac{1}{\rho}(\mathcal{P}_1 - \mathcal{P}_2) = 0, \tag{7.50}$$

can be used instead of the equation for α.

7.2 One–Dimensional Two–Phase Flow Model–Hyperbolic Conservative Model

Two–phase flows always involve some relative motion of one phase with respect to the other. Therefore, a two–phase flow problem should be formulated in terms of two velocity fields [32, 33, 34]. Two–phase flow has applications within several areas and is known for being quite complicated both from a modeling and numerical point of view. Following Romenski [145], one–dimensional two–phase two–fluid flow with different phase velocities can be derived from the general three–dimensional equations (7.39)–(7.45) and is governed by six first order non–linear partial differential equations. They include conservation laws of mass, momentum and energy for the mixture, a balance law for the volume concentration of the second phase, a balance law for mass concentration of the second phase and a balance law for the relative velocity between the two phases. The dynamics of two–phase flow are determined by

these balance equations which involve complicated terms for interphase exchanges of volume concentration and relative velocity between phases. In addition, the relaxation of volume concentration to equilibrium state and interfacial friction are highly responsible for the development of the flow.

The two–fluid model is widely used within the chemical reactors and it is well known that modeling of flows involving mixtures is a difficult task. Another area of application for two–phase fluid flows concerns, for example, safety of nuclear reactors which is an area of great importance for the industrial field. Considering two–phase flow in the nuclear industry it is convenient to identify a class of physical phenomena such as pressure wave propagation through a gas and liquid flow. Pressure wave propagation study is useful for safety purposes, for flow regulation, and to give information about flow properties. Further knowledge about pressure wave propagation can aid in flow control because a change in flow rate or pressure at the inlet or outlet generates a pressure wave. From a numerical point of view, the correct description of pressure waves requires high–order schemes possessing little numerical diffusion. In addition, it is very important that the schemes can produce solutions within a reasonable amount of accuracy and time. The effects of viscosity are assumed to be absent and there is no mass transfer between the phases. The one–dimensional hyperbolic conservative model then takes the following form:

The mixture mass conservation equation

$$\partial_t(\rho) + \partial_x(\rho u) = 0. \tag{7.51}$$

The mixture momentum conservation equation

$$\partial_t(\rho u) + \partial_x(\rho u^2 + \mathcal{P} + \rho u_r \mathcal{E}_{u_r}) = 0. \tag{7.52}$$

The mixture energy conservation equation

$$\partial_t(\rho(\mathcal{E} + \frac{u^2}{2})) + \partial_x(\rho u(\mathcal{E} + \frac{u^2}{2}) + \mathcal{P}u + \rho u u_r \mathcal{E}_{u_r} + \rho \mathcal{E}_c \mathcal{E}_{u_r}) = 0. \tag{7.53}$$

In (7.51)–(7.52)–(7.53), t is the time; x is the flow direction (space coordinate); α is the volume fraction of the gas phase; $\rho = (1-\alpha)\rho_1 + \alpha\rho_2$ is the mixture density; $\rho u = (1-\alpha)\rho_1 u_1 + \alpha\rho_2 u_2$ is the mixture momentum and the subscripts 1 and 2 refers to the liquid and gas phases respectively. The conserved quantities in (7.51)–(7.52)–(7.53) represent the mixture mass, mixture momentum and mixture energy. In addition, several closure laws must be given which involve the gas volume concentration law, the mass gas concentration law and the relative velocity law.

The gas volume concentration balance law is

$$\partial_t(\rho\alpha) + \partial_x(\rho u\alpha) = \phi. \tag{7.54}$$

The source term ϕ is found to be

$$\phi = -\frac{\rho}{\tau}\mathcal{E}_\alpha, \tag{7.55}$$

describing the relaxation of volume concentration to equilibrium state with relaxation time τ (which can be a function of parameters of state).

The mass gas concentration conservation law is

$$\partial_t(\rho c) + \partial_x(\rho u c) = 0. \tag{7.56}$$

Finally, the relative velocity balance law can be written as

$$\partial_t(u_r) + \partial_x(u u_r + \mathcal{E}_c) = \pi, \tag{7.57}$$

where the source term π is the interfacial friction defined as

$$\pi = -\kappa c(1-c)u_r, \tag{7.58}$$

with κ depending on the parameter of state.

To close the system (7.51)–(7.52)–(7.53) and (7.54)–(7.56)–(7.57) we define the pres-

sure as

$$\mathcal{P} = \rho^2 \mathcal{E}_\rho, \tag{7.59}$$

and the mixture internal energy (EOS) as

$$\mathcal{E}(\rho, \alpha, c, u_r, \mathcal{S}) = \mathfrak{e}(\rho, \alpha, c, \mathcal{S}) + c(1-c)\frac{u_r u_r}{2}, \tag{7.60}$$

where $\mathcal{S}$ is the entropy of the mixture and $\mathfrak{e}(\rho, \alpha, c, \mathcal{S})$ is the specific potential energy of the mixture defined as

$$\mathfrak{e}(\rho, \alpha, c, \mathcal{S}) = c_1 \mathfrak{e}_1(\rho_1, \mathcal{S}) + c_2 \mathfrak{e}_2(\rho_2, \mathcal{S}) + \mathfrak{e}_0(c), \tag{7.61}$$

where $\mathfrak{e}_1$, $\mathfrak{e}_2$ are the EOS of each phase and $\mathfrak{e}_0$ is the excess energy as given in (7.25). Now if we let

$$\mathbb{U} = \begin{pmatrix} \rho \\ \rho\alpha \\ \rho u \\ \rho c \\ u_r \\ \rho(\mathcal{E} + \frac{u^2}{2}) \end{pmatrix}, \quad \mathbb{F}(\mathbb{U}) = \begin{pmatrix} \rho u \\ \rho u \alpha \\ \rho u^2 + \mathcal{P} + \rho u_r \mathcal{E}_{u_r} \\ \rho u c + \rho \mathcal{E}_{u_r} \\ u u_r + \mathcal{E}_c \\ \rho u(\mathcal{E} + \frac{u^2}{2}) + \mathcal{P} u + \rho u u_r \mathcal{E}_{u_r} + \rho \mathcal{E}_c \mathcal{E}_{u_r} \end{pmatrix}, \tag{7.62}$$

and

$$\mathbb{S}(\mathbb{U}) = \left[0, \phi, 0, 0, \pi, 0\right]^T, \tag{7.63}$$

then (7.51)–(7.52)–(7.53) and (7.54)–(7.56)–(7.57) can be written as a 6×6 system of conservation laws

$$\partial_t \mathbb{U} + \partial_x \mathbb{F}(\mathbb{U}) = \mathbb{S}(\mathbb{U}), \quad -\infty < x < \infty, \quad t > 0. \tag{7.64}$$

Letting J denote the Jacobian matrix of $\mathbb{F}$ with respect to the conservative variables $\mathbb{U}$, we can write

$$\partial_t \mathbb{U} + J\partial_x \mathbb{U} = \mathbb{S}(\mathbb{U}). \tag{7.65}$$

Generally, it is difficult to express explicitly the flux function $\mathbb{F}$ in terms of conservative variables. From a physical point of view, the vector of conservative variables $\mathbb{U}$ is not a convenient state vector to work with. The closure laws are formulated in terms of physical variables (primitive variables). Also, from a numerical point of view, numerical schemes based on conservative variables will require some iterative procedure to transform these variables into primitive variables for each calculation. This leads us to consider other alternatives based on primitive formulations. For the one–dimensional conservative two–fluid model one possible primitive formulation is the vector $\mathbb{W}$ defined as

$$\mathbb{W} = \left[\rho, \alpha, u, c, u_r, \mathcal{S}\right]^T. \tag{7.66}$$

Thus, in quasi–linear form we have

$$\partial_t \mathbb{W} + \mathbb{A}(\mathbb{W})\partial_x \mathbb{W} = \mathbb{Q}(\mathbb{W}), \tag{7.67}$$

where the Jacobian matrix $\mathbb{A}(\mathbb{W})$ is

$$\begin{pmatrix} u & 0 & \rho & 0 & 0 & 0 \\ 0 & u & 0 & 0 & 0 & 0 \\ \frac{1}{\rho}(\mathcal{P}_\rho + c(1-c)u_r^2) & \frac{\mathcal{P}_\alpha}{\rho} & u & \frac{1}{\rho}(\mathcal{P}_c + \rho(1-2c)u_r^2) & 2c(1-c)u_r & \frac{\mathcal{P}_\mathcal{S}}{\rho} \\ c(1-c)\frac{u_r}{\rho} & 0 & 0 & u + (1-2c)u_r & c(1-c) & 0 \\ \mathfrak{e}_{c\rho} & \mathfrak{e}_{\alpha c} & u_r & \mathfrak{e}_{cc} - u_r^2 & u + (1-2c)u_r & \mathfrak{e}_{c\mathcal{S}} \\ 0 & 0 & 0 & 0 & 0 & u \end{pmatrix}, \tag{7.68}$$

and the source terms are

$$\begin{aligned}\mathbb{Q}(\mathbb{W}) &= (\mathbb{U}_{\mathbb{W}})^{-1}\,\mathbb{S}(\mathbb{U}(\mathbb{W})),\\ &= \left[0, \frac{\phi}{\rho}, 0, 0, \pi, \Lambda\right]^T,\end{aligned} \tag{7.69}$$

where

$$\Lambda = -\frac{1}{\mathcal{E}_\rho}(\mathcal{E}_\alpha \phi + \mathcal{E}_{u_r}\pi) \geq 0,$$

is the entropy production.

This hyperbolic conservative two–fluid model will be useful to study shock waves in two–phase medium.

7.3 Hyperbolicity Analysis of the Equations

The analysis is presented in a one–dimensional setting. At the outset, the equations for conservative, one–dimensional two–phase flow model in process without dissipation can be written in the form of conservation laws:

$$\partial_t \mathbb{U} + \partial_x \mathbb{F}(\mathbb{U}) = 0, \quad -\infty < x < \infty, \quad t > 0, \tag{7.70}$$

where $\mathbb{U}$ and $\mathbb{F}(\mathbb{U})$ are the set of conservative variables and flux vector respectively. Here $\mathbb{U}(x,t)$ is a vector–valued function. $\mathbb{R} \times [0,\infty) \to \Omega$, Ω is the set of (physically acceptable) states and we assume that each component of $\mathbb{U}$ is a piecewise C^1 function in the sense that there is only a finite set in $\mathbb{R}$ which is not in C^1 and where the shock conditions hold. The components of $\mathbb{U}$ are the conserved quantities

$$\mathbb{U} = \left[\rho, \rho\alpha, \rho u, \rho c, u_r, \rho(\mathcal{E} + \frac{u^2}{2})\right]^T, \tag{7.71}$$

and the flux function is

$$\mathbb{F}(\mathbb{U}) = \begin{pmatrix} \rho u \\ \rho u \alpha \\ \rho u^2 + \mathcal{P} + \rho u_r \mathcal{E}_{u_r} \\ \rho u c + \rho \mathcal{E}_{u_r} \\ u u_r + \mathcal{E}_c \\ \rho u(\mathcal{E} + \frac{u^2}{2}) + \mathcal{P} u + \rho u u_r \mathcal{E}_{u_r} + \rho \mathcal{E}_c \mathcal{E}_{u_r} \end{pmatrix}. \tag{7.72}$$

As discussed in the previous section the two–phase flow equations (7.70) may be formulated in terms of variables other than the conserved variables. The mathematical structure of the system is more clearly revealed and the characteristic analysis given below is simplified in terms of primitive variables. For a choice given as in (7.66), the conservative two–fluid model can be written in terms of primitive variables as

$$\partial_t \mathbb{W} + \mathbb{A}(\mathbb{W}) \partial_x \mathbb{W} = 0, \tag{7.73}$$

where the Jacobian matrix $\mathbb{A}(\mathbb{W})$ is

$$\begin{pmatrix} u & 0 & \rho & 0 & 0 & 0 \\ 0 & u & 0 & 0 & 0 & 0 \\ \frac{1}{\rho}(\mathcal{P}_\rho + c(1-c)u_r^2) & \frac{\mathcal{P}_\alpha}{\rho} & u & \frac{1}{\rho}(\mathcal{P}_c + \rho(1-2c)u_r^2) & 2c(1-c)u_r & \frac{\mathcal{P}_\mathcal{S}}{\rho} \\ c(1-c)\frac{u_r}{\rho} & 0 & 0 & u + (1-2c)u_r & c(1-c) & 0 \\ \mathfrak{e}_{c\rho} & \mathfrak{e}_{\alpha c} & u_r & \mathfrak{e}_{cc} - u_r^2 & u + (1-2c)u_r & \mathfrak{e}_{c\mathcal{S}} \\ 0 & 0 & 0 & 0 & 0 & u \end{pmatrix}.$$

Let us introduce the set Ω of physically admissible states, $\Omega = \{\mathbb{U} \in \mathbb{R}^6; \rho, \mathcal{S} > 0, \alpha, c \in]0,1[, u, u_r \in \mathbb{R}\}$. Further we will see that there exists a positive number $u_r^\star$ such that for any $\mathbb{U}$ that lies in the set $\Omega^\star$ defined by $\Omega^\star = \{\mathbb{U} \in \Omega; |u_r| \leq u_r^\star\}$ the eigenvalues λ_j, $1 \leq j \leq 6$ are real for u_r small enough. Thus the eigenvalues of the

matrix $\mathbb{A}(\mathbb{W})$ are the solutions of the characteristic polynomial

$$\det\Big[\mathbb{A}(\mathbb{W}) - \lambda I\Big] = 0, \tag{7.74}$$

which becomes

$$\mathcal{Y}^2\Big[\mathcal{Y}^4 + \varsigma_3\mathcal{Y}^3 + \varsigma_2\mathcal{Y}^2 + \varsigma_1\mathcal{Y} + \varsigma_0\Big] = 0, \tag{7.75}$$

where

$$\mathcal{Y} \equiv u - \lambda, \tag{7.76}$$

and

$$\varsigma_3 = 2(1-2c)u_r, \tag{7.77}$$

$$\varsigma_2 = -\big(\mathcal{P}_\rho + c(1-c)\mathfrak{e}_{cc}\big) + b_0 u_r^2, \tag{7.78}$$

$$\varsigma_1 = 2\big(2\rho c(1-c)\mathfrak{e}_{c\rho} - (1-2c)\mathcal{P}_\rho\big)u_r + b_1 u_r^3, \tag{7.79}$$

$$\varsigma_0 = c(1-c)\big(\mathcal{P}_\rho\mathfrak{e}_{cc} - \mathcal{P}_c\mathfrak{e}_{c\rho}\big) + b_2 u_r^2 + b_3 u_r^4, \tag{7.80}$$

with

$$b_0 = (1-2c)^2 + 2c(1-c), \tag{7.81}$$

$$b_1 = 2c(1-c)(1-2c), \tag{7.82}$$

$$\begin{aligned} b_2 &= \rho c(1-c)(1-2c)\mathfrak{e}_{c\rho} \\ &- c^2(1-c)^2\mathfrak{e}_{cc} - \mathcal{P}_\rho(1-2c)^2 \\ &- \mathcal{P}_\rho c(1-c) + \frac{\mathcal{P}_c}{\rho}c(1-c)(1-2c), \end{aligned} \tag{7.83}$$

$$b_3 = c^2(1-c)^2. \tag{7.84}$$

Note that the coefficients of equation (7.75) have the form

$$\varsigma_\imath = \varsigma_\imath^0 + \varsigma_\imath^1 u_r + \mathcal{O}(u_r^2), \quad \imath = 0, 1, 2. \tag{7.85}$$

Solving equation (7.75) for the non-trivial roots is difficult, therefore we assume that the relative velocity u_r is sufficiently small we can use perturbation method around $u_r = 0$ and write the solution in the following form

$$\mathcal{Y} = \mathcal{Y}_0 + \mathcal{Y}_1 u_r + O(u_r^2). \tag{7.86}$$

At zero order in u_r we derive from (7.75)

$$\mathcal{Y}_0^4 - \varsigma_2^0 \mathcal{Y}_0^2 + \varsigma_0^0 = 0, \tag{7.87}$$

and the roots of this equation are

$$\mathcal{Y}_0 = \pm \left[\frac{-\varsigma_2^0 \pm \sqrt{\xi}}{2} \right]^{\frac{1}{2}}. \tag{7.88}$$

where

$$\xi = (\varsigma_2^0)^2 - 4\varsigma_0^0. \tag{7.89}$$

We mentioned that the system under consideration can be transformed to a symmetric hyperbolic system and its hyperbolicity is guaranteed by the convexity of the equation of state. Now we prove that the convexity of the specific potential energy $\mathfrak{e}$ guarantees that all roots $\mathcal{Y}_0$ of the equation (7.87) are real. To do this it is convenient to use the variables

$$\mathcal{V} = (\frac{1}{\rho}, c, \mathcal{S}). \tag{7.90}$$

where $\mathcal{V}$ is the specific volume. In terms of these variables we have

$$\mathcal{P} = -\mathfrak{e}_{\mathcal{V}}, \tag{7.91}$$

and the following formulae are satisfied:

$$\begin{aligned}
\mathcal{P}_\rho &= V^2 \mathfrak{e}_{VV}, && (7.92)\\
\mathcal{P}_c &= -\mathfrak{e}_{Vc}, && (7.93)\\
\mathfrak{e}_{\rho c} &= -V^2 \mathfrak{e}_{Vc}, && (7.94)\\
\mathcal{P}_\rho + c(1-c)\mathfrak{e}_{cc} &= \Big[\mathfrak{e}_{VV} + \frac{c(1-c)}{V}\frac{\mathfrak{e}_{cc}}{V}\Big]^2 V^2. && (7.95)
\end{aligned}$$

It follows from (7.88) that

$$\begin{aligned}
\frac{1}{V^4}\xi &= \Big[\mathfrak{e}_{VV} + \frac{c(1-c)}{V}\frac{\mathfrak{e}_{cc}}{V}\Big]^2 - \frac{4c(1-c)}{V}\frac{\mathfrak{e}_{VV}\mathfrak{e}_{cc} - \mathfrak{e}_{Vc}^2}{V},\\
&= \Big[\mathfrak{e}_{VV} - \frac{c(1-c)}{V}\frac{\mathfrak{e}_{cc}}{V}\Big]^2 + \frac{4c(1-c)}{V}\frac{\mathfrak{e}_{Vc}^2}{V} > 0, && (7.96)
\end{aligned}$$

which means that the values

$$\mathcal{Y}_0^2 = \frac{1}{2}\Big[-\varsigma_2^0 \pm \sqrt{\xi}\Big], \tag{7.97}$$

defined by (7.88) are real. Furthermore the positiveness of $\mathcal{Y}_0^2$ (and hence the reality of $\mathcal{Y}_0$) is guaranteed by the inequality

$$\mathfrak{e}_{VV}\mathfrak{e}_{cc} - \mathfrak{e}_{Vc}^2 > 0. \tag{7.98}$$

The above inequality (7.98) is one of the convexity conditions which is the positive definiteness condition of the matrix

$$\begin{pmatrix} \mathfrak{e}_{VV} & \mathfrak{e}_{Vc} & \mathfrak{e}_{V\mathcal{S}} \\ \mathfrak{e}_{cV} & \mathfrak{e}_{cc} & \mathfrak{e}_{c\mathcal{S}} \\ \mathfrak{e}_{\mathcal{S}V} & \mathfrak{e}_{\mathcal{S}c} & \mathfrak{e}_{\mathcal{S}\mathcal{S}} \end{pmatrix}. \tag{7.99}$$

From (7.75) the first–order terms in u_r lead to

$$2\big(\varsigma_2^0 + 2\mathcal{Y}_0^2\big)\mathcal{Y}_1 + \varsigma_3^1\mathcal{Y}_0^2 + \varsigma_1^1 = 0, \tag{7.100}$$

and the solution is

$$\mathcal{Y}_1 = -\frac{\varsigma_1^1 + \varsigma_3^1 \mathcal{Y}_0^2}{2(\varsigma_2^0 + 2\mathcal{Y}_0^2)}. \tag{7.101}$$

Thus, the system (7.70) admits the following six eigenvalues up to first order in u_r

$$\lambda_1 = u - a_{m_1} + \mathcal{Y}(a_{m_1})u_r + \mathcal{O}(u_r^2), \tag{7.102}$$

$$\lambda_2 = u - a_{m_2} + \mathcal{Y}(a_{m_2})u_r + \mathcal{O}(u_r^2), \tag{7.103}$$

$$\lambda_3 = \lambda_4 = u, \tag{7.104}$$

$$\lambda_5 = u + a_{m_1} + \mathcal{Y}(a_{m_1})u_r + \mathcal{O}(u_r^2), \tag{7.105}$$

$$\lambda_6 = u + a_{m_2} + \mathcal{Y}(a_{m_2})u_r + \mathcal{O}(u_r^2), \tag{7.106}$$

where

$$a_{m_1} = \frac{1}{\sqrt{2}}\Big[-\varsigma_2^0 + \sqrt{(\varsigma_2^0)^2 - 4\varsigma_0^0}\Big]^{\frac{1}{2}}, \tag{7.107}$$

$$a_{m_2} = \frac{1}{\sqrt{2}}\Big[-\varsigma_2^0 - \sqrt{(\varsigma_2^0)^2 - 4\varsigma_0^0}\Big]^{\frac{1}{2}}, \tag{7.108}$$

and

$$\mathcal{Y}(a_{mi}) = \mathcal{Y}_1(a_{mi}) = -\frac{\varsigma_1^1 + \varsigma_3^1 a_{mi}^2}{2(\varsigma_2^0 + 2a_{mi}^2)}, \quad \mathrm{i} = 1, 2. \tag{7.109}$$

The eigenvalues $\lambda_{3,4}$ are clearly the mixture velocity u, whereas the other eigenvalues correspond to the acoustic wave propagation for the mixture. Further, the associated linearly independent set of eigenvectors

$$\mathcal{K}_{\mathrm{j}} = \Big[\mathcal{K}_1,\ \mathcal{K}_2,\ \mathcal{K}_3, \mathcal{K}_4,\ \mathcal{K}_5,\ \mathcal{K}_6\Big]_{\mathrm{j}}^T \quad \mathrm{j} = 1, \cdots, 6, \tag{7.110}$$

can be found from the equation

$$\Big[\mathbb{A}(\mathbb{W}) - \lambda I\Big]\mathcal{K} = 0, \tag{7.111}$$

and determined as

$$\mathcal{K}_3 = \big(0,\ 0,\ 1,\ 0,\ 0,\ 0\big)^T, \quad \mathcal{K}_4 = \big(0,\ 0,\ 0,\ 1,\ 0,\ 0\big)^T, \tag{7.112}$$

$$\mathcal{K}_i = \big(k,\ k_2(a_{m\mathrm{j}}, k),\ 0,\ 0,\ k_5(a_{m\mathrm{j}}, k),\ k_6(a_{m\mathrm{j}}, k)\big)^T, \quad \mathrm{j} = 1, 2, \tag{7.113}$$

$$\mathcal{K}_{4+i} = \big(k,\ k_2(-a_{m\mathrm{j}}, k),\ 0,\ 0,\ k_5(-a_{m\mathrm{j}}, k),\ k_6(-a_{m\mathrm{j}}, k)\big)^T, \quad \mathrm{j} = 1, 2, \tag{7.114}$$

where k is an arbitrary parameter and

$$k_2\big(a_{m\mathrm{j}}, k\big) = -\frac{1}{\rho}\big(a_{m\mathrm{j}} - \mathcal{Y}_1(a_{m\mathrm{j}})u_r\big)\, k, \tag{7.115}$$

and $k_5(a_{m\mathrm{j}}, k), k_6(a_{m\mathrm{j}}, k)$ are the solutions to the linear system of algebraic equations

$$\big(a_{m\mathrm{j}} + ((1-2c) - \mathcal{Y}_1(a_{m\mathrm{j}}))u_r\big)\, k_5 + c(1-c)\, k_6 = -\frac{1}{\rho}c(1-c)u_r\, k, \tag{7.116}$$

$$\mathfrak{e}_{cc}\, k_5 + \big(a_{m\mathrm{j}} + ((1-2c) - \mathcal{Y}_1(a_{m\mathrm{j}}))u_r\big)\, k_6 = -\big(\mathfrak{e}_{c\rho} - \frac{1}{\rho}a_{m\mathrm{j}}u_r\big)\, k. \tag{7.117}$$

More precisely the associated eigenvectors of system (7.70) in the system of variables $\mathbb{W}$ for u_r small enough are found to be

$$\mathcal{K}^{\pm}(\mathbb{W}) \;=\; k \begin{pmatrix} 1 \\ \vartheta_0 + \vartheta_1 u_r \\ \vartheta_2 + \vartheta_3 u_r \\ \vartheta_4 + \vartheta_5 u_r \end{pmatrix}, \tag{7.118}$$

$$\mathcal{K}^{0-}(\mathbb{W}) \;=\; \begin{pmatrix} 0 \\ 1 \end{pmatrix},\ \mathcal{K}^{0+}(\mathbb{W}) = \begin{pmatrix} 1 \\ 0 \end{pmatrix}, \tag{7.119}$$

where

$$\vartheta_0 = \pm\frac{a_{m_{1,2}}}{\rho},$$
$$\vartheta_1 = -\frac{\mathcal{Y}_1}{\rho},$$
$$\vartheta_2 = -\frac{c(1-c)\mathfrak{e}_{c\rho}}{c(1-c)\mathfrak{e}_{cc} - a^2_{m_{1,2}}},$$

$$\vartheta_3 = \pm\frac{2a_{m_{1,2}}((1-2c)+\mathcal{Y}_1)}{c(1-c)\mathfrak{e}_{cc} - a^2_{m_{1,2}}},$$
$$\vartheta_4 = \pm\frac{\mathfrak{e}_{c\rho}}{a_{m_{1,2}}} \pm \frac{c(1-c)\mathfrak{e}_{c\rho}\mathfrak{e}_{cc}}{a_{m_{1,2}}[c(1-c)\mathfrak{e}_{cc} - a^2_{m_{1,2}}]},$$
$$\vartheta_5 = \frac{1}{\rho} + \frac{2c(1-c)\mathfrak{e}_{c\rho}\mathfrak{e}_{cc}((1-2c)+\mathcal{Y}_1)}{[\mathfrak{e}_{cc}(1-c) - a^2_{m_{1,2}}]^2} \pm \vartheta_4\frac{(1-2c)-\mathcal{Y}_1}{a_{m_{1,2}}}.$$

The eigenvalues are all real and the eigenvectors $\mathcal{K}^{\pm}$ and $\mathcal{K}^{0\pm}$ form a complete set of linearly independent eigenvectors. Thus we have proved that the one–dimensional conservative two–fluid model is hyperbolic and hyperbolicity remains a property of the conservative two–fluid model for more general equations of state.

7.4 Nature of Characteristic Fields

As the conservative complete two–fluid model is hyperbolic, for small enough u_r we study in this section the nature of characteristic fields for the basic structure of the solution of the Riemann problem as a set of elementary waves which can be described as follows: from the eigenvalues (7.102)–(7.106) we obtain

$$\lim_{u_r\to 0} \nabla\lambda_{\pm}(\mathbb{W}) = \left[\pm\frac{\partial a_{m_{1,2}}}{\partial\rho} + \frac{\partial\mathcal{Y}_1}{\partial\rho}\,u_r, 1, \pm\frac{\partial a_{m_{1,2}}}{\partial c} + \frac{\partial\mathcal{Y}_1}{\partial\rho}\,u_r, \mathcal{Y}_1\right], \tag{7.120}$$

$$\lim_{u_r\to 0} \nabla\lambda_{0\pm}(\mathbb{W}) = \Big[0, 0\Big]. \tag{7.121}$$

So that

$$\begin{aligned}\lim_{u_r\to 0}\nabla\lambda_{\pm}(\mathbb{W})\cdot\mathcal{K}^{\pm}(\mathbb{W}) &= k\Bigg[\pm\frac{\partial a_{m_{1,2}}}{\partial\rho}+\frac{\partial \mathcal{Y}_1}{\partial\rho}\,u_r+\vartheta_0+\vartheta_1 u_r\\ &+ \Big(\frac{\partial a_{m_{1,2}}}{\partial c}+\frac{\partial \mathcal{Y}_1}{\partial\rho}\,u_r\Big)\vartheta_2\\ &\pm \vartheta_3\frac{\partial \mathcal{Y}_1}{\partial c}\,u_r+\big(\vartheta_4+\vartheta_5 u_r\big)\mathcal{Y}_1\Bigg]\neq 0, \qquad (7.122)\end{aligned}$$

$$\lim_{u_r\to 0}\nabla\lambda_{0\pm}(\mathbb{W})\cdot\mathcal{K}^{0\pm}(\mathbb{W}) = 0. \qquad (7.123)$$

Thus, the characteristic fields up to first order in u_r associated with the eigenvalues $\lambda_{\mathrm{i}}(\mathbb{W})$, $\mathrm{j}=1,\,2,\,5,\,6$ are genuinely non–linear while those associated with $\lambda_{\mathrm{j}}(\mathbb{W})$, $\mathrm{j}=3,4$, are linearly degenerate.

Characteristic analysis shows that there are two types of sound wave and hence two types of shock waves exist, these being fast and slow shock waves.

7.5 Conclusions

Based on an extended thermodynamics approach initiated by Romensky [145] a new model "the hyperbolic conservative two–fluid model" for two–phase flow is developed in this chapter. The fundamental three–dimensional governing equations and their corresponding closure relations for two–phase two–fluid continuous media were derived. All the field equations form a symmetric hyperbolic system of equations in conservative form and are used to model a compressible non–equilibrium two–phase flow. The mathematical character of the model for the one–dimensional case in a process without dissipation for the hyperbolic conservative two–fluid model is examined in detail. The mathematical analysis shows that there are six real eigenvalues. Two of these eigenvalues are equal to the mixture velocity and correspond to the convective waves while the other four eigenvalues correspond to the left and right sound waves. Through analysis, the derived eigenvectors and the characteristic fields corresponding to the acoustic waves are shown to be genuinely non–linear while the

last two are linearly degenerate.

The hyperbolic conservative two–fluid model seems to be more attractive from the mathematical and numerical point of view. Due to the well defined mathematical properties of the dissipation–free model, one can formulate a single wave solution such as shock, contact and centred wave to solve the Riemann problem for the model. From a numerical point of view, the hyperbolic conservative two–fluid model will be useful to develop an accurate numerical methods for the proposed model.

It is hoped that the theory developed in this chapter will motivate other researchers to use, and further develop, extended thermodynamics methodology for the analysis of two–phase flow in systems and processes of practical concern.

CHAPTER 8

THE RIEMANN PROBLEM FOR THE HYPERBOLIC CONSERVATIVE TWO–FLUID MODEL

In the previous chapter we have formally established the mathematical foundation for the hyperbolic conservative two–fluid model. In this chapter we introduce the Riemann problem for the model to study possible wave pattern.

8.1 The Riemann Problem and a Solution Strategy

The Riemann problem for the one–dimensional complete two–fluid model is the initial value problem (IVP) for the conservation laws

$$\left.\begin{aligned} \partial_t \mathbb{U} + \partial_x \mathbb{F}(\mathbb{U}) &= 0, \\ \mathbb{U}(x,0) &= \begin{cases} \mathbb{U}_{\mathcal{L}} & \text{if } x < 0, \\ \mathbb{U}_{\mathcal{R}} & \text{if } x > 0, \end{cases} \end{aligned}\right\} \tag{8.1}$$

for which the vectors of conserved variables $\mathbb{U}$ is

$$\mathbb{U} = \begin{pmatrix} \rho \\ \rho\alpha \\ \rho u \\ \rho c \\ u_r \\ \rho(\mathcal{E} + \frac{u^2}{2}) \end{pmatrix}, \tag{8.2}$$

and the flux

$$\mathbb{F}(\mathbb{U}) = \begin{pmatrix} \rho u \\ \rho u \alpha \\ \rho u^2 + \mathcal{P} + \rho u_r \mathcal{E}_{u_r} \\ \rho u c + \rho \mathcal{E}_{u_r} \\ u u_r + \mathcal{E}_c \\ \rho u(\mathcal{E} + \frac{u^2}{2}) + \mathcal{P} u + \rho u u_r \mathcal{E}_{u_r} + \rho \mathcal{E}_c \mathcal{E}_{u_r} \end{pmatrix}. \tag{8.3}$$

The structure of the similarity solution $\mathbb{U}(\frac{x}{t})$ of (8.1) is as shown in figure 8.1. There

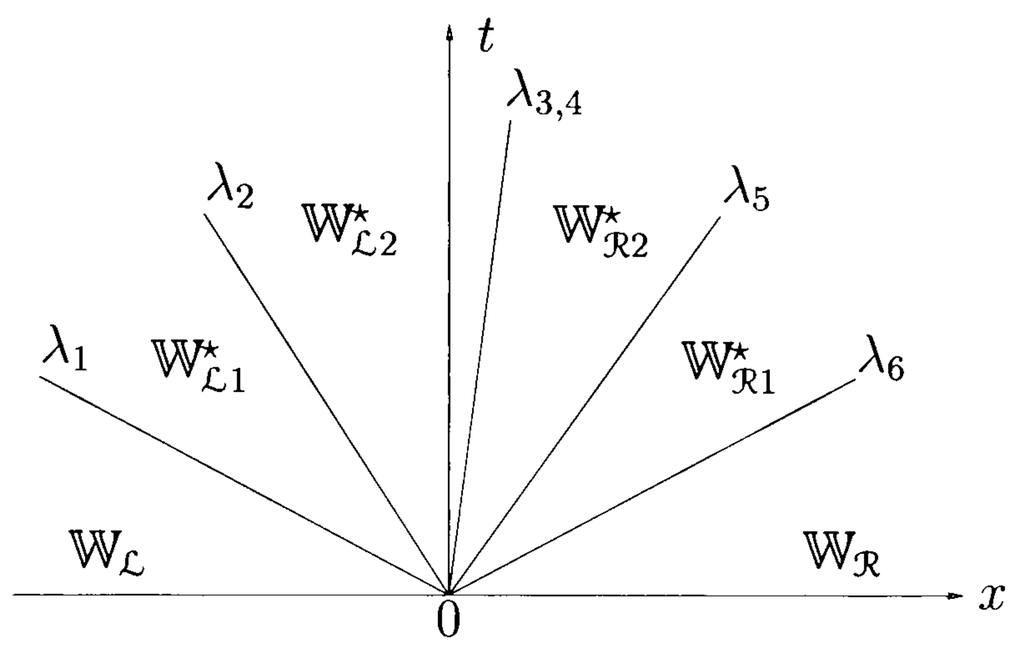

Figure 8.1: Structure of the solution of the Riemann problem on the x–t plane for the hyperbolic conservative two–fluid model.

are six waves associated with the six characteristic fields corresponding to the eigenvectors $\mathcal{K}^{\mathrm{j}}, \mathrm{j} = 1, \ldots, 6$. The six waves separate six constant states. In terms of primitive variables

$$\mathbb{W} = \Big[\rho, \alpha, u, c, u_r, \mathcal{S}\Big]^T, \tag{8.4}$$

the six constant states are denoted, from left to right $\mathbb{W}_{\mathcal{L}}$ (left data), $\mathbb{W}^{\star}_{\mathcal{L}1}$, $\mathbb{W}^{\star}_{\mathcal{L}2}$, $\mathbb{W}^{\star}_{\mathcal{R}2}$, $\mathbb{W}^{\star}_{\mathcal{R}1}$, $\mathbb{W}_{\mathcal{R}}$ (right data). The states $\mathbb{W}^{\star}_{\mathcal{L}1}$, $\mathbb{W}^{\star}_{\mathcal{L}2}$ and $\mathbb{W}^{\star}_{\mathcal{R}2}$, $\mathbb{W}^{\star}_{\mathcal{R}1}$ cover the star region and emerge from the interaction of the data states $\mathbb{W}_{\mathcal{L}}$ and $\mathbb{W}_{\mathcal{R}}$. In general, the two–left and two–right waves are shocks or rarefactions, while the middle waves are always contact waves. Therefore, depending on the type of non–linear wave there

can be sixteen wave patterns to construct as shown in figures 8.2, 8.3, 8.4 and 8.5, noting that there are six waves in each case. Case (a) in figure 8.2 is where the one–

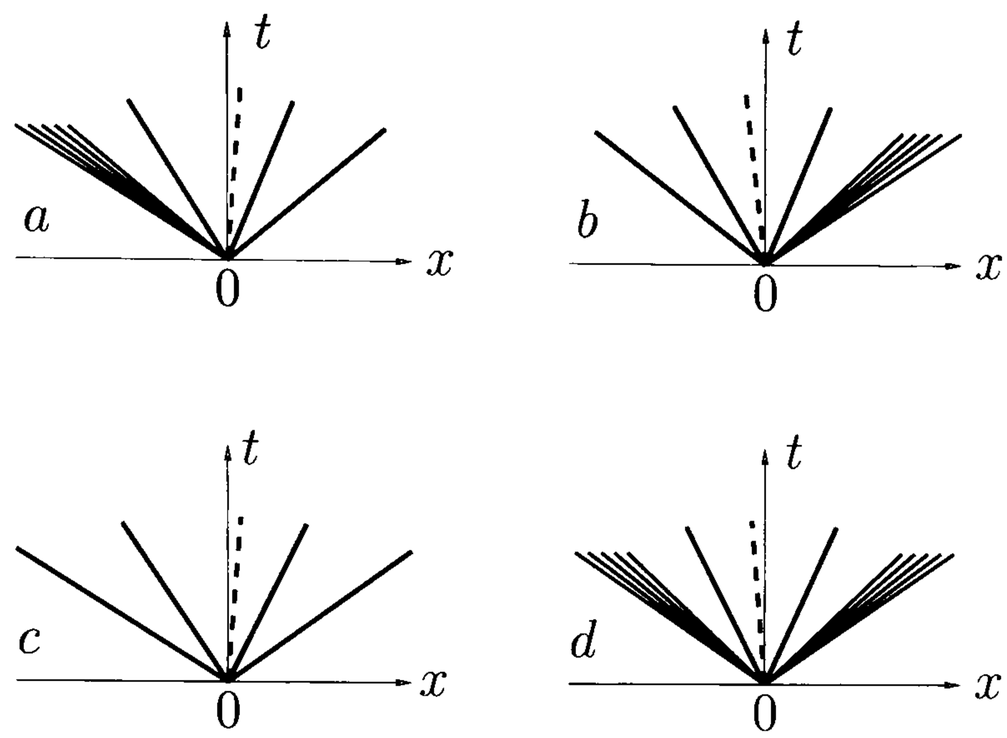

Figure 8.2: Possible wave patterns in the solution of the Riemann problem for the hyperbolic conservative two–fluid model where one–left wave and one–right wave are shock waves.

left wave is a rarefaction and one–left wave is a shock wave while the two–right waves are shocks. Case (b) is where the two–left waves are shocks and one–right wave is a rarefaction and one–right wave is a shock. Case (c) is where both the two–left and two–right waves are shocks. Case (d) is where one–left wave is a rarefaction, one–left wave is a shock while one–right wave is a rarefaction and one–right wave is a shock.

In case (a) in figure 8.3 one–left wave is a rarefaction, one–left wave is a shock and one–right wave is a shock, one–right wave is a rarefaction. Case (b) is where both two–left waves are shocks while the two–right waves are rarefactions. Case (c) is where the two–left waves are shocks and one–right wave is a rarefaction, one–right is a shock. Case (d) is the case where one–left wave is a rarefaction and one–left wave is a shock, two–right waves are rarefactions.

Case (a) in figure 8.4 is the case where the two–left waves are rarefactions while the two–right waves are shocks. Case (b) is where one–left wave is a shock and one left wave a is rarefaction, and one–right wave is rarefaction with one–right shock wave.

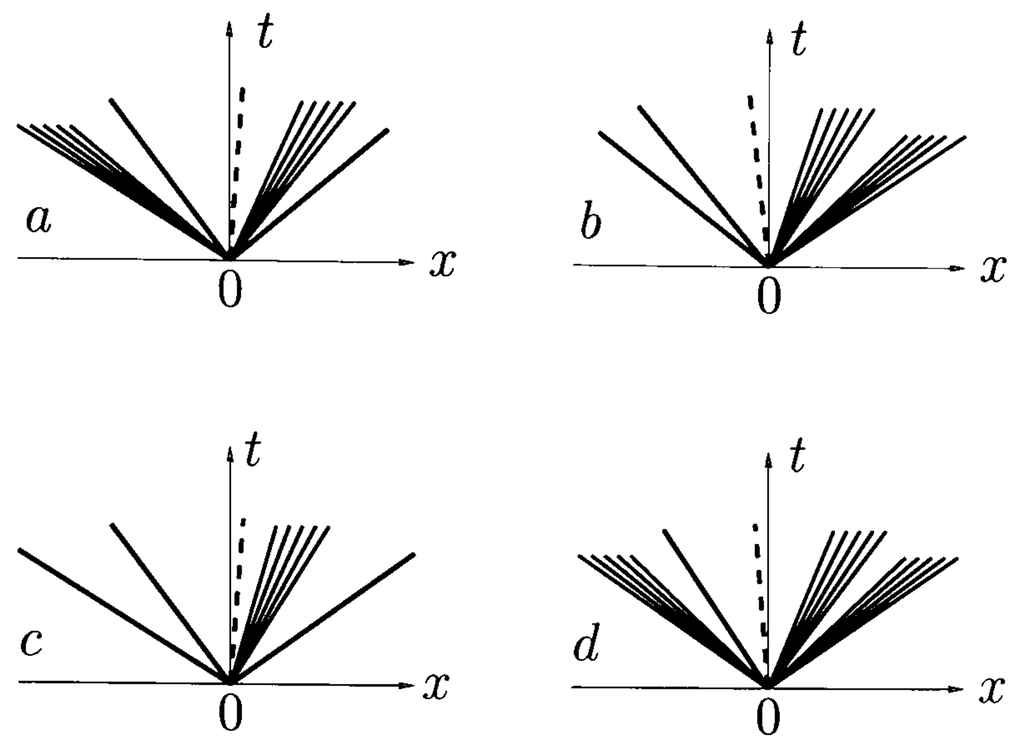

Figure 8.3: Possible wave patterns in the solution of the Riemann problem for the hyperbolic conservative two–fluid model where one–left wave is a shock wave and one–right wave is a rarefaction wave.

Case (c) is where one–left wave is a shock and one–left wave is rarefaction while the two–right waves are shocks. Case (d) is where the two–left waves are rarefaction waves and one–right wave is a rarefaction and one–right wave is a shock.

Case (a) in figure 8.5 is where the two–left waves are rarefactions and one–right wave is a shock, one–right wave is a rarefaction. Case (b) is where one–left wave is a shock and one–left is a rarefaction while both two–right waves are rarefactions. Case (c) is the case where the one–left wave is a shock while one–left wave is a rarefaction with one–right wave shock and one–right wave rarefaction. Case (d) is the case where both two–left and two–right waves are rarefactions.

The main step in solving the Riemann problem is the determination of the solution in the star region. This depends on appropriate relations through the left and right waves connecting $\mathbb{W}^{\star}_{\mathcal{L}1}$, $\mathbb{W}^{\star}_{\mathcal{L}2}$ to $\mathbb{W}_{\mathcal{L}}$ and $\mathbb{W}^{\star}_{\mathcal{R}2}$, $\mathbb{W}^{\star}_{\mathcal{R}1}$ to $\mathbb{W}_{\mathcal{R}}$ respectively. In practice the determination of the solution in the star region is difficult and time consuming because it typically requires iterations for non–linear equations. Since the model possesses a large number of non–linear waves it is not easy to analyse the star region mathematically. In addition, the number of non–linear equations will depend on the number of the non–linear waves considered. The problem in determining the analyti-

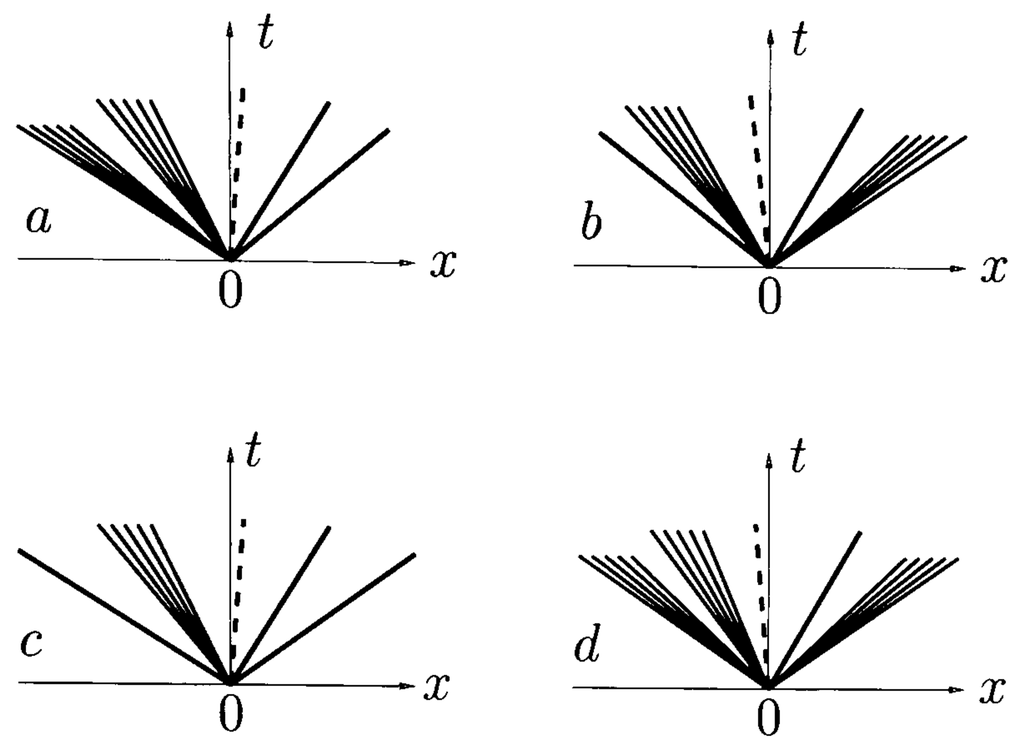

Figure 8.4: Possible wave patterns in the solution of the Riemann problem for the hyperbolic conservative two–fluid model where one–left wave is a rarefaction wave and one–right wave is a shock wave.

cal explicit solution of the Riemann problem is very useful for a better understanding of the physical meaning of the model and to develop an efficient numerical method. Thus this leads us to consider numerical approximations by using modern shock–capturing schemes. The scheme we will use must be flexible enough to handle the model without relying on mathematical results obtained analytically. The numerical scheme will give more insight into the Riemann problem for the hyperbolic conservative two–fluid model and will resolve both rarefaction waves and shock waves as we shall see in the later chapters.

8.2 Study of the Sound Wave Propagation

The analysis of the eigenstructure given in the previous chapter has shown that there are four eigenvalues corresponding to two sound velocities. Now we clarify the values of the velocity of sound in static two–fluid media and its dependence on the volume concentration relaxation illustrated by the example of a air–water mixture. Consider the generalization of the system (7.73) by adding a source term to the equation for the volume concentration equation as given in equation (7.4) with the partial case of

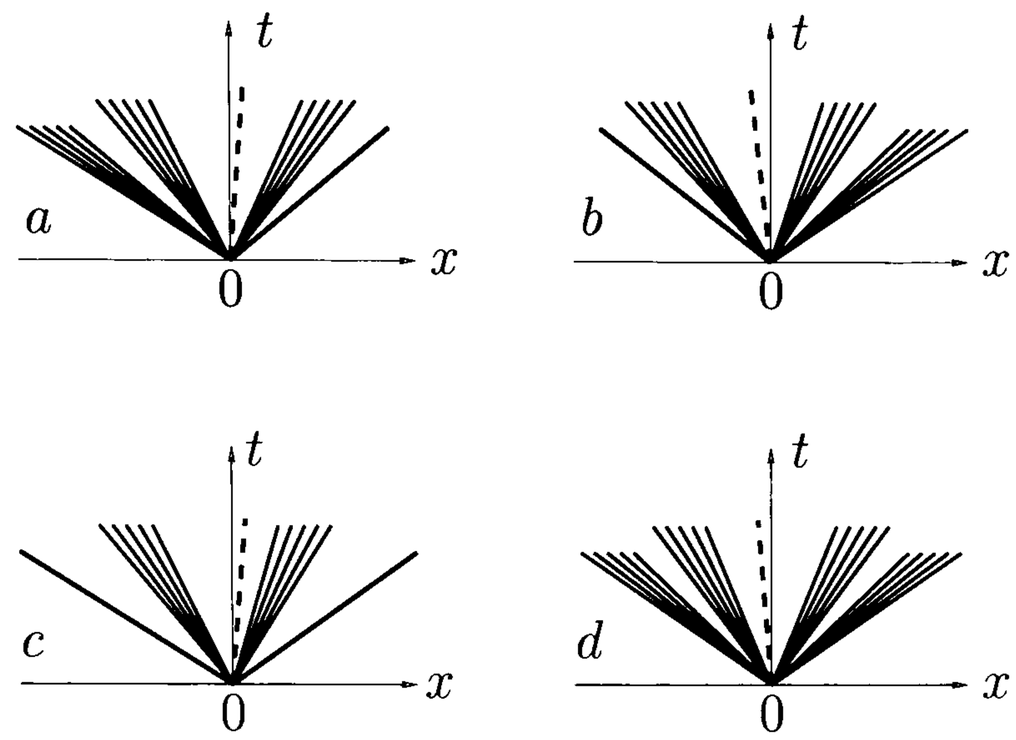

Figure 8.5: Possible wave patterns in the solution of the Riemann problem for the hyperbolic conservative two–fluid model where one–left wave and one–right wave are rarefaction waves.

the system (7.69) to obtain

$$\partial_t \mathbb{W} + \mathbb{A}(\mathbb{W})\partial_x \mathbb{W} = \mathbb{Q}(\mathbb{W}), \tag{8.5}$$

where

$$\mathbb{Q}(\mathbb{W}) = \left(0, -\frac{1}{\tau}\mathcal{E}_\alpha, 0, 0, 0, \frac{\mathcal{E}_\alpha^2}{\tau \mathcal{E}_{\mathcal{S}}}\right)^T. \tag{8.6}$$

We study small–amplitude wave propagation in the static two–fluid media which is also in the thermodynamic equilibrium (in particular $\mathcal{E}_\alpha = 0$). A solution of (8.5) can be represented in the form

$$\begin{aligned} \mathbb{W} &= \mathbb{W}^0 + \mathbb{W}^1 \\ &= \left(\rho^0 + \rho^1, \alpha^0 + \alpha^1, u^1, c^0 + c^1, u_r^1, \mathcal{S}^1\right), \end{aligned} \tag{8.7}$$

where $\mathbb{W}^1$ is the vector of small perturbation of the primitive variables. The smallness of $\mathbb{W}^1$ allows us to derive a linear system of partial differential equations

$$\partial_t \mathbb{W}^1 + \mathbb{A}(\mathbb{W}^0)\partial_x \mathbb{W}^1 = \mathbb{Q}_{\mathbb{W}}(\mathbb{W}^0)\mathbb{W}^1, \tag{8.8}$$

where

$$\mathbb{A}(\mathbb{W}^0) = \begin{pmatrix} 0 & 0 & \rho^0 & 0 & 0 & 0 \\ 0 & 0 & 0 & 0 & 0 & 0 \\ \frac{\mathcal{P}_\rho}{\rho^0} & \frac{\mathcal{P}_\alpha}{\rho^0} & 0 & \frac{\mathcal{P}_c}{\rho^0} & 0 & \frac{\mathcal{P}_\mathcal{S}}{\rho^0} \\ 0 & 0 & 0 & 0 & c^0(1-c^0) & 0 \\ \mathfrak{e}_{c\rho} & \mathfrak{e}_{\alpha c} & 0 & \mathfrak{e}_{cc} & 0 & \mathfrak{e}_{c\mathcal{S}} \\ 0 & 0 & 0 & 0 & 0 & 0 \end{pmatrix},$$

and the entries of the Jacobian matrix $\mathbb{Q}_\mathbb{W}$ is

$$\mathbb{Q}_\mathbb{W}(\mathbb{W}^0) = \begin{pmatrix} 0 & 0 & 0 & 0 & 0 & 0 \\ -\frac{1}{\tau}\mathfrak{e}_{\alpha\rho} & -\frac{1}{\tau}\mathfrak{e}_{\alpha\alpha} & 0 & -\frac{1}{\tau}\mathfrak{e}_{\alpha c} & 0 & -\frac{1}{\tau}\mathfrak{e}_{\alpha\mathcal{S}} \\ 0 & 0 & 0 & 0 & 0 & 0 \\ 0 & 0 & 0 & 0 & 0 & 0 \\ 0 & 0 & 0 & 0 & 0 & 0 \\ 0 & 0 & 0 & 0 & 0 & 0 \end{pmatrix}. \tag{8.9}$$

Here all derivatives of thermodynamic parameters are computed at the values $\rho = \rho^0, \alpha = \alpha^0, c = c^0, \mathcal{S} = 0$. The sound waves are harmonic solutions of the form

$$\mathbb{W}^1 = \mathbb{W}^1_0 \exp\big(i(\nu t - \mathfrak{k}x)\big). \tag{8.10}$$

If we substitute this expression into (8.8) we observe that only the solution with $\mathcal{S}^1 = 0$ exists. The equation connecting the frequency ν and wavelength $\mathfrak{k}$ can then be derived:

$$\nu^4 - \sigma_2(i\nu)\nu^2\mathfrak{k}^2 + \sigma_0(i\nu)\mathfrak{k}^4 = 0, \tag{8.11}$$

where

$$\sigma_2(i\nu) \;=\; \mathcal{P}_\rho + c^0(1-c^0)\mathfrak{e}_{cc} - \frac{\rho^2\mathfrak{e}_{\alpha\rho}^2 + \mathfrak{e}_{\alpha c}^2}{i\nu\tau + \mathfrak{e}_{\alpha\alpha}}, \tag{8.12}$$

$$\begin{aligned}\sigma_0(i\nu) &= c^0(1-c^0)\left(\mathcal{P}_\rho - \frac{\rho^2\mathfrak{e}_{\alpha\rho}^2}{i\nu\tau+\mathfrak{e}_{\alpha\alpha}}\right)\left(\mathfrak{e}_{cc} - \frac{\mathfrak{e}_{\alpha c}^2}{i\nu\tau+\mathfrak{e}_{\alpha\alpha}}\right)\\ &- c^0(1-c^0)\left(\mathcal{P}_c - \frac{\rho^2\mathfrak{e}_{\alpha\rho}\mathfrak{e}_{\alpha c}}{i\nu\tau+\mathfrak{e}_{\alpha\alpha}}\right)\left(\mathfrak{e}_{c\rho} - \frac{\mathfrak{e}_{\alpha\rho}\mathfrak{e}_{\alpha c}}{i\nu\tau+\mathfrak{e}_{\alpha\alpha}}\right). \qquad (8.13)\end{aligned}$$

It is obvious that if the wavelength is prescribed then the sound wave behaviour depends on the value of relaxation time τ (note that τ can depend on the thermodynamic parameters of state). We consider only two interesting limiting cases $\tau = \infty$ and $\tau = 0$ which correspond to the case when the characteristic time of a process is respectively less or greater then the relaxation time.

In the first case ($\tau = \infty$) we have

$$\sigma_2 = \mathcal{P}_\rho + c^0(1-c^0)\mathfrak{e}_{cc}, \quad \sigma_0 = c^0(1-c^0)(\mathcal{P}_\rho\mathfrak{e}_{cc} - \mathcal{P}_c\mathfrak{e}_{c\rho}), \qquad (8.14)$$

and the roots $\nu/\mathfrak{k}$ of equation (8.10) coincide with eigenvalues of the system (7.73) corresponding to acoustic waves (at $u = 0$).

In the second case ($\tau = 0$)

$$\sigma_2 = \mathcal{P}_\rho + c^0(1-c^0)\mathfrak{e}_{cc} - \frac{\rho^2\mathfrak{e}_{\alpha\rho}^2 + \mathfrak{e}_{\alpha c}^2}{\mathfrak{e}_{\alpha\alpha}}, \qquad (8.15)$$

$$\begin{aligned}\sigma_0 &= c^0(1-c^0)\left\{\left(\mathcal{P}_\rho - \frac{\rho^2\mathfrak{e}_{\alpha\rho}^2}{\mathfrak{e}_{\alpha\alpha}}\right)\left[\mathfrak{e}_{cc} - \frac{\mathfrak{e}_{\alpha c}^2}{\mathfrak{e}_{\alpha\alpha}}\right]\right.\\ &- \left.\left(\mathcal{P}_c - \frac{\rho^2\mathfrak{e}_{\alpha\rho}\mathfrak{e}_{\alpha c}}{\mathfrak{e}_{\alpha\alpha}}\right)\left[\mathfrak{e}_{c\rho} - \frac{\mathfrak{e}_{\alpha\rho}\mathfrak{e}_{\alpha c}}{\mathfrak{e}_{\alpha\alpha}}\right]\right\}. \qquad (8.16)\end{aligned}$$

For both cases we have the common formula for sound wave velocities obtained by solving the equation (8.11) (choosing only positive roots):

$$a_{m_{1,2}} = \frac{\nu}{\mathfrak{k}} = \sqrt{\frac{1}{2}\left[\sigma_2 \pm \sqrt{\sigma_2^2 - 4\sigma_0}\right]}. \qquad (8.17)$$

Considering now an example of air–water mixture and checking the dependence of the velocity of sound on the volume concentration of the gas (void fraction) for the two cases above described supposing that the mixture is at normal conditions. The

equation of state for such a mixture is given by (7.60) and determined by the equations of state for air and water. The EOS for air is the perfect gas EOS [68, 104] given by

$$\mathfrak{e}_2 = \frac{A_2}{\gamma_2 - 1}\left(\frac{\rho_2}{\rho_2^0}\right)^{\gamma_2 - 1} \exp\left(\frac{\mathcal{S}}{c_V^2}\right). \tag{8.18}$$

The EOS for water is defined as

$$\mathfrak{e}_1 = \frac{A_1}{\gamma_1 - 1}\left(\frac{\rho_1}{\rho_1^0}\right)^{\gamma_1 - 1} \exp\left(\frac{\mathcal{S}}{c_V^1}\right) + A_0\frac{\rho_1^0}{\rho_1}, \tag{8.19}$$

which is the stiffened gas EOS rewritten in terms of density and entropy [68, 108] and the constants are defined in table 8.1.

Direct calculation of the speeds of sound at normal conditions ($\rho_1 = \rho_1^0, \rho_2 = \rho_2^0, \mathcal{S} =$

Constants in the equations of state for liquid and gas							
γ_1	=	2.8		γ_2	=	1.4	
ρ_1^0	=	10^3	kg/m^3	ρ_2^0	=	1	kg/m^3
c_v^1	=	1495	J/kgK	c_v^2	=	720	J/kgK
A_0	=	$8.4999\ 10^5$	m^2/s^2	A_2	=	10^5	m^2/s^2
A_1	=	$8.5\ 10^5$	m^2/s^2				

Table 8.1: Constants for the study of the sound wave propagation.

0) gives the following results for the case $\tau = \infty$:

$$a_{m1} = \sqrt{\gamma_1 A_1}, \quad a_{m2} = \sqrt{\gamma_2 A_2}. \tag{8.20}$$

We can see that both speeds of sound do not depend on the void fraction and coincide with the speeds of sound in the pure water and air respectively. The dependence of the speeds of sound on the void fraction in the case when $\tau = 0$ (equal pressure approximation) was calculated numerically (8.17). It is found that one of the speeds is equal to 0. The non–zero speed of sound is presented in figure 8.6.

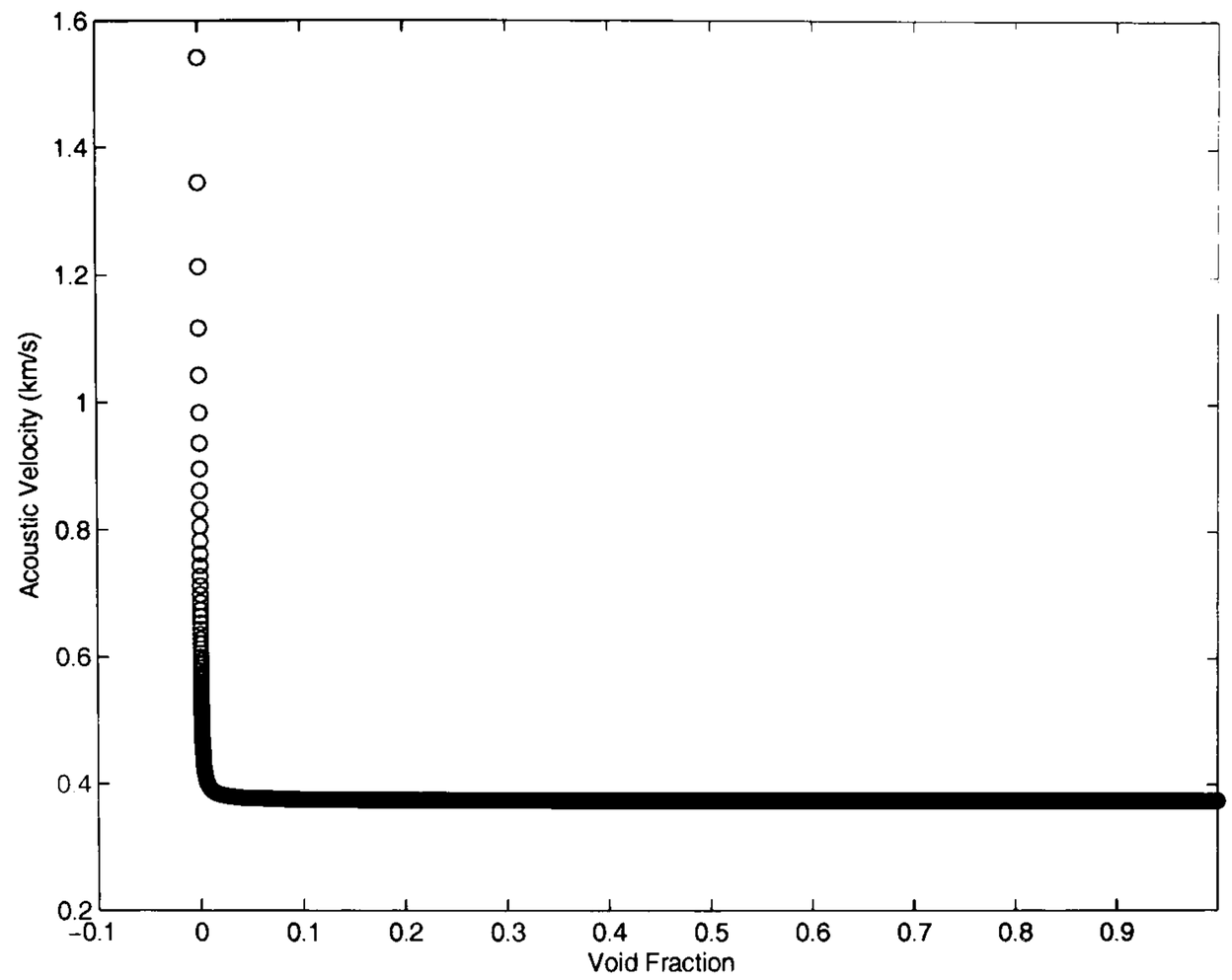

Figure 8.6: The acoustic velocity for a air–water mixture for the case of single pressure approximation as a function of void fraction α. The water and air are at rest under atmospheric conditions.

8.3 Discontinuities in Two–Phase Flow Models

In this section we consider a special wave solution for the hyperbolic conservative two–fluid model. We are interested in the shock waves connecting a state $\mathbb{U}$ on the left of the discontinuity to a state $\mathbb{U}^0$ placed on the right side of the discontinuity, which depends on $\zeta = x - St$ as the wave moves from the left to the right as shown in figure 8.7. If $\mathbb{U}$ is a weak solution of (8.1), $\mathbb{U}$ satisfies the jump condition

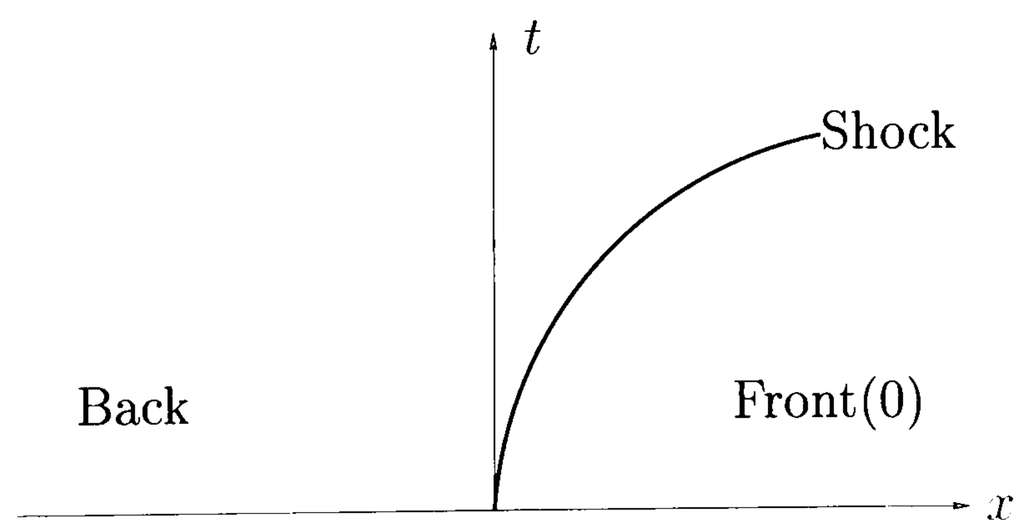

Figure 8.7: The shock in moving coordinates.

$$S\Big[\,\mathbb{U}\Big] = \Big[\,\mathbb{F}(\mathbb{U})\Big], \tag{8.21}$$

where S is the shock speed and $[\cdot]$ represents the jump across discontinuity. The system (8.1) is hyperbolic and equation (8.21) has six waves as solutions. We are interested in four of these waves (two–left shocks and two–right shocks). For the jump condition (8.21) applied to the system of conservation laws (8.1) without dissipation we find that the jump relations across a discontinuity in the x–t plane with velocity $\frac{dx}{dt} = S$ are given as follows

$$S[\rho] = [\rho u] = Q, \tag{8.22}$$

$$S[\rho\alpha] = [\rho\alpha u], \tag{8.23}$$

$$S[\rho u] = [\rho u^2 + \mathcal{P} + \rho u_r \mathcal{E}_{u_r}], \tag{8.24}$$

$$S[\rho c] = [\rho u c + \rho \mathcal{E}_{u_r}], \tag{8.25}$$

$$S[u_r] = [u u_r + \mathcal{E}_c], \tag{8.26}$$

$$S[\rho(\mathcal{E} + \frac{u^2}{2})] = [\rho u(\mathcal{E} + \frac{u^2}{2}) + \mathcal{P}u + \rho u u_r \mathcal{E}_{u_r} + \rho \mathcal{E}_c \mathcal{E}_{u_r}], \tag{8.27}$$

where Q denotes the mass flux through the shock wave.

These are called the shock relations. The equations of fluid mechanics, like those of classical particle mechanics, are Galilean invariant. Therefore, it is legitimate to transform variables to a coordinate system moving with uniform velocity. It is convenient to pick a coordinate system whose velocity at some fixed time t_0, say $t_0 = 0$, equals that of the discontinuity and such that the discontinuity is at $x = 0$ at $t = 0$ (see figure 8.7). In this coordinate system, the shock relations at the origin become

$$\rho u = \rho^0 u^0, \tag{8.28}$$

$$\rho\alpha u = \rho^0 \alpha^0 u^0, \tag{8.29}$$

$$\frac{Q^2}{\rho} + \mathcal{P} + \rho u_r \mathcal{E}_{u_r} = \frac{Q^2}{\rho^0} + \mathcal{P}^0 + \rho^0 u_r^0 \mathcal{E}_{u_r}^0, \tag{8.30}$$

$$Qc + \rho \mathcal{E}_{u_r} = Qc^0 + \rho^0 \mathcal{E}_{u_r}^0, \tag{8.31}$$

$$\frac{Qu_r}{\rho} + \mathcal{E}_c = \frac{Qu_r^0}{\rho^0} + \mathcal{E}_c^0, \tag{8.32}$$

$$\begin{aligned} Q(\mathcal{E} + \frac{u^2}{2}) + \mathcal{P}u + \rho u u_r \mathcal{E}_{u_r} + \rho \mathcal{E}_c \mathcal{E}_{u_r} &= Q(\mathcal{E}^0 + \frac{u^0 u^0}{2}) + \mathcal{P}^0 u^0 \\ &+ \rho^0 u^0 u_r^0 \mathcal{E}_{u_r}^0 + \rho^0 \mathcal{E}_c^0 \mathcal{E}_{u_r}^0, \end{aligned} \tag{8.33}$$

where the superscript (0) indicates one side of the discontinuity (front of the shock). Now the equations (8.28)–(8.33) are written in terms of the thermodynamics potential equation given by (7.60). First we can write the jump of momentum equation given by (8.30) as

$$Q(u - u^0) + \mathcal{P} + \rho c(1-c)u_r^2 - \mathcal{P}^0 + \rho^0 c^0 (1 - c^0) u_r^0 u_r^0 = 0. \tag{8.34}$$

To transform the equation for the energy we use the following formula obtained using equation (8.27)

$$\begin{aligned} Q\frac{u^2}{2} &+ \mathcal{P}u + u\rho c(1-c)u_r^2 - Q\frac{u^0 u^0}{2} + \mathcal{P}^0 u^0 + u^0 \rho^0 c^0 (1-c^0) u_r^0 u_r^0 \\ &= \frac{Q(u-u^0)(u+u^0)}{2} + \frac{(\mathcal{P} - \mathcal{P}^0)(u+u^0)}{2} + \frac{(\mathcal{P} - \mathcal{P}^0)(u-u^0)}{2} \\ &+ u\rho c(1-c)u_r^2 - \rho^0 c^0 (1-c^0) u_r^0 u_r^0 \\ &= \frac{\mathcal{P} + \rho c(1-c)u_r^2 + \mathcal{P}^0 + \rho^0 c^0 (1-c^0) u_r^0 u_r^0}{2} (u - u^0). \end{aligned} \tag{8.35}$$

Thus the new system to consider after the transformation takes the following form

$$\rho u = \rho^0 u^0 = Q, \tag{8.36}$$

$$\rho u \alpha = \rho^0 u^0 \alpha_0, \tag{8.37}$$

$$\frac{Q^2}{\rho} + \mathcal{P} + \rho c(1-c)u_r^2 = \frac{Q^2}{\rho^0} + \mathcal{P}^0 + \rho^0 c^0 (1-c^0) u_r^0 u_r^0, \tag{8.38}$$

$$Qc + \rho c(1-c)u_r = Qc^0 + \rho^0 c^0 (1-c^0) u_r^0. \tag{8.39}$$

$$\frac{Qu_r}{\rho} + \mathfrak{e}_c + (1-2c)\frac{u_r^2}{2} = \frac{Qu_r^0}{\rho^0} + \mathfrak{e}_c^0 + (1-2c^0)\frac{u_r^0 u_r^0}{2}, \tag{8.40}$$

$$
\begin{aligned}
\mathfrak{e} + c(1-c)\frac{u_r^2}{2} \quad &+ \quad \frac{\rho c(1-c)u_r}{Q}\Big(\mathfrak{e}_c + (1-2c)\frac{u_r^2}{2}\Big) \\
+\frac{1}{2}\Big(\mathcal{P} + \rho c(1-c)u_r^2 \quad &+ \quad \mathcal{P}^0 + \rho^0 c^0(1-c^0)u_r^0 u_r^0\Big)\Big(\frac{1}{\rho} - \frac{1}{\rho^0}\Big) \\
-\mathfrak{e}^0 + c^0(1-c^0)\frac{u_r^0 u_r^0}{2} \quad &+ \quad \frac{\rho^0 c^0(1-c^0)u_r^0}{Q}\Big(\mathfrak{e}_c^0 + (1-2c^0)\frac{u_r^0 u_r^0}{2}\Big) = 0. \qquad (8.41)
\end{aligned}
$$

If $Q = 0$ we call the discontinuity a contact discontinuity or a slip line. Since $u^0 = u = 0$, these discontinuities move with the two–phase flow. If $Q \neq 0$, we call the discontinuity a shock since $u^0 \neq 0$, $u \neq 0$, two–phase flow is crossing the shock, or equivalently, the shock is moving through the mixture where the superscript 0 denotes the mixture parameters ahead the shock.

8.4 Study of Shock Waves of Small Amplitude

In this section we study shock waves of small amplitude. This allows us to perform an analysis to describe the qualitative behaviour of such discontinuities. The system (8.36)–(8.41) may be formulated in terms of the specific volume $V = \frac{1}{\rho}$ instead of the mixture density ρ. Thus system (8.22)–(8.27) can be written in the following form

$$
\begin{aligned}
\frac{u-S}{V} &= \frac{u^0 - S}{V^0} = Q, && (8.42)\\
\frac{\alpha(u-S)}{V} &= \frac{\alpha^0(u^0-S)}{V^0}, && (8.43)\\
Q^2V + \mathcal{P} + \frac{c(1-c)}{V}u_r^2 &= Q^2V^0 + \mathcal{P}^0 + \frac{c^0(1-c^0)}{V^0}u_r^0 u_r^0, && (8.44)\\
Qc + \frac{c(1-c)}{V}u_r &= Qc^0 + \frac{c^0(1-c^0)}{V^0}u_r^0, && (8.45)\\
QVu_r + \mathfrak{e}_c + (1-2c)\frac{u_r^2}{2} &= QV^0u_r^0 + \mathfrak{e}_c^0 + (1-2c^0)\frac{u_r^0u_r^0}{2}, && (8.46)\\
\mathfrak{e} + u_rc(1-c)\frac{u_r^2}{2} \quad &+ \quad \frac{c(1-c)u_r}{QV}\Big(\mathfrak{e}_c + (1-2c)\frac{u_r^2}{2}\Big) \\
-\mathfrak{e}^0 - u_r^0c^0(1-c^0)\frac{u_r^0u_r^0}{2} \quad &- \quad \frac{c^0(1-c^0)u_r^0}{QV^0}\Big(\mathfrak{e}_c^0 + (1-2c^0)\frac{u_r^0u_r^0}{2}\Big) \\
+\frac{1}{2}\Big(\mathcal{P} + \frac{c(1-c)}{V}u_r^2 \quad &+ \quad \mathcal{P}^0 + \frac{c^0(1-c^0)}{V^0}u_r^0u_r^0\Big)(V - V^0) = 0. \qquad (8.47)
\end{aligned}
$$

where

$$\mathcal{P} = -\mathfrak{e}_V. \tag{8.48}$$

More precisely, we study a shock wave propagating in the two–phase medium where there is no relative motion, that is

$$u_r^0 = 0. \tag{8.49}$$

Assume that the medium ahead of the shock is not a pure phase such as

$$0 < c^0 < 1, \tag{8.50}$$

as the cases $c^0 = 0$ or $c^0 = 1$ lead to a degenerate form of the equations and require special consideration. Then substituting (8.49) into (8.42)–(8.47), system (8.42)–(8.47) can be linearized to give

$$\frac{u - S}{V} = \frac{u^0 - S}{V^0} = Q, \tag{8.51}$$

$$\frac{\alpha(u - S)}{V} = \frac{\alpha^0(u^0 - S)}{V^0} \tag{8.52}$$

$$Q^2 V + \mathcal{P} + \frac{c(1-c)}{V} u_r^2 = Q^2 V^0 + \mathcal{P}^0, \tag{8.53}$$

$$Qc + \frac{c(1-c)}{V} u_r = Qc^0, \tag{8.54}$$

$$QVu_r + \mathfrak{e}_c + (1-2c)\frac{u_r^2}{2} = \mathfrak{e}_c^0, \tag{8.55}$$

$$\begin{aligned} \mathfrak{e} + c(1-c)\frac{u_r^2}{2} + \frac{c(1-c)u_r}{QV}\Big(\mathfrak{e}_c + (1-2c)\frac{u_r^2}{2}\Big) &- \mathfrak{e}^0 \\ + \frac{1}{2}\Big(\mathcal{P} + \frac{c(1-c)}{V} u_r^2 + \mathcal{P}^0\Big)(V - V^0) &= 0. \end{aligned} \tag{8.56}$$

Now let us assume that the mass flux Q is constant and let the parameters of state ahead of and behind the shock wave be connected by the following relations

$$u_r = \Delta u_r. \tag{8.57}$$

$$V = V^0 - \Delta V, \tag{8.58}$$

$$c = c^0 - \Delta c, \tag{8.59}$$

$$\mathcal{S} = \mathcal{S}^0 + \Delta \mathcal{S}, \tag{8.60}$$

where $\Delta V > 0$, $\Delta c > 0$, Δu_r and $\Delta \mathcal{S}$ are sufficiently small quantities. We also assume the following approximate formulae

$$u_r = \Delta u_r, \tag{8.61}$$

$$u_r^2 = (\Delta u_r)^2, \tag{8.62}$$

$$\frac{1}{V} = \frac{1}{V^0} + \frac{\Delta V}{V^0 V^0}, \tag{8.63}$$

$$c(1-c) = c^0(1-c^0) - (1-2c^0)\Delta c, \tag{8.64}$$

$$\frac{c(1-c)}{V} = \frac{c^0(1-c^0)}{V^0} + \frac{c^0(1-c^0)}{V^0 V^0}\Delta V - \frac{1-2c^0}{V^0}\Delta c, \tag{8.65}$$

and use equation (8.56) to derive the entropy variation behind the shock wave. Using (8.54) into (8.56) gives

$$\begin{aligned} \mathfrak{e} \quad - \quad & \mathfrak{e}^0 + c(1-c)\frac{u_r^2}{2} - (c-c^0)\Big(\mathfrak{e}_c + (1-2c)\frac{u_r^2}{2}\Big) \\ + \quad & \frac{1}{2}\Big(\mathcal{P} + \mathcal{P}^0 + \frac{c(1-c)}{V}u_r^2\Big)(V - V^0) = 0. \end{aligned} \tag{8.66}$$

Expanding each term in (8.66) up to first order in the entropy variation to obtain

$$\begin{aligned} \mathfrak{e}_{\mathcal{S}}\Delta\mathcal{S} - \mathfrak{e}_V\Delta V - \mathfrak{e}_c\Delta c + \mathfrak{e}_{VV}(\Delta V)^2 \quad & + \\ \mathfrak{e}_{cc}(\Delta c)^2 + \mathfrak{e}_{Vc}\Delta V\Delta c + \frac{1}{2}c^0(1-c^0)(\Delta u_r)^2 \quad & - \\ \frac{1}{6}\big[\mathfrak{e}_{VVV}(\Delta V)^3 + \mathfrak{e}_{ccc}(\Delta c)^3\big] \quad & - \\ \frac{1}{2}\big[\mathfrak{e}_{VVc}(\Delta V)^2\Delta c + \mathfrak{e}_{Vcc}\Delta V(\Delta c)^2\big] \quad & + \\ \Delta c\big[\mathfrak{e}_c - \mathfrak{e}_{cV}\Delta V - \mathfrak{e}_{cc}\Delta c + \frac{1}{2}\mathfrak{e}_{cVV}(\Delta V)^2 \quad & + \\ \frac{1}{2}\mathfrak{e}_{ccc}(\Delta c)^2 + \mathfrak{e}_{Vcc}\Delta V\Delta c + \frac{1}{2}(1-2c^0)(\Delta u_r)^2\big] \quad & - \end{aligned}$$

$$\frac{\Delta V}{2}\Big[2\mathcal{P}^0 + \mathfrak{e}_{VV}\Delta V + \mathfrak{e}_{Vc}\Delta c - \frac{1}{2}\mathfrak{e}_{VVV}(\Delta V)^2 - \frac{1}{2}\mathfrak{e}_{Vcc}(\Delta c)^2 - \mathfrak{e}_{VVc}\Delta V\Delta c\Big] = 0, \tag{8.67}$$

where all the derivatives of the EOS are calculated at ρ^0, c^0, $\mathcal{S}^0$. Substituting (8.48) into (8.67) we find

$$\begin{aligned}\mathfrak{e}_{\mathcal{S}}\Delta\mathcal{S} &= \frac{1}{2}\mathfrak{e}_{cc}(\Delta c)^2 + \frac{1}{2}\mathfrak{e}_{Vc}\Delta V\Delta c - \frac{1}{2}c^0(1-c^0)(\Delta u_r)^2 \\ &- \frac{1}{12}\mathfrak{e}_{VVV}(\Delta V)^3 - \frac{1}{3}\mathfrak{e}_{ccc}(\Delta c)^3 - \frac{3}{4}\mathfrak{e}_{Vcc}\Delta V(\Delta c)^2 \\ &- \frac{1}{2}\mathfrak{e}_{VVc}(\Delta V)^2\Delta c - \frac{1}{2}(1-2c^0)\Delta c(\Delta u_r)^2,\end{aligned} \tag{8.68}$$

which gives the entropy variation behind the shock wave of small amplitude . Equation (8.68) allow us to neglect entropy variation terms in expanding equations (8.51)–(8.55). Thus linearization of (8.53), (8.54) and (8.55) can be written in the form

$$(\mathfrak{e}_{VV} - Q^2)\Delta V + \mathfrak{e}_{Vc}\Delta c = 0, \tag{8.69}$$

$$\frac{c^0(1-c^0)}{V^0}\Delta u_r - Q\Delta c = 0, \tag{8.70}$$

$$QV^0\Delta u_r - \mathfrak{e}_{Vc}\Delta V - \mathfrak{e}_{cc}\Delta c = 0. \tag{8.71}$$

Using (8.70) into (8.71) the above system reduces to

$$(\mathfrak{e}_{VV} - Q^2)\Delta V + \mathfrak{e}_{Vc}\Delta c = 0, \tag{8.72}$$

$$c^0(1-c^0)\mathfrak{e}_{Vc}\Delta V + \big(c^0(1-c^0)\mathfrak{e}_{cc} - Q^2V^0V^0\big)\Delta c = 0. \tag{8.73}$$

There exists a non–trivial solution for (8.72)–(8.73) if the determinant of the system is equal to zero, that is

$$\begin{vmatrix} \mathfrak{e}_{VV} - Q^2 & \mathfrak{e}_{Vc} \\ c^0(1-c^0)\mathfrak{e}_{Vc} & c^0(1-c^0)\mathfrak{e}_{cc} - Q^2V^0V^0 \end{vmatrix} = 0, \tag{8.74}$$

or in a biquadratic form as

$$Q^4 - \left[\mathfrak{e}_{VV} + \frac{c^0(1-c^0)}{V^0}\frac{\mathfrak{e}_{cc}}{V^0}\right] Q^2 + \frac{c^0(1-c^0)}{V^0}\frac{\mathfrak{e}_{VV}\mathfrak{e}_{cc} - \mathfrak{e}_{Vc}^2}{V^0} = 0. \tag{8.75}$$

Solving (8.75) for the mass flux Q we find that

$$\begin{aligned} Q^2 &= \frac{1}{2}\left[\mathfrak{e}_{VV} + \frac{c^0(1-c^0)}{V^0}\frac{\mathfrak{e}_{cc}}{V^0}\right] \\ &\pm \frac{1}{2}\sqrt{\left[\left(\mathfrak{e}_{VV} + \frac{c^0(1-c^0)}{V^0}\frac{\mathfrak{e}_{cc}}{V^0}\right)^2 - 4\frac{c^0(1-c^0)}{V^0}\frac{\mathfrak{e}_{VV}\mathfrak{e}_{cc} - \mathfrak{e}_{Vc}^2}{V^0}\right]}. \end{aligned} \tag{8.76}$$

If we assume that the shock wave is determined by the jump of the specific volume V, then other parameters of state behind the shock can be obtained using (8.70)–(8.71) and (8.75) by the expressions

$$\Delta u = -Q\Delta V, \tag{8.77}$$

$$\Delta c = -\frac{\mathfrak{e}_{VV} - Q^2}{\mathfrak{e}_{Vc}}\Delta V, \tag{8.78}$$

$$\Delta u_r = \frac{QV^0}{c^0(1-c^0)}\frac{\mathfrak{e}_{VV} - Q^2}{\mathfrak{e}_{Vc}}\Delta V. \tag{8.79}$$

Finally, we conclude that there are two possible shock waves of small amplitude. The velocities of those two waves are close to the velocities of two sound waves. It follows from (8.51) that

$$S = u^0 - QV^0. \tag{8.80}$$

From (8.70) we find that

$$\Delta u_r = \frac{QV^0}{c^0(1-c^0)}\Delta c. \tag{8.81}$$

Thus we have for the second order terms of (8.68) the expression

$$\begin{aligned}
&\mathfrak{e}_{cc}(\Delta c)^2 + \mathfrak{e}_{Vc}\Delta V\Delta c - c^0(1-c^0)(\Delta u_r)^2 = \\
&\frac{c^0(1-c^0)\mathfrak{e}_{cc} - Q^2V^0V^0}{c^0(1-c^0)}(\Delta c)^2 + \mathfrak{e}_{Vc}\Delta V\Delta c,
\end{aligned} \tag{8.82}$$

which is equal to zero as it follows from (8.73). Therefore the entropy variation has the following expression

$$\begin{aligned}
\mathfrak{e}_{\mathcal{S}}\Delta\mathcal{S} &= \frac{1}{12}\mathfrak{e}_{VVV}(\Delta V)^3 - \frac{1}{3}\mathfrak{e}_{ccc}(\Delta c)^3 - \frac{3}{4}\mathfrak{e}_{Vcc}\Delta V(\Delta c)^2 \\
&- \frac{1}{2}\mathfrak{e}_{VVc}(\Delta V)^2\Delta c - \frac{1}{2}(1-2c^0)\Delta c(\Delta u_r)^2.
\end{aligned} \tag{8.83}$$

Thus, the entropy variation is proportional to the cube of the variations of other parameters of state. The laws of thermodynamics require the positiveness of $\Delta\mathcal{S}$. This requirement leads to some restrictions on the third derivatives of the equation of state. In the gas dynamics equations where the equation of state depends on the specific volume and entropy $\mathfrak{e} = \mathfrak{e}(V, \mathcal{S})$ this restriction is $\mathfrak{e}_{VVV} < 0$. Under which condition this restriction is physically realizable for (8.83) remains the subject of future study.

8.5 Conclusions

This chapter presents the basis of the Riemann problem for the hyperbolic conservative two–fluid model. Possible wave patterns in the solution of the Riemann problem are proposed and it is shown that, depending on the type of non–linear wave, there can be sixteen wave patterns to construct with six waves in each case. It is shown that for the case of single pressure approximation the dependence of the speed of sound on the void fraction is monotonic. The sound wave propagation in static two–fluid media is derived and its dependence on the volume concentration relaxation is assessed. The conservative form of the model allows the formulation of discontinuous solutions such as shock waves. The analysis of the discontinuities of the model is carried out by investigating small amplitude shock waves where there is no relative motion ahead of

the shock and where the medium is not a pure phase. In addition, the study of shock waves of small amplitude presented in this chapter concludes that there are two types of shock waves corresponding to the types of sound wave in the two–phase flow. The analysis of the shock waves presented in this chapter implies that it is not easy to analyse the Riemann problem mathematically to obtain an explicit solution of the Riemann problem. This therefore leads one to consider numerical approximations by using modern shock–capturing schemes. The numerical scheme will give more insight into the Riemann problem for the hyperbolic conservative two–fluid model and will resolve both rarefaction waves and shock waves as we shall see in the next chapter.

CHAPTER 9

NUMERICAL STUDY OF WAVE PROPAGATION IN COMPRESSIBLE TWO–PHASE FLOW

This chapter is concerned with the numerical solution of a system of conservation laws modeling one–dimensional compressible two–phase flow.

9.1 The Numerical Method

The hyperbolic conservative two–fluid model presented in chapters 7 and 8 is difficult to solve analytically since the model possesses a large number of acoustic and convective waves. In addition the number of equations will depend on the number of waves considered, and the closure laws supplied will typically vary and change the solution. Thus, a small modification of the model, will require us to repeat the mathematical analysis and this does not seem practical. Therefore, it seems unnatural to look for analytical solutions to the model. We must instead consider numerical approximations using modern shock–capturing schemes. The method we will use must be flexible enough to handle the modifications of the model without relying on mathematical results obtained analytically. The numerical method will give further insight into the model and will resolve both rarefaction waves and shocks.

Before presenting our numerical method for the hyperbolic conservative two–fluid model, we review some of the basic theory of Godunov–type numerical schemes [71, 177]. We discretise the x–t plane by choosing a mesh width Δx and a time step Δt, and we define the mesh size $\Delta x = x_{i+\frac{1}{2}} - x_{i-\frac{1}{2}}$, with $i = 1, \ldots, M$. Thus for a given cell $I_i = [x_{i-\frac{1}{2}}, x_{i+\frac{1}{2}}]$ the location of cell x_i and the cell boundaries $x_{i-\frac{1}{2}}$, $x_{i+\frac{1}{2}}$ are given by

$$x_{i-\frac{1}{2}} = (i-1)\Delta x, \;\; x_i = (i - \frac{1}{2})\Delta x, \;\; x_{i+\frac{1}{2}} = i\Delta x. \tag{9.1}$$

The time step Δt ($\Delta t = t^{n+1} - t^n$) is calculated as marching in time proceeds and satisfies the condition

$$\Delta t = C \frac{\Delta x}{S_{\max}^{(n)}}, \tag{9.2}$$

where C is the CFL (Courant–Friedrichs–Lewy) number with $0 < C \leq 1$ and $S_{\max}^{(n)}$ is the maximum wave speed present throughout the domain at the time level n chosen

$$S_{\max}^{(n)} = \max_i \left\{ |\lambda_i| \right\}, \tag{9.3}$$

where λ_i are eigenvalues corresponding to sound waves.

In Godunov's methods, the approximate solution $\mathbb{U}^{n+1}$, at time t^{n+1}, is obtained by solving Riemann problems at cell interfaces

$$\mathbb{U}_i^{n+1} = \mathbb{U}_i^n - \frac{\Delta t}{\Delta x}[\mathbb{F}_{i+\frac{1}{2}} - \mathbb{F}_{i-\frac{1}{2}}], \tag{9.4}$$

with the numerical flux $\mathbb{F}_{i+\frac{1}{2}}$ corresponding to the intercell boundary at $x = x_{i+\frac{1}{2}}$ between i and $i+1$. The Godunov flux $\mathbb{F}_{i+\frac{1}{2}}$ may be defined as the physical flux $\mathbb{F}(\mathbb{U})$ evaluated at the solution $\mathbb{U}_{i+\frac{1}{2}}(\frac{x}{t})$ along t–axis in the local coordinates, that is

$$\mathbb{F}_{i+\frac{1}{2}} = \mathbb{F}(\mathbb{U}_{i+\frac{1}{2}}(0)), \tag{9.5}$$

which is the exact solution of the Riemann problem

$$\partial_t \mathbb{U} + \partial_x \mathbb{F}(\mathbb{U}) = 0, \tag{9.6}$$

$$\mathbb{U}(x, t^n) = \begin{cases} \mathbb{U}_{i-1}^n & x < x_{i-\frac{1}{2}}, \\ \mathbb{U}_i^n & x > x_{i-\frac{1}{2}}. \end{cases} \tag{9.7}$$

In practice, solving the non–linear Riemann problem for the hyperbolic conservative two–fluid model may be difficult and time consuming because it requires some itera-

tions for non–linear equations. This suggests using approximate Riemann solvers to build more efficient Godunov–type numerical methods. One of the more modern approximate Riemann solvers is a TVD centred scheme such as the SLIC scheme. The SLIC scheme is a second–order extension of the FORCE scheme. To solve the non–linear Riemann problem (9.5) for hyperbolic conservative systems, the SLIC scheme results from replacing the Godunov upwind flux in the MUSCL–Hancock scheme by the FORCE flux. For the set of variables $\mathbb{W}$ chosen as in (7.66), the SLIC scheme lies in three steps to implement. We follow the procedures given by Toro [177, 178] to recall these steps:

Step (I): Data Reconstruction, for a given set of constant average data states $\mathbb{W}_i^n$, the reconstruction of piecewise constant data $\mathbb{W}_i^n$ into a piecewise linear distribution of the data given as

$$\mathbb{W}_i(x) = \mathbb{W}_i^n + (x - x_i)\frac{\Delta_i}{\Delta x}, \ x \in I_i, \tag{9.8}$$

where $x_i = (i - \frac{1}{2})\Delta x$ is the centre of the computing cells I_i, Δ_i are the slopes of six components for the hyperbolic conservative two–fluid model defined as

$$\Delta_i = \frac{1}{2}(1 + \Im)\mathbb{W}_{i-\frac{1}{2}} + \frac{1}{2}(1 - \Im)\mathbb{W}_{i+\frac{1}{2}}, \tag{9.9}$$

where the parameter $\Im \in [-1, 1]$, for the hyperbolic conservative two–fluid model $\Im = 0$ and the average between the intercell slopes

$$\mathbb{W}_{i-\frac{1}{2}} = \mathbb{W}_i - \mathbb{W}_{i-1}, \ \mathbb{W}_{i+\frac{1}{2}} = \mathbb{W}_{i+1} - \mathbb{W}_i. \tag{9.10}$$

Now the boundary extrapolated values are obtained by setting $x = 0$ and $x = \Delta x$ in (9.8)

$$\mathbb{W}_i^{\mathcal{L}} = \mathbb{W}_i^n - \frac{1}{2}\Delta_i; \ \mathbb{W}_i^{\mathcal{R}} = \mathbb{W}_i^n + \frac{1}{2}\Delta_i. \tag{9.11}$$

which is the values of the vector function (9.8) at the left and right boundaries of I_i.

Step (II): Evolution of extrapolated values, the boundary extrapolated values $\mathbb{W}_i^{\mathcal{L}}$ and $\mathbb{W}_i^{\mathcal{R}}$ evolved in each cell I_i by a time $t = \frac{1}{2}\Delta t$ in terms of conservative variables according to

$$\overline{\mathbb{U}}_i^{\mathcal{L}} = \mathbb{U}_i^{\mathcal{L}} + \frac{1}{2}\frac{\Delta t}{\Delta x}[\mathbb{F}(\mathbb{W}_i^{\mathcal{L}}) - \mathbb{F}(\mathbb{W}_i^{\mathcal{R}})], \tag{9.12}$$

$$\overline{\mathbb{U}}_i^{\mathcal{R}} = \mathbb{U}_i^{\mathcal{R}} + \frac{1}{2}\frac{\Delta t}{\Delta x}[\mathbb{F}(\mathbb{W}_i^{\mathcal{L}}) - \mathbb{F}(\mathbb{W}_i^{\mathcal{R}})], \tag{9.13}$$

where $\mathbb{U}_i^{\mathcal{L}}$ and $\mathbb{U}_i^{\mathcal{R}}$ are computed from the boundary extrapolated variables $\mathbb{W}_i^{\mathcal{L}}$ and $\mathbb{W}_i^{\mathcal{R}}$.

Step (III): The Riemann problem, we solve the conventional, piecewise constant data Riemann problem for the hyperbolic conservative two–fluid model with initial data

$$\mathbb{W}_{\mathcal{L}} \equiv \overline{\mathbb{U}}_{\mathrm{i}}^{\mathcal{R}};\ \mathbb{W}_{\mathcal{R}} \equiv \overline{\mathbb{U}}_{\mathrm{i+1}}^{\mathcal{L}}, \tag{9.14}$$

at each interface $x_{i+\frac{1}{2}}$ to find the similarity solution $\mathbb{W}_{i+\frac{1}{2}}(\frac{x}{t})$.
Now to obtain the Godunov flux (9.5) at the intercell position $i + \frac{1}{2}$, we evaluate the FORCE flux

$$\mathbb{F}_{i+\frac{1}{2}}^{\mathrm{FORCE}} = \mathbb{F}_{i+\frac{1}{2}}(\overline{\mathbb{U}}_i^{\mathcal{R}}, \overline{\mathbb{U}}_{i+1}^{\mathcal{L}}) = \frac{1}{2}(\mathbb{F}_{i+\frac{1}{2}}^{\mathrm{LF}} + \mathbb{F}_{i+\frac{1}{2}}^{\mathrm{RI}}), \tag{9.15}$$

where $\mathbb{F}_{i+\frac{1}{2}}^{LF}$ is the Lax–Friedrichs flux given by

$$\mathbb{F}_{i+\frac{1}{2}}^{\mathrm{LF}} = \frac{1}{2}(\mathbb{F}_i^n + \mathbb{F}_{i+1}^n) + \frac{1}{2}\frac{\Delta x}{\Delta t}[\mathbb{U}_i^n - \mathbb{U}_{i+1}^n], \tag{9.16}$$

and the Richtmyer flux defined as

$$\mathbb{F}^{\mathrm{RI}}_{i+\frac{1}{2}} = \mathbb{F}(\mathbb{U}^{\mathrm{RI}}_{i+\frac{1}{2}}), \tag{9.17}$$

$$\mathbb{U}^{\mathrm{RI}}_{i+\frac{1}{2}} = \frac{1}{2}(\mathbb{U}^n_i + \mathbb{U}^n_{i+1}) + \frac{1}{2}\frac{\Delta t}{\Delta x}[\mathbb{F}^n_i - \mathbb{F}^n_{i+1}]. \tag{9.18}$$

Implementing the TVD version of the scheme for the hyperbolic conservative two–fluid model is similar to the case of the simplified two–fluid model of chapter 2.

9.2 Treatment of Source Terms

In this section we are concerned with the numerical solution for the hyperbolic conservative two–fluid model with a source term which can be written in a system of conservation laws as

$$\partial_t \mathbb{U} + \partial_x \mathbb{F}(\mathbb{U}) = \mathbb{S}(\mathbb{U}), \tag{9.19}$$

where $\mathbb{U}$ is the vector of unknowns, the vector of fluxes is $\mathbb{F}(\mathbb{U})$ and $\mathbb{S}(\mathbb{U})$ is the vector of source terms taken as physical parameters (see chapter 7 for background in the hyperbolic conservative two–fluid model).

The numerical solution of (9.19) with initial conditions (IC's) at time $t = t^n$ given by

$$\mathbb{U}(x, t^n) = \mathbb{U}^n, \tag{9.20}$$

can be found using the splitting scheme [177] which relies on solving in succession the following pair of IVPs (initial–value problems)

$$\left.\begin{aligned} \text{PDE's}: \ \partial_t \mathbb{U} + \partial_x \mathbb{F}(\mathbb{U}) &= 0, \\ \text{IC's}: \ \mathbb{U}(x, t^n) &= \mathbb{U}^n, \end{aligned}\right\} \tag{9.21}$$

and

$$\left.\begin{aligned} \text{PDE's}: \ \frac{d}{dt}\mathbb{U} &= \mathbb{S}(\mathbb{U}), \\ \text{IC's}: \ \overline{\mathbb{U}}^{n+1}. \end{aligned}\right\} \tag{9.22}$$

Simplification of (9.19) results from the assumption of no spatial variations, that is

$$\partial_x \mathbb{F}(\mathbb{U}) = 0. \tag{9.23}$$

Thus each numerical sub–problem (9.21), (9.22) is dealt with separately. One requires a numerical method to solve the homogeneous system (9.21) and another numerical method to solve (9.22), with the initial data taken from the solution of (9.21). Generally, one may choose the best scheme for the type of problems. In the previous section we have presented a numerical scheme for solving (9.21). Now we want to evolve $\mathbb{U}^n$ from time $t = t^n$ to the new value $\mathbb{U}^{n+1}$ and at $t = t^{n+1}$ by a time step $\Delta t = t^{n+1} - t^n$. The initial condition of the homogeneous system (9.21) is the initial condition $\mathbb{U}^n$ of the full problem (9.19) and the solution after a time step Δt is $\overline{\mathbb{U}}^{n+1}$, which may be regarded as a predicted (approximate) solution. The IVP (9.22) is then solved by a time Δt and with initial condition given by the solution of the homogeneous IVP namely $\overline{\mathbb{U}}^{n+1}$. The solution of IVP (9.22) is then regarded as the approximate solution of the full problem (9.19).

Interpreting $\mathfrak{C}(\mathbb{U})$ as the solution operator for system (9.21) and $\mathfrak{S}(\mathbb{U})$ as the source operator for system (9.22) over a time t we can write

$$\text{Solution } \mathfrak{C}: \quad \overline{\mathbb{U}}_i^{n+1} = \mathbb{U}_i^n - \frac{\Delta t}{\Delta x}[\mathbb{F}_{i+\frac{1}{2}} - \mathbb{F}_{i-\frac{1}{2}}], \tag{9.24}$$

and

$$\text{Source } \mathfrak{S}: \quad \mathbb{U}_i^{n+1} = \overline{\mathbb{U}}_i^{n+1} + \Delta t \mathbb{S}(\overline{\mathbb{U}}_i^{(n+1)}), \tag{9.25}$$

where $\overline{\mathbb{U}}^{(n+1)}$ is a value at which the source term vector $\mathbb{S}$ is evaluated. Hence the splitting scheme (9.21) and (9.22) can be expressed as

$$\mathbb{U}^{n+1} = \mathfrak{S}^{(\Delta t)}\mathfrak{C}^{(\Delta t)}(\mathbb{U}^n), \tag{9.26}$$

which is a first–order splitting scheme accuracy in time. A scheme that is second–order accurate in time is

$$\mathbb{U}^{n+1} = \mathfrak{S}^{(\frac{1}{2}\Delta t)}\mathfrak{C}^{(\Delta t)}\mathfrak{S}^{(\frac{1}{2}\Delta t)}(\mathbb{U}^n). \tag{9.27}$$

The full scheme (9.24) and (9.25) can be written as

$$\mathbb{U}_i^{n+1} = \mathbb{U}_i^n - \frac{\Delta t}{\Delta x}[\mathbb{F}_{i+\frac{1}{2}} - \mathbb{F}_{i-\frac{1}{2}}] + \Delta t \mathbb{S}(\overline{\mathbb{U}}_i^{(n+1)}). \tag{9.28}$$

We refer to [54, 177] for further approaches on splitting schemes for non–linear systems of hyperbolic conservation laws with source terms.

9.3 Test Problems and Numerical Results

Using the aforementioned theory and model inputs, we present and discuss seven numerical test problems. The main purpose of this section is to illustrate the capabilities of the numerical method to capture pressure wave propagation and to present a suite of carefully selected one–dimensional test problems for the hyperbolic conservative two–fluid model with source terms. In the first test problem, we consider an air–water mixture collision which consists of a symmetric Riemann problem. In the second test problem, we present a grid convergence study for the solution of the Riemann problem obtained in Test 1. In the third test we consider pressure wave

Parameters for the liquid and gas phases							
γ_1	=	2.8		γ_2	=	1.4	
ρ_1^0	=	10^3	kg/m^3	ρ_2^0	=	1	kg/m^3
c_v^1	=	1495	J/kgK	c_v^2	=	720	J/kgK
A_0	=	$8.4999\ 10^5$	m^2/s^2	A_2	=	10^5	m^2/s^2
A_1	=	$8.5\ 10^5$	m^2/s^2				

Table 9.1: Parameters for the numerical study of wave propagation in compressible two–phase flow.

propagation for a constructed case and examine the effect of the mixture velocity on the description of these waves. In the fourth test problem, we consider a relaxation

of volume concentration to study the effect of this relaxation on the air–water mixture collision. In the fifth test problem we consider additionally an interfacial friction source terms in the air–water mixture collision. In the sixth test problem we consider a two–phase shock–tube problem which consists of a Riemann problem for the hyperbolic conservative two–fluid model. Finally, in the last test problem we consider a 2–left and 2–right rarefactions and study the symmetric Riemann problem. The air–water mixture is governed by EOS (see section 7.2 of chapter 7))

$$\mathcal{E}(\rho, \alpha, c, u_r, \mathcal{S}) = \mathfrak{e}(\rho, \alpha, c, \mathcal{S}) + c(1-c)\frac{u_r u_r}{2}, \tag{9.29}$$

which is determined by the equations of state for the air and water as described in section 8.2 of chapter 8.

In all chosen tests, the data consists of two constant states $\mathbb{W}_{\mathcal{L}} = [\rho_{\mathcal{L}}, \alpha_{\mathcal{L}}, u_{\mathcal{L}}, c_{\mathcal{L}}, u_{r\mathcal{L}}, \mathcal{S}_{\mathcal{L}}]^T$ and $\mathbb{W}_{\mathcal{R}} = [\rho_{\mathcal{R}}, \alpha_{\mathcal{R}}, u_{\mathcal{R}}, c_{\mathcal{R}}, u_{r\mathcal{R}}, \mathcal{S}_{\mathcal{R}}]^T$, separated by a discontinuity at a position $x = x_0$ with $\rho_{\mathcal{L}}$ and $\rho_{\mathcal{R}}$ are computed by the given pressures $\mathcal{P}_{\mathcal{L}}$ and $\mathcal{P}_{\mathcal{R}}$. The numerical

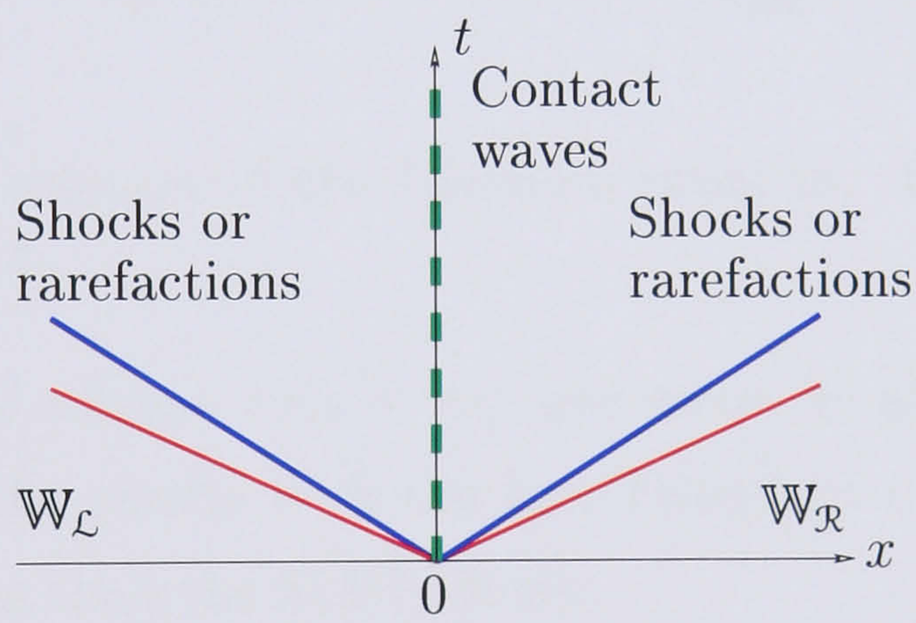

Figure 9.1: Structure of the exact solution of the symmetric Riemann problem in the x–t plane for the hyperbolic conservative two–fluid model. There are six wave families associated with the eigenvalues (7.102)–(7.106).

solutions are found in the spatial domain $-10 \leq x \leq 10$, which is discretized with M computing cells ($M = 100$ or $M = 1000$ for a coarse mesh or a fine mesh, respectively). The Courant number coefficient is $C = 0.9$; boundary conditions are transmissive; $S_{\max}$ is found using the simplified formula (9.3); the SUPERBEE limiter was used to obtain second–order accuracy in space and the units for the time, pressure, mixture

velocity and spatial domain are; $[t] = 10^{-5}\ s$, $[\mathcal{P}] = 10^9$ Pa, $[u] = 10^3\ m/s$ and $[x] = 10^{-2}\ m$. The calculations have been carried out using the parameters defined in table 9.1. The numerical results were then compared with a reference solution

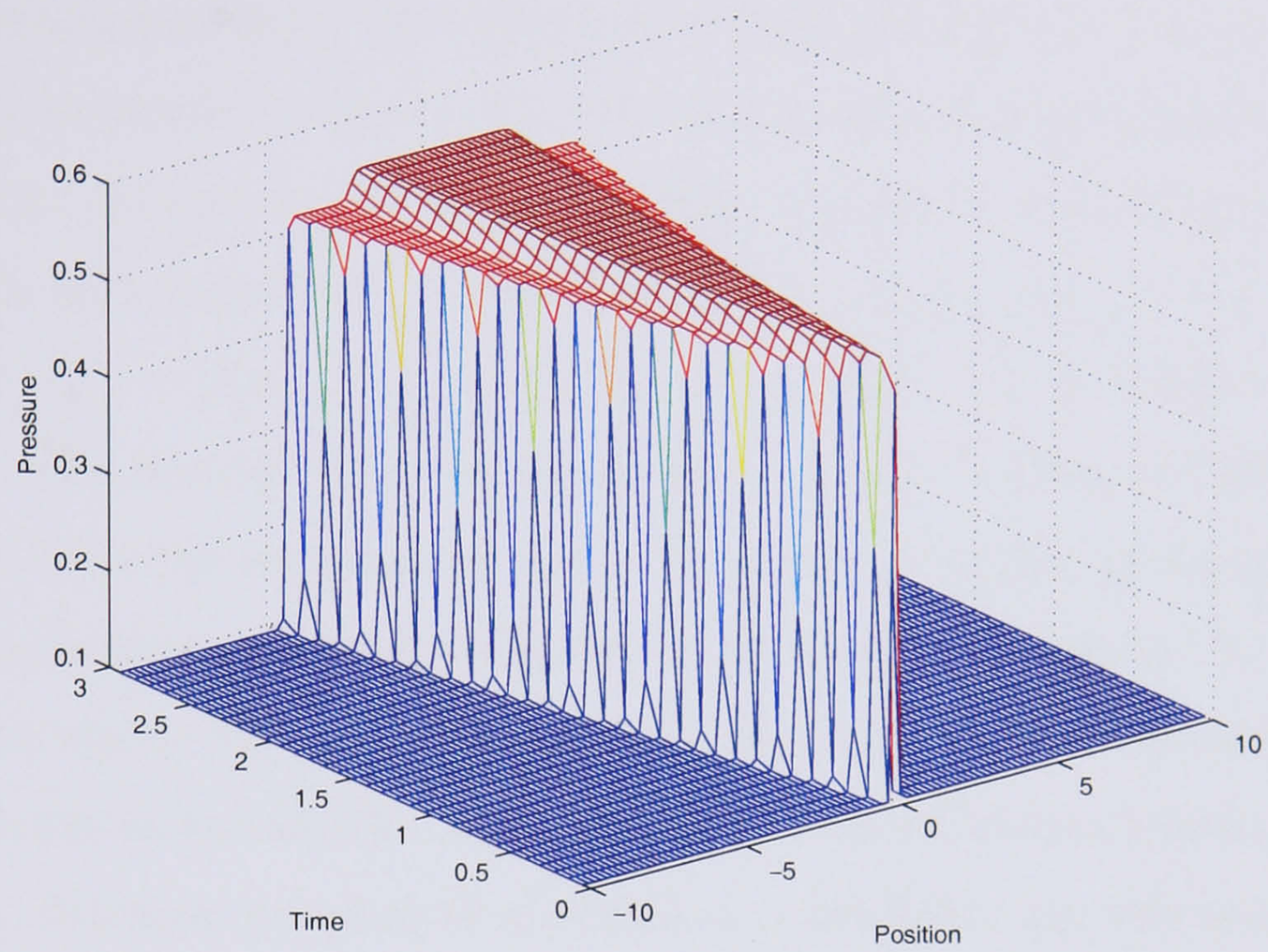

Figure 9.2: Numerical solution of the Riemann problem. Pressure distribution in three–dimension at $t = 3$.

obtained using the SLIC scheme with a very fine mesh. In all test cases, as we shall see later, we compare the results with the Lax–Friedrichs method which has much more numerical diffusion than the SLIC scheme.

9.3.1 Test 1: Air–Water Mixture Collision

The purpose of this first test is to choose the reference solution for the numerical solution with a very fine mesh and compare the numerical scheme described in section 9.1 with this reference solution as well as the standard Lax–Friedrichs method on the solution of the Riemann problem for the hyperbolic conservative two–fluid model. Computational experience suggests that the TVD SLIC scheme with a very fine mesh, $M = 1000$, is the reference solution for the hyperbolic conservative two–fluid model. Thus in all the test problems we will compare our results with the reference so-

lution. The left and right states for this Riemann problem are; $\mathcal{P}_{\mathcal{L}} = \mathcal{P}_{\mathcal{R}} = 0.1$, $\alpha_{\mathcal{L}} = 0.5 = \alpha_{\mathcal{R}}$, $u_{\mathcal{L}} = 0.4$, $u_{\mathcal{R}} = -0.4$, $u_{r\mathcal{L}} = 0 = u_{r\mathcal{R}}$, $\mathcal{S}_{\mathcal{L}} = 0 = \mathcal{S}_{\mathcal{R}}$, with $c_{\mathcal{L}}$ and $c_{\mathcal{R}}$ can be calculated using relation (7.23). As the data for the pressure is constant on the left and right states and for the mixture velocity u is symmetric, this is a symmetric Riemann problem. The solution of the symmetric Riemann problem (9.6) is schematically depicted in figure 9.1, which consists of a symmetric wave pattern about the t–axis. There are six wave families, the outer waves corresponds to the non–linear fields associated with the eigenvalues $\lambda_{1,2} = u - a_{m_{1,2}} + \mathcal{Y}(a_{m_{1,2}})u_r + \mathcal{O}(u_r^2)$ and $\lambda_{5,6} = u + a_{m_{1,2}} + \mathcal{Y}(a_{m_{1,2}})u_r + \mathcal{O}(u_r^2)$, where $a_{mi}(\mathrm{i} = 1, 2)$ is the speed of sound of the mixture. The middle wave families correspond to the linearly degenerate fields associated with multiple eigenvalues $\lambda_{3,4} = u$, which is in this problem $\lambda_{3,4} = u = 0$. It is difficult to construct an exact solution for the Riemann problem in a general case. However, for the states $\mathbb{W}_{\mathcal{L}}$ and $\mathbb{W}_{\mathcal{R}}$ we know that the exact solution is composed of six waves which are either shocks, rarefactions or contact discontinuities separated by constant states. Because no analytical solution is available numerical evidence shows that there are four symmetric shock waves travelling in opposite directions that have become shock waves and trivial contact discontinuities centred at $x = x_0 = 0$ as shown in figures 9.2 and 9.3. The benefit of shock wave capturing is more clearly seen in figure 9.4 in the comparison with figures 9.2 and 9.3. In figure 9.4 we give a comparison between SLIC and Lax–Friedrichs methods for the pressure. In figure 9.5 we show the effect of the initial pressure ($\mathcal{P}_{\mathcal{L}} = \mathcal{P}_{\mathcal{R}} = 0.0001,\ 0.001,\ 0.1$) on the waves propagation to the left and right after the collision. The increase of the pressure generates left–going two–shock and right–going two–shock waves as shown in figure 9.5.

9.3.2 Test 2: Grid Convergence Study

Since no analytical solution is available, a grid convergence study is performed in order to gain some insight into the structure of the solution and to test the convergence, and the stability character of SLIC scheme described in section 9.1. In this test case the initial conditions for the Riemann problem are chosen as in Test 1. A series of 7

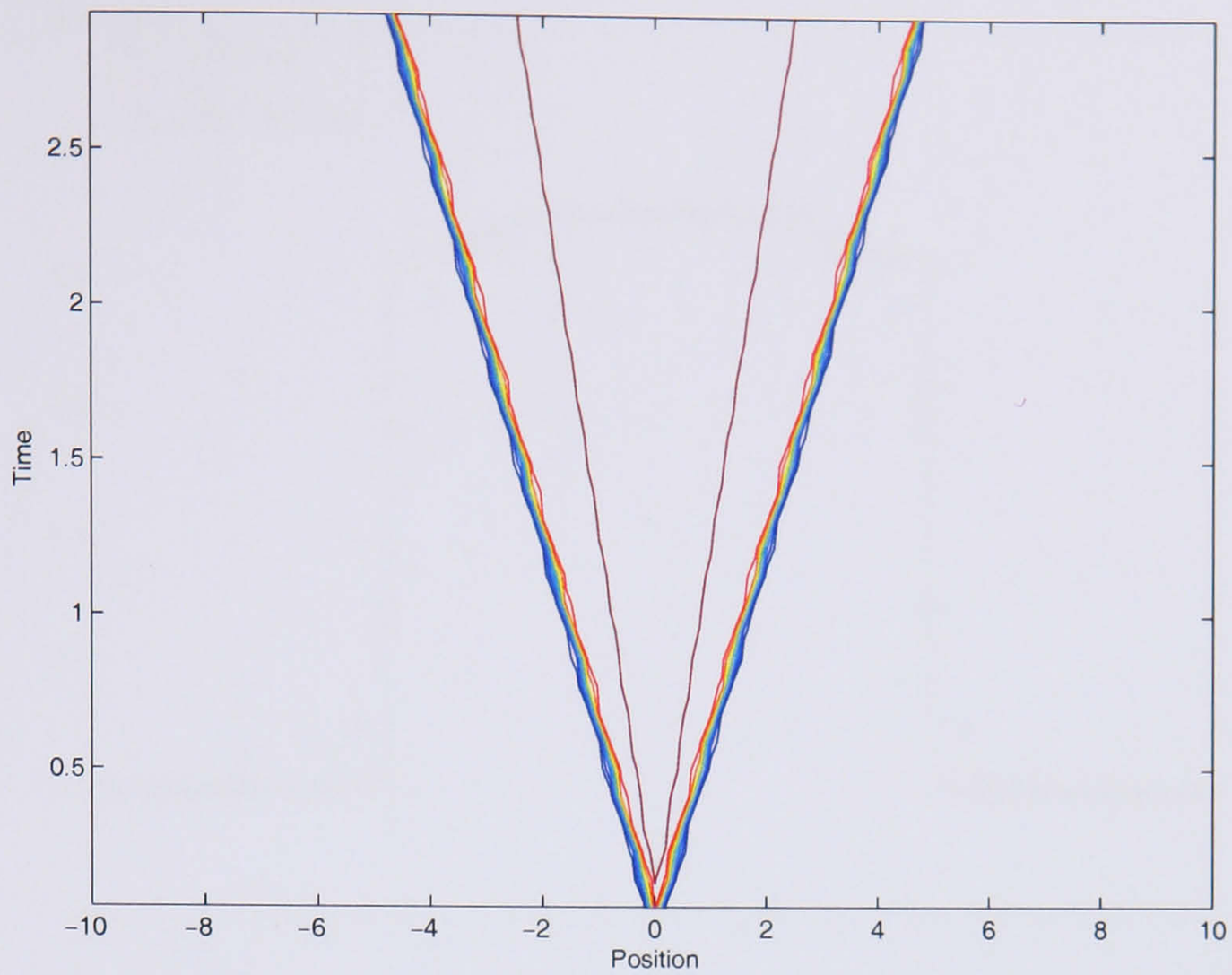

Figure 9.3: Pressure contours for the Riemann problem at $t = 3$.

meshes, from 100 to 1000 cells, have been considered in this study. From the results plotted in figure 9.6, one can identify two–shock waves propagating to the far left and to the far right, and a contact wave in the middle of the structure, through which the pressure remains constant. An interesting feature of the study shown in figure 9.6 is that there are no oscillations at the discontinuity of the pressure when the meshing is refined. This study clearly demonstrates the ability of the SLIC scheme to capture discontinuities.

9.3.3 Test 3: Pressure Wave Propagation

Results of Test 1 shows that there are four pressure waves. These waves can be split into two families of two shock waves. The purpose of this test problem is to study the structure of the pressure wave and its dependence on the value of the pressure. Such a problem should be considered by the study of Hugoniot shock conditions; but this problem is a subject of further research. Here we present results of calculations of pressure waves, which satisfy the Hugoniot conditions numerically. To do this we use the values of parameters of state in the star region in Test 1, which correspond

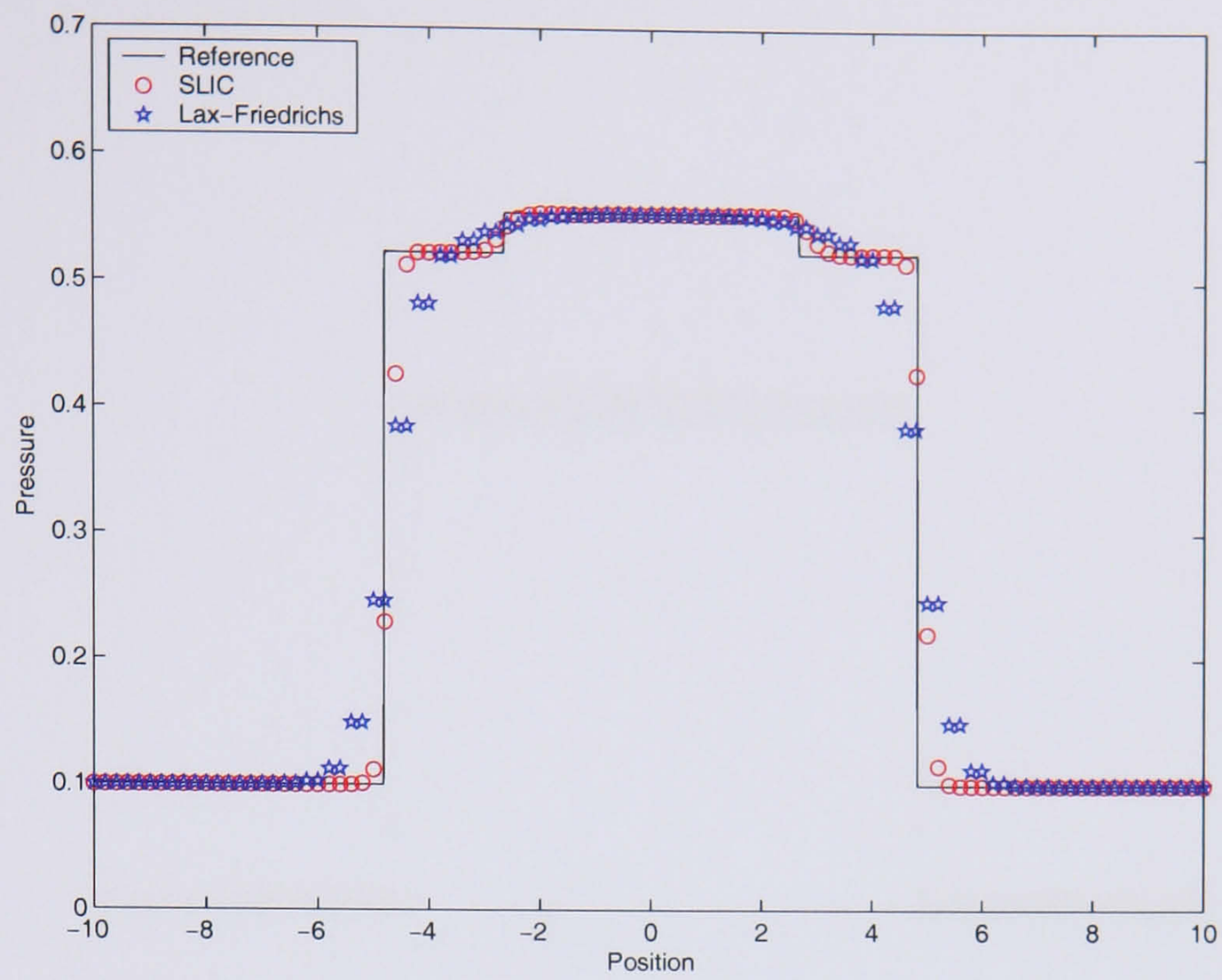

Figure 9.4: Numerical solution (symbols) for pressure at time 3. SLIC and Lax–Friedrichs methods are compared with the reference solution at 1000 cells.

to the values behind the shock wave on the Hugoniot curve. We take these values as the initial data on the left side in the Riemann problem. The initial pressure value from the right side is set equal to 0.1. We are interested in simulating a pressure wave generated by increasing the mixture velocity from 0.1 to 0.4 and setting the obtained star states equal to the left data, i.e. $\mathbb{W}^\star = \mathbb{W}_\mathcal{L}$ in each case of the simulation. If we recall Test 1, we notice that there are right–going two–shock waves in the mixture region (see figure 9.4). It is clear that the velocity of the shock waves is equal for all the different cases where the mixture velocity increases. The amplitude of the second wave with less velocity increases as the pressure behind the wave becomes stronger. The increase in the mixture velocity generates kinks in the shocks for the pressure solution as shown in figure 9.7. These kinks at $u_\mathcal{R} = 0.4$ are referred to as "start–up errors" and were first reported in [202]. In addition, a strong two–shocks will form which continues to travel to the right in the mixture two–phase region with reduced mixture velocity as shown in figure 9.7. These results were obtained by the SLIC scheme with $M = 300$ cells.

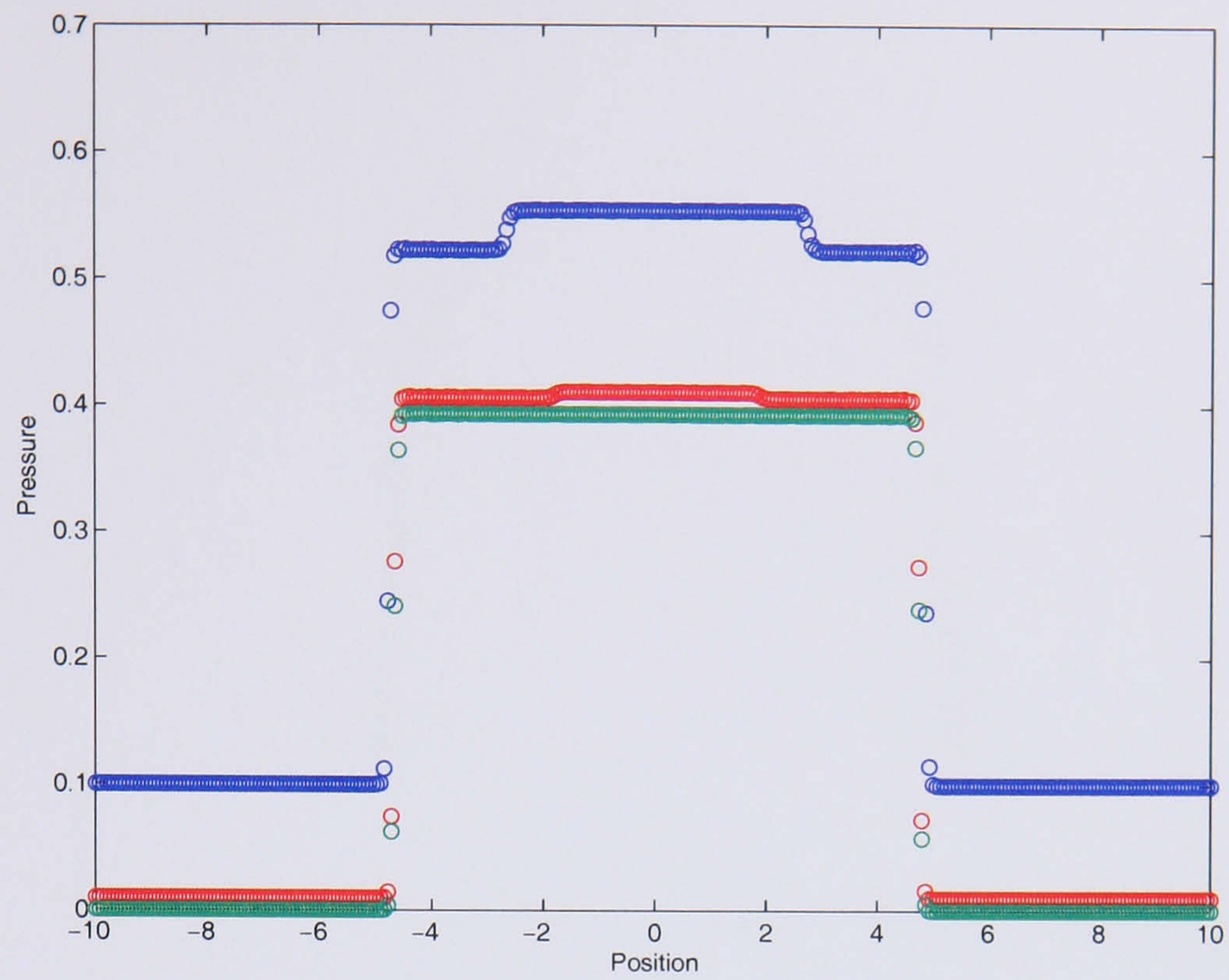

Figure 9.5: Numerical solution (SLIC scheme). Effect of the initial pressure on the structure of the solution at $t = 3$.

9.3.4 Test 4: Relaxation of Volume Concentration

A source term is considered in Test 3 to study the effect of the relaxation of volume concentration on the pressure wave propagation. The source term in the volume concentration equation (7.54) describes the relaxation of volume concentration to equilibrium state with relaxation time τ, that is the pressures for the phases are equal. In this test problem, the initial conditions are chosen as in Test 1 where the pressure is kept constant and equal to 0.1 at the left and right states. For the numerical calculations, the SLIC scheme tested as explained in section 9.1. The results are shown in figure 9.8. We have chosen to present plots of the pressure. In figure 9.8, it is seen that the effect of τ at $t = 3$ has a decreased amplitude due to the physical attenuation caused by the interphase exchange of volume concentration ($\tau^{-1} = 0.1,\ 1.0,\ 10$).

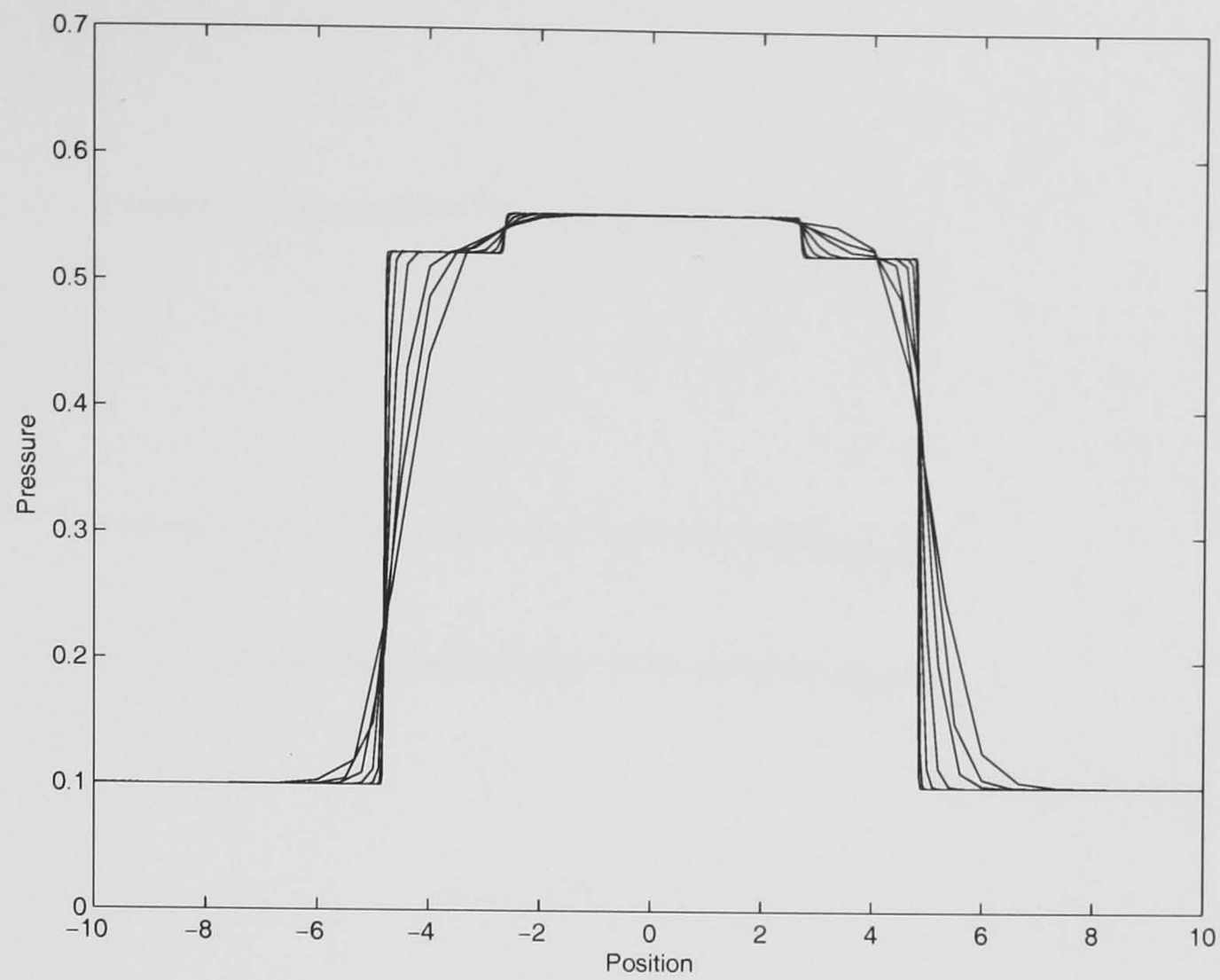

Figure 9.6: Riemann problem: grid convergence study for the pressure profile with SLIC scheme at $t = 3$.

9.3.5 Test 5: Effect of Volume Concentration Relaxation and Interfacial Friction

The purpose of this test problem is to evaluate the capabilities of the SLIC scheme to compute pressure wave propagation with source terms. In this test case we study the effect of the source terms on the hyperbolic conservative two–fluid model. The source terms correspond to the relaxation of volume concentration to equilibrium state with relaxation time τ and to the interfacial friction π as expressed in (7.58) with κ defined as

$$\kappa = \frac{1}{8} C_{\mathrm{D}} \frac{\rho^2}{\rho_2} |u_r|, \tag{9.30}$$

with the drag coefficient $C_{\mathrm{D}} = 500$, and $\rho_2 = c\rho/\alpha$ is the air mass density.

As mentioned before the relaxation of volume concentration and interfacial friction are highly responsible for the development of the flow. Three computations were performed on a mesh of 100 cells, using the SLIC scheme, and for three values of

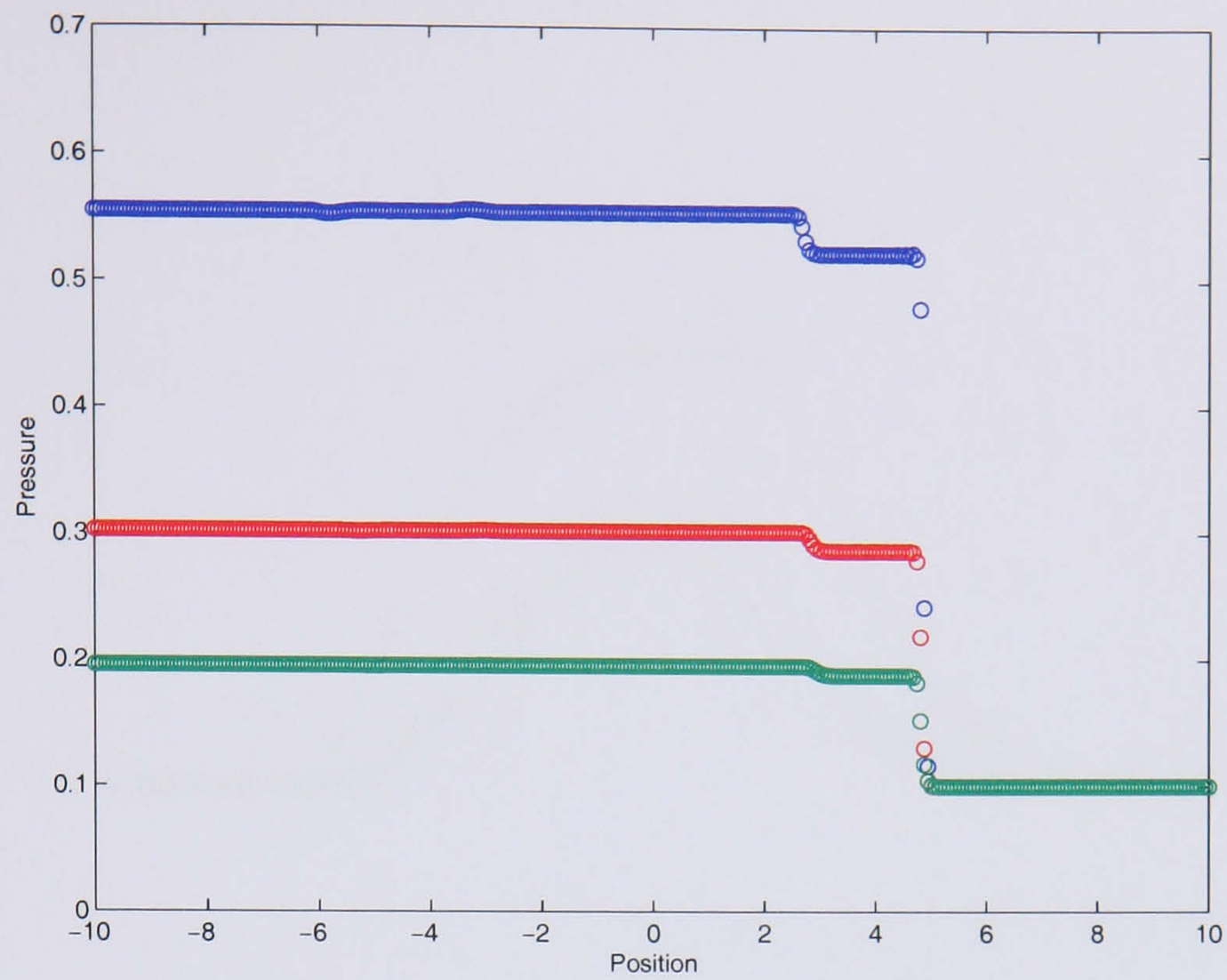

Figure 9.7: A closer look at the strong 2–shocks propagating to the right obtained by SLIC scheme at $t = 3$.

$\mathbb{S}(\mathbb{W})$, $\mathbb{S}(\mathbb{W}) = (0, 0, 0, 0, 0, 0)$, $\mathbb{S}(\mathbb{W}) = (0, \phi, 0, 0, \pi, 0)$ and $\mathbb{S}(\mathbb{W}) = (0, \phi, 0, 0, 0, 0)$. Figure 9.9 shows that the effect of the source terms on the pressure wave propagation is significant.

9.3.6 Test 6: Mixture Two–Phase Shock–Tube Problem

We consider a shock tube filled with a air–water mixture under a high pressure in the left section and under a lower pressure in the right section. This test consists of a Riemann problem for the hyperbolic conservative two–fluid model without a source term and with the left and right states defined as $\mathcal{P}_{\mathcal{L}} = 0.1, \mathcal{P}_{\mathcal{R}} = 0.01$, $\alpha_{\mathcal{L}} = 0.4, \alpha_{\mathcal{R}} = 0.6$, $u_{\mathcal{L}} = u_{\mathcal{R}} = 0$, $u_{r\mathcal{L}} = u_{r\mathcal{R}} = 0$, $c_{\mathcal{L}} = 0.0004$, $c_{\mathcal{R}} = 0.0006$, $\mathcal{S}_{\mathcal{L}} = \mathcal{S}_{\mathcal{R}} = 0$. A mesh with 100 cells is used to show the solution numerically. The corresponding results are shown in figure 9.10 at time $t = 3$. Bearing in mind the reference solution obtained with a very fine mesh using the SLIC scheme, we compared the numerical results for SLIC and Lax–Friedrichs schemes with the reference solution at time $t = 3$. As expected, the SLIC scheme gives a much sharper result of discontinuities compared

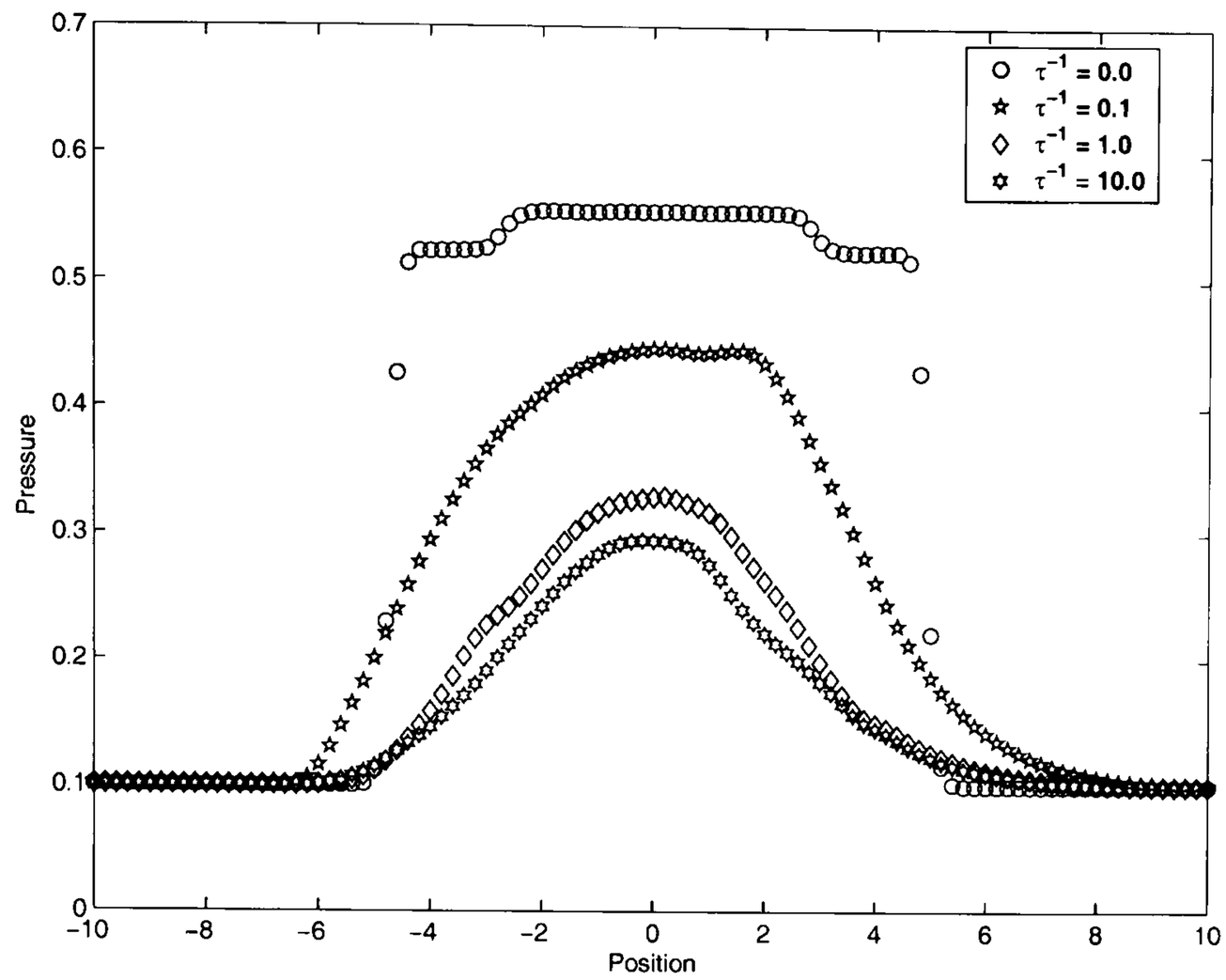

Figure 9.8: Effect of the relaxation of volume concentration τ on the Pressure.

to the Lax–Friedrichs method.

9.3.7 Test 7: Four–Rarefactions Test Problem

This test problem consists of a symmetric Riemann problem for the hyperbolic conservative two–fluid model with the left and right states given as $\mathcal{P}_{\mathcal{L}} = 0.5 = \mathcal{P}_{\mathcal{R}}$, $\alpha_{\mathcal{L}} = 0.4, \alpha_{\mathcal{R}} = 0.4$, $u_{\mathcal{L}} = -0.1$, $u_{\mathcal{R}} = 0.1$, $u_{r\mathcal{L}} = u_{r\mathcal{R}} = 0$, $c_{\mathcal{L}} = 0.0004$, $c_{\mathcal{R}} = 0.0004$, $\mathcal{S}_{\mathcal{L}} = \mathcal{S}_{\mathcal{R}} = 0$. As mentioned before our reference solution is the SLIC scheme with a very fine mesh. The numerical solution of the symmetric Riemann problem consists of four symmetric rarefaction waves and a trivial contact discontinuity at $x = x_0 = 0$. Figure 9.11 shows a comparison between the SLIC and Lax–Friedrichs methods. The dip in mixture density and concentration produced in the vicinity of the trivial contact discontinuity is due to spurious mixture density perturbations which are characteristic of typical anomalies of hyperbolic systems [180] . We do not know or have analytical results for this problem but numerical computations consistently show erroneous solutions for this case. An important conclusion that is valid for this test problem, anticipated from the numerical solution, is that anomalies in the

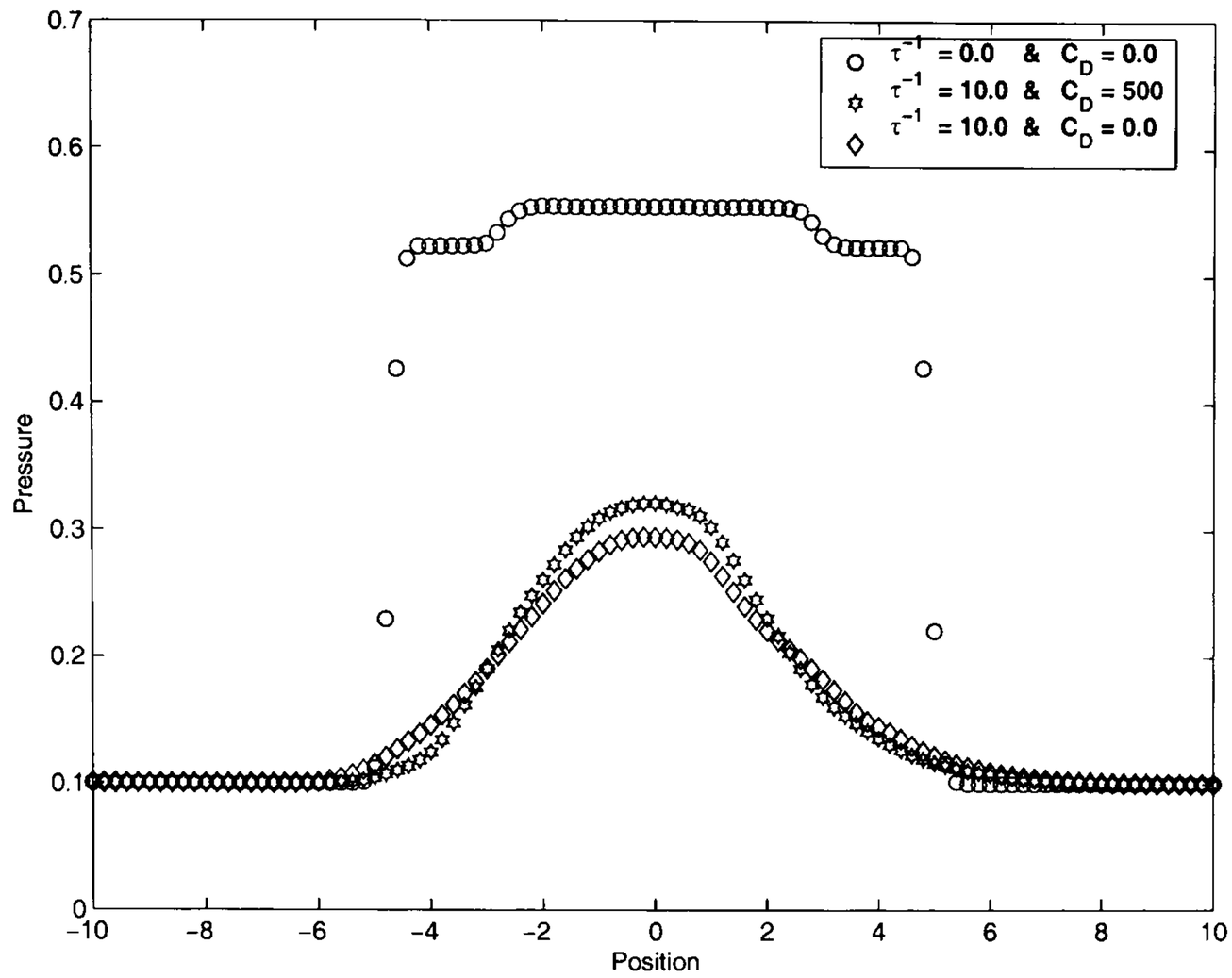

Figure 9.9: A closer look at the effect of source terms with relaxation time τ and interfacial friction on the structure of the solution of the Riemann problem (pressure).

conservative methods deployed here, take the form of a mixture density perturbation in the vicinity of trivial contact discontinuities. Anomalies reported here do affect other hyperbolic systems such as Euler equations, artificial compressibility equations associated with steady incompressible Navier–Stokes equations and equations of Magnetohydrodynamics [180].

9.4 Conclusions

In this study, a TVD slope limiter centred scheme SLIC for wave propagation in compressible two–phase flow model which describes a mixture of air and water was developed. The model is given by a non–linear hyperbolic system that cannot easily be solved by upwind schemes. Since the model possesses a large number of acoustic waves it is not easy to upwind all these waves accurately and simply. The concept of TVD centred schemes totally avoids the details of the Riemann problem solution. The method developed in this chapter can be seen as a formalization of the SLIC scheme suggested by Toro [178] for hyperbolic conservation laws. The centred schemes

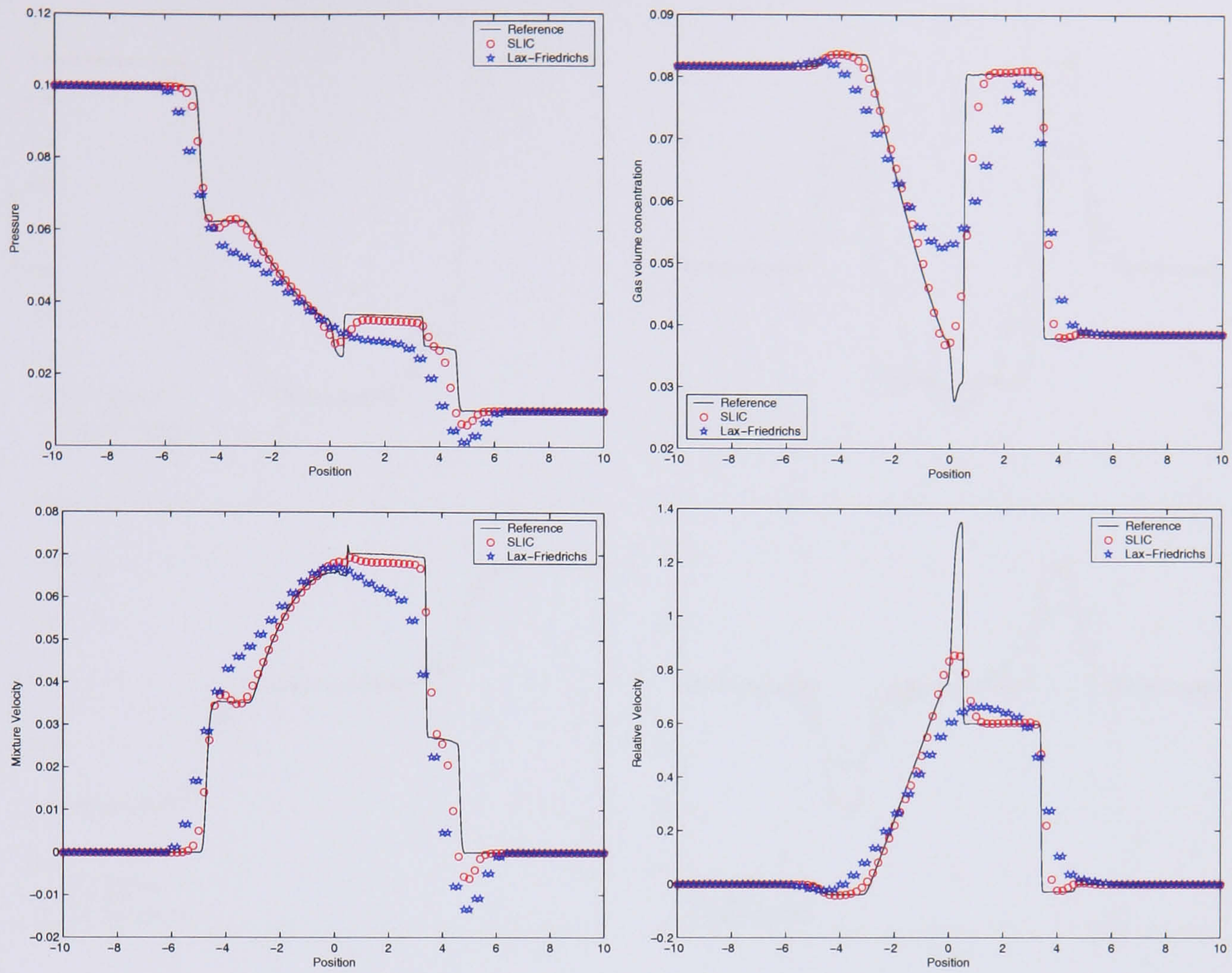

Figure 9.10: Solution of the Riemann problem for the air–water mixture shock tube. SLIC and Lax–Friedrichs methods (symbols) compared with the reference solution (line) at 1000 cells.

represent a competitive alternative to the existing upwind schemes for simulating gas–liquid flow. The developed scheme has been applied to the calculation of a one–dimensional mixture of air and water two–phase flow to study the Riemann problem numerically. The high–resolution property of the scheme was tested in standard two–phase flow problems. In particular, it was demonstrated that the SLIC scheme gives very accurate numerical solutions of the wave propagation as demonstrated through the test problems presented in this chapter. This is an essential property in order to obtain accurate simulation of gas–liquid flow. In these test problems the source terms have a strong influence on the equations and therefore these problems provide excellent references to test the stated theory. They have been useful in showing the performance of the SLIC scheme under extreme conditions which would ensure

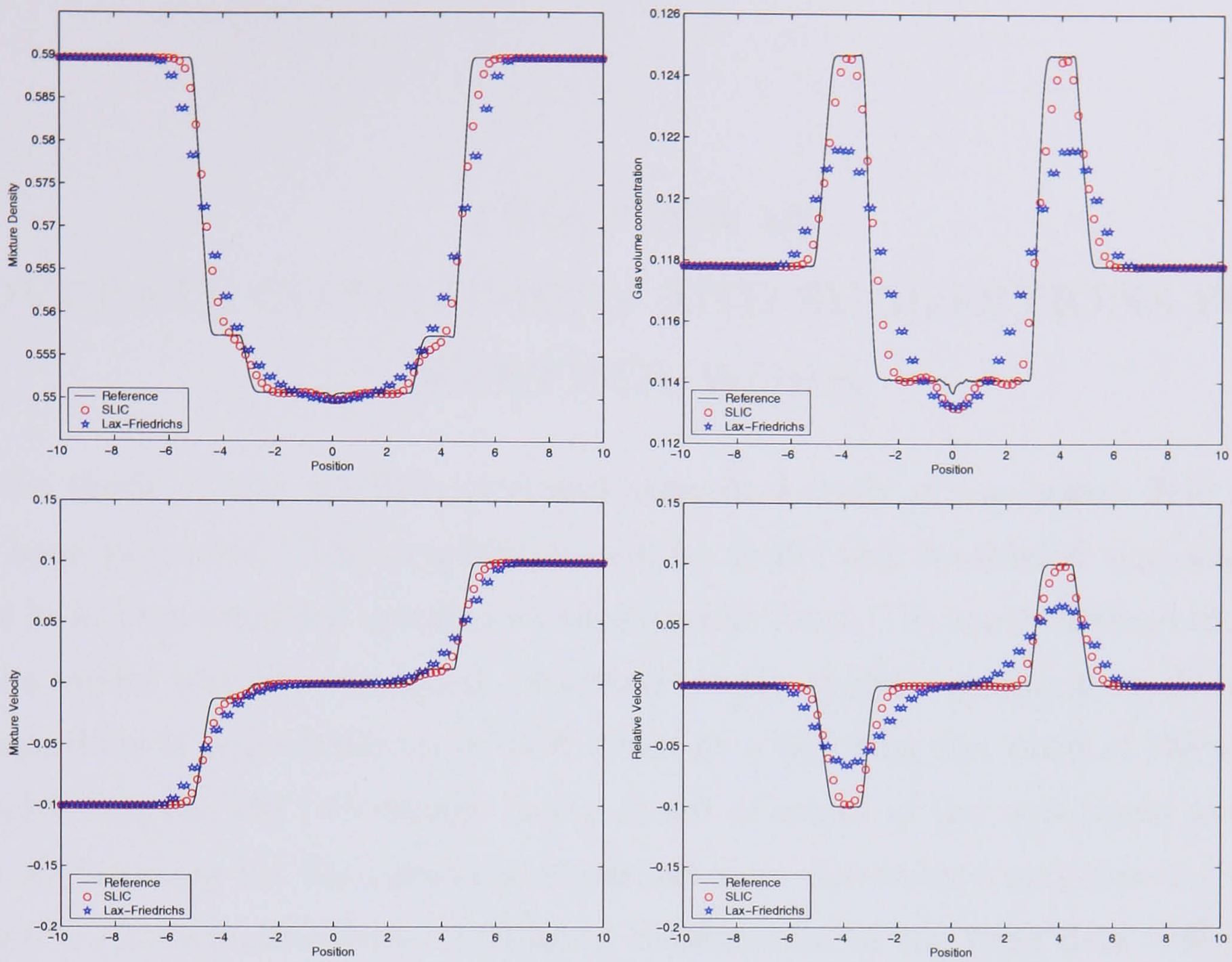

Figure 9.11: Solution of the Riemann problem for the four rarefaction waves. SLIC and Lax–Friedrichs methods (symbols) compared with the reference solution (line) at 1000 cells.

high–quality results under more ordinary circumstances. Numerical results show that the derived SLIC scheme is robust with the ability to capture solutions accurately. Additionally the interest of this chapter has been on the development of high–order numerical schemes with a capacity to recognize anomalies of conservative methods for inhomogeneous hyperbolic conservation laws arising in two–phase flow models. This numerical study seems very promising for the numerical solution of two–phase flows as shown by the numerical results for standard two–phase flow problems. As a conclusion, the SLIC scheme turns out to be a very promising scheme for more complex models like the hyperbolic conservative two–fluid model studied in this thesis.

CHAPTER 10

OVERALL CONCLUSIONS AND SUGGESTIONS FOR FURTHER WORK

In this thesis, a new mathematical and numerical study of two–phase flow models has been presented. The simplified two–fluid model was considered first which results in a three–equation system in a conservative form. The mathematical character of the model was also examined. A characteristic analysis reveals that the system of equations is hyperbolic up to first order in η (η being the ratio of the relative velocity between the two–phases to the speed of sound of the two–phase mixture). The eigenvectors for the system of equations were determined and this description recast in characteristic form. Following classification of the wave field a discontinuous solution of the model was determined, the corresponding Riemann invariants were derived and simple wave solutions were constructed. Additionally, an efficient solver for computing the exact solution of the Riemann problem was derived [207]. The mixture density $\rho^\star$ between the acoustic waves was found by solving a single, non–linear algebraic equation [206].

Having established this mathematical foundation for the simplified two–fluid model, approximate Riemann solvers were derived for the model. The HLLC Riemann solver derived is accurate and robust in comparison with other approximate Riemann solvers such as Roe's solver which would require an entropy fix. These solvers have been used locally in second–order TVD methods to compute the global solution to the general initial–boundary value problem for the simplified two–fluid model. The methods have the ability to capture discontinuities in conservative form with high–resolution and without the spurious oscillations of traditional higher–order finite difference methods. This was illustrated by the numerical results presented. The results suggest that the model has applications for the two–phase flow cases where the solution would exhibit high gradients and non–linear effects. The comparison between the centred schemes

and the upwind schemes was done in terms of accuracy and efficiency. The upwind methods produce more accurate results than the centred methods, but overall numerical results by centred schemes are satisfactory and can reflect the basic physical phenomena inherent to two–phase flow equations. In terms of simplicity and efficiency, the centred schemes have a better performance than the upwind schemes [205].

The next model considered in this thesis is the hyperbolic conservative two–fluid model. Based on extended thermodynamics the governing equations for a two–phase mixture description used to model fully compressible non–equilibrium two–phase flows were formulated. The field equations form a symmetric hyperbolic system of balance equations in a conservative form. In addition to the usual conservation equations of mixture mass, mixture momentum and mixture energy, the balance equations of volume concentration and relative velocity are important consisting parts of the description of the two–phase flow mixture. The mathematical character of the one–dimensional governing equations was investigated and the mathematical analysis showed that the model is hyperbolic with six real eigenvalues. Through analysis of the eigenstructure, it was found that two of the eigenvalues are equal to the mixture velocity whereas the other eigenvalues correspond to the acoustic wave propagation for the mixture. Via a detailed analysis, the derived eigenvectors and the characteristic fields corresponding to the acoustic waves were shown to be genuinely non–linear while the last two are linearly degenerate. In addition to the mathematical analysis of the hyperbolic conservative two–fluid model we investigated sound wave propagation. It is shown that for the case of single pressure approximation the dependence of the speed of sound on the void fraction is monotonic [147]. From the analysis of the discontinuities of the model, an investigation of shock waves of small amplitude where there is no relative motion ahead of the shock and where the medium is not a pure phase was conducted. Thus a well–posed two–fluid model together with a set of closure relations is proposed which satisfies the corresponding entropy conditions and takes account of the interfacial non–equilibrium effects due to the velocity between the phases. Moreover, this model allows the application of relatively modern shock–capturing methods of centred types such as the TVD SLIC scheme. The centred schemes represent a competitive alternative to the existing upwind schemes for

simulating gas–liquid flow. The developed scheme has been applied to the calculation of one–dimensional mixture of air and water two–phase flow to study the Riemann problem numerically [208]. The calculations reveal good agreement with the reference solution. At the same time, we demonstrated the importance of proper treatment of source terms in the field equations. The high–resolution property of the scheme was tested in standard two–phase flow problems. Numerical results show that the derived SLIC scheme is robust with the ability to capture solutions accurately [209]. The great attraction of the SLIC scheme is its simplicity and efficiency, especially for the hyperbolic conservative two–fluid model which is too complicated to be solved by upwind–based schemes.

Currently used two–phase flow models of the non–conservative two–fluid model type are of importance to industrial applications. The mathematical properties of these models are still poorly developed. They are complicated and even often ill–posed which emphasises the need to develop new models and to provide a variety of numerical schemes to investigate their properties.

Overall, in this thesis, we have observed that through a deeper understanding of numerical schemes of conservation laws, one can develop models and schemes which reveal an improved performance in dealing with realistic two–phase flow problems.

For the simplified two–fluid model, our results clearly illustrated that the upwind and centred schemes seemed most promising. Some further work would therefore be to generalize these numerical schemes for complete non–conservative two–fluid models. However, this task is quite complex and requires a good understanding of the intricate mathematical concepts involved in the two–phase flow models.

For the hyperbolic conservative two–fluid model one area of further investigation would be to derive the analytical solution of the governing differential equations which will be composed of simple waves, discontinuous waves (shocks and contacts) and centred waves. This analysis would provide the possibility to construct the analytical solution of the Riemann Problem. This will lead to a better understanding of the physical meaning of the model [206, 207]. Another area of future work would be to generalize the numerical investigation of the hyperbolic conservative two fluid model using the exact Riemann solutions. Also, as the Godunov type method of

upwind–type such as the TVD WAF (Weighted Average Flux) scheme was successfully implemented for the simplified two–fluid model [205], a similar approach can be followed for the hyperbolic conservative two–fluid model using the same scheme in the exact and approximate Riemann solvers.

REFERENCES

[1] Abgrall R. How to Prevent Pressure Oscillations in Multicomponent Flow Calculations: A Quasi Conservative Approach. *J. Comp. Phys.* 1996; **125**: 150–160.

[2] Acheson D. *Elementary Fluid Dynamics.* Oxford University Press, 1990.

[3] Anderson T. and Jackson R. A Fluid Mechanical Description of Fluidized Beds. *I & E. C. Fund.* 1967; **6**: 527–539.

[4] Anderson J. *Computational Fluid Dynamics.* The Basics with Applications. McGraw–Hill, Inc., 1995.

[5] Baer M. and Nunziato J. A Two–Phase Mixture Theory for the Deflagration–to–Detonation Transition (DDT) in Reactive Granular Materials. *Int. J. Multiphase Flow.* 1986; **12**, 861–889.

[6] Barre F. The CATHARE Code Strategy and Assessment. *Nucl. Eng. Design.* 1990; **124**: 257–284.

[7] Bdzil J., Menikoff R., Son S., Kapila A. and Stewart D. Two–Phase Modeling of Deflagration–To–Detonation Transition in Granular Materials: a Critical Examination of Modeling Issues. *Physics of Fluids* 1999; **11**: 378–402.

[8] Ben–Artzi M. and Falcovitz J. A Second–Order Godunov–Type Scheme for Compressible Fluid Dynamics. *J. Comp. Phys.* 1984; **55**: 1–31.

[9] Bendiksen k., Malnes D., Moe R. and Nuland S. The Dynamic Two–Fluid Model OLGA: Theory and Application. *SPE Production Engineering.* May 1991; **6**: 171–180.

[10] Bergles A., Collier J., Delhaye J., Hewitt G. and Mayinger F. *Two–Phase Flow and Heat Transfer in the Power and Process Industries.* McGraw–Hill. New–York, 1981.

[11] Bouré J., Reocreux M., Flamannd J. and Schipfer P. *Critical Flow Rates in Water–Vapor Diphasic Flow.* Atomic Energy Commission/Center For Nuclear Studies of Grenoble Service of Thermal Transfer. TT No. 106, 1971.

[12] Bouré J. and Delhaye J. *General Equations and Two–Phase Flow Modeling.* In *Handbook of Multiphase Systems.* G. Hetsroni. Hemipshere, 1982.

[13] Bowen R. Toward a Thermodynamics and Mechanics of Mixtures. *Arch. Rational Mech. Anal.* 1967; **24**: 370–403.

[14] Black P., Daniels L., Hoyle N. and Jepson W. Studying Transit Multiphase Flow Using the Pipline Analysis Code (PLAC). *J. Energy Resources Technology.* 1990; **112**: 25–29.

[15] Campbell I. and Pitcher A. Shock Waves in a Liquid Containing gas bubbles. *Proc. Roy. Soc. London Ser.* 1958; A243: 534–545.

[16] Chang T. and Hsiao L. *The Riemann Problem and Interaction of Waves in Gas Dynamics.* Harlow, 1989.

[17] Chorin A. J. and Marsden J. E. *A Mathematical Introduction to Fluid Mechanics.* Springer Verlag, 1993.

[18] Chorlton F. *Textbook of Fluid Dynamics.* CBS Publishers & Distributors. India, 1985.

[19] Cassaude B., Fabre J., Jean C., Ozon P. and Théron. Unsteady Phenomena in Horizontal Gas–Liquid Slug Flow. In *Proc. 4th Int. Conf. Multi–Phase Flow.* June 1989; 469–484. Nice, France.

[20] Colella P. and Woodward P. The Piecewise Parabolic Method (PPM) for Gas Dynamical Simulation. *J. Comp. Phys.* 1984; **54**: 174–201.

[21] Collier J. *Convective Boiling and Condensation.* McGraw–Hill, 2nd Ed. New York, 1981.

[22] Colombeau J. and Le Roux A. In Non–Linear Hyperbolic Problems. *Lecture Notes in Mathematic.* Vol. 1270, Springer–Verlag. New York/Berlin, 1987.

[23] Cocchi J. and Saurel R. A Riemann Problem Based Method for Compressible Multifluid Flows. *J. Comp. Phys.* 1997; **137**: 265–298.

[24] Coleman B and Noll W. The Thermomechanics of Elastic Materials with Heat Conduction and Viscosity. *Arch. Rational Mech. Anal.* 1963; **13**: 265–298.

[25] Coquel F., El Amine k., Godlewski E., Perthame B. and Rascle P. A Numerical Method Using Upwind for the Resolution of Two–Phase Flows. *J. Comp. Phys.* 1997; **136**: 272–288.

[26] Courant R., Isaacson E. and Rees M. On the Solution Nonlinear Hyperbolic Differential Equations by Finite Differences. *Comm. Pure. Appl. Math.* 1952; **5**: 243–255.

[27] Courant R., Friedrichs K. *Supersonic Flow and Shock Waves.* Springer–Verlag, 1985.

[28] Craine R. Oscillations of a Plate in a Binary Mixture of Incompressible Newtonian Fluids. *Int. J. Engng. Sci.* 1971; **9**: 1177–1192.

[29] Dafermos C. *Hyperbolic Conservation Laws in Continuum Physics.* Springer, 2000.

[30] Delhaye J. General Equations of Two–Phase Systems and Their Applications to Air–Water Bubble Flow and to Steam–Water Flashing Flow. *ASME Preprint.* 69–HT–63. 1969.

[31] Dimenna R. *RELAP5/MOD2 Models and Correlations.* NUREG/CR–5194. EGG–2531, 1988.

[32] Dorovsky V. Coninual Theory of Filtration. *Sov. Geology and Geophysics.* 1989; **30**(7): 39–45.

[33] Dorovsky V. and Perepechko Y. Phenomenological Description of Two–Velocity Media with Relaxing Shear Stresses. *J. Appl. Mech. and Tech. Phys.* 1992; **33**(3): 403–409.

[34] Dorovsky V., Perepechko Y. and Romensky E. Godunov's Scheme for the Analysis of the Nonlinear Wave Process in the Two–Velocity Media with Elastic Interaction. In *FED* Vol. 196, *Advanced in Computational Methods in Fluid Dynamics, ASME.* 1994; 355–366.

[35] Drew D. and Segel A. Averaged Equations for Two–Phase Flows. *Stud. Appl. Math.* 1971; **1**: 205–231.

[36] Drew D. The Analysis of Virtual Mass Effects in Two–Phase Flow. *Int. J. Multiphase Flow.* 1979; **5**: 233–258.

[37] Drew D. and Lahey R. Application of General Constitutive Principles to the Derivation of Multidimensional Two–Phase Flow Equations. *Int. J. Multiphase Flow.* 1979; **5**: 243–264.

[38] Drew D. and Passman S. *Theory of Multicomponent Fluids.* Springer–Verlag. New York, 1999.

[39] Dugdale J. S. *Entropy and Its Physical Meaning.* Taylor & Francis, September 1996.

[40] Dunwoody N. and Müller I. A Thermodynamic Theory of Two Chemically Reacting Ideal Gases with Different Temperatures. *Arch. Rational Mech. Anal.* 1968; **29**: 344–369.

[41] Ekrann S. and Rommetveit R. A Simulator for Gas Kicks in Oil–Based Drilling Muds. Paper SPE 14182 Presented at the *1985 SPE Annual Technical Conference and Exhibition* Held in Las Vegas, Sept. 22–25.

[42] Embid P. and Baer M. Mathematical Analysis of a Two–Phase Continuum Mixture Theory. *Continuum Mechanics and Thermodynamics.* 1992; **4**: 279–312.

[43] Engquist B. and Gustafsson B. Proc. Third International Conference on Hyperbolic Problems. Vol. I and II. Chartwell–Bratt, 1991.

[44] Eringen A. and Ingram J. A Continuum Theory of Chemically Reacting Media–I. *Int. J. Eng. Sci.* 1965; **3**: 197–212.

[45] Falcovitz J. and Ben–Artzi M. Recent Development of the GRP method. *JSME Int. J. B–Fluids Therm. Eng.* 1995; **38**(4): 497–517.

[46] Faille I. and Heintzé E. A Rough Finite Volume Scheme for Modeling Two–Phase Flow in a Pipeline. *Computers & Fluids* 1999; **28**: 213–241.

[47] Fermi E. *Thermodynamics.* Dover. New York.1956.

[48] Fitt A. The Character of Two–Phase Gas/Particulate Flow Equations. *Appl. Math. Modelling.* 1993; **17**: 338–354.

[49] Fjelde K. and Karlsen K. High–resolution hybrid primitive–conservative upwind schemes for the drift flux model. In *Elsevier Science Ltd.*, Vol. 31/3, pp. 335-367. Elsevier Science Limited, The Boulevard , Langford Lane, Oxford OX5 1GB, U.K 2001

[50] Fox R. and McDonald A. *Introduction to Fluid Mechanics.* John Wiley & Sons, Inc., 1998.

[51] Franca F. and Lahey R. The Use of Drift–Flux Techniques for the Analysis of Horizontal 2–Phase Flows. *Int. J. Multiphase Flow.* 1992; **18**(6): 787–801.

[52] Friedrichs K. Symmetric Positive Linear Differential Equations. *Comm. Pure Appl. Math.* 1958; **11**: 333–418.

[53] Garabedian P. *Partial Differential Equations.* Wiley. New York, 1964

[54] Gascón L. and Corberán M. Construction of Second–Order TVD Schemes for Nonhomogeneous Hyperbolic Conservation Laws. *J. Comp. Phys.* 2001; **172**: 261–297.

[55] Gavage S. *Analyse numérique des modèles hydrodynamiques d'écoulements diphasiques instationnaires dans Les réseaux de production pétrolière.* Thèse, ENS Lyon France, 1991.

[56] Gavrilyuk S. and Saurel R. Mathematical and Numerical Modeling of Two–Phase Compressible Flows with Micro–Inertia. *J. Comp. Phys.* 2002; **175**: 326–360.

[57] Glimm J., Graham M., Grove J. and Plohr B. *Proc. Fifth International Conference on Hyperbolic Problems.* World Scientific, 1996

[58] Godlewski E. and Raviart P. *Numerical Approximation of Hyperbolic Systems of Conservation Laws.* Applied Mathematical Sciences, Vol. 118, Springer–Verlag, New York, 1996.

[59] Godunov G. Finite Difference Methods for the Computation of Discontinuous Solutions of the Equations of Fluid Dynamics. *Mat. Sb.* 1959; **47**: 271–306.

[60] Godunov S. and Romensky E. Thermodynamics, Conservation Laws and Symmetric Forms of Differential Equations in Mechanics of Continuous Media. In *Comput. Fluid Dynamic Review.* PP.19–31. New York. John Wiley & Sons., 1995

[61] Gokhale S. and Krier H. Modeling of Unsteady Two–Phase Reactive Flow in Porous Beds of Propellant. *Prog. Energy. Combust. Sci.* 1982; **8**: 1–39.

[62] Gouin H. and Gavrilyuk S. Hamilton's Principle and Rankine–Hugoniot Conditions for General Motions of Mixtures. *Meccanica.* 1999; **34**: 39–47.

[63] Goursat E. *Cours d'Analyse Mathématique, Tome II.* Gauthiers Villars. Paris, 1933.

[64] Green A. and Naghdi P. A Dynamical Theory of Interacting Continua. *Int. J. Eng. Sci.* 1965; **3**: 231–241.

[65] Green A. and Naghdi P. A Theory of Mixtures.*Arch. Rational Mech. Anal.* 1967; **24**: 243–263.

[66] Green A. and Naghdi P. On Basic Equations for Mixtures. *Quart. J. Mech. and Applied Math.* 1969; **22**: 427–438.

[67] Green A. and Naghdi P. Entropy Inqualities for Mixtures. *Quart. J. Mech. and Applied Math.* 1971; **24**: 473–485.

[68] Harlow F. and Amsden A. *Fluid Dynamics.* Monograph LA–4700, Los Alamos National Laboratory, Los Alamos, NM, 1971.

[69] Harlow F. and Amsden A. A Numerical Fluid Dynamics Calculation Method for All Flow Speeds. *J. Comp. Phys.* 1971; **8**: 197–213.

[70] Harlow F. and Amsden A. Numerical Calculation of Multiphase Fluid Flow. *J. Comp. Phys.* 1975; **17**: 19–52.

[71] Harten A., Lax P. and van Leer B. On Upstream Differencing and Godunov–Type Schemes for Hyperbolic Conservation Laws. *SIAM Review.* 1983; **25**(1): 35–61.

[72] Harten A. High Resolution Schemes for Hyperbolic Conservation Laws. *J. Comp. Phys.* 1983; **49**: 357–393.

[73] Heibig A. and Serre D. Etude Variationnelle du Problème de Riemann. *J. Diff. Eqs.* 1992; **96**: 56–88.

[74] Henriot V., Pauchon C., Duchet–Suachaux P. and Leibovici C. TACITE: Contribution of Fluid Composition Tracking on Transient Multiphase Flow Simulation. Paper OTC 8563 Presented at *the 1997 Offshore Technology Conference.* Houston, Texas, 5–6 May.

[75] Hörmander L. *Lectures on Nonlinear Hyperbolic Differential Equations, Mathématiques et Applications 26*, Springer–Verlag, 1997.

[76] Hoffmann K. *Computational Fluid Dynamics for Engineers.* Engineering Education Systems. Austin, Texas, USA, 1989

[77] Hoffman Joe D. *Numerical Methods for Engineers and Scientists.* Marcel Dekker; 2nd edition, September 2001.

[78] Holden H. and Risebro N. H. *Front Tracking for Hyperbolic Conservation Laws.* Applied Mathematical Sciences, volume 152, Springer Verlag, New York, 2002.

[79] Hou T. and LeFloch P. Why Non–Conservative Schemes Converge to the Wrong Solutions: Error Analysis. *Math of Comput.* 1994; **62**: 497–530.

[80] Hirsh C. *Numerical Computation of Internal and External Flows.* Vol. I: *Computational Methods For Inviscid and Viscous Flows.* Wiley, 1988.

[81] Hirsh C. *Numerical Computation of Internal and External Flows.* Vol. II: *Computational Methods For Inviscid and Viscous Flows.* Wiley, 1990.

[82] Hsu Y. and Graham H., *Transport Processes in Two–Phase Boiling Systems.* Hemisphere. New York, 1977.

[83] Ingram J. and Eringen A. A Continuum Theory of Chemically Reacting Media–II. *Int. J. Eng. Sci.* 1967; **5**: 289–322.

[84] Ishii M. *Thermo–Fluid Dynamic Theory of Two–Phase Flow.* Eyrolles. Paris. 1975.

[85] Ishii M. One–Dimensional Drift-Flux Model and Constitutive Equations for Relative Motion Between Phases in Various Two–Phase Flow Regimes. Argonne National Report, ANL 77–47, October 1977.

[86] John F. *Partial Differential Equations*, Springer–Verlag, 1982.

[87] Jiang G. and Tadmor E. Nonoscillatory Central Schemes for Multidimensional Hyperbolic Conservation Laws. *SIAM J. Sci. Comput.* 1998; **19**(6), 1892–1917.

[88] Jiang G., Levy D., Lin C. Osher S. and Tadmor E. High–resolution Nonoscillatory Central Schemes with Nonstaggered Grids for Hyperbolic Conservation Laws. *SIAM J. Num. Anal.* 1998; **35**(6), 2147–2168.

[89] Kalinin A. Derivation of Fluid–Mechanics Equations for a Two–Phase Medium with Phase Changes. *Heat Transfer–Soviet Research.* 1970; **2**: 83–96.

[90] Kelly P. A Reacting Continuum. *Int. J. Eng. Sci.* 1964; **2**: 129–153.

[91] Kröner D. *Numerical Schemes for Conservation Laws.* Wiely Teubner, 1997.

[92] Kumbaro A. and Caremoli C. Modelisation, Analyse Mathematique Et Numerique Des Modeles Bi–Fluides D'Ecoulement Diphasique. Thèse, EDF Clamart France, 1994.

[93] Lahey R, Cheng L, Drew D, Flaherty E. The Effect of Virtual Mass on the Numerical Stability of Accelerating Two–Phase Flows. *Int. J. Multiphase flow.* 1980; **6**: 281–294.

[94] Landau L. and Lifshitz E. *Fluid Mechanics.* Pergamon Press, 1982.

[95] Larsen M., Hustvedt E., Hedne P. and Straume T. PeTra: A Novel Computer Code for Simulation of Slug Flow. Paper SPE 38841 Presented at *the 1997 SPE Annual Technical Conference and Exhibition Held in San Antonio, Texas, 5–8 Oct. 1997.*

[96] Lax P. Weak Solutions of Nonlinear Hyperbolic Equations and Their Numerical Computation. *Comm. Pure Appl. Math.* 1954; VII: 159–193.

[97] Lax P. and Wendroff B. Systems of Conservation Laws. *Comm. Pure Appl. Math.* 1960; **13**: 217–237.

[98] LeFloch P. Entropy Weak Solutions to Nonlinear Hyperbolic Systems Under Nonconservative Form. *Commun. Part. Diff. Equa.* 1988; **13**(6): 669–727.

[99] LeVeque R. *Numerical Methods for Conservation Laws.* Birkhäuser Verlag Basel, 2nd Ed., 1992.

[100] LeVeque R. *Finite Volume Methods for Hyperbolic Problems.* Cambridge University Press, August 2002.

[101] Liles D. and Reed W. A Semi–Implicit Method for Two–Phase Fluid Dynamics. *J. Comp. Phys.* 1978; **26**: 77–102 1978.

[102] Lindquist W. *Current Progress in Hyperbolic Systems: Riemann Problems and Computations.* American Mathematical Society, 1989.

[103] Liu X. and Tadmor E. Third order Nonoscillatory Central Scheme for Hyperbolic Conservation Laws. *Numeriche Mathematik.* 1998; **79**(3): 397–425.

[104] Mader C. *Numerical Modeling of Detonations.* University of California Press Ltd. London, England, 1979.

[105] Maron M. and Lopez R. *Numerical Analysis.* Wadsworth, 1991.

[106] Masella J., Faille I. and Gallouet T. On Approximate Godunov Scheme. *Int. J. Computational Fluid Dynamics.* 1999; *12*(2): 133–149.

[107] Mecredy R. and Hamilton L. The Effects of Nonequilibrium Heat, Mass and Momentum Transfer on Two–Phase Sound Speed. Int. J. Heat Mass Trans. 1972; **15**: 61–72.

[108] Menikoff R, Plohr B. The Riemann Problem for Fluid Flow of Real Materials. *Rev. of Mod. Phys.* 1989; **61**: 75–130.

[109] Minami K. *Transient Flow and Pigging Dynamics in Two–Phase Piplines.* Ph.D. Dissertation, University of Tulsa. 1991.

[110] Minami K. and Shoham O. Transient Two–Phase Flow Behaviour in Piplines–Experiment and Modeling. *Int. J. Multiphase Flow.* 1994; **20**(4): 739–752.

[111] Moretti G. and Bleich G. A Time–Dependent Computational Method for Blunt–Body Flows. *AIAA J.* 1966; **4**: 2136–2141.

[112] Moretti G. The λ–Scheme. *Computers and Fluids.* 1979; **7**: 191–205.

[113] Müller I. On the Entropy Inequality. *Arch. Rational Mech. Anal.* 1967; **26**: 118–141.

[114] Müller I. A Thermodynamic Theory of Mixtures of Fluids. *Arch. Rational Mech. Anal.* 1968; **28**: 1–39.

[115] Müller I. A New Systematic Approach to Non–Equilibrium Thermodynamics. *Pure and Applied Chemistry.* 1970; **22**.

[116] Müller I. and Ruggeri T. *Rational Extended Thermodynamics.* Springer–Verlag. New York, 1998.

[117] Murray J. On the Mathematics of Fluidization. Part 1, Fundamental Equations and Wave Propagation. *J. Fluid Mech.* 1965; **21**: 465–493.

[118] Nessyahu H. and Tadmor E. Non–Oscillatory Central Differencing for Hyperbolic Conservation–Laws. *J. Comp. Phys.* 1990; **87**(2): 408–463.

[119] Nickens H. A Dynamic Computer Model of a Kicking Well. Paper SPE 14183 First Presented at *the 1985 SPE Annual Technical Conference and Exhibition* Held in Las Vegas. Sept. 22–25.

[120] Nigmatulin R. *Dynamics of Multiphase Media.* Hemisphere. New York, 1991.

[121] Okazava N. and Unai A. Abstract Quasilinear Evolution Equations in a Hilbert Space with Applications to Symmetric Hyperbolic Systems. *SUT J. Math* 1993; **29**(N2): 263–240.

[122] Oran E. and Boris J. *Numerical Simulation of Reactive Flow.* Elsevier. New York, 1987.

[123] Osher S. and Solomon F. Upwind Difference Scheme for Hyperbolic Systems of Conservation Laws. *Math. Comp.* 1982; **38**: 339–374.

[124] Panton R. Flow Properties for the Continuum Viewpoint of a Nonequilibrium Gas–particle Mixture. *J. Fluid Mech.* 1968; **31**: 273–303.

[125] Patankar S. *Numerical Heat Transfer and Fluid Flow.* Hemisphere, 1975.

[126] Pauchon C., Dhulesia H., Binh–Cirlot G. and Fabre J. TACITE: A Transient Tool for Multiphase Pipline and Well Simulation. Paper SPE 28545 Presented at *the 1994 SPE Annual and Technical Conference and Exhibition.* New Orleans, LA Sept. 25–28.

[127] Pauchon C., Dhulesia H., Lopez D. and Fabre J. TACITE: A Comprehensive Mechanistic Model for Two–Phase Flow. In *Proceedings of the 6th International Conference on Multiphase Production.* Cannes, France, June 1993.

[128] Petrovskii I. *Partial Differential Equations.* Philadephia: W. B. Saunders Co., 1967.

[129] Pokharna H. Mori M. and Ransom V. Regularization of Two–Phase Flow Models: A Comparison of Numerical and Differential Approaches. *J. Comp. Phys.* 1997; **134**: 282–295.

[130] Prigogine I. *Introduction to Thermodynamics of Irreversible Processes.* Charles C Thomas, Publishers, 1961.

[131] Progress and challenges in CFD methods and algorithms, *Proc. AGARD* conference, Seville, Spain, 2–5 October 1995. AGARD–CP–578.

[132] Prosperetti A. and Satrape J. Stability of Two–Phase Flow Models. In D.D. Joseph and D.G. Schaeffer, (eds.) *Two–Phase Flows and Waves.* pp. 98–117. Springer–Verlag, 1990.

[133] Ramshaw J. and Trapp J. Characteristics, Stability and Short–Wavelength Phenomena in Two–Phase Flow Equation Systems. *Nuclear Science and Engineering.* 1978; **66**: 93–118 1978.

[134] Ransom V. and Hicks D. Hyperbolic Two–Pressure Models for Two–Phase Flow. *J. Comp. Phys.* 1984; **53**, 124–151.

[135] Ransom V. *REALP5/MOD1 Code Manual Volume 1: Code Structure, System Models, and Numerical Method.* NUREG/CR–1826, U.S. Nuclear Regulatory Commission, 1982

[136] Ransom V. and Mousseau V. Convergence and Accuracy of the REAL5 Two–Phase Flow Model. *Proc. INT. Topl. Mtg. Advances in Mathematics, Computations and Reactor Physics.* American Nuclear Society. Pittsburgh, Pennsylvania, April 28–May 2, 1991.

[137] Romstedt P. A Split–Matrix Method for the Numerical Solution of Two–Phase Flow Equations. *Nucl. Sci. Eng.* 1990; **104** 1–25.

[138] Roe P. Approximate Riemann Solvers, Parameter Vectors and Difference Schemes. *J. Comp. Phys.* 1981;**43**: 357–372.

[139] Roe P. Characteristic–Based Schemes for the Euler Equations. *Ann. Rev. Fluid Mech.* 1986; **43**:337–365.

[140] Romate J. and Meiring W. Solving a Hyperbolic Two–Phase Flow Model With Flow–Dependent Slip Relation. In *Numerical Methods for Fluid Dynamics V*, K. Morton and M. Baines (eds.) Clarendon Press, Oxford, 1995; pp.557–564.

[141] Romate J. Approximate Riemann Solvers for a Hyperbolic Two–Phase Flow Model. In *Numerical Modeling in Continuum Mechanics.* M. Feistauer, R. Rannacher and K. Kozel (Eds.), Proc. 3rd Summer Conference, Prague, 8–11 September, 1997.

[142] Romate J. An approximate Riemann Solver for a Two–Phase Flow Model with Numerically Given Slip Relation. *Computers & fluids.* 1998; **27**: 445–477.

[143] Romensky E. Symmetric Form of the Equations of a Nonlinear Maxwell's Medium. *Siberian Adv. Math.* 1995; **5**: 113–150.

[144] Romensky E. Hyperbolic Systems of Thermodynamically Compatible Conservation Laws in Continuum Mechnics. *Mathl. Comput. Modelling.* 1998; **28**: 115–130.

[145] Romensky E. Thermodynamics and Hyperbolic Systems of Balance Laws in Continuum Mechanics. In *Godunov Methods:theory and applications*, E. F. Toro (ed.); pp. 745–761 Kluwer Academic/Plenum publishers, 2001.

[146] Romenskii Evgenii I. and Godunov Sergei K. *Elements of Continuum Mechanics and Conservation Laws* Kluwer Academic Publishers. 2003

[147] Romenski E., Zeidan D., Slaouti A. and Toro E. F. Hyperbolic Conservative Model for Compressible Two–Phase Flow. Submitted to Continuum Mechanics and Thermodynamics.

[148] Rosenhead L. *Laminar Boundary Layers.* Oxford University Press, 1963.

[149] Richtmyer R. and Morton K. *Difference Methods for Initial Value Problems.* Interscience–Wiley, New York, 1967.

[150] Rider W. Advanced numerical techniques for thermal–hydraulics. Presented *National Heat Transfer Conf.*, 1993.

[151] Riemann B. Under die Fortflanzung ebener Luftwellen von endlicher Schwingungsweite. *Gött. Abh. Math. Cl.* 1860; 8: 43–65.

[152] Ruan Y. *On Entropy Balance Analyses of Non–Equilibrium Two–Phase Flow Models for Thermal–Hydraulic Computer Simulation.* Herbert Utz Verlag Wissenschaft. Munchen, 1997.

[153] Sainsaulieu L. Finite Volume Approximation of Two–Phase Fluid Flows Based on an Approximate Roe–Type Riemann Solver. *J. Comp. Phys.* 1995; **121**: 1–28.

[154] Sainsaulieu L. *Thèse de doctorat. Ecole Polytechnique.* 1991.

[155] Saurel R, Abgrall R. A Multiphase Godunov Method for Compressible Multi–Fluid and Multiphase Flows. *J. Comput. Phys.* 1999; **150**: 425–467.

[156] Schlichting H. *Boundary Layer Theory.* McGraw Hill, Inc., 1960.

[157] Serrin J. Mathematical Principles of Classical Fluid Mechanics. In *Encyclopedia of Physics,* VIII/1. pp. 125–263. Springer–Verlag, 1959.

[158] Sever M. Estimate of the Time Rate of Entropy Dissipation for Systems of Conservation Laws. *J. Differential Equations.* 1996; **130**: 127–141.

[159] Smoller J. *Shock Waves and Reaction–Diffusion Equations.* Springer–Verlag, 1994.

[160] Smith G. *Numerical Solution of Partial Differential Equations.* Clarendon Press, Oxford, 1978.

[161] Smith R. The Riemann Problem in Gas Dynamics. *Trans. AMS.* 1970; **249**: 1–50.

[162] Soo S. *Fluid Dynamics of Multiphase Systems.* Blaisdell. Waltham, 1967.

[163] Shapiro A. *The Dynamics and Thermodynamics of Compressible Fluid Flow.* Vol. I, II. John Wiley & Sons, Inc., 1953.

[164] Shyue K. A Fluid–Mixture Type Algorithm for Compressible Multicomponent Flow with van der Waals Equation of State. *J. Comput. Phys.* 1999; **156**: 43–88.

[165] Shyue K. A Fluid–Mixture Type Algorithm for Compressible Multicomponent Flow with Mie–Grüneisen Equation of State. *J. Comput. Phys.* 2001; **171**: 678–707.

[166] Städtke H., Worth B. and Franchello G. On the Hyperbolic Nature of Two–Phase Flow Equations: Characteristic Analysis and Related Numerical Methods. In *Godunov Methods: Theory and Applications*, E. F. Toro (ed.); 841–862. Kluwer Academic/Plenum publishers, 2001.

[167] Stewart H. Stability of Two–Phase Flow Calculations Using Two–Fluid Model. *J. Comp. Phys.* 1979; **33**: 259–284.

[168] Stewart H. and Wendroff B. Two–Phase Flow: Models and Methods, *J. Comp. Phys.* 1984; **56**: 363–409.

[169] Tang H., Huang D. A second–Order Accurate Capturing Scheme for 1D Inviscid Flows of Gas and Water with Vacuum Zones. *J. Comp. Phys.* 1996; **128**: 301–318.

[170] Tiselj I. and Petelin S. Modeling of Two–Phase Flow With Second–Order Accurate Scheme. *J. Comp. Phys.* 1997; **136**: 503–521.

[171] Toro E. F. Riemann–problem Based Techniques for Computing Reactive Two-Phase Flows. In *Numerical Combustion.* A. Dervieux & B. Larrouturou (eds.), no 351, 427–481. Springer Lecture Notes in Physics, 1989.

[172] Toro E. F. A Weighted Average Flux Method for Hyperbolic Conservation Laws. *Proc. Roy. Soc. Lond. A.* 1989; **423**: 401–418.

[173] Toro E. F. A Linearised Riemann Solver for the Time–Dependent Euler Equations of Gas Dynamics. *Proc. Roy. Soc. Lond. A.* 1991; **434**: 683–693.

[174] Toro E. F., Spruce M. and Speares W. Restoration of the Contact Surface in the HLL–Riemann Solver. *Shock Waves.* 1994; **4**: 25–34.

[175] Toro E. F. Direct Riemann Solvers for the Time–Dependent Euler Equations. *Shock Waves.* 1995; **5**: 75–80.

[176] Toro E. F. *On Glimm–related Schemes for Conservation Laws.* Technical Report MMU–9602. Manchester Metropolitan University, 1996.

[177] Toro E. F. *Riemann Solvers and Numerical Methods for Fluid Dynamics.* A Practical Introduction. Springer–Verlag. Berlin, 1999.

[178] Toro E. F. and Billett S. Centred TVD Schemes for Hyperbolic Conservation Laws. *IMA. J. Numerical Analysis.* 2000; **20**: 47–79.

[179] Toro E. F. *Shock–Capturing Methods for Free–Surface Shallow Flows.* John Wiley & Sons. 2001.

[180] Toro E. F. Anomalies of Conservative Methods: Analysis, Numerical Evidence and Possible Cures. *Computational Fluid Dynamics Journal.* 2002; **11**(2): 128–143.

[181] Toumi I. A Weak Formulation of Roe's Approximate Riemann Solver. *J. Comp. Phys.* 1992; **102**: 360–373.

[182] Toumi I, Kumbaro A. An Approximate Linearized Riemann Solver for a Two–Fluid Model. *J. Comp. Phys.* 1996; **124**: 286–303.

[183] Toumi I. An Upwind Numerical Method for Two–Fluid Two–Phase Flow Models. *Nucl. Sci. Eng.* 1996; **123**: 147–168.

[184] Toumi I. and Caruge D. An Implicit Second Order Numerical Method for Three–Dimensional Two–Phase Flow Calculations. *Nucl. Sci. Eng.*1998; **130**: 213–225.

[185] Toumi I, Kumbaro A, Seignole V, Paillère H. Development of a multi–dimensional upwind solver for two–phase water/steam flows. 8th *ICONE*, April 2–6, 2000, Baltimore, MD USA.

[186] TRAC–PFI/MOD1. *An Advanced Best–Estimate Computer Program for Pressurized Water Reactor Thermal–Hydraulic Analysis.* NUREG/CR–3858, LA 10157 -MS, Los Alamos National Laboratory, 1986.

[187] Trapp J. and Riemke R. A Nearly–Implicit Hydrodynamic Numerical Scheme for Two–Phase Flows. *J. Comp. Phys.* 1986; **66**: 62–87.

[188] Truesdell C. and Toupin R. The Classical Field Theories. In *Handbuch der Physik.* Vol. III/1. Springer–Verlag. Berlin–Gottingen–Heidelberg, 1960.

[189] Truesdell C. Mechanical Basis of Diffusion. *J. Chem. Phys* 1962; **17**: 2336–2343.

[190] Truesdell C. and Noll W. The Non–Linear Field Theories of Mechanics. In *Handbuch der Physik.* Bd 111/3. Springer–Verlag. Berlin, 1965.

[191] Truesdell C. Rational Thermodynamics. McGraw–Hill. New York, 1969.

[192] Tveito A. and Winther R. *Introduction to Partial Differential Equations*, Springer–Verlag, 1998.

[193] van Leer B. Towards the Ultimate Conservative Difference Scheme III. Upstream–centred Finite Difference Schemes for Ideal Compressible Flow. *J. Comp. Phys.* 1977; **23**: 263–275.

[194] van Leer B. Towards the Ultimate Conservative Difference Scheme V. A. Second Order Sequel to Godunov's Method. *J. Comp. Phys.* 1979; **32**: 101–136.

[195] van Leer B. On the Relationship Between the Upwind Differencing Schemes of Godunov, Enguist–Osher and Roe. *SIAM J. Sci Comp.* 1984; **5**: 1–20.

[196] Venkateswaran S., Lindau J., Kunz R. and Merkle C. Computation of Multiphase Mixture Flows with Compressibility Effects. *J. Comp. Phys.* 2002; **180**: 54–77.

[197] Wallis G. *One–Dimensional Two–Phase Flow.* McGraw–Hill. New York, 1969.

[198] Wallis G. Review–Theoretical Models of Gas–Liquid Flows. *J. Fluids Engineering.* 1982; **104**: 279–283.

[199] White D. and Walton I. A Computer Model for Kicks in Water and Oil Based Muds. Paper SPE 19975 Presented at *the 1990 IADC–SPE Drilling Conference* Held in Houston, Texas, Februray 27–March 2, 1990.

[200] Wijngaarden L. One–Dimensional Flow of Liquids Containing Small Gas Bubbles. *Ann. Rev. Fluid Mech.* 1972; **4**: 369–396.

[201] Witte J. Mixing Shocks in Two–Phase Flow. *J. Fluid Mech.* 1969; **36**(4): 639–655.

[202] Woodward P. and Colella P. The Numerical Simulation of Two-Dimensional Fluid Flow with Strong Shocks *J. Comp. Phys.* 1984; **54**: 115-173.

[203] Yee H. A Class of High–Resolution Explicit and Implicite Shock–Capturing Methods. *Von Karman Institute of Fluid Dynamics*, Lecture Series 1989–4, 1989.

[204] Zachmanoglou E. and Thoe D. *Introduction to Partial Differential Equations*, Dover Publications, Inc. New York, 1986.

[205] Zeidan D., Toro E. F. and Slaouti A. Numerical Simulation of Compressible Two–Phase Flow Model Based on the Riemann Problem. *ACOMEN 2002*, May 28–31, 2002, Liège University, Belgium.

[206] Zeidan D., Toro E. F. and Slaouti A. On the Riemann Problem for a Hyperbolic Two–Phase Flow Model. 2nd *European Multiphase Systems Institute Meeting and* 40th *European Two–Phase Flow Group Meeting*, June 10–13, 2002, Royal Institute of Technology, Stockholm, Sweden.

[207] Zeidan D., Slaouti A. and Toro E. F. Mathematical and Numerical Study of a Simplified Two–Fluid Model. To be submitted.

[208] Zeidan D., Slaouti A., Romenski E. and Toro E. F. Numerical Modeling of the Riemann Problem for the Hyperbolic Conservative Two–Fluid Model. To be submitted.

[209] Zeidan D., Romenski E., Slaouti A. and Toro E. F. Numerical Study of Wave Propagation in Compressible Two–Phase Flow. Submitted to International Journal for Numerical Methods in Fluids.

[210] Zuber N. and Findley J. Average Volumetric Concentration in Two–Phase Flow Systems. *J. Heat Transfer.* 1965; **87**: 453–468.

APPENDIX A
EXACT RIEMANN PROBLEM SOLVER FOR TWO–PHASE FLOW MODELS

```
!~~~
```

```
 OPEN(1,file='dexact.out'); OPEN(2,file='uexact.out')
 OPEN(3,file='urexact.out');OPEN(4,file='pexact.out')
 WRITE(1, 201)xpos, Ds;     WRITE(2, 202)xpos, US
 WRITE(3, 203)xpos, U21s;   WRITE(4, 204)xpos, PS/Psle
11   CONTINUE
     CLOSE(1); CLOSE(2); CLOSE(3); CLOSE(4)
201  FORMAT(F15.8,2X, F15.8)
202  FORMAT(F15.8,2X, F15.8)
203  FORMAT(F15.8,2X, F15.8)
204  FORMAT(F15.8,2X, F15.8)
END PROGRAM exact_solver
!! <-----------------------------| READER |------------------------------->
SUBROUTINE READER
!! Purpose: to read initial parameters of the problem
 IMPLICIT NONE
 INTEGER  NX
 DOUBLE PRECISION IDIS, TM, CL, ML, MR, D1, Cref, Psle, DL, UL, U21L, &
 DR, UR, U21R, G, GI, G1, G2, G3, G4, G5, G6, G7, G8, G9, G10, ALF2L, &
 G11, G12, G13, PL, CT, PR, D2R, ALF2R, CR, AMR, D21L, D21R, D2L, DX, &
 COMMON/DATAIN/NX, TM, IDIS
 COMMON/GAMMAS/G, GI, G1, G2, G3, G4, G5, G6, G7, G8, G9,            &
 G10, G11, G12, G13
 COMMON/STATES/DL, UL, U21L, PL, amL, DR, UR, U21R, PR, amR, CT, Psle
 COMMON/DELTAX/dx
 COMMON/CONSTS/D21L, D21R, C, D1, Cref
 COMMON/VAP/D2L, D2R, alf2L, alf2R
 COMMON/XPOSI/ML, MR
 OPEN(UNIT = 1,FILE = '2rar.inp')
 READ(1,*)NX, IDIS, G, TM, C
 READ(1,*)ML, MR, D1, Cref, Psle
 READ(1,*)DL, UL, U21L
 READ(1,*)DR, UR, U21R
 GI  = (1.0d0/G)
 G1  = (G - 1.0d0)/2.0D0
 G2  = 2.0/(G - 1.0d0)
 G3  = (G - 1.0d0)
 G4  = (G + 1.0d0)/2.0d0
 G5  = 2.0d0/(G + 1.0d0)
 G6  = ((G + 1.0d0)/(G - 1.0d0))
 G7  = ((G - 1.0d0)/(G + 1.0d0))
 G8  = G/(G - 1.0d0)
 G9  = (G - 1.0d0)/G
```

```
G10 = (G + 3.0d0)/2.0d0
G11 = (G - 3.0)/(G - 1.0)
G12 = (G - 3.0)/2.0
G13 = (3.0 - G)/(G - 1.0)
dx  = (MR - ML)/REAL(NX)
alf2L = 1.0d0 - DL/D1 + C*(DL/D1)
D2L   = C*(DL/alf2L)
PL    = Cref*(D2L)**G
CT = PL/(DL**G)
PR    = CT*DR**G
D2R   = (PR/Cref)**GI
alf2R = ((DR - D1)/(D2R - D1))
amL   = SQRT(G*PL/DL)
amR   = SQRT(G*PR/DR)
D21L  = ((1.0/D2L) -(1.0/D1))
D21R  = (D1 - D2R)/(D1*D2R)
IF(G2*(amL+amR) <= (UR-UL))THEN
WRITE(*,*)'-***Vacuum is generated by data***-'
WRITE(6,*)'-***Program stopped***-'
STOP
ENDIF
CLOSE(1)
END SUBROUTINE READER
!! <-------------------------------| STARDU |----------------------------->
SUBROUTINE STARDU(D, U)
!! Purpose: to compute the solution for mixture density and velocity
!! in star region
 IMPLICIT NONE
 INTEGER I, NITER
 DOUBLE PRECISION FL, FLD, FR, FRD, D, U, CT, DL, UL, U21L, PL, amL, &
 DR, UR, U21R, PR, amR, Dstart, Dold, UDIF, Change, Psle, TOL
 COMMON/STATES/DL, UL, U21L, PL, amL, DR, UR, U21R, PR, amR, CT, Psle
 DATA TOL, NITER/1.0E-06, 20/
 CALL GUSSD(Dstart)
 Dold = Dstart
 UDIF = UR - UL
 WRITE(6,*)'----------------------------------------'
 WRITE(6,*)'   Iteration number      Change   '
 WRITE(6,*)'----------------------------------------'
 DO 3 I = 1, NITER
 CALL DENFUN(FL, FLD, Dold, DL, amL, CT)
 CALL DENFUN(FR, FRD, Dold, DR, amR, CT)
```

```
 D       = Dold - (FL + FR + UDIF)/(FLD + FRD)
 Change = 2.0D0*ABS((D - Dold)/(D + Dold))
 WRITE(*, 50) I, Change
 IF(Change <= TOL) GOTO 33
 IF(D < 0.0) D = TOL
 Dold   = D
3  CONTINUE
 WRITE(*,*)'-...Divergence in Newton-Raphson iteration...?...!'
33 CONTINUE
 U = 0.5*(UL + UR + FR - FL)
 WRITE(6,*)'----------------------------------------'
 WRITE(6,*)'Mixture Density   '!     Mixture Velocity'
 WRITE(6,*)'----------------------------------------'
 WRITE(6,40)D, U
 WRITE(6,*)'----------------------------------------'
50   FORMAT(5x,I5, 12x, f12.7,9x,F12.7)
40   FORMAT(2(F14.5, 5X))
END SUBROUTINE STARDU
!! <--------------------------| GUSSD |------------------------------->
SUBROUTINE GUSSD(DM)
!! TO provide a guessed value for mixture density DM in the star region.
!! The choice is made according to adaptive Riemann solver using the PVRS,
!! TRRS and TSRS approximate Riemann solvers.
 IMPLICIT NONE
 DOUBLE PRECISION   DM, CT, ap6, G, GI, G1, G2, G3, DL, UL,          &
 amL, DR, UR, U21R, PR, amR,  DaLR, UaLR, DCLR, CR, CL, D21L,        &
 D21R, DPV, DMIN, DMAX, QMAX, DLR, UM, DTL, DTR, NL1, NL2, gL,       &
 gR, NR1, NR2, Cref, upv, UDa, UDLR, u21pvL, U21pvR,U21ML,ppv,       &
 H1L, H2L, HL, U21MR, H1R, H2R, HR, J1, J2, J3, J4,re,re1,reu,       &
 rel, rer, rep,ppvr, Psle, pa, pma, Pmf, pf, G4, G5, U21LPV,         &
 U21RPV, alf2pv,  D2pv, c, d1, G6,  ALF2M, KC, D2M, J5,J6,H3L,       &
 H4L, H5L, H6L, H7L, H3R, H4R, H5R, H6R, H7R, PM, PS, eq1,eq2,       &
 eq3, G7, ap1, ap2, ap4, ap5, G8, G9, G10, G11, G12, G13,            &
 QUSER, ap9, ap8, ap7, ap3, ap10, U21L, PL, ap11
 COMMON/GAMMAS/G, GI, G1,G2, G3, G4, G5, G6, G7, G8, G9,             &
 G12, G13, G10, G11
 COMMON/STATES/DL, UL, U21L, PL, amL, DR, UR, U21R, PR, amR, CT, Psle
 COMMON/CONSTS/D21L, D21R, C, D1, Cref
 QUSER = 2.0
 ap1    = (DL + DR)*(amL + amR)
 ap2    = (DL+DR)/(D21L + D21R)
 ap3    = (U21L+U21R)/(amL + amR)
```

```
ap5    = (2*(C + C)-(C + C)**2)
ap6    = (UL + UR)/(DL + DR)
ap7    = (DR-DL)/(amL+amR)
ap8    = (1.0/(DL+DR))
ap9    = (1.0/(D21L+D21R))
ap10   = (1.0/(amL+amR))
DPV    = (0.5*(DL + DR) + 0.125*(UL - UR)*ap1                          &
       + 0.125*ap2*ap3*(DR - DL)*ap5)
Upv    = (0.5*(UL + UR) - (2*AP7*AP8) - (0.5*ap5*ap3*ap7*ap9)          &
       + (0.5*ap3*ap5*ap9*Dpv*ap10))
DPV    = MAX(0.0, DPV)
DMIN   = MIN(DL, DR)
DMAX   = MAX(DL, DR)
QMAX   = DMAX/DMIN
IF(QMAX.LE.QUSER.AND.(DMIN.LE.Dpv.AND.Dpv.LE.DMAX))THEN
DM     = DPV
ELSE
IF(Dpv.LT.DMIN) THEN
DLR    = (DL/DR)**G1
UM     = ((DLR*UL/amL)+UR/amR+G2*(DLR - 1))/(DLR/amL+1.0D0/amR)
DTL    = (1.0D0 + G1*(UL - UM)/amL)
DTR    = (1.0D0 + G1*(UM - UR)/amR)
 DM    = 0.5*(DL*DTL**G2 + DR*DTR**G2)
 ELSE
!! SELECT 2-SHOCK  RIEMANN SOLVER; TSRS, WITH PVRS as ESTIMATE
 NL1   = (CT*(DPV**G - DL**G))
 NL2   = (DL*(DPV - DL)*DPV)
 gL    = SQRT(NL1/NL2)
 NR1   = (CT*(DPV**G - DR**G))
 NR2   = (DR*(DPV - DR)*DPV)
 gR    = SQRT(NR1/NR2)
 DM    = (gL*DL + gR*DR - (uR - uL))/(gR+gL)
 UM    = 0.5*(UL + UR)+ 0.5*(gL*(DM - DL) - gR*(DM - DR))
 END IF
 END IF
END SUBROUTINE GUSSD
!! <-----------------------------| DENFUN |------------------------------>
SUBROUTINE DENFUN(F, FD, D, DK, amK, CT)
!! EVALUATE the DENSITY FUNCTIONS FL & FR in exact Riemann solver
!! and their first derivatives
 IMPLICIT NONE
 DOUBLE PRECISION  F, FD, D, DK, DRAF, amK, CT, G, GI, G1, G2, G3, SW, &
```

```
 HW, SH, V1, V2, G4, G5, G6, G7, G8, G9, G10, G11, G12, G13
 COMMON/GAMMAS/ G, GI, G1, G2, G3, G4, G5, G6, G7, G8, G9, G10,        &
 G11, G12, G13
 IF(D.LE.DK)THEN
!! Rarefaction wave
 DRAF = D/DK
 F    = G2*amK*(DRAF**G1 - 1.0D0)
 FD   = amK*((DRAF)**G1)/D
 ELSE
!! Shock wave
 SW   = SQRT(CT/(D*DK))
 HW   = SQRT((D**G - DK**G)*(D - DK))
 V1   = (DK/(D - DK))
 V2   = ((G*D**G)/(D**G - DK**G))
 SH   = (V1 + V2)
 F    = (SW*HW)
 FD   = 0.5*F*SH/D
  END IF
END SUBROUTINE DENFUN
!! <---------------------------| SAMPLE |------------------------------->
Subroutine SAMPLE(DM, UM, S, D, U21, U)
!! Purpose: to sample the solution  throughout the wave pattern.
!! Mixture density DM and mixture velocity UM in the Star Region are known.
!! Sampling is performed in terms of the 'speed' S = x/t.
!! Sampled values are D, U, U21
 IMPLICIT NONE
 DOUBLE PRECISION G, G1, G2, G3, G4, G5, G6, G7, DL, UL, U21L, PL,    &
 UR, U21R, PR, amR, CT, Psle, D21L, D21R, CL, CR, C, D1, Cref,        &
 D2L, D2R, alf2L, alf2R, DM, UM, SHL, D, U, U21, amM, STL, KC,X2,     &
 X1, X3, DANL, PM, DSL, SL, Z1, ZY0, D2M, ZY1, E1, E2, E3, Z2,        &
 DSR, SR, ZQ1, ZQ2, ZQ3, EQ1, EQ2, EQ3, QE, SHR, STR, Z5, ZY2,Z4,     &
 DANR, PANR, P, NR1, NR2, GI, G8, G9 , S, U21ML, U21MR, LF, Laf,      &
 RF, RAF, G10, G11, G12, DOLD, DRF, DRFD, Chge, dfn, G13, NL1,        &
 NL2, alf2m, d21m, gd2, d2f,gd2l, d2fl, X11, X22, X33, Z55, ZY22,     &
 Z44, CM, alf2, D2, CLFAN, CRFAN, amL, DR
 COMMON/GAMMAS/G, GI, G1, G2, G3, G4, G5, G6, G7, G8, G9, G10,        &
       G12, G13, G11
 COMMON/STATES/DL, UL, U21L, PL, amL, DR, UR, U21R, PR, amR, CT, Psle
 COMMON/CONSTS/D21L, D21R, C, D1, Cref
 COMMON/VAP/D2L, D2R, alf2L, alf2R
 IF(S <= UM) THEN
!! Sampling point lies to the left of the contact discontinuity
```

```
 IF(DM <= DL)THEN
!! Left rarefaction
 SHL   = (UL - amL + (C*(1.0 - C)*U21L*DL*D21L))
 IF(S <= SHL)THEN
!! Sampled point is left data state
 D     = DL
 U21   = U21L
 U     = UL
 ELSE
 PM    = CT*DM**G
 D21M  = (D1 - D2M)/(D1*D2M)
 KC    = (Cref/CT)**GI
 X11   = (DM/DL)
 X22   = G6*((X11**G1) - 1.0)*KC
 X33   = (DM*((DL/DM) - (X11**G1))/D1)
 U21ML = U21L - G5*(X22 + X33)*amL
 amM   = amL*(DM/DL)**G1
 STL   = (UM - amM + (C*(1.0 - C)*U21ML*DM*D21M))
 IF(S > STL)THEN
!! Sampled point is Star Left state
 D     = DM
 X1    = (DM/DL)
 X2    = G6*((X1**G1) - 1.0)*KC
 X3    = (DM*((DL/DM) - (X1**G1))/D1)
 U21   = U21L - G5*(X2 + X3)*amL
 U     = UM
 ELSE
!! Sampled point is inside left fan
 KC    = (Cref/CT)**GI
 CALL FANL(DFN, DM, S, KC)
 D     = DFN
 P     = CT*D**G
 D2FL  = ((1.0/D2) - (1.0/D1))
 DANL  = (D/DL)
 NL1   = G6*((DANL**G1) - 1.0d0)*KC
 NL2   = (D*((DL/D) - (DANL**G1))/D1)
 U21   = (U21L - (G5*(NL1 + NL2)*amL))
 U     = G5*(S + amL + G1*UL - (D*C*(1.0 - C)*U21*D2FL))
 END IF
 END IF
 ELSE
!! LEFT SHOCK
```

```
 PM     = CT*DM**G
 alf2M = 1.0d0 - DM/D1 + C*(DM/D1)
 D2M    = C*(DM/alf2M)
 DSL    = (((DM*(PM - PL))/(DL*(DM - DL))))
 SL     = UL - SQRT(DSL)
 amM    = amL*(DM/DL)**G1
 IF(S <= SL)THEN
!! Sampled point is left data state
 D      = DL
 U21    = U21L
 U      = UL
 ELSE
!! Sampled point is Star Left state
 D      = DM
 Z1     = ((DM/DL)*U21L)
 Zy0    = Cref**GI*G8*(PM**G9 - PL**G9)
 Zy1    =  (PM - PL)/D1
 E1     = (ZY0 - ZY1)
 E2     = ((DM*(DM - DL)))
 E3     = ((DL*(PM - PL)))
 Z2     = SQRT(E2/E3)
 U21    = (Z1 - E1*Z2)
 U      = UM
 END IF
 END IF
 ELSE
!! Sampling lies to the right of the contact  discontinuity
 IF(DM > DR)THEN
!! RIGHT SHOCK
 PM     = CT*DM**G
 alf2M = 1.0d0 - DM/D1 + C*(DM/D1)
 D2M    = C*(DM/alf2M)
 DSR    = ((DM*(DM**G - DR**G))/(DR*(DM - DR)))
 SR     = UR + SQRT(CT*DSR)
 IF(S >= SR)THEN
!! Sampled point is right data state
 D    = DR
 U21 = U21R
 U    = UR
 ELSE
!! Sampled point is Star Right state
 D    = DM
```

```
ZQ1 = ((DM/DR)*U21R)
ZQ2 = Cref**GI*G8*(PM**G9 - PR**G9)
ZQ3 = (PM - PR)/D1
EQ1 = (ZQ2 - ZQ3)
EQ2 = ((DM*(DM - DR)))
EQ3 = ((DR*(PM - PR)))
QE  = SQRT(EQ2/EQ3)
U21 = (ZQ1 + EQ1*QE)
U   = UM
 END IF
 ELSE
!! RIGHT RAREFACTION
 SHR   = (UR + amR + (C*(1.0 - C)*U21R*DR*D21R))
 IF(S >= SHR)THEN
!! Sampled point is right data state
 D     = DR
 U21   = U21R
 U     = UR
 ELSE
 PM    = CT*DM**G
 D2M   = (PM/Cref)**GI
 alf2M = ((DM - D1)/(D2M - D1))
 D21M  = (D1 - D2M)/(D1*D2M)
 KC    = (Cref/CT)**GI
 Z55   = (DM/DR)
 ZY22  = G6*((Z55**G1) - 1.0)*KC
 Z44   = (DM*((DR/DM) - (Z55**G1))/D1)
 U21MR = U21R + G5*(ZY22 + Z44)*amR
 amM   = amR*(DM/DR)**G1
 STR   = (UM + amM  + (C*(1.0 - C)*U21MR*DM*D21M))
 IF(S <= STR)THEN
!! Sampled point is Star Right state
 D     = DM
 KC    = (Cref/CT)**GI
 Z5    = (DM/DR)
 ZY2   = G6*((Z5**G1) - 1.0)*KC
 Z4    = (DM*((DR/DM) - (Z5**G1))/D1)
 U21   = U21R + G5*(ZY2 + Z4)*amR
 U     = UM
 ELSE
!! Sampled point is inside right fan
 KC    = (Cref/CT)**GI
```

```
CALL FANR(DFN, DM, S, KC)
D      = DFN
P      = CT*D**G
D2     = (P/Cref)**GI
alf2   = ((D - D1)/(D2 - D1))
D2F    = ((1.0/D2) - (1.0/D1))
DANR   = (D/DR)
NR1    = G6*((DANR**G1) - 1.0d0)*KC
NR2    = (D*((DR/D) - (DANR**G1))/D1)
 U21    = (U21R + (G5*(NR1 + NR2)*amR))
 U      = G5*(S - amR + G1*UR - (D*C*(1.0 - C)*U21*D2F))
 END IF; END IF; END IF; END IF
END SUBROUTINE SAMPLE
!! <-----------------------------| FANL |----------------------------->
SUBROUTINE FANL(D, DM, S, KC)
 IMPLICIT NONE
 INTEGER    J, FITEL
 DOUBLE PRECISION EXL1, EXL2, EXL3, EXL4, EXL5,EXL6, EXL7, EXL8, EXL9,   &
 EXL10, EXTL1,  EXTL2, FANVL, DLF, EXTL1D, EXL1D, EXL2D, EXTL2D, EXL6D,  &
 EXL7D, EXL8D, EXL9D, EXL10D, FANVLD, DLFD, D, G, GI, G1, G2, G3,        &
 G4, G5, G6, G7, G8, G9, G10, G11, G12, D21L, D21R, CL, CR, C, D1,       &
 Cref, KC, DL, UL, U21L, PL, amL, DR, UR, U21R, PR, amR, CT, Psle,       &
 EXTR, S, chge, dold, dm, G13, str,  DOLDL, FANTOL
 COMMON/STATES/DL, UL, U21L, PL, amL, DR, UR, U21R, PR, amR, CT, Psle
 FITEL = 80
 FANTOL=1.0E-08
 DoldL  =  DM
 DO 9 J = 1, FITEL
 CALL FANLdia(DLF, DLFD, DoldL, S, KC)
 D    = DoldL - (DLF)/(DLFD
 Chge = 2.0D0*ABS((D - DoldL)/(D + DoldL))
 WRITE(*, 50) j, Chge
 IF(Chge <= FANTOL) GOTO 99
 IF(D < 0.0) D = FANTOL
 DoldL = D
9  CONTINUE
 WRITE(*,*)'-.....Divergence L-FAN..... '
99 CONTINUE
 WRITE(6,40)D
50 FORMAT(5x,I5, 12x, f12.7,9x,F12.7)
40 FORMAT(2(F14.5, 5X))
END SUBROUTINE FANL
```

```
!! <-----------------------|FANLdia|------------------------------------>
SUBROUTINE FANLdia(DLF, DLFD, D, S, KC)
 IMPLICIT NONE
 DOUBLE PRECISION EXL1, EXL2, EXL3, EXL4, EXL5,EXL6, EXL7, EXL8, EXL9,   &
 EXL10, EXTL1,  EXTL2, FANVL, DLF, EXTL1D, EXL1D, EXL2D, EXTL2D, EXL6D,  &
 EXL7D, EXL8D, EXL9D, EXL10D, FANVLD, DLFD, D, G, GI, G1, G2, G3,        &
 G4, G5, G6, G7, G8, G9, G10, G11, G12, D21L, D21R,  C, D1,              &
 Cref, KC, DL, UL, U21L, PL, amL, DR, UR, U21R, PR, amR, CT, Psle,       &
 EXTR, G13, exL4d, exL3d, exL5d, EXTL, S
 COMMON/GAMMAS/G, GI, G1, G2, G3, G4, G5, G6, G7, G8, G9, G10, G11,G12, G13
 COMMON/CONSTS/D21L, D21R, C,  D1, Cref
 COMMON/STATES/DL, UL, U21L, PL, amL, DR, UR, U21R, PR, amR, CT, Psle
 EXL1   = (G7*C*(1.0 - C)*U21L*KC/amL)
 EXL2   = (G5*C*(1.0 - C)*(D**G1/DL**G1)*KC**2)
 EXL3   = (G5*C*(1.0 - C)*KC**2)
 EXL4   = (G5*G7*C*(1.0 - C)*KC*(D**G4)/(D1*DL**G1))
 EXL5   = (G5*G7*C*(1.0 - C)*KC*DL/D1)
 EXL6   = (G7*C*(C - 1.0)*U21L*D/(D1*amL))
 EXL7   = (G5*C*(C - 1.0)*((D**G4)/(D1*DL**G1))*KC)
 EXL8   = (G5*C*(C - 1.0)*KC*D/D1)
 EXL9   = (G5*G7*C*(C - 1.0)*((D**G10)/(D1**2*DL**G1)))
 EXL10  = (G5*G7*C*(C - 1.0)*DL*(D/D1**2))
 EXTL1  = (EXL1 - EXL2 + EXL3 + EXL4 - EXL5)
 EXTL2  = (EXL6 - EXL7 + EXL8 + EXL9 - EXL10)
 EXTL   = (EXTL1 + EXTL2)
 FANVL  = (G5 + (G7*(UL - S)/amL) + EXTL)
 DLF    = (DL*FANVL**G2 - D)  !!
 EXL1D  = (G7*C*(1.0 - C)*KC**2*(D**G12/DL**G1)
 EXL2D  = (G7*C*(1.0 - C)*KC*(D**G1/(D1*DL**G1)))
 EXL3D  = (G7*C*(C - 1.0)*U21L/(D1*amL))
 EXL4D  = (C*(C - 1.0)*((D**G1)/(D1*DL**G1))*KC)
 EXL5D  = (G5*C*(C - 1.0)*KC/D1)
 EXL6D  = (G5*G7*G10*C*(C - 1.0)*((D**G4)/(D1**2*DL**G1)))
 EXL7D  = (G5*G7*C*(C - 1.0)*(DL/D1**2))
 EXTL1D = (EXL2D - EXL1D)
 EXTL2D = (EXL3D - EXL4D + EXL5D + EXL6D - EXL7D)
 FANVLD = (EXTL1D + EXTL2D)
 DLFD   = ((G2*DL*FANVLD*FANVL**G13) - 1.0)
END SUBROUTINE  FANLdia
!! <-----------------------------| FANR |------------------------------>
SUBROUTINE FANR(D, DM, S, KC)
 IMPLICIT NONE
```

```
      INTEGER J, FITER
      DOUBLE PRECISION EXR1, EXR2, EXR3, EXR4, EXR5,EXR6, EXR7, EXR8, EXR9,    &
      EXR10, EXTR1,  EXTR2, FANVR, DRF, EXTR1D, EXR1D, EXR2D, EXTR2D, EXR6D,   &
      EXR7D, EXR8D, EXR9D, EXR10D, FANVRD, DRFD, D, G, GI, G1, G2, G3,         &
      G4, G5, G6, G7, G8, G9, G10, G11, G12, D21L, D21R, CL, CR, C, D1,        &
      Cref, KC, DL, UL, U21L, PL, amL, DR, UR, U21R, PR, amR, CT, Psle,        &
      EXTR, S, chge, dold, dm, G13, str, FANTOL
      COMMON/STATES/DL, UL, U21L, PL, amL, DR, UR, U21R, PR, amR, CT, Psle
      FITER  = 80
       FANTOL =1.0E-08
       Dold   =  DM
       DO 9 J = 1, FITER
       CALL FANRdia(DRF, DRFD, Dold, S, KC)
       D      = Dold - (DRF)/(DRFD)
       Chge   = 2.0D0*ABS((D - Dold)/(D + Dold))
       WRITE(*, 50) j, Chge
       IF(Chge <= FANTOL) GOTO 99
       IF(D < 0.0) D = FANTOL
       Dold   = D
      9  CONTINUE
      99 CONTINUE
       WRITE(6,40)D
      50 FORMAT(5x,I5, 12x, f12.7,9x,F12.7)
      40 FORMAT(2(F14.5, 5X))
      END SUBROUTINE FANR
      !! <----------------------------|FANRdia|------------------------------->
      SUBROUTINE FANRdia(DRF, DRFD, D, S, KC)
       IMPLICIT NONE
       DOUBLE PRECISION EXR1, EXR2, EXR3, EXR4, EXR5,EXR6, EXR7, EXR8, EXR9,    &
       EXR10, EXTR1,  EXTR2, FANVR, DRF, EXTR1D, EXR1D, EXR2D, EXTR2D, EXR6D,   &
       EXR7D, EXR8D, EXR9D, EXR10D, FANVRD, DRFD, D, G, GI, G1, G2, G3,         &
       G4, G5, G6, G7, G8, G9, G10, G11, G12, D21L, D21R, C, D1,                &
       Cref, KC, DL, UL, U21L, PL, amL, DR, UR, U21R, PR, amR, CT, Psle,        &
       EXTR, G13, exr4d, exr3d, EXR5D, S
       COMMON/GAMMAS/G, GI, G1, G2, G3, G4, G5, G6, G7, G8, G9, G10, G11,G12, G13
       COMMON/CONSTS/D21L, D21R, C, D1, Cref
       COMMON/STATES/DL, UL, U21L, PL, amL, DR, UR, U21R, PR, amR, CT, Psle
       EXR1    = (G7*C*(C - 1.0)*U21R*KC/amR)
       EXR2    = (G5*C*(C - 1.0)*(D**G1/DR**G1)*KC**2)
       EXR3    = (G5*C*(C - 1.0)*KC**2)
       EXR4    = (G5*G7*C*(C - 1.0)*KC*DR/D1)
       EXR5    = (G5*G7*C*(C - 1.0)*KC*(D**G4)/(D1*DR**G1))
```

```
EXR6   = (G7*C*(1.0 - C)*U21R*D/(D1*amR))
EXR7   = (G5*C*(1.0 - C)*((D**G4)/(D1*DR**G1))*KC)
EXR8   = (G5*C*(1.0 - C)*KC*D/D1)
EXR9   = (G5*G7*C*(1.0 - C)*DR*(D/D1**2))
EXR10  = (G5*G7*C*(1.0 - C)*((D**G10)/(D1**2*DR**G1)))
EXTR1  = (EXR1 + EXR2 - EXR3 + EXR4 - EXR5)
EXTR2  = (EXR6 + EXR7 - EXR8 + EXR9 - EXR10)
EXTR   = (EXTR1 + EXTR2)
FANVR  = (G5 + (G7*(S - UR)/amR) + EXTR)
 DRF    = (DR*FANVR**G2 - D)     !!
 EXR1D  = (G7*C*(C - 1.0)*KC**2*(D**G12/DR**G1))
 EXR2D  = (G7*C*(C - 1.0)*KC*(D**G1/(D1*DR**G1)))
 EXR3D  = (G7*C*(1.0 - C)*U21R/(D1*amR))
 EXR4D  = (C*(1.0 - C)*((D**G1)/(D1*DR**G1))*KC)
 EXR5D  = (G5*C*(1.0 - C)*KC/D1)
 EXR6D  = (G5*G7*C*(1.0 - C)*(DR/D1**2))
 EXR7D  = (G5*G7*G10*C*(1.0 - C)*((D**G4)/(D1**2*DR**G1)))
 EXTR1D = (EXR1D - EXR2D)
 EXTR2D = (EXR3D + EXR4D - EXR5D + EXR6D - EXR7D)
 FANVRD = (EXTR1D + EXTR2D)
 DRFD   = ((G2*DR*FANVRD*FANVR**G13) - 1.0)
END SUBROUTINE FANRdia
```

APPENDIX B
THE LAX–FRIEDRICHS SCHEME FOR TWO–PHASE FLOW MODELS

```
!~~~
```

```
END PROGRAM dia_ LaxFriedrichs_Scheme
!! <-----------------------------| READER |------------------------------->
SUBROUTINE READER
 IMPLICIT NONE
 INTEGER MAXNT, cells, NFREQ, TLIFBC, TRIGBC
 DOUBLE PRECISION  ML, MR, RHOL, VL, V21L, RHOR, VR, V21R, CFL, CCL, &
 CREF, D1, TIMEOU, G, GI, G1, G2, G3, G4, G5, G6, G7, G8, G9,        &
 G10, G11, G12, G13
 COMMON/GAMMAS/G, GI, G1, G2, G3, G4, G5, G6, G7, G8, G9,            &
 G12, G13, G10, G11
 COMMON/DATAIN/CELLS, NFREQ, CFL, MAXNT, timeou
 COMMON/PARAM/D1, Cref, CCL
 COMMON/INISTA/RHOL, VL, V21L, RHOR, VR, V21R
 COMMON/DOMAIN/ML, MR
 COMMON/BOCON/TLIFBC, TRIGBC
 OPEN(UNIT = 1, FILE = '2rrnum.inp')
 READ(1,*)CELLS, NFREQ, timeou, CFL, MAXNT, G
 READ(1,*)ML, MR, TLIFBC, TRIGBC, Cref, D1, CCL
 READ(1,*)RHOL, VL, V21L
 READ(1,*)RHOR, VR, V21R
 CLOSE(1)
END SUBROUTINE READER
!! <-----------------------------| INITIA |------------------------------->
SUBROUTINE INITIA(CELLS, CT)
 IMPLICIT NONE
 INTEGER I, CELLS, IDIM
 PARAMETER (IDIM = 6000)
 DOUBLE PRECISION G, GI, G1, G2, G3, G4, G5, G6, G7, G8, G9, G10,  &
 G11, G12, G13, D1, CCL, CREF, ALF2LL, RHOL, D2LL , PLL, CT,       &
 RHOR, D2RR, ALF2RR, amLL, amRR, CCR, D21LL, D21RR, PRR, VL,       &
 V21L, VR, V21R, D, U, U21, XPOS, ML, MR, dx, dt, CS
 DIMENSION D(-1:IDIM+2), U(-1:IDIM+2), U21(-1:IDIM+2), CS(3,-1:IDIM+2)
 COMMON/GAMMAS/G, GI, G1, G2, G3, G4, G5, G6, G7, G8, G9,          &
 G12, G13, G10, G11
 COMMON/PARAM/D1, Cref, CCL
 COMMON/INISTA/RHOL, VL, V21L, RHOR, VR, V21R
 COMMON/DOMAIN/ML, MR
 COMMON/PRMTV/D, U, U21
 COMMON/dtdx/DT, DX
 COMMON/CONSER/CS
 GI        = (1.0d0/G)
 G1        = (G - 1.0d0)/2.0D0
```

```
G2          = 2/(G - 1.0d0)
G3          = (G - 1.0d0)
G4          = (G + 1.0d0)/2.0d0
G5          = 2.0d0/(G + 1.0d0)
G6          = ((G + 1.0d0)/(G - 1.0d0))
G7          = ((G - 1.0d0)/(G + 1.0d0))
G8          = G/(G - 1.0d0)
G9          = (G - 1.0d0)/G
G10         = (G + 3.0d0)/2.0d0
G11         = (G - 3.0)/(G - 1.0)
G12         = (G - 3.0)/2.0
G13         = (3.0 - G)/(G - 1.0)
alf2LL      = 1.0d0 - RHOL/D1 + CCL*(RHOL/D1)
D2LL        = CCL*(RHOL/alf2LL)
PLL         = Cref*(D2LL)**G
CT          = PLL/(RHOL**G)
PRR         = CT*RHOR**G
D2RR        = (PRR/Cref)**GI
alf2RR      = ((RHOR - D1)/(D2RR - D1))
amLL        = SQRT(G*PLL/RHOL)
amRR        = SQRT(G*PRR/RHOR)
D21LL       = ((1.0/D2LL)-(1.0/D1))
D21RR       = (D1 - D2RR)/(D1*D2RR)
dx          = (MR - ML)/REAL(CELLS)
DO 101 I = 1, cells
Xpos        = ML + (MR - ML)*REAL(I-1)/REAL(CELLS)
IF(Xpos.LE.0.0) THEN
D(I)        = rhoL
U(I)        = VL
U21(I)      = V21L
ENDIF
IF(XPOS.GT.0.0)THEN
D(I)        = rhoR
U(I)        = VR
U21(I)    = V21R
ENDIF
 CS(1,I) = D(I)
 CS(2,I) = D(I)*U(I)
 CS(3,I) = U21(I)
101  CONTINUE
END SUBROUTINE INITIA
! |~~~~~~~~~~~~~~~~~~~~~~~~~~| BCONDI |~~~~~~~~~~~~~~~~~~~~~~~~~~~~~~~~~~~~~~|
```

```
SUBROUTINE BCONDI(CELLS)
 IMPLICIT NONE
 INTEGER CELLS, IDIM, TLIFBC, TRIGBC
 DOUBLE PRECISION D, U, U21
 PARAMETER (IDIM = 6000)
 DIMENSION D(-1:IDIM+2), U(-1:IDIM+2), U21(-1:IDIM+2)
 COMMON/PRMTV/D, U, U21
 COMMON/BOCON/TLIFBC, TRIGBC
 IF(TLIFBC.EQ.0)THEN
 D(0)    = D(1)
 U(0)    = U(1)
 U21(0) = U21(1)
 ELSE
 D(0)    =  D(1)
 U(0)    = -U(1)
 U21(0) =  U21(1)
 ENDIF
 IF(TRIGBC.EQ.0)THEN
 D(CELLS + 1)    = D(CELLS)
 U(CELLS + 1)    = U(CELLS)
 U21(CELLS + 1) = U21(CELLS)
 ELSE
 D(CELLS + 1)    = D(CELLS)
 U(CELLS + 1)    = -U(CELLS)
 U21(CELLS + 1) =  U21(CELLS)
      ENDIF
END SUBROUTINE BCONDI
! |~~~~~~~~~~~~~~~~~~~~~~~~~~| CFLCON |~~~~~~~~~~~~~~~~~~~~~~~~~~~~~~~~~~~~~~|
SUBROUTINE CFLCON(CFL, CELLS, CT, N, TIME, TIMEOU)
!!Purpose: to apply the CFL condition to find a stable time
!!step size DT
 IMPLICIT NONE
 INTEGER CELLS, N, IDIM, I
 PARAMETER (IDIM = 6000)
 DOUBLE PRECISION D, U, U21, D2, P, C, ALF2, am, XS, MAXS, SMAX, G,  &
 GI, G1, G2, G3, G4, G5, G6, G7, G8, G9, G10, G11, G12, G13, D1,     &
 Cref, CCL, cfl, time, timeou, CT, dt, dx , D2D
 DIMENSION D(-1:IDIM+2), U(-1:IDIM+2), U21(-1:IDIM+2), P(-1:IDIM+2), &
 am(-1:IDIM+2), D2(-1:IDIM+2), alf2(-1:IDIM+2), XS(-1:IDIM+2)
 COMMON/PRMTV/D, U, U21
 COMMON/PARAM/D1, Cref, CCL
 COMMON/GAMMAS/G, GI, G1, G2, G3, G4, G5, G6, G7, G8, G9,           &
```

```
      G12, G13, G10, G11
COMMON/dtdx/DT, DX
DO 10 I       = 0, CELLS + 1
P(I)          = CT*D(I)**G
am(I)         = SQRT(G*P(I)/D(I))
D2(I)         = (P(I)/Cref)**GI
XS(I)         = (D(I)*((1.0/D2(I))-(1.0/D1))*CCL*(1.0 - CCL)*U21(I))
MAXS          = (ABS(U(I)) + am(I) + XS(I))
IF (MAXS > SMAX )SMAX = MAXS
10 CONTINUE
 dt            = CFL*DX/SMAX
 IF(N.LE.5)DT = 0.2*DT
 IF((TIME+DT).GT.TIMEOU)THEN
 DT = TIMEOU - TIME
 ENDIF
 TIME = TIME + DT
END SUBROUTINE CFLCON
! |~~~~~~~~~~~~~~~~~~~~~~~~~~~| Lax-Flux |~~~~~~~~~~~~~~~~~~~~~~~~~~~~~~~~~~~~~~|
SUBROUTINE LAXFRI(CELLS, CT)
 IMPLICIT NONE
 INTEGER  I, CELLS, IDIM, K
 PARAMETER (IDIM = 6000)
 DOUBLE PRECISION  D, U, U21, D2, P, C, ALF2, am, XS, MAXS, SMAX, G,  &
 GI, G1, G2, G3, G4, G5, G6, G7, G8, G9, G10, G11, G12, G13, D1,      &
 Cref, CCL, CS, FD, CT, FI, DT, DX
 DIMENSION D(-1:IDIM+2), U(-1:IDIM+2), U21(-1:IDIM+2), P(-1:IDIM+2),  &
 am(-1:IDIM+2), D2(-1:IDIM+2), alf2(-1:IDIM+2), C(-1:IDIM+2),         &
 CS(3,-1:IDIM+2), FD(3,-1:IDIM+2), FI(3,-1:IDIM+2)
 COMMON/PRMTV/D, U, U21
 COMMON/PARAM/D1, Cref, CCL
 COMMON/GAMMAS/G, GI, G1, G2, G3, G4, G5, G6, G7, G8, G9,            &
       G12, G13, G10, G11
 COMMON/CONSER/CS
 COMMON/dtdx/DT, DX
 COMMON/FLUXES/FI
 DO 10 I  = 0, CELLS + 1
 CS(1,I)  = D(I)
 CS(2,I)  = D(I)*U(I)
 CS(3,I)  = U21(I)
 P(I)     = (CT*D(I)**G)
 D2(I)    = (P(I)/Cref)**GI
 FD(1,I)  = CS(2,I)
```

```
 FD(2,I)  = (CS(2,I)*U(I) + (P(I)) +                                    &
  (D(I)*CCL*(1.0 - CCL)*U21(I)*U21(I)))
 FD(3,I)  = (U(I)*U21(I) + 0.5*(1.0 - 2*CCL)*U21(I)*U21(I) +            &
  ((Cref**GI*G8*P(I)**G9) - (P(I)/D1)))
10 CONTINUE
 DO 20 I  = 0, CELLS
 DO 30 K  = 1, 3
 FI(K, I) = (0.5*(FD(K, I) + FD(K, I + 1)) +                            &
 0.5*(DX/DT)*(CS(K, I) - CS(K, I + 1)))

30 CONTINUE
20 CONTINUE
END SUBROUTINE LAXFRI
! |~~~~~~~~~~~~~~~~~~~~~~~~~~| UPDATE |~~~~~~~~~~~~~~~~~~~~~~~~~~~~~~~~~~~~~~|
SUBROUTINE UPDATE(CELLS)
!! Purpose: to update the solution according to the conservative
!! formula and compute physical variables
 IMPLICIT NONE
 INTEGER I, IDIM, K, CELLS
 PARAMETER (IDIM = 6000)
 DOUBLE PRECISION   DT, DTODX, DX, FI, U, D, U21, CS
 DIMENSION D(-1:IDIM+2), U(-1:IDIM+2), U21(-1:IDIM+2),                  &
       CS(3,-1:IDIM+2), FI(3, -1:IDIM+2)
 COMMON/PRMTV/D, U, U21
 COMMON/dtdx/DT, DX
 COMMON/CONSER/CS
 COMMON/FLUXES/FI
 DTODX    = DT/DX
 DO 10 I  = 1, CELLS
 DO 20 K  = 1, 3
 CS(K, I) = (CS(K, I) + DTODX*(FI(K, I-1) - FI(K, I)))
20 CONTINUE
10 CONTINUE
 DO 30 I  = 1, CELLS
 D(I)     = CS(1,I)
 U(I)     = CS(2,I)/D(I)
 U21(I)   = CS(3,I)
30 CONTINUE
END SUBROUTINE UPDATE
! |~~~~~~~~~~~~~~~~~~~~~~~~~~| OUTPUT |~~~~~~~~~~~~~~~~~~~~~~~~~~~~~~~~~~~~~~|
SUBROUTINE OUTPUT(CELLS, CT)
!! Purpose: to output the solution at a specified time TIMEOU
```

```
      IMPLICIT NONE
      INTEGER CELLS, I, IDIM
      PARAMETER (IDIM = 6000)
      DOUBLE PRECISION DX, XPOS, ML, MR, D, U, U21, P, am, G, GI, G1, G2, &
      G3, G4, G5, G6, G7, G8, G9, G10, G11, G12, G13, CT, Psle, D2,       &
      alf2, C, D1, Cref, CCL
      DIMENSION D(-1:IDIM+2), U(-1:IDIM+2), U21(-1:IDIM+2), P(-1:IDIM+2), &
      am(-1:IDIM+2), D2(-1:IDIM+2), alf2(-1:IDIM+2)
      COMMON/DOMAIN/ML, MR
      COMMON/GAMMAS/G, GI, G1, G2, G3, G4, G5, G6, G7, G8, G9,            &
            G12, G13, G10, G11
      COMMON/PRMTV/D, U, U21
      COMMON/PARAM/D1, Cref, CCL
      Psle = 100000.0
      OPEN(1, FILE = 'dlax.out');  OPEN(2, FILE = 'ulax.out')
      OPEN(3, FILE = 'urlax.out'); OPEN(4, FILE = 'plax.out')
      DO 110 I = 1, CELLS +1
      Xpos    = ML + (MR - ML)*REAL(I - 1)/REAL(CELLS)
      P(I)    = CT*D(I)**G
      D2(I)   = (P(I)/Cref)**GI
      alf2(I) = ((D(I) - D1)/(D2(I) - D1))
      am(I)   = SQRT(G*P(I)/D(I))
       Write(1,20)Xpos, D(I);   Write(2,30)Xpos, U(I)
       WRITE(3,40)xpos, u21(I); WRITE(4,50)xpos, P(I)/Psle
      110 CONTINUE
           Close(1); Close(2); Close(3); Close(4)
      20   FORMAT(F15.8,2X, F15.8)
      30   FORMAT(F15.8,2X, F15.8)
      40   FORMAT(F15.8,2X, F15.8)
      50   FORMAT(F15.8,2X, F15.8)
      END SUBROUTINE OUTPUT
```

APPENDIX C
MUSCL–HANCOCK SCHEME FOR TWO–PHASE FLOW MODELS

```
!~~~
```

```
END PROGRAM dia_MUSCL--Hancock_scheme
! |~~~~~~~~~~~~~~~~~~~~~~~~~~| READER |~~~~~~~~~~~~~~~~~~~~~~~~~~~~~~~~~~~~~~|
SUBROUTINE READER
 IMPLICIT NONE
 INTEGER MAXNT, cells, NFREQ, TLIFBC, TRIGBC, influx, LIMITE
 DOUBLE PRECISION  ML, MR, RHOL, VL, V21L, RHOR, VR, V21R, CFL, CC,G12,  &
 CREF, D1, TIMEOU, G, GI, G1, G2, G3, G4, G5, G6, G7, G8, G9, G10, G11,  &
 COMMON/DATAIN/CELLS, NFREQ, CFL, MAXNT, timeou, influx, LIMITE
 COMMON/GAMMAS/G, GI, G1, G2, G3, G4, G5, G6, G7, G8, G9,                &
 G10, G11, G12, G13
 COMMON/PARAM/D1, Cref, CC
 COMMON/INISTA/RHOL, VL, V21L, RHOR, VR, V21R
 COMMON/DOMAIN/ML, MR
 COMMON/BOCON/TLIFBC, TRIGBC
 OPEN(UNIT = 1, FILE = '2rrnum.inp')
 READ(1,*)CELLS, NFREQ, timeou, CFL, MAXNT, G, influx, LIMITE
 READ(1,*)ML, MR, TLIFBC, TRIGBC, Cref, D1, CC
 READ(1,*)RHOL, VL, V21L
 READ(1,*)RHOR, VR, V21R
 CLOSE(1)
END SUBROUTINE READER
! |~~~~~~~~~~~~~~~~~~~~~~~~~~| INITIA |~~~~~~~~~~~~~~~~~~~~~~~~~~~~~~~~~~~~~~|
SUBROUTINE INITIA(CELLS, CT)
 IMPLICIT NONE
 INTEGER I, CELLS, IDIM
 PARAMETER (IDIM = 6000)
 DOUBLE PRECISION G, GI, G1, G2, G3, G4, G5, G6, G7, G8, G9, G10,  &
 G11, G12, G13, D1, CC, CREF, ALF2LL, RHOL, D2LL , PLL, CT,        &
 RHOR, D2RR, ALF2RR, amLL, amRR, CCR, D21LL, D21RR, PRR, VL,       &
 V21L, VR, V21R, D, U, U21, XPOS, ML, MR, dx, dt, CS
 DIMENSION D(-1:IDIM+2), U(-1:IDIM+2), U21(-1:IDIM+2) , CS(3,-1:IDIM+2)
 COMMON/GAMMAS/G, GI, G1, G2, G3, G4, G5, G6, G7, G8, G9,          &
       G12, G13, G10, G11
 COMMON/PARAM/D1, Cref, CC
 COMMON/INISTA/RHOL, VL, V21L, RHOR, VR, V21R
 COMMON/DOMAIN/ML, MR
 COMMON/PRMTV/D, U, U21
 COMMON/dtdx/DT, DX
 COMMON/CONSER/CS
 GI        = (1.0d0/G)
 G1        = (G - 1.0d0)/2.0D0
 G2        = 2/(G - 1.0d0)
```

```
G3        = (G - 1.0d0)
G4        = (G + 1.0d0)/2.0d0
G5        = 2.0d0/(G + 1.0d0)
G6        = ((G + 1.0d0)/(G - 1.0d0))
G7        = ((G - 1.0d0)/(G + 1.0d0))
G8        = G/(G - 1.0d0)
G9        = (G - 1.0d0)/G
G10       = (G + 3.0d0)/2.0d0
G11       = (G - 3.0)/(G - 1.0)
G12       = (G - 3.0)/2.0
G13       = (3.0 - G)/(G - 1.0)
alf2LL    = 1.0d0 - RHOL/D1 + CC*(RHOL/D1)
D2LL      = CC*(RHOL/alf2LL)
PLL       = Cref*(D2LL)**G
CT        = PLL/(RHOL**G)
PRR       = CT*RHOR**G
D2RR      = (PRR/Cref)**GI
alf2RR    = ((RHOR - D1)/(D2RR - D1))
amLL      = SQRT(G*PLL/RHOL)
amRR      = SQRT(G*PRR/RHOR)
D21LL     = ((1.0/D2LL) -(1.0/D1))
D21RR     = (D1 - D2RR)/(D1*D2RR)
dx        = (MR - ML)/REAL(CELLS)
DO 101 I = 1, cells
Xpos      = ML + (MR - ML)*REAL(I - 1.0)/REAL(CELLS)
IF(Xpos.LE.0) THEN
D(I)      = rhoL
U(I)      = VL
U21(I)    = V21L
ENDIF
IF(XPOS.GT.0)THEN
D(I)      = rhoR
U(I)      = VR
U21(I)    = V21R
ENDIF
CS(1,I)   = D(I)
 CS(2,I)   = D(I)*U(I)
 CS(3,I)   = U21(I)
101 CONTINUE
END SUBROUTINE INITIA
! |~~~~~~~~~~~~~~~~~~~~~~~~~~| BCONDI |~~~~~~~~~~~~~~~~~~~~~~~~~~~~~~~~~~~~~~~~~~~~~~|
SUBROUTINE BCONDI(CELLS)
```

```
      IMPLICIT NONE
      INTEGER CELLS, IDIM, TLIFBC, TRIGBC
      DOUBLE PRECISION D, U, U21
      PARAMETER (IDIM = 6000)
      DIMENSION D(-1:IDIM+2), U(-1:IDIM+2), U21(-1:IDIM+2)
      COMMON/PRMTV/D, U, U21
      COMMON/BOCON/TLIFBC, TRIGBC
      IF(TLIFBC.EQ.0)THEN
      D(0)     = D(1)
      U(0)     = U(1)
      U21(0)   = U21(1)
      D(-1)    =  D(2)
      U(-1)    =  U(2)
      U21(-1)  = U21(2)
      ELSE
      D(0)     =  D(1)
      U(0)     = -U(1)
      U21(0)   =  U21(1)
      D(-1)    =  D(2)
      U(-1)    = -U(2)
      U21(-1)  = U21(2)
      ENDIF
      IF(TRIGBC.EQ.0)THEN
      D(CELLS + 1)    = D(CELLS)
      U(CELLS + 1)    = U(CELLS)
      U21(CELLS + 1)  = U21(CELLS)
      D(CELLS + 2)    =  D(CELLS-1)
      U(CELLS + 2)    =  U(CELLS-1)
      U21(CELLS + 2)  = U21(CELLS-1)
      ELSE
      D(CELLS + 1)    = D(CELLS)
      U(CELLS + 1)    = -U(CELLS)
      U21(CELLS + 1)  =  U21(CELLS)
      D(CELLS + 2)    =  D(CELLS-1)
      U(CELLS + 2)    = -U(CELLS-1)
      U21(CELLS + 2)  = U21(CELLS-1)
      ENDIF
    END SUBROUTINE BCONDI
    ! |~~~~~~~~~~~~~~~~~~~~~~~~~~~| CFLCON |~~~~~~~~~~~~~~~~~~~~~~~~~~~~~~~~~~~~~~|
    SUBROUTINE CFLCON(CFL, CELLS, CT, N, TIME, TIMEOU)
    !! Purpose: to apply the CFL condition to find a stable time
    !! step size DT
```

```
      IMPLICIT NONE
      INTEGER CELLS, N, IDIM, I
      PARAMETER (IDIM = 6000)
      DOUBLE PRECISION D, U, U21, D2, P, C, ALF2, am, XS, MAXS, SMAX, G,  &
      GI, G1, G2, G3, G4, G5, G6, G7, G8, G9, G10, G11, G12, G13, D1,     &
      Cref, CC, cfl, time, timeou, CT, dt, dx , D21
      DIMENSION D(-1:IDIM+2), U(-1:IDIM+2), U21(-1:IDIM+2), P(-1:IDIM+2), &
      am(-1:IDIM+2), D2(-1:IDIM+2), alf2(-1:IDIM+2),                      &
      XS(-1:IDIM+2), D21(-1:IDIM+2)
      COMMON/PRMTV/D, U, U21
      COMMON/PARAM/D1, Cref, CC
      COMMON/GAMMAS/G, GI, G1, G2, G3, G4, G5, G6, G7, G8, G9,            &
      G10, G11, G12, G13
      COMMON/dtdx/DT, DX
      DO 10 I = 0, CELLS + 1
      P(I)     = CT*D(I)**G
      am(I)    = SQRT(G*P(I)/D(I))
      D2(I)    = (P(I)/Cref)**GI
      alf2(I) = ((D(I) - D1)/(D2(I) - D1))
      D21(I)   = ((1.0/D2(I)) - (1.0/D1))
      XS(I)    = (D(I)*((1.0/D2(I)) - (1.0/D1))*CC*(1.0 - CC)*U21(I))
      MAXS     = (ABS(U(I)) + am(I) + XS(I))
       IF (MAXS.GT.SMAX )SMAX = MAXS
      10 CONTINUE
       dt       = CFL*DX/SMAX
       IF(N.LE.5)DT = 0.2*DT
       IF((TIME + DT).GT.TIMEOU)THEN
       DT = TIMEOU - TIME
       ENDIF
       TIME = TIME + DT
      END SUBROUTINE CFLCON
      ! |~~~~~~~~~~~~~~~~~~~~~~~~~~| MUSFLUX  |~~~~~~~~~~~~~~~~~~~~~~~~~~~~~~~~~~~~~~|
      SUBROUTINE MUSFLUX(CELLS, CT, influx, LIMITE)
       IMPLICIT NONE
       INTEGER  I, CELLS, IDIM, K, IUPW, influx, LIMITE
       PARAMETER (IDIM = 6000)
       DOUBLE PRECISION  D, U, U21, D2, P, C, ALF2, am, XS, MAXS, SMAX, G,  &
       GI, G1, G2, G3, G4, G5, G6, G7, G8, G9, G10, G11, G12, G13, D1,     &
       Cref, CC, CT, PL, DL, UL, U21L, D2L, ALF2L, CL, AML, PR, DR,  FIR,  &
       UR, U21R, D2R, ALF2R, CR, AMR, DM, UM, D21L, D21R, D21, DS, US,     &
       U21S, PS, CS, ALF2S, FI, D2S, TOLLIM, FD, SL, SM, SR, PM, DSL,      &
       DSR, U21ML, U21MR, KC, X1, X2, X3, E1, E2, E3, Z1, ZY0, ZY1, Z2,    &
```

```
Z5, ZY2, Z4, ZQ1, ZQ2, ZQ3, EQ1, EQ2, EQ3, QE, D2M, ALF2M, CM, FIL,  &
FSL, FSR, WS, WJ, DT, DX, CN, DTODX, DLOC, DUPW, RATIO, WAFLIM,      &
WML, WMR, WL, WR, S, D21s, Omega, DELTA, PIL, PIR, BEXT, DELFLUX,    &
DIMENSION D(-1:IDIM+2), U(-1:IDIM+2), U21(-1:IDIM+2), P(-1:IDIM+2),  &
am(-1:IDIM+2), D2(-1:IDIM+2), alf2(-1:IDIM+2),                       &
D21(-1:IDIM+2), FI(3,-1:IDIM+2), FD(3, -1:IDIM+2),                   &
CS(3,-1:IDIM+2), FSL(3, -1:IDIM+2), FSR(3, -1:IDIM+2),               &
WS(3, -1:IDIM+2), WJ(3, -1:IDIM+2), CN(3), WAFLIM(3),                &
PIL(3), PIR(3), FIL(3), FIR(3), BEXT(2, 3, -1:IDIM+2)
 COMMON/PRMTV/D, U, U21
 COMMON/PARAM/D1, Cref, CC
 COMMON/GAMMAS/G, GI, G1, G2, G3, G4, G5, G6, G7, G8, G9,            &
 G10, G11, G12, G13
 COMMON/CONSER/CS
 COMMON/dtdx/DT, DX
 COMMON /BEXTRA/ BEXT
 DATA TOLLIM, Omega/1.0E-06, 0.0/
 DO 999 I = -1, CELLS + 2
 CS(1, I) = D(I)
 CS(2, I) = D(I)*U(I)
 CS(3, I) = U21(I)
999  CONTINUE
 DTODX    = DT/DX
 DO 20 I  =  0, CELLS + 1
 DO 30 K  = 1, 3
 DUPW     = CS(K, I)      - CS(K, I - 1)
 DLOC     = CS(K, I + 1) - CS(K, I)
 IF(ABS(DUPW).LE.TOLLIM)DUPW=TOLLIM*SIGN(1.0d0,DUPW)
 IF(ABS(DLOC).LE.TOLLIM)DLOC=TOLLIM*SIGN(1.0d0,DLOC)
 DELTA = 0.5*(1.0+OMEGA)*DUPW + 0.5*(1.0d0-OMEGA)*DLOC
 RATIO = DUPW/DLOC
 IF(LIMITE.EQ.10)DELTA = 0.0
 IF(LIMITE.EQ.20)DELTA = DELTA
 IF(LIMITE.EQ.2)CALL SBSLIC(RATIO, OMEGA, DELTA)
 IF(LIMITE.EQ.4)CALL VLSLIC(RATIO, OMEGA, DELTA)
 IF(LIMITE.EQ.5)CALL VASLIC(RATIO, OMEGA, DELTA)
 IF(LIMITE.EQ.6)CALL MISLIC(RATIO, OMEGA, DELTA)
 IF(LIMITE.EQ.7)CALL MINMAX(DUPW, DLOC, DELTA)
 PIL(K) = CS(K, I) - 0.5*DELTA
 PIR(K) = CS(K, I) + 0.5*DELTA
30 CONTINUE
 CALL FLUEVAL(PIL, FIL, CT)
```

```
 CALL FLUEVAL(PIR, FIR, CT)
 DO 40 K      = 1, 3
 DELFLUX      = 0.5*DTODX*(FIL(K) - FIR(K))
 BEXT(1,K,I) = PIL(K) + DELFLUX
 BEXT(2,K,I) = PIR(K) + DELFLUX
40 CONTINUE
20 CONTINUE
 CALL HLLC(CELLS, CT)
END SUBROUTINE MUSFLUX
! |~~~~~~~~~~~~~~~~~~~~~~~~~~| SBSLIC |~~~~~~~~~~~~~~~~~~~~~~~~~~~~~~~~~~~~~~|
SUBROUTINE SBSLIC(R, OMEGA, DELTA)
!! To compute a SUPERBEE type slope limiter DELTA
 IMPLICIT NONE
 DOUBLE PRECISION  DELTA, DENOR, OMEGA, PHI, PHIR, R
 PHI              = 0.0
 IF(R.GE.0.0)PHI = 2.0*R
 IF(R.GE.0.5)PHI = 1.0
 IF(R.GE.1.0)THEN
 DENOR = 1.0 - OMEGA + (1.0 + OMEGA)*R
 PHIR  = 2.0/DENOR
 PHI   = MIN(PHIR, R)
 PHI   = MIN(PHI, 2.0)
 ENDIF
 DELTA = PHI*DELTA
END SUBROUTINE SBSLIC
! |~~~~~~~~~~~~~~~~~~~~~~~~~~| VLSLIC |~~~~~~~~~~~~~~~~~~~~~~~~~~~~~~~~~~~~~~|
SUBROUTINE VLSLIC(R, OMEGA, DELTA)
 IMPLICIT NONE
 DOUBLE PRECISION DELTA, DENOR, OMEGA, PHI, PHIR, R
 PHI   = 0.0
 IF(R.GE.0.0)THEN
 DENOR = 1.0 - OMEGA + (1.0 + OMEGA)*R
 PHIR  = 2.0/DENOR
 PHI   = 2.0*R/(1.0 + R)
 PHI   = MIN(PHI, PHIR)
 ENDIF
 DELTA = PHI*DELTA
END SUBROUTINE VLSLIC
! |~~~~~~~~~~~~~~~~~~~~~~~~~~| VASLIC |~~~~~~~~~~~~~~~~~~~~~~~~~~~~~~~~~~~~~~|
SUBROUTINE VASLIC(R, OMEGA, DELTA)
 IMPLICIT NONE
 DOUBLE PRECISION  DELTA, DENOR, OMEGA, PHI, PHIR, R
```

```
 PHI = 0.0
 IF(R.GE.0.0)THEN
 DENOR = 1.0 - OMEGA + (1.0 + OMEGA)*R
 PHIR  = 2.0/DENOR
 PHI   = R*(1.0 + R)/(1.0 + R*R)
 PHI   = MIN(PHI, PHIR)
 ENDIF
 DELTA    = PHI*DELTA
END SUBROUTINE VASLIC
! |~~~~~~~~~~~~~~~~~~~~~~~~~~| MISLIC |~~~~~~~~~~~~~~~~~~~~~~~~~~~~~~~~~~~~~~|
SUBROUTINE MISLIC(R, OMEGA, DELTA)
 IMPLICIT NONE
 DOUBLE PRECISION DELTA, DENOR, OMEGA, PHI, PHIR, R
 PHI              = 0.0
 IF(R.GE.0.0)PHI = R
 IF(R.GE.1.0)THEN
 DENOR = 2.0*(1.0 - OMEGA + (1.0 + OMEGA)*R)
 PHIR  = 4.0/DENOR
 PHI   = MIN(1.0, PHIR)
 ENDIF
 DELTA = PHI*DELTA
END SUBROUTINE MISLIC
! |~~~~~~~~~~~~~~~~~~~~~~~~~~| MINMAX |~~~~~~~~~~~~~~~~~~~~~~~~~~~~~~~~~~~~~~|
SUBROUTINE MINMAX(DUPW, DLOC, DELTA)
 IMPLICIT NONE
 DOUBLE PRECISION BETAL, BETAR, DELTA, DLOC, DUPW, SIGNO
 BETAL = 1.0
 BETAR = 1.0
 SIGNO = 0.5*(SIGN(1.0d0,DUPW) + SIGN(1.0d0,DLOC))
 DELTA = SIGNO*(MIN(BETAL*ABS(DUPW),BETAR*ABS(DLOC)))
END SUBROUTINE MINMAX
! |~~~~~~~~~~~~~~~~~~~~~~~~~~| HLLC |~~~~~~~~~~~~~~~~~~~~~~~~~~~~~~~~~~~~~~|
SUBROUTINE HLLC(CELLS, CT)
!! To compute the intercell flux FI(K, I) according
!! to the Godunov method with the HLL approximate
 IMPLICIT NONE
 INTEGER  I, K, CELLS, IDIM
 PARAMETER (IDIM = 6000)
 DOUBLE PRECISION BEXT, DL, UL, U21L, PL, D21L, amL,  DR, UR, U21R, PR, &
 D21R, amR, CDL, CDR, FI, FDL, FDR, G, GI, G1, G2, G3, G4, G5, G6,      &
 G7, G8, G9, G10, G11, G12, G13, CT, D1, Cref, CC, D2L, ALF2L,          &
 D2R, ALF2R, SL, SM, SR, CSTAL, CSTAR, dm, um, pm,                      &
```

```
      VU1L, VU2L, VU3L, VU4L, VU5L, VU6L, VU1R, VU2R, VU3R, VU4R, VU5R,&
      VU6R, RELUL, RELUR, U21ML, U21MR
      DIMENSION CDL(3), CDR(3), FDL(3), FDR(3), FI(3, -1:IDIM+2), &
      BEXT(2, 3, -1:IDIM+2), CSTAL(3), CSTAR(3)
      COMMON/STATES/DL, UL, U21L, PL, D21L, amL,  DR, UR, U21R, PR, D21R, amR
      COMMON /BEXTRA/BEXT
      COMMON/GAMMAS/G, GI, G1, G2, G3,G4, G5, G6, G7, G8, G9, G10, G11,G12, G13
      COMMON /FLUXES/ FI
      COMMON/PARAM/D1, Cref, CC
       DO 10 I = 0, CELLS
       DO 20 K = 1, 3
       CDL(K)  = BEXT(2, K, I)
       CDR(K)  = BEXT(1, K, I + 1)
      20 CONTINUE
       DL      = CDL(1)
       UL      = CDL(2)/DL
       U21L    = CDL(3)
       PL      = CT*DL**G
       D2L     = (PL/Cref)**GI
       alf2L   = (1.0 - (DL/D1) + (CC*DL/D1))
       amL     = SQRT(G*PL/DL)
       D21L    = ((1.0/D2L) - (1.0/D1))
       DR      = CDR(1)
       UR      = CDR(2)/DR
       U21R    = CDR(3)
       PR      = CT*DR**G
       D2R     =  (PR/Cref)**GI
       alf2R   = (1.0 - (DR/D1) + (CC*DR/D1))
       amR     =  SQRT(G*PR/DR)
       D21R    = ((1.0/D2R) - (1.0/D1))
       CALL FLUEVAL(CDL, FDL, CT)
       CALL FLUEVAL(CDR, FDR, CT)
       CALL TworarefaSolver(DM, UM, CT)
       CALL ESTIME(SL, SM, SR, CT, DM, UM, U21ML, U21MR)
       PM        = CT*DM**G
       IF(SL.GE.0.0)THEN
       DO 30 K  = 1, 3
       FI(K, I) = FDL(K)
      30 CONTINUE
       ENDIF
       IF(SL.LE.0.0.AND.SR.GE.0.0)THEN
       IF(SM.GE.0.0)THEN
```

```
      VU1L      = ((CDL(3)*(SL - UL))/(DM*(SL - SM)))
      VU2L      = ((1.0)/(DM*(SL - SM)))
      VU3L      = (0.5*(1.0 - 2*CC)*(U21ML**2 - U21L**2))
      VU4L      = (Cref**GI*G8*(PM**G9 - PL**G9))
      VU5L      = ((PM - PL)/D1)
      VU6L      = (VU4L - VU5L)
      RELUL     =  (VU1L + VU2L*(VU3L + VU6L))
      CSTAL(1)  =  DL*(SL - UL)/(SL - SM)
      CSTAL(2)  = CSTAL(1)*SM
      CSTAL(3)  = CSTAL(1)*RELUL
      DO 40 K   = 1, 3
      FI(K, I)  = FDL(K) + SL*(CSTAL(K) - CDL(K))
   40 CONTINUE
      ELSE
      VU1R      = ((CDR(3)*(SR - UR))/(DM*(SR - SM)))
      VU2R      = ((1.0)/(DM*(SR - SM)))
      VU3R      = (0.5*(1.0 - 2*CC)*(U21MR**2 - U21R**2))
      VU4R      = (Cref**GI*G8*(PM**G9 - PR**G9))
      VU5R      = ((PM - PR)/D1)
      VU6R      = (VU4R - VU5R)
      RELUR     = (VU1R + VU2R*(VU3R + VU6R))
      CSTAR(1)  = DR*(SR - UR)/(SR - SM)
      CSTAR(2)  = CSTAR(1)*SM
      CSTAR(3)  = CSTAR(1)*RELUR
      DO 50 K   = 1, 3
      FI(K, I)  = FDR(K) + SR*(CSTAR(K) - CDR(K))
   50 CONTINUE
      ENDIF; ENDIF
      IF(SR.LE.0.0)THEN
      DO 506 K = 1, 3
      FI(K, I) = FDR(K)
  506 CONTINUE
      ENDIF
   10 CONTINUE
      END SUBROUTINE HLLC
      ! |~~~~~~~~~~~~~~~~~~~~~~~~~~~~| FLUEVAL  |~~~~~~~~~~~~~~~~~~~~~~~~~~~~~~~~~~~~~~~~~~~~~|
      SUBROUTINE FLUEVAL(CS, FLUX, CT)
      IMPLICIT NONE
      DOUBLE PRECISION G, GI, G1, G2, G3, G4, G5, G6, G7, G8, G9, G10, G11, &
      G12, G13, CS, FLUX, D1, Cref, CC, D, U, U21, P, CT
      DIMENSION CS(3), FLUX(3)
      COMMON/GAMMAS/G, GI, G1, G2, G3,G4, G5, G6,G7, G8, G9, G10, G11,G12, G13
```

```
COMMON/PARAM/D1, Cref, CC
D          = CS(1)
U          = CS(2)/D
U21        = CS(3)
P          =  CT*D**G
FLUX(1)    = D*U
FLUX(2)    = (D*U*U + P + D*CC*(1.0 - CC)*U21*U21)
FLUX(3)    = ((U*U21) + (0.5*(1.0 - 2.0*CC)*U21*U21) + &
             ((Cref**GI*G8*P**G9) - (P/D1)))
 END SUBROUTINE FLUEVAL
! |~~~~~~~~~~~~~~~~~~~~~~~~~~~| Tworare |~~~~~~~~~~~~~~~~~~~~~~~~~~~~~~~~~~~~~~|
SUBROUTINE TworarefaSolver(DM, UM, CT)
 IMPLICIT NONE
 DOUBLE PRECISION  DM, DL, UL, U21L, PL, amL, DR, UR, U21R, PR, amR,    &
 CL, D21L, CR, D21R, G, GI, G1, G2, G3, G4, G5, G6, G7, ap1, ap2, ap4,  &
 ap6, gL, gR, CT, NL1, NL2, NR1, NR2, DPV, DMIN, DMAX, QMAX, DLR,       &
 UM, DTL, DTR, D1, T, R, S0, S1, SE, P0, C, Cref, G8, G9, G10, G11,     &
 G12, G13, CCL, QUSER , cc, ap9, ap8, ap7, ap3, ap10, ap5
 COMMON/GAMMAS/G, GI, G1,G2, G3, G4,G5, G6, G7, G8, G9, G10, G11,G12, G13
 COMMON/STATES/DL, UL, U21L, PL, D21L, amL,  DR, UR, U21R, PR,D21R, amR
 COMMON/PARAM/D1, Cref, CC
 ap1  = (DL + DR)*(amL + amR)
 ap2  = (DL+DR)/(D21L + D21R)
 ap3  = (U21L+U21R)/(amL + amR)
 ap5  = (2*(CC + CC)-(CC + CC)**2)
 ap6  = (UL + UR)/(DL + DR)
 AP7  = (DR-DL)/(amL+amR)
 ap8  = (1.0/(DL+DR))
 ap9  = (1.0/(D21L+D21R))
 ap10 = (1.0/(amL+amR))
 DPV  = (0.5*(DL + DR) + 0.125*(UL - UR)*ap1                            &
      + 0.125*ap2*ap3*(DR - DL)*ap5)
 DPV  = MAX(0.0, DPV)
 DLR = (DL/DR)**G1
 UM  = ((DLR*UL/amL)+UR/amR+G2*(DLR - 1))/(DLR/amL+1.0D0/amR)
 DTL = (1.0D0 + G1*(UL - UM)/amL)
 DTR = (1.0D0 + G1*(UM - UR)/amR)
 DM  = 0.5*(DL*DTL**G2 + DR*DTR**G2)
END SUBROUTINE TworarefaSolver
! |~~~~~~~~~~~~~~~~~~~~~~~~~~~| ESTIME |~~~~~~~~~~~~~~~~~~~~~~~~~~~~~~~~~~~~~~|
SUBROUTINE ESTIME(SL, SM, SR, CT, DM, UM, U21ML, U21MR)
 IMPLICIT NONE
```

```
DOUBLE PRECISION  DL, UL, U21L, PL, D21L, amL,  DR, UR, U21R, PR,     &
D21R, amR, G, GI, G1, G2, G3, G4, G5, G6, G7, G8, G9, G10, G11,       &
G12, G13, D1, Cref, CC, QUSER, DM, UM, PM, ap1, ap2, ap4, ap5,        &
ap6, gL, gR, CT, NL1, NL2, NR1, NR2, DPV, DMIN, DMAX, QMAX, DLR,      &
SL, SM, SR, DTL, DTR, DSL, DSR, U21ML, U21MR, KC, X1, X2, X3,         &
E1, E2, E3, Z1, ZY0, ZY1, Z2, Z5, ZY2, Z4, ZQ1, ZQ2, ZQ3, EQ1,        &
EQ2, EQ3, QE, ap3, ap7, ap8, ap9
COMMON/STATES/DL, UL, U21L, PL, D21L, amL, DR, UR, U21R, PR, D21R, amR
COMMON/GAMMAS/G, GI,G1, G2, G3, G4, G5, G6, G7, G8,G9, G10, G11,G12, G13
COMMON/PARAM/D1, Cref, CC
IF(DM.LE.DL)THEN
SL     = (UL - amL + (CC*(1.0 - CC)*U21L*DL*D21L))
X1     = (DM/DL)
X2     = G6*((X1**G1) - 1.0)*KC
X3     = (DM*((DL/DM) - (X1**G1))/D1)
U21ML = U21L - G5*(X2 + X3)*amL
ELSE
PM     = CT*DM**G
DSL    = (((DM*(PM - PL))/(DL*(DM - DL))))
SL     = UL - SQRT(DSL)
Z1     = ((DM/DL)*U21L)
Zy0    = Cref**GI*G8*(PM**G9 - PL**G9)
Zy1    =  (PM - PL)/D1
E1     = (ZY0 - ZY1)
E2     = ((DM*(DM - DL)))
E3     = ((DL*(PM - PL)))
Z2     = SQRT(E2/E3)
U21ML = (Z1 - E1*Z2)
END IF
SM     = UM
IF(DM.LE.DR)THEN
SR     = (UR + amR + (CC*(1.0 - CC)*U21R*DR*D21R))
KC     = (Cref/CT)**GI
Z5     = (DM/DR)
ZY2    = G6*((Z5**G1) - 1.0)*KC
Z4     = (DM*((DR/DM) - (Z5**G1))/D1)
U21MR = U21R + G5*(ZY2 + Z4)*amR
ELSE
PM     = CT*DM**G
DSR    = ((DM*(PM - PR))/(DR*(DM - DR)))
SR     = UR + SQRT(DSR)
ZQ1    = ((DM/DR)*U21R)
```

```
  ZQ2    = Cref**GI*G8*(PM**G9 - PR**G9)
  ZQ3    = (PM - PR)/D1
  EQ1    = (ZQ2 - ZQ3)
  EQ2    = ((DM*(DM - DR)))
  EQ3    = ((DR*(PM - PR)))
  QE     = SQRT(EQ2/EQ3)
  U21MR  = (ZQ1 + EQ1*QE)
    END IF
END SUBROUTINE ESTIME
! |~~~~~~~~~~~~~~~~~~~~~~~~~~~| UPDATE |~~~~~~~~~~~~~~~~~~~
```

```
DIMENSION D(-1:IDIM+2), U(-1:IDIM+2), U21(-1:IDIM+2), P(-1:IDIM+2), &
am(-1:IDIM+2), D2(-1:IDIM+2), alf2(-1:IDIM+2)
COMMON/DOMAIN/ML, MR
COMMON/GAMMAS/G, GI, G1, G2, G3, G4, G5, G6, G7, G8, G9,          &
      G12, G13, G10, G11
COMMON/PRMTV/D, U, U21
COMMON/PARAM/D1, Cref, CCL
Psle = 100000.0
OPEN(1, FILE = 'dmusc.out');  OPEN(2, FILE = 'umusc.out')
 OPEN(3, FILE = 'urmusc.out'); OPEN(4, FILE = 'pmusc.out')
 DO 110 I = 1, CELLS +1
 Xpos     = ML + (MR - ML)*REAL(I - 1)/REAL(CELLS)
 P(I)     = CT*D(I)**G
 D2(I)    = (P(I)/Cref)**GI
 alf2(I) = ((D(I) - D1)/(D2(I) - D1))
 am(I)    = SQRT(G*P(I)/D(I))
 Write(1,20)Xpos, D(I);   Write(2,30)Xpos, U(I)
 WRITE(3,40)xpos, u21(I); WRITE(4,50)xpos, P(I)/Psle
110 CONTINUE
    Close(1); Close(2); Close(3); Close(4)
20 FORMAT(F15.8,2X, F15.8)
30 FORMAT(F15.8,2X, F15.8)
40 FORMAT(F15.8,2X, F15.8)
50 FORMAT(F15.8,2X, F15.8)
END SUBROUTINE OUTPUT
```